The University Of Sheffield.

Development of a Long-Acting Parathyroid Hormone for the Treatment of Hypoparathyroidism

Faez Falah Alshehri

A thesis submitted in partial fulfilment of the requirements for the degree of Doctor of Philosophy

The University of Sheffield

Faculty of Medicine, Dentistry and Health

Department of Oncology and metabolism

First Supervisor: Prof. Richard Ross

Second Supervisor: Dr. Ian Wilkinson

June 2021

Declaration

I hereby declare that this thesis has been composed by myself and has not been previously presented for an award at this, or any other, university. The work reported in this thesis is novel and has been carried out by myself with all source of information being specifically acknowledged by means of references.

Faez Alshehri

June, 2021

Abstract

Background: Parathyroid hormone (PTH) is a peptide hormone consisting of 84 amino acids with residues 1-34 responsible for its biological activity. In Hypoparathyroidism, patients lack PTH due to loss or damage to the parathyroid glands leading to impaired mineral homeostasis. Hypoparathyroidism is commonly treated with oral calcium and active vitamin D and more recently with Natpara (PTH 1-84). However, because of a short serum half-life, PTH 1-84 requires daily injections and treatments are complicated by fluctuating calcium levels. An unmet need exists for a long-acting PTH that is effective, easy to administer and has realistic manufacturing costs. It is hypothesised that a fusion of PTH to a native binding protein, Growth Hormone Binding Protein (GHBP), will retain biological activity, and have a prolonged serum half-life through increased size and reduced proteolysis. This hypothesis has been tested in this thesis by studying three PTH fusion proteins: 14A7 (PTH linked to GHBP), 14A2c (PTH linked to the extracellular domain of PTH receptor and GHBP) and 14A8 as control for 14A2c wherein the PTH binding site on the receptor has been mutated to prevent PTH binding.

Methods: Stable PTH fusions generated in CHO Flp-In cells were confirmed by RT-PCR and sequencing. Fusions were expressed in suspension culture in roller bottles as a secreted product and purified by ion exchange and affinity chromatography. Potency of Fusions was assessed using a Dual Luciferase Reporter Assay (DLRA) in the PTH responsive rat osteosarcoma cell line, UMR-106. EC_{50} values were obtained using GraphPad Prism software.

Results: Protein expression for all PTH fusions was confirmed by western blotting. 14A7 separated as diffuse bands between 37 and 50 kDa and purified to 0.93 mg/mL. 14A2c and 14A8 separated as diffuse bands between 75 and 100 kDa and purified to 2.57 mg/mL and 2.29 mg/mL, respectively. During the DLRA validation process, pRL-TK was shown to be superior to pRL-CMV as an internal control. pRL-TK at 10 or 20 ng per transfection yielded more consistent results with no variation in Renilla expression with increasing concentrations of PTH 1-34 or PTH fusions. Using the validated DLRA, Mean ± SD EC_{50}'s nM were: PTH 1-34 = 2.39 ± 0.58 (n = 8), 14A7 = 68.02 ± 4.01 (n = 4), 14A2c = 699.4 ± 55.6 (n = 3), and 14A8 = 253.8 ± 26.3 (n = 3).

Conclusion: All three PTH fusions were successfully expressed and for 14A8 and 14A7 stable CHO Flp-In cell lines were created. Protein was obtained in the expression media and purified for all PTH fusions. All three fusion proteins showed biological activity although this was less than that for PTH 1-34. The addition of the extracellular PTH receptor to the fusion, as in 14A2c, reduced biological activity which was partially restored in 14A8, by mutating the PTH receptor moiety, suggesting that inter- or intra-molecular binding was taking place. In conclusion, it is possible to express PTH linked to a binding protein and retain biological activity providing potential for a long-acting PTH molecule.

Acknowledgement

This thesis was finalised during the most challenging time, the COVID-19 quarantine. At this time, I was working on my thesis between the UK and Saudi Arabia and I experienced drastic changes where the world was fighting the pandemic: cities were locked down, curfews were imposed and social distancing was a necessary requirement.

Praise be to God the Lord of the universe. After an intensive time of three years, today is the day: writing these few paragraphs of thanks is the crowning achievement of my thesis. It has been a time of exceptional learning for me, in the scientific field, as well as on an individual level. On behalf of myself, I would like to express my sincerest and humble gratitude to my supervisors Professor Richard Ross and Dr Ian Wilkinson. This research work would not have been produced without their consistent guidance, advice, constructive comments and suggestions that helped me bring this study into success. For that, I am utmost grateful for their time and their effort. I would also like to thank my laboratory's technician assistant Mrs Sue Justice who the department would not run so smoothly without her.

As always, I am extremely grateful to my family and friends for their support. I am especially grateful to my parents and all my family members for their unconditional support, not only this year but throughout my life, leading me to where I am today. I am likewise grateful to all my teachers and mentors who contributed any portion of knowledge or guidance till this date.

My deepest appreciation belongs to my Wife, Mrs Faizah, who is my champion and who blessed me with a life of joy. To my two little kids, Musk and Falah for their endless support and belief in me.

Lastly and most of all, I am very grateful to Allah without whom nothing is possible.

Table of Contents

List of Figures

List of Tables

List of Abbreviations

%CV	Coefficient of variation
(1 α,25(OH)$_2$D)	1 α,25-dihydroxyvitamin D
α	alpha
β	Beta
γ	Gama
A_{260}	Absorbance 260nm
A_{280}	Absorbance 280nm
Ab	Antibody
AC	Adenylyl cyclases
anti-GHBP	Antibody Growth hormone binding protein
Arr	Arrestin
APS	Ammonium persulphate
ATP	Adenosine triphosphate
BMD	Bone mineral density
BSA	Bovine Serum Albumin
Bp	Base pair
Ca^{2+}	Ionic calcium
cAMP	Cyclic adenosine monophosphate
CaSR	Calcium-sensing receptors
CBD	Collagen Binding Domain
cDNA	Complementary deoxyribonucleic acid
CHO	Chinese Hamster Ovary
COS-7	African green monkey kidney fibroblast-like cell line
CNBr Activited	Cyanogen Bromide-Activated Sepharose
C_{max}	Maximum Concentration
CMV	Cytomegalovirus
CRE	cAMP Response Element
CREB	cAMP Response Element Binding
CV	Column Volume
Cys	Cysteine
CV-1 cells	African Green Monkey Kidney
C-terminus	Carboxyl-terminus
DAG	Diacylglycerol
DB	DMEM Buffer/0.1% BSA
dd H_2O	Double distilled water
DLA	Dual Luciferase Reporter Assay
DMEM	Dulbecco's Modified Eagle Medium
DMSO	Dimethylsulfoxide
DNA	Deoxyribonucleic Acid
dNTP	Deoxyribonucleotide Triphosphate
ds DNA	Double-stranded DNA

EB	Elution buffer
EC_{50}	Half Maximal response
ECD	Extracellular demand
EDTA	Ethylenediaminetetraacetic acid
eGFR	Estimated glomerular filtration rate
ELISA	Enzyme-linked immunosorbent assay
ER	Endoplasmic Reticulum
ERK1/2	Extracellular signal-regulated kinase 1 & 2
E.coli	Escherichia coli
FD	Fold difference
FDA	Food and Drug Administration
FGF-23	Fibroblast growth factor-23
FL/RL	Ratio of Firefly to Renilla Luciferase
FMI	Future Market Insights
FRT	Flp Recombinant Target
GC	Guanylyl cyclases
GH	Growth Hormone
GHBP	Growth hormone binding protein
GHss	Growth hormone signal sequence
GDP	Guanosine diphosphate
GRK	G protein-coupled receptor kinase
GPCR's	G protein-coupled receptors
GTP	Guanosine triphosphate
H_2O	Water
HEK	Human Embryonic Kidney
HIC	Hydrophobic interaction chromatography
HRP	Horseradish Peroxidase
IEX	Ion Exchange Chromatography
IGF-I	Insulin-like growth factor-I
IP3	Inositol (1,4,5)-triphosphate
I135K	A single amino acid change of Isoleucine-135 to lysine
Kb	Kilo base pair
kDa	Kilo Dalton
LA	Long-Acting
LA-PTH	Long-Acting- Parathyroid hormone
MCB	Master Cell Bank
MM	Master Mix
mPEG	methoxy polyethylene glycol
mRNA	Messenger ribonucleic acid
MWCO	Molecular Weight cut-off
Mwt	Molecular Weight
ng	Nanogram
N-terminus	Amino-terminus
OD_{260}	The optical density at 260nm

oligo d(T)$_{20}$	Oligodeoxynucleotide
PBS	phosphate-buffered saline
PBS-T	Phosphate Buffered Saline –Tween 20
PC	Post-concentration
PCR	Polymerase chain reaction
PD	Pharmacodynamics
PDE4	Phosphodiesterases Type-4
PE	Pooled elutions
PEG	Polyethylene glycol
PI3Ks	Phosphoinositide 3-kinases
PIP2	Phosphatidylinositol (4,5)-bisphosphate
PK	Pharmacokinetic
PKA	Protein kinase A
PLA2	Phospholipase A2
PLC	Phospholipase C
pRL-CMV	cytomegalovirus immediate-early enhancer/promoter region
pRL-TK	Herpes Simplex Virus thymidine kinase promoter
PTH	Parathyroid hormone
PTHrP	Parathyroid hormone-related protein
PTHR1	PTH type 1 receptor
PTHR2	PTH type 2 receptor
PTHss	Parathyroid hormone signal sequence
PTHrExt	Parathyroid hormone Extracellular Receptor
PTH-Fc	PTH 1-34 joined to the Fc fragment of human IgG1
Ppase	Protein phosphatase
PVDF	Polyvinylidene fluoride
Q-Unbound	Q-Sepharose column unbound fraction
R^0	G-protein-independent conformational state
R^G	G-protein-dependent conformational state
RB	Roller Bottle
rhPTH	Recombinant Full Length PTH
RL	Renilla Luciferase
RLU	Relative light units
RNA	Ribonucleic Acid
RT-PCR	Reverse Transcription Polymerase Chain Reaction
SaOS-2	Sarcoma Osteogenic Cells Line
SDS-PAGE	Sodium Dodecyl Sulphate-Polyacrylamide Gel Electrophoresis
StDev	Standard Deviation
Sir	Serine
ss DNA	Single-stranded DNA
TE	Trypsin/EDTA
TEMED	Tetremethylenediamine

TFX	transfection
TIP39	Tuberoinfundibular peptide containing 39 residues
TM	Transmembrane
TPTX	Thyroparathyroidectomized
Trp	Tryptophan
UB	Unbound fraction
µg	Microgram
UGS-56 cells	Derived from the UMR-106
µL	Microliter
UMR-106 cells	Rat osteosarcoma cell line
UV	Ultraviolet
V	Volt
vATPase	Vacuolar H+-ATPase
WCB	Working Cell Bank
W104A	A single amino acid change of tryptophan-104 to alanine

Chapter One – Introduction

1.1 Parathyroid Hormone

Parathyroid Hormone (PTH) is an endocrine hormone that is produced by the parathyroid gland (Clemens et al., 2001), and plays a significant role in the regulation of blood calcium levels (Collip, 1925) as well as control bone maintenance and mineral ion homeostasis (Raisz, 1963). PTH production is regulated by calcium-sensing receptors (CaSR), which control the secretion of PTH in the event of a low plasma calcium level in the blood (Egbuna and Brown, 2008, Loupy et al., 2012); which in turn increases the reabsorption of calcium in the kidney tubule, and thus reduces further loss in plasma calcium through renal excretion (Conigrave and Ward, 2013). In addition to regulating blood calcium levels, PTH also regulates the concentration of phosphate ions in circulation by maintaining the phosphate homeostatic concentration via the inhibition of phosphate reabsorption in the kidney tubules (Bergwitz and Juppner, 2010, Lederer, 2014).

As intracellular calcium and phosphate ions play essential roles in various biochemical processes in humans, such as hormonal secretion, neurotransmission, and cardiac contraction (Wettschureck and Offermanns, 2005, Blaine et al., 2015), their regulation by PTH underscores the importance of PTH in maintaining the homeostatic balance of these physiological processes. Hence, the initiation of the bone resorption to release calcium from the bone, as well as the stimulation of the reabsorption of calcium in the kidney, occurs through the secretion of PTH, which has the main purpose of targeting the kidney and the bone, in order for the aforementioned physiological processes to be executed (Blaine et al., 2015, Gardella and Vilardaga, 2015).

1.1.1 Structure of PTH and Function

The PTH gene is located on the short arm of chromosome 11 and consists of three exons (Naylor et al., 1983). As shown in Figure 1.1, PTH is synthesised as a large precursor Prepro-PTH polypeptide chain of 115 amino acids by the parathyroid cells (Habener et al., 1978). Subsequently, it loses its hydrophobic N-terminal signal sequence of 25 amino acids through cleavage by the action of microsomal-associated peptidase in the endoplasmic reticulum. The resulting pro-PTH (90 amino acids) is translocated into the Golgi apparatus, where it undergoes further proteolysis, resulting in the loss of additional 6 residue prosequences, and thus forms the mature PTH (Murray et al., 2005). The mature PTH is secreted as a single chain polypeptide hormone that consists of 84 amino acids (Clemens et al., 2001), with most of its biological action associated with the first 34 N- terminal amino-acid residues (Potts et al., 1980). Consequently, the truncated length of PTH, which consists of residues 1-34, is more often used instead of full length PTH 1-84 in functional and clinical studies of PTH (Hodsman et al., 2005). Following its biosynthesis, the mature PTH is stored in the secretory vesicles until released in response to hypocalcaemia (Brown, 1983).

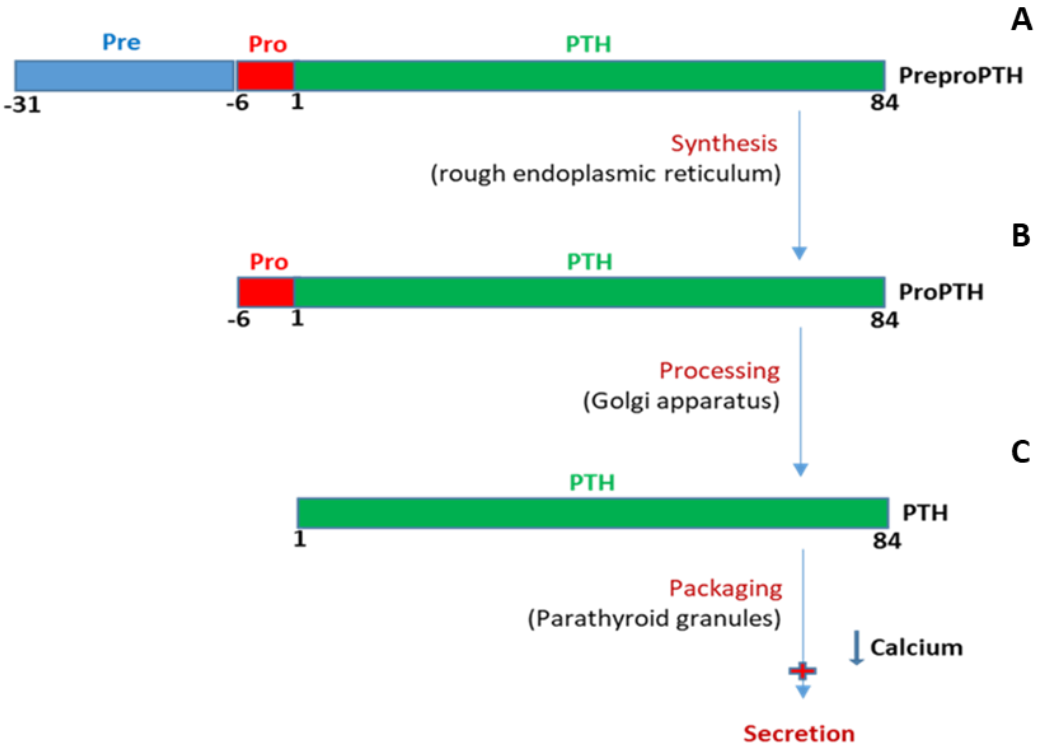

Figure 1.1: Schematic explaining PTH synthesis.

PTH is synthesised as a large precursor Prepro-PTH polypeptide chain of 115 amino acids consisting of a prepro N-terminal signal sequence of 25 amino acids and 6 amino acid protease cleavage site linked to 1-84 mature PTH **(A)**. The signal sequence is cleaved by the action of microsomal-associated peptidase in the endoplasmic reticulum **(B)**. Further processing is completed in the Golgi apparatus with the removal of the 6 amino acid prosequence, to give the mature PTH 1-84 **(C)**. PTH is stored in parathyroid granules ready for secretion, and released in response to hypocalcaemia. Constructed using Venngage website.

1.1.2 Crystal Structure of Parathyroid Hormone

Structurally, for decades, PTH was thought to exist as a long straight peptide (Jin et al., 2000, Barden and Kemp, 1993). NMR spectroscopy studies of PTH tertiary structure revealed that the mature peptide consists of two alpha (α) helices at the N and C-terminal. The respective helices were thought to be connected via a flexible linker (Marx et al., 1995) (See Figure 1.2). However, through X-ray crystallography PTH has been shown as a continuous α helix with two amphiphilic sections - one at residues 6-20 and the other at residues 21-33 - and identified

with a slight bend 15° between residues 12 and 21. In addition, studies on PTH structure-activity revealed the role of the amphipathic α-helix in facilitating the binding of the PTH to its receptor, in a manner that is consistent with how GPCRs bind to their ligand (Piserchio et al., 2000, Jin et al., 2000, Pioszak et al., 2009).

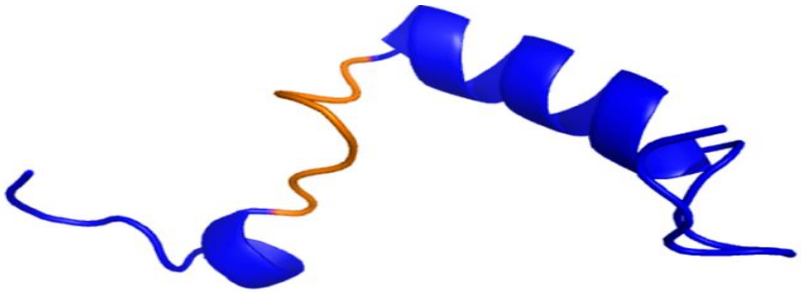

Figure 1.2: Schematic structure of PTH.
The picture features PTH (1-37) structure was identified by using NMR spectroscopy. The image is from the protein Database.

1.1.3 The Regulation of PTH Secretion

The parathyroid glands play a pivotal role in vertebrates in regulating calcium ions homeostatic balance, which is achieved by modulating bone metabolism and the reabsorption of calcium ions in the distal tubules, as well as regulating the synthesis of 1 α,25-dihydroxyvitamin D (1 α,25$(OH)_2$D) in proximal tubules (Kumar and Thompson, 2011). The secretion of PTH from the parathyroid glands is modulated by CaSR, which are homodimer structures that are found on the surface of the parathyroid gland (Egbuna and Brown, 2008). The CaSR belongs to the family of G protein-coupled receptors' (GPCRs') type C that comprises of a large N-terminal extracellular calcium-binding domain and a small intracellular C-terminal domain associated with protein signalling (Katritch et al., 2013). The role of CaSR in the regulation of the PTH gene expression is affected through a change in preproPTH mRNA levels. The CaSR dimer is able to bind ionised calcium, which leads to the stimulation of the

receptor (Nechama et al., 2009), and in turn leads to the inhibition of PTH secretion, and ultimately, the inhibition of calcium reabsorption. Therefore, ionised calcium in the blood can regulate the functions of both the kidney and parathyroid glands, in order to achieve normal calcium ions levels in circulation (Grant et al., 2012).

Studies have shown an inverse relationship between calcium ion levels and PTH secretion, whereby high calcium ions levels result in a decline in PTH secretion. Conversely, lower calcium ions levels result in an increase in PTH secretion and a concomitant increase in parathyroid chief cell number (Egbuna and Brown, 2008, Kumar and Thompson, 2011). The downregulation of PTH secretion by elevated ionised calcium levels in the blood is commonly associated with two underlying mechanisms, beginning with the activation of the proteases within the PTH vesicles and the cleavage of PTH 1-84, which generates fragmented PTH peptides that are functionally inactive. Furthermore, the second mechanism involves the prevention of the PTH vesicle fusion within the parathyroid chief cell membrane (Potts, 2005).

1.1.4 Metabolism of PTH

PTH has a relatively short plasma half-life few minutes once secreted, as it is rapidly cleared from the circulation by peripheral clearance (Allgrove and O'Riordan, 1985); predominantly through the hepatic and renal clearance routes (Juppner et al., 1991, D'Amour et al., 2006). In the liver, extensive cleavage and proteolysis of the PTH is mediated by the Kupffer cells, which facilitate its rapid clearance. In the kidney, reabsorption of PTH occurs from the urine into the renal tubules, where it is subsequently cleaved, degraded and cleared from circulation (Murray et al., 2005).

1.2 G- Protein Coupled Receptors (GPCRs)

GPCR's are members of the largest family of membrane proteins and function as mediators of several cellular responses of hormonal/neurotransmitter origin (Palczewski and Orban, 2013). The characteristic features of the receptors in this family include a seven hydrophobic transmembrane (TM) structure, a large N-terminal extracellular and an intracellular C-terminal domain (Gardella and Juppner, 2001, Gardella and Vilardaga, 2015) (See Figure 1.3).

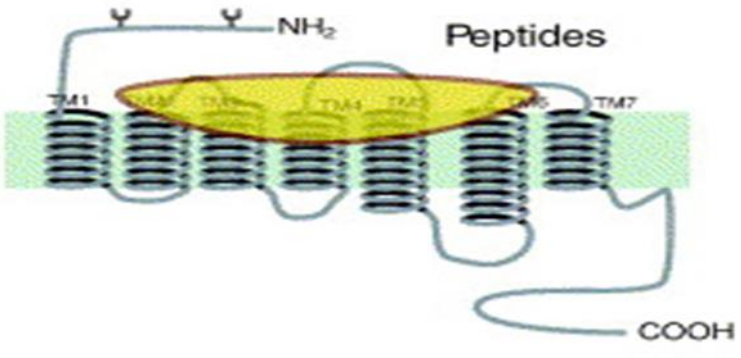

Figure 1.3: Schematic structure of GPCRs.
The figure shows a seven transmembrane helix segment flanked by an extracellular N-terminus and an intracellular C terminus in a GCPR peptide. The cell membrane is shown in green and the ligand peptide is shown in yellow. Adapted from (Kobilka, 2007), the image is with permission from PMC.

Structurally, the G-proteins are heterotrimeric with α, β, and γ subunits. The first subunit (i.e. α) plays a role in the hydrolysis of GTP by facilitating both GTP and GDP binding, and the β and γ subunits form a βγ complex to function (Sprang, 2016). The G-proteins are activated as a heterotrimer when the bound GDP in the G-protein α-subunit is displaced by GTP. The displacement by GTP triggers a disintegration of the αβγ complex into functionally active α-subunit monomer and βγ dimer (Hermans, 2003, Wong, 2003). Therefore, both the α- and βγ-subunits of G-protein are able to induce signal transduction of various molecules, such as phosphoinositide 3-kinases (PI3Ks), phospholipase A2 and C (PLA2 and PLC respectively),

adenylyl and guanylyl cyclases (AC and GC respectively) and elicit further downstream cellular responses, which include increases in the intracellular concentration of Ca^{2+} and regulating ion channels (Marinissen and Gutkind, 2001, Smrcka, 2008).

1.2.1 PTH Receptor

Parathyroid hormone-related protein (PTHrP) and parathyroid hormone (PTH) both bind the PTH type 1 receptor (PTHR1). However, even though PTH exerts its functions through PTHR1 to mediate the regulation of PTH-dependent mineral homeostasis (Juppner et al., 1991, Gardella and Vilardaga, 2015), it can also bind to another receptor known as PTH type 2 receptor (PTHR2) (Gensure et al., 2005). Indeed, PTHR1 expression has been found in many tissues, such as kidney, bone and cartilage, liver, smooth muscle, heart, skin, mammary glands, ovary, testis, placenta and the uterus (Ureña et al., 1993, Hiremath and Wysolmerski, 2013). While PTHR1 is expressed in several tissues, the expression of PTHR2 is limited to a few tissues, such as the brain, pancreas, placenta, testis and blood vessels (Usdin et al., 1995, Dobolyi et al., 2012).

1.2.1.1 Structure and Function of PTHR1

In 1991, PTHR1 complementary deoxyribonucleic acid (cDNA) was first cloned from a kidney cell cDNA library of an opossum in 1991 and the protein expressed in COS-7 cells (Juppner et al., 1991). PTHR1 is a member of the class B family of GPCR's and consists of 593 amino acids (Subramanian et al., 2016), with a molecular weight of 60 kDa for the non-glycosylated polypeptide backbone, which increases to 80 kDa upon glycosylation (Bisello et al., 1996, Shigeno et al., 1988). Structurally, both PTHR1 and PTHR2 possess distinguishing features that separate them from other classes of GPCR (Gardella and Vilardaga, 2015). As shown in Figure

1.4, these features include six highly conserved cysteines that interact to generate three disulphide bridges and a characteristically large glycosylated N-terminal extracellular domain. This domain contains four N-glycosylation sites that are crucial to the biological activity of the receptor (Grauschopf et al., 2000, Zhou et al., 2000). The N-glycosylation sites have been mapped to residues N151, N161, N166 and N176 (Zhou et al., 2000) and are in close proximity to the first transmembrane domain. Therefore, glycosylation occurs at all possible N-glycosylation sites in PTH/PTHrP receptor. Ligand binding and signal transduction require at least one N-linked glycosylation of the receptor for its expression (Zhou et al., 2000, Gardella and Vilardaga, 2015) (See Figure 1.4). The C-terminal domain includes several serine residues that are phosphorylated, due to the binding of ligand (Hodsman et al., 2005, Gardella and Vilardaga, 2015).

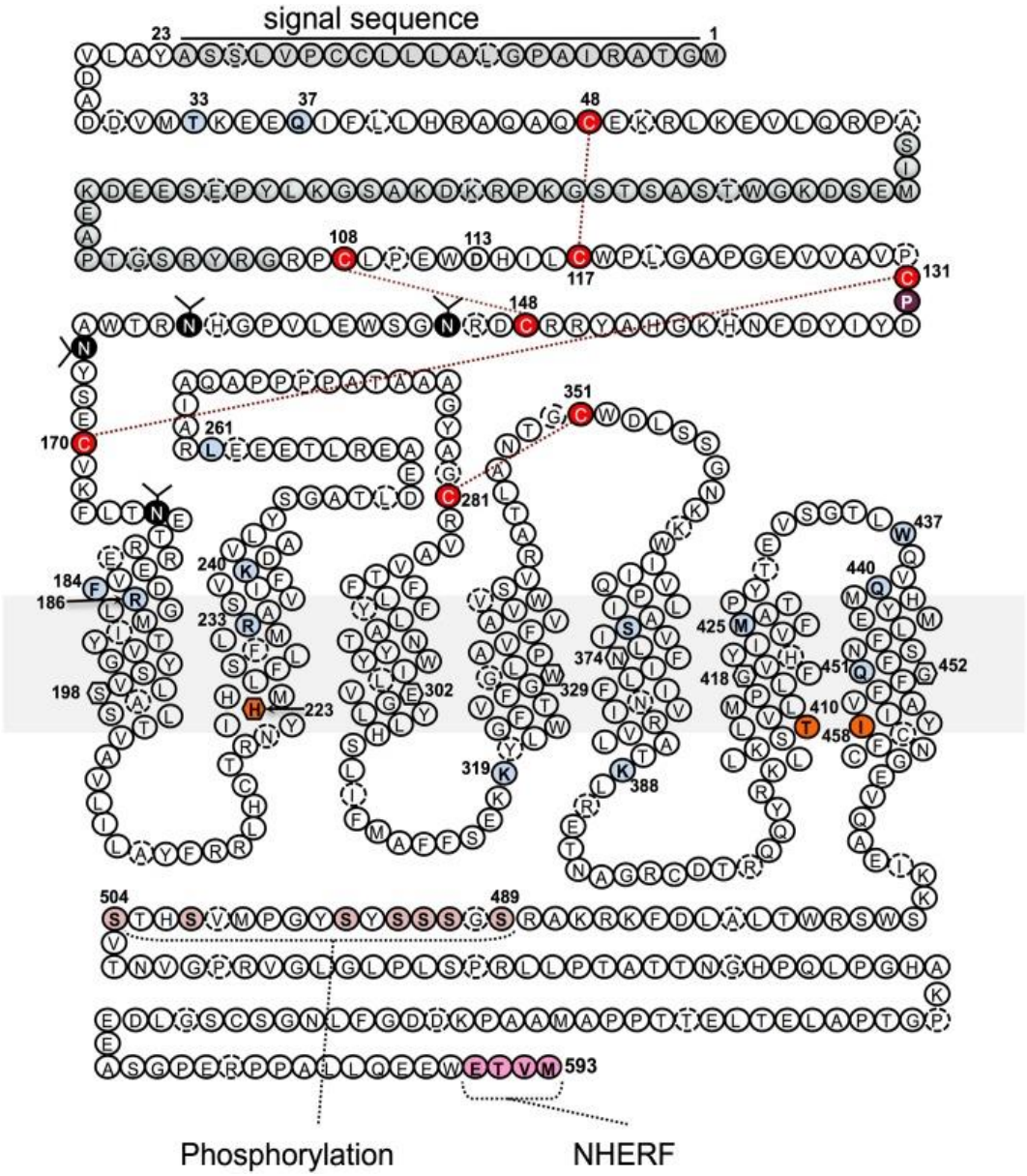

Figure 1.4: Schematic representation of the PTHR1.

The open circles is amino acid code in a position of represents the amino acid sequence 593 of the PTHR1 whereby loops connection which arbitrates against receptor activation and signal transduction locates the possible locations of the transmembrane domains. Amino acids positions are represented by the black circles for N-linked glycosylation. The cleavage site is specified by the inverted triangle for the 23-amino acid. In addition, C terminal tail is 130 amino acids. The receptor is shown to be made up of 160 amino acids ECD. Several serine residues which are phosphorylated make up the C-terminal domain 130 amino acid because the binding of a ligand in the C-tail. The receptor also contains six conserved cysteine residues, which interact to generate three disulphide bridges. NHERF family of proteins indicate interaction with the ETVM sequence in the C-terminal site. Adapted from (Gardella and Vilardaga, 2015), the image is with permission from PMC.

The active fragment of PTH 15-34 has been modelled with the PTHR1 ECD amino acid (See Figure 1.5). The PTHR1 ECD amino acid modelled structure features an elongated N-terminal flanking α-helix; a prominent loop; three disulphide bridges that provide stability to the molecular structure; and two pairs of antiparallel beta strands at the central core of the molecule (Jin et al., 2000). The C-terminal end features an amphipathic α-helix with a prominent groove. In addition, studies on PTH structure-activity reveal the role of the amphipathic α-helix in facilitating the binding of the PTH to its receptor (Piserchio et al., 2000, Jin et al., 2000, Pioszak et al., 2009).

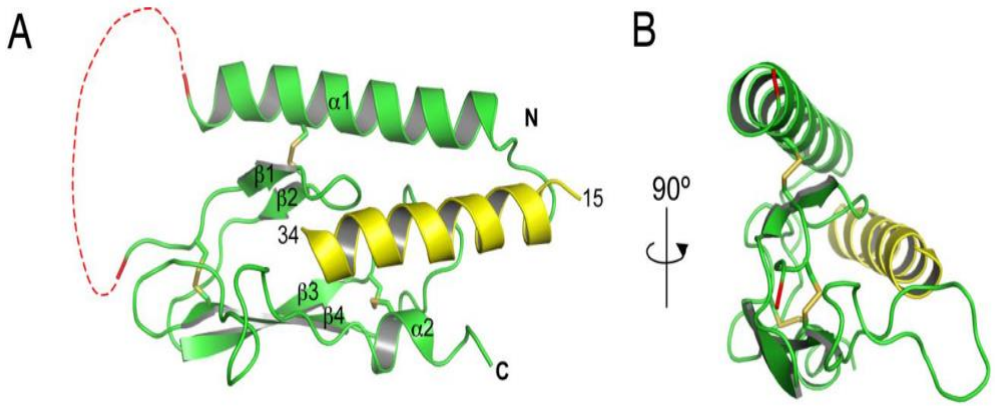

Figure 1.5: Molecular model of the PTH (15-34) with ECD region of PTHR1 complex.
The X-ray crystal structures (Diagram A and B) that are exposed are of PTH (15–34) (yellow), which bounds to the extracellular domain region of the PTHR1 residues 56–105 and 175–187 (green); the red dashed line shows that the break in the chain is located between residues 57 and 105, due to a disordered loop. Furthermore, there is the N-terminal flanking α-helix of the ECD PTHR1, while α-helix is connected with β-strands 4 in the loop. There are four types of β-strands in several residues. Adapted from (Pioszak and Xu, 2008), the image is with permission from PMC.

1.2.1.2 PTH and PTHR1 Interactions and Signalling

The mechanism of interaction of PTH with PTHR1 has been proposed to depend on the conformation of PTHR1, which could either be a long-acting G-protein-independent

conformational state (R^0) or a short-lived G-protein-dependent conformational state (R^G) in eliciting induced different cAMP signal transduction when bound by a G-protein ligand (Ferrandon et al., 2009, Vilardaga et al., 2012). In the R^0 conformation, PTHR1 can persistently bind its Gαs ligand with a very high-affinity and induce cAMP responses in cells over a longer period of time (Maeda et al., 2013, Vilardaga et al., 2012). Recent evidence suggests that this persistent action has been associated to the stability of the PTHR1/ligand complex as cellular responses have been reported after internalisation into endosomal vesicles, as shown in Figure 1.6 (Vilardaga et al., 2014). PTHR1 signal transduction in the R^0 conformation is commonly associated with prolonged hypophosphatemic and hypercalcaemic cellular responses in animals, which makes the R^0 receptor conformation an attractive candidate for novel treatment against hypoparathyroidism (Ichikawa et al., 2008).

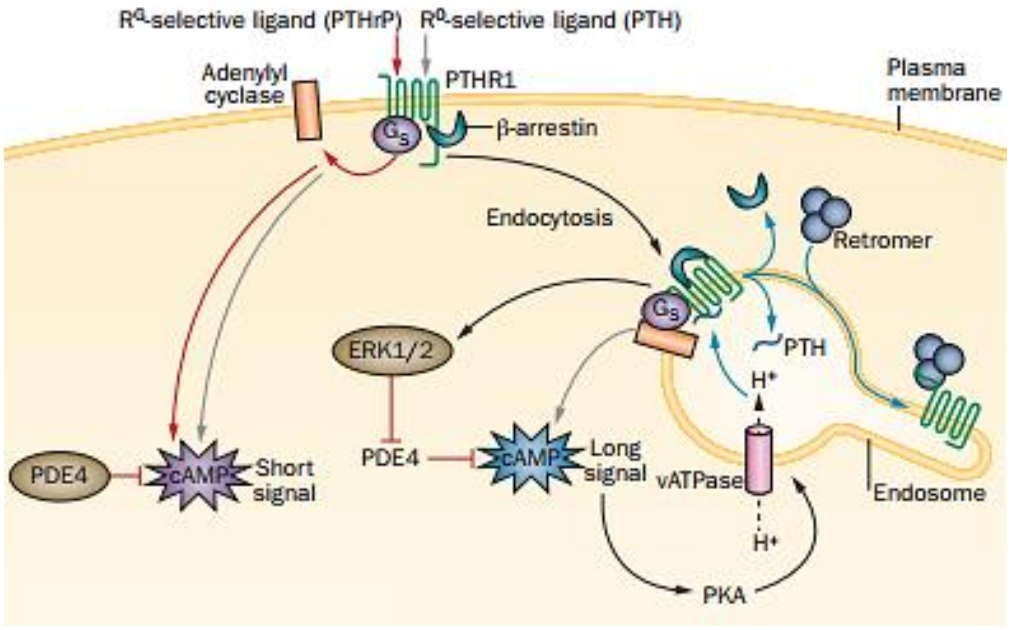

Figure 1.6: Schematic representation of the PTH and PTHrP with PTHR1 interactions and signalling. The diagram above shows that the PTH signal takes a long signal R^0 to respond within prolonged cAMP responses from signalling divided at the internalised endosomal domain, which contains β arrestin. While PTHrP works with $G\alpha_s$ at the plasma membrane through the cAMP response, there is then a dissociated short signal R^G. The dimer initiates a cascade of cellular responses, ranging from vATPase activation, cAMP synthesis, and then PKA activation. Activation of ERK1/2 contributes to the inhibition PDE4, which suspends cAMP. PTHR binding with retromer leads to the isolation of the receptor to retrograde trafficking domains, and thus, stops cAMP generation. Adapted from (Cheloha et al., 2015): **ERK1/2** extracellular signal-regulated kinase 1/2; **PDE4,** Phosphodiesterases Type IV **vATPase**; vacuolar H^+-ATPase. Image is with permission from PMC.

PTHR1 activation by either PTHrP or PTH induces a change in the receptor conformation and facilitates its interaction with G protein heterotrimers (Gαβγ). The resulting complex catalyses the replacement of the Gα-subunit GDP for GTP, which in turn triggers the disintegration of the G-protein heterotrimeric complex into two units - the Gα monomer and Gβγ dimer (Wehbi et al., 2013, Sprang, 2016). The dimer initiates a cascade of cellular responses, ranging from adenylyl cyclase (AC) activation, cAMP synthesis, and then PKA activation (See Figure

1.7). Similarly, the Gα monomer initiates a series of signal transductions, starting with PLC activation, which in turn generated inositol (1, 4, 5) -trisphosphate (IP3) and diacylglycerol (DAG) from phosphatidylinositol (4, 5)-bisphosphate (PIP2) by cleavage (Vilardaga et al., 2011, Taylor, 2017). Subsequently, protein kinase C (PKC) is activated by the DAG, while the IP3 induces the release of calcium ions into the cytosol (Guo et al., 2010). The increased cytoplasmic calcium ions in turn promote the translocation of PKC into the plasma membrane to be activated by DAG (Schipani and Provot, 2003). Therefore, PTHR1 is capable of activating various signalling pathways and elevates the concentration of ionised cytoplasmic calcium (Hodsman et al., 2005, Gardella and Vilardaga, 2015). In addition, recent studies reveal that GPCRs mediate G-protein signalling from endosomal membranes (See Figure 1.8). The regulation and maintenance of GPCRs signalling for an extended period of time assists in the understanding of the mechanism of action of drugs which target this receptor through internalising and redistributing into early endosomes (Vilardaga et al., 2014).

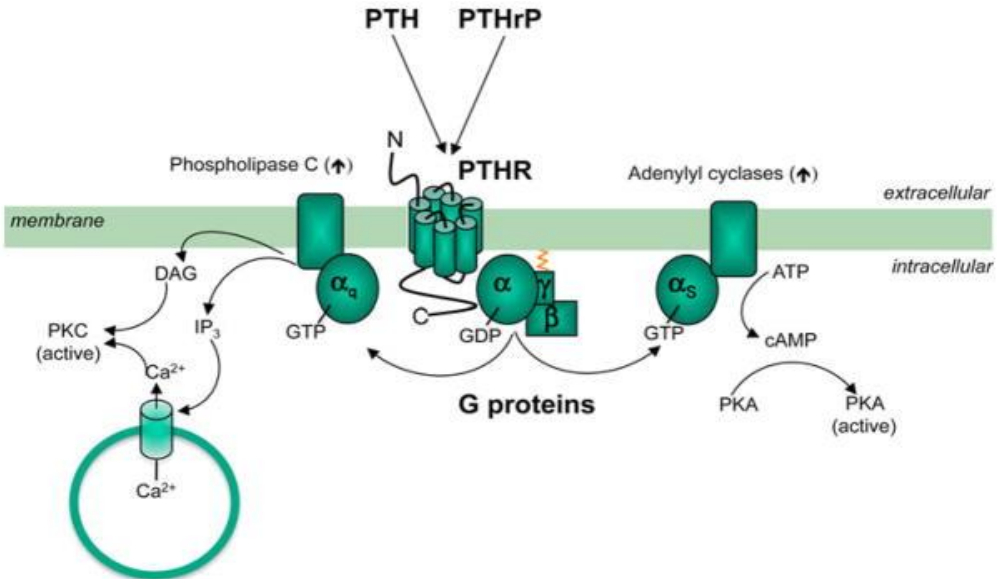

Figure 1.7: Multiple signalling pathways mediated by PTHR1.

The activation of PTHR1 induces a series of cellular responses that culminate in the activation of multiple pathways, such as AC, PKA, PKC, DAG, as well as increasing the concentration of cytosolic calcium ions. Different ligands are capable of inducing signal transduction interacting with GPCRs on the surface of membrane, which regulates many essential biological responses adapted from (Vilardaga et al., 2014), the image is used with kind permission from PMC.

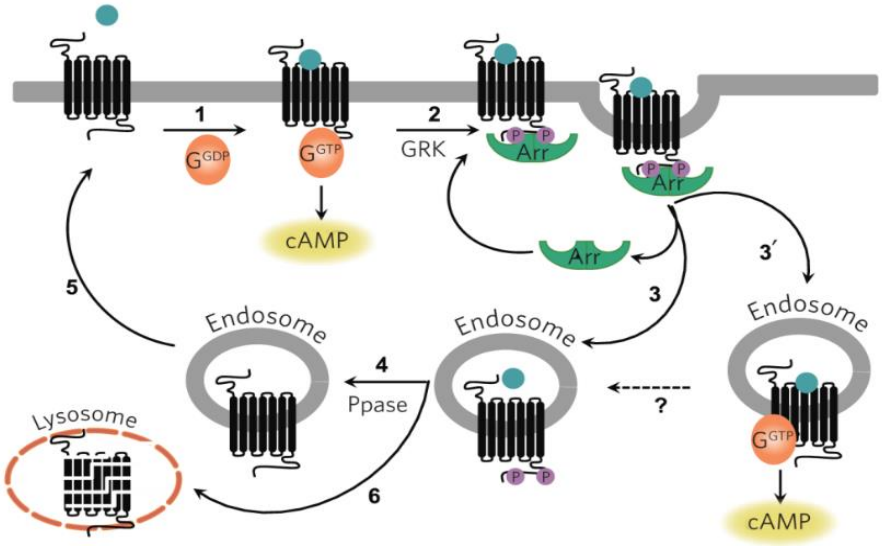

Figure 1.8: The depiction of models of GPCR one is classical versus another endosomal signalling models.

Arbitration by GPCR–GS systems of the activation and desensitisation of a cAMP response which occurs through a sequence of cellular as well as biochemical events where the primary phase originates at the cell membrane and the resulting effect is the induction, propagation and termination of the second messenger molecule described in steps 1 to 6. As seen in the classical model, the GPCR–G protein scheme exhibits activeness only on the cell surface and internalise to be watered-down as well as disintegrated and it might be replaced by newly synthesised GPCRs. Later models show the GS and cAMP signalling might continue to occur even after the internalisation of ligand– GPCR complexes in endosomes described by step 3. Adapted from (Vilardaga et al., 2014), the image is with permission from PMC: Arr, arrestin; GRK, GPCR (G protein-coupled receptors); Ppase, protein phosphatase.

1.2.2 PTHR2

PTHR2 cDNA was first cloned from the human brain cDNA library (Usdin et al., 1995), and about 70% of the PTHR2 amino acid sequence is homologous to that of PTHR1, which is predominantly within the transmembrane domain. Also, both receptors exhibit 50% identity similarity (Bisello et al., 2004) and elicit a similar dual signal transduction in response to truncated PTH (1–34) through cAMP stimulation and accumulation, which increases in intracellularly Ca^{2+} (Usdin et al., 2002, Ferrandon et al., 2009). However, in contrast to the PTHR1, PTHR2 is selectively activated by TIP39 (tuberoinfundibular peptide containing 39

residues) (John et al., 2002, Hoare et al., 2000, Bhattacharya et al., 2011) despite the striking similarity between TIP39 and PTH, whereby the truncated peptides of both molecules, consisting of the first 34 residues, exhibit full activity (Dobolyi et al., 2010). Moreover, cellular responses that result from TIP39 stimulation of cAMP formation is relatively desensitised and last longer than those induced by PTH, which is brief and resensitises rapidly (Bisello et al., 2004). Additionally, TIP39 is significantly expressed in testis as a secreted protein and in the hepatic, renal and several central nervous system cells at a trace amount (Dobolyi et al., 2012, John et al., 2002).

1.3 Hypoparathyroidism: Causes and Treatments

1.3.1 Causes and Symptoms

Hypoparathyroidism is a rare disease that results from reduced activity or secretion of PTH. The clinical manifestation of the disease includes blood hypocalcemia (i.e. significantly low calcium levels) and hyperphosphatemia (i.e. high phosphorus levels), with about 77000 individuals diagnosed in the United States alone (Clarke et al., 2016). The condition is associated with a lack of PTH production or insufficient amounts of PTH production, due to an absent or damaged parathyroid gland, respectively (Shoback, 2008, Cusano et al., 2015). Specifically, hypoparathyroidism could be either acquired as a result of surgical removal or damage to the parathyroid glands (Puzziello et al., 2014), or autoimmune (Goswami et al., 2010). Due to the pivotal role of PTH in calcium and phosphorus ions' regulation in the body, patients with hypoparathyroidism are predisposed to impaired mineral homeostasis, which includes hypocalcemia (low blood calcium) and hyperphosphatemia (high blood phosphate) (Shoback, 2008). The inherited causes of hypoparathyroidism are less common, and these include genetic defects, autoimmune disease, congenital agenesis of the glands, and defective

PTH secretion. For example, DiGeorge syndrome is a failure of the parathyroid glands tissue following sporadic mutations on chromosome 22 (Kobrynski and Sullivan, 2007). Common symptoms of hypoparathyroidism or PTH deficiency include problems in their muscles, such as numbness, twitching and tingling, or in the bone and cartilage, heart, kidney damage, cognitive issues, emotional swings (Abate and Clarke, 2016), and seizures as a consequence of low blood calcium levels (Cooper and Gittoes, 2008). Over the past 10 years, the challenge of treatment of hypoparathyroidism is to maintain the management of the hypocalcemia and to avoid imbalances in hypercalciuria and other complications (Brandi et al., 2016).

1.3.2 Current Treatments

Hypoparathyroidism is characterised by hypocalcaemia and is commonly treated with oral calcium and active vitamin D analogues, with a view to relieving the symptoms and improve the quality of life of the patients (Sikjaer et al., 2011a, Liebman et al., 2006, Shoback, 2008). Therefore, conventional treatment focuses on maintaining both calcium and phosphate levels in the serum within the physiological range whilst trying to avoiding hypercalciuria (Shoback, 2008). Despite the safety and efficacy of conventional treatment, patients suffer from several major drawbacks through renal complications as a consequence of hypercalciuria and reduced quality of life (Brandi et al., 2016). However, it is easier for patients to comply with mineral supplement due to ease of administration as it can be taken orally as required, and is affordable.

1.3.3 PTH Replacement Therapy

The first serious discussions and analyses of alternative therapies through clinical trials for hypoparathyroidism emerged in the 1920's when a 14-year-old boy's hypoparathyroidism

was alleviated for four weeks treatment with bovine PTH (Albright and Ellsworth, 1929). Nevertheless, this treatment was abolished due to antibody formation and costs. (Melick et al., 1967). Recently, PTH 1-34 (Teriparatide) and PTH 1-84 (NATPARA) were approved by the Food and Drug Administration (FDA) for the treatment of osteoporosis and hypoparathyroidism, respectively.

1.3.3.1 Recombinant PTH 1–34

In a series of classic studies, Winer et al. (1996), evaluated synthetic N-terminal human PTH 1–34 which was FDA approved for osteoporosis, and has been utilised in clinical trials for testing maintaining normal serum calcium and urinary calcium excretion levels. They found that PTH 1-34 treatment reduced urine calcium excretion compared with calcitriol and vitamin D supplementation in adults. In an attempt to avoid the short half-life of PTH 1–34 dosing at least twice daily was required (Winer et al., 1998). They also compared PTH 1-34 once daily to twice daily and found that the twice daily injection lowered the tendency toward low serum calcium levels during the second half of the day. In another study, they found PTH 1–34 delivery by insulin pump reduced urine calcium excretion by more than 50% and with less variability in serum calcium compared with PTH 1-34 twice daily injection (Winer et al., 2012).

Other studies showed that it was possible to maintain stable serum calcium over 2 years with twice daily PTH 1–34 treatment in postsurgical hypoparathyroidism adults and children (Winer et al., 2003, Palermo et al., 2018). Moreover, PTH 1–34 treatment indicated an improvement in some mental and physical aspects of patient quality of life (Santonati et al., 2015). Despite not being approved for treatment of hypoparathyroidism, the data was promising in adults and children (Zavatta and Clarke, 2020).

1.3.3.2 Recombinant Full Length PTH (1–84) in Hypoparathyroidism

Some studies have focused on investigating the potential of the full length PTH 1–84 for the treatment of hypoparathyroidism (Cusano et al., 2013, Sikjaer et al., 2011b). Interestingly, recombinant full length PTH 1–84 exhibits a remarkably different pharmacokinetic profile in comparison to the truncated PTH 1–34. For instance, studies have shown the truncated PTH 1–34 reached its peak within 30 minutes of injection and calcium peak levels within 4–6 hours (Bollerslev et al., 2015, Sikjaer et al., 2013), whereas the full length PTH 1–84 reached its peak after 1–2 hours of injection with calcium peaking between 6 -8 hours and was possible to maintain stable serum calcium while significantly reducing the need for conventional treatment (Sikjaer et al., 2011a). The longer *in vivo* and biological half-life of full length PTH 1–84 makes once-daily dosing more feasible than PTH 1–34 (Clarke et al., 2014, Sikjaer et al., 2013). Subsequently, a full length PTH (NATPARA) was approved for use in hypoparathyroidism in 2015 by the FDA (Marcucci et al., 2016). NATPARA has a black box warning, because of concerns regarding the potential osteosarcoma effects observed in rats (Zavatta and Clarke, 2020, Marcucci et al., 2016). However, in a recent study, safety and efficacy were demonstrated under treatment with PTH over a period of 5 years. This 5-years randomised control study, REPLACE trial, of once-daily injection demonstrated that rhPTH 1-84 was able to reduce oral supplementation with calcium and vitamin D. Also, they observed estimated glomerular filtration rate (eGFR) and serum creatinine levels remained stable with improved serum phosphorus and maintaining urinary calcium excretion normalized (Mannstadt et al., 2019).

Although, the recently approved PTH 1-84 has treated some of the problems associated with current treatments and is an improvement over the prevailing treatment regimen for

hypoparathyroidism. Using PTH 1-84 presents other emerging health issues that are of clinical significance. For instance, recent studies have looked at the effects on bone mineral density (BMD) and skeletal microstructure and reported an increase in BMD at the lumbar spine and femoral neck in the hypoparathyroidism patient, with declines at the total hip and ultradistal radius (Cusano et al., 2020). Despite this, an accurate prediction cannot be made if there will be prolonged effects on fracture risk in treated patients (Cusano et al., 2014, Cusano et al., 2020). Therefore, a gap remains with regards to a longer-term therapy that mimics the physiological action of PTH in combination with having a prolonged effect. Thus, there is a need for the development of a long-acting PTH.

1.4 Development of Long Acting PTH Molecules

An unmet need exists for a long-acting treatment for hypoparathyroidism that is effective, easy to administer, has realistic manufacturing costs, and improves the health and quality of life of patients. There are several *in vivo* studies by various groups that have contributed to the development of treatments for hypoparathyroidism and osteoporosis using several PTH constructs with long-acting properties.

One alternative strategy that has been explored is by creating a fusion of PTH to another molecule. The main objective being to increase molecular weight leading to a reduced clearance rate and/or an altered pharmacodynamic profile. A prominent example is the fusion of PTH 1-34 joined at its C terminus to the Fc fragment of human IgG1 (PTH-Fc) (Kostenuik et al., 2007). A comparative analysis of the PTH-Fc fusion with PTH 1-34 in Sprague-Dawley rats revealed that both molecules have similar arrestin and PTHR1 trafficking. However, even though PTH-Fc had a 5-fold longer half-life with a 33-fold longer residence time it

demonstrated a lower maximum serum concentration (Cmax) and bioavailability (See Figure 1.9).

Other notable properties were increases in serum calcium, bone strength and bone mass density. For all doses and frequencies, the serum calcium levels were consistently above baselines for about 24 hours post-administration. Consequently, due to the transient hypercalcaemia observed, this may limit the use of PTH-Fc without an antiresorptive therapy as a monotherapy. However, there is a high therapeutic potential for the use of PTH-fusions molecules in osteoporosis or hypoparathyroidism therapy due to their delayed clearance and positive effects on serum calcium and bone mass (Kostenuik et al., 2007).

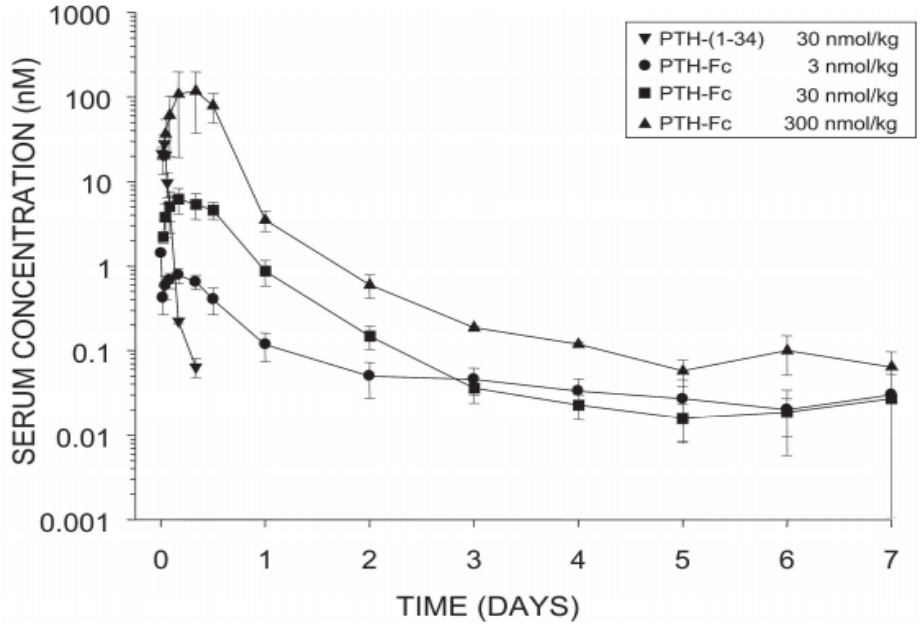

Figure 1.9: *In vivo* clearance profile of PTH-Fc against PTH 1-34.
Sprague-Dawley rats were treated with either a single dose of at 30 nmol/kg, or PTH-Fc at doses of 3, 30 and 300 nmol/kg. The PK profiles were estimated by measuring the serum levels of both molecules for 7 days. Whilst PTH-Fc remained in the circulation for all doses for the duration of the study, PTH 1-34 was rapidly cleared from circulation shortly after administration (Kostenuik et al., 2007). The image is with kind permission from PMC.

Another interesting PTH-fusion, which was designed as a treatment for osteoporosis, consists of the N-terminal of PTH 1-33 linked to the collagen binding domain (CBD) of Clostridium Histolyticum (Stratford et al., 2014). The pharmacokinetic and pharmacodynamics profiles of the PTH–CBD were compared to PTH 1-34 in Sprague-Dawley rats (See Figure 1.10). Both PTH 1-34 and PTH-CBD exhibited similar time to peaks of 20-60 minutes post-dose, with PTH-CBD demonstrating a higher Cmax and longer half-life. Similar serum calcium levels were recorded for both molecules which suggested that the PTH-CBD has the advantage of a longer duration of action without elevating serum calcium levels. Furthermore, the fusion molecule had anabolic effects on bone which was associated with the accumulation of the PTH-CBD within bone (Stratford et al., 2014). Concerns over PTH-CBD having relatively similar serum calcium concentration as PTH 1-34 as well as a rapid clearance rate of 95% within a day following administration significantly limits the use of the fusion as a potential therapy for hypoparathyroidism.

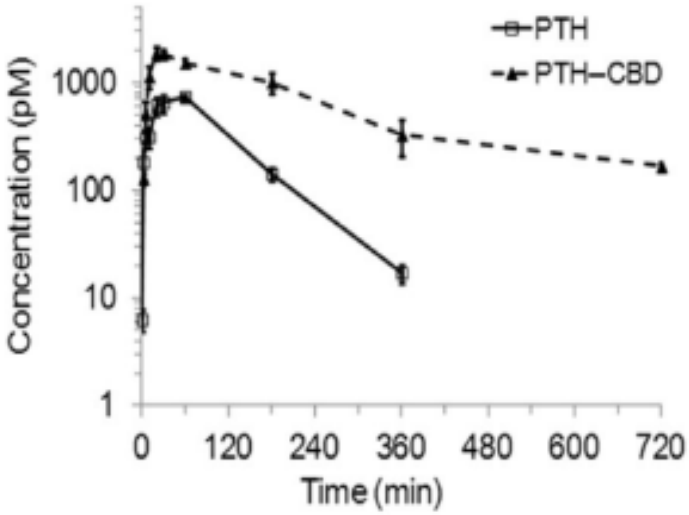

Figure 1.10: Clearance profile of PTH 1-34 and PTH-CBD in circulation.

Sprague-Dawley rats were treated with a bolus subcutaneous injection of either PTH 1-34 at 19.4 nmol/kg or PTH-CBD at 18.1 nmol/kg and the serum level of both products assessed over the 12-hour period. Whilst PTH-CBD was still detectable up to 12 hours post-dose, PTH 1-34 disappeared from circulation within 6 hours after administration (Stratford et al., 2014). The image is with kind permission from PMC.

More recently, two constructs have been developed specifically for the treatment of hypoparathyroidism. These are a Long-Acting (LA) PTH analogue and a PEGylated form of PTH 1-34.

Investigators at Massachusetts General Hospital developed a long acting PTH termed LA-PTH. This is a fusion of a modified N-terminal residues 1-14 of PTH to residues 15-36 of PTHrP (See Figure 1.11). LA-PTH binds to the high affinity PTHR1 conformation, R^0, thus inducing sustained cAMP signalling from endosomes as described in Section 1.2.1 (Maeda et al., 2013, Shimizu et al., 2016, Bi et al., 2016, Noda et al., 2020).

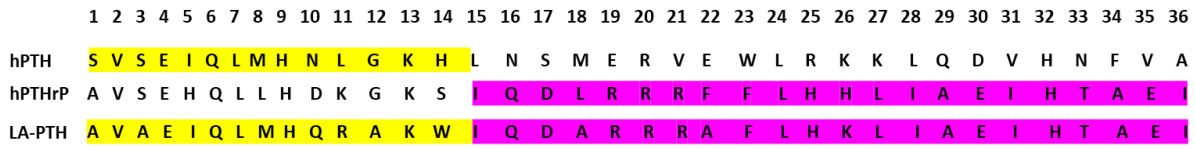

Figure 1.11: Sequence of LA-PTH aligned with PTH 1-36 and PTHrP 1-36.
The amino acid sequence of LA-PTH consists of a modified N-terminal PTH 1-14 (Yellow) linked to the C-terminal 15-36 of the PTHrP (Pink).

The pharmacokinetic and pharmacodynamic profiles of LA-PTH were studied in thyroparathyroidectomized (TPTX) rats and normal monkeys using hPTH 1-84 and PTH1-34 as comparative agents (Shimizu et al., 2016). Surprisingly, no correlation was observed between the pharmacokinetic and pharmacodynamic properties of LA-PTH. LA-PTH had a similar rapid plasma clearance rate as PTH 1-34 and PTH 1-84 (See Figure 1.12), however it exhibited a longer duration of action on plasma levels of calcium and phosphate (Shimizu et al., 2016, Bi et al., 2016). One potential drawback of LA-PTH was its negative effect on cortical bone density which was only apparent when LA-PTH was given at the highest dose of 7.2 nmol/kg. However, by using a reduced dose and staggering the repeat doses, it is improbable that LA-PTH will have a detrimental bone resorptive effect due to its longevity of action (Shimizu et

al., 2016). This treatment strategy will both minimise the dose frequency and allow the analogues to clear in between doses. Therefore, LA-PTH has a very promising therapeutic potential for hypoparathyroidism because of these prolonged signalling properties, for which the target of treatment is to achieve a sustained normalization of blood calcium (Cusano et al., 2015).

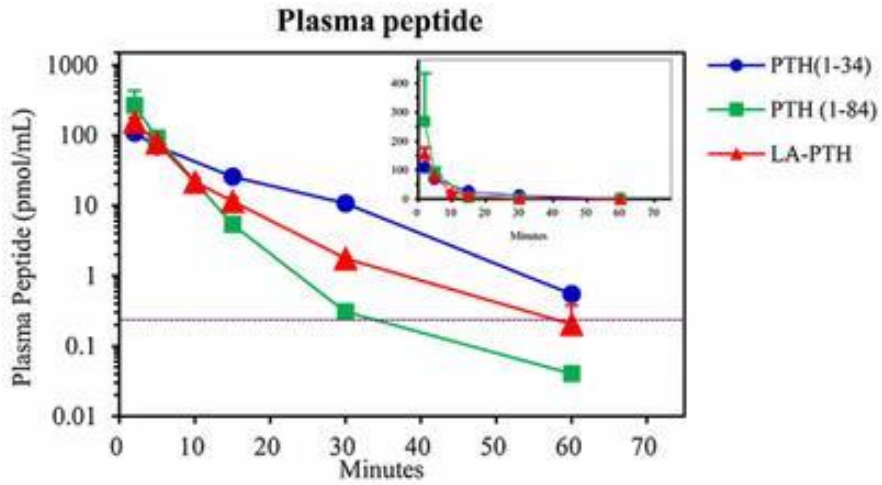

Figure 1.12: Pharmacokinetics of PTH 1-34, PTH (1-84 and LA-PTH).
Sprague-Dawley rats were administered 24.3 nmol/kg dose concentration of either PTH 1-34, PTH 1-84 or LA-PTH, via subcutaneous. Blood samples were taken over 70 minutes and all molecules were rapidly cleared from circulation within 60 minutes of injection (Shimizu et al., 2016). The image is with kind permission from PMC.

LA-PTH has been taken forward for further development in clinical trials in collaboration with Amolyt Pharmaceuticals (Lyon, France) under the name, AZP-3601. A Phase 1 clinical trial has been initiated in September 2020 and no published data are available yet (Amolytpharma.com, 2020, September 20).

Another method for extending the half-life of molecules is PEGylation. To extend the *in vivo* pharmacokinetic profile, the Polyethylene glycol (PEG) moieties is attached to PTH, via a thiol-linkage, to a C-terminal Cys35 residue with a view to decreasing its clearance rate via the glomerulus (Guo et al., 2017). Many biotherapeutic clinical profiles have been enhanced

through PEGylation. A notable example is the PEGylation of the growth hormone receptor antagonist, also known as Pegvisomant, for the treatment of acromegaly (Pradhananga et al., 2002). This approach was applied to PTH to develop PEG-PTH (Na and Lee, 2004). *In vivo* studies with PEG-PTH in mice demonstrated better control of calcium levels when compared against non-PEGylated PTH. For instance, after injections of PEG-PTH calcium levels were still elevated at 48 h and maintained baseline levels until 96 h post intravenous injection at a dose of 50 nmol/kg. A reduction in the phosphate levels was also observed. In contrast, non-PEGylated PTH was short acting and showed a minimal increase in serum calcium levels and slight reduction in phosphate levels. These data showed that PEG-PTH has an extended plasma half-life (Guo et al., 2017).

Another construct developed, known as LY627-2K is a PTH 1–34 backbone with specific amino acid substitutions and coupled to a 2 kDa PEG polymer via Lysine-26 (See Figure 1.13). Initially developed to avoid daily injections in postmenopausal osteoporosis treatment this compound may be repurposed for hypoparathyroidism therapy. LY627-2K has the potential to improve efficacy by reducing the risk of hypercalciuria-related complications, maintaining bone mass, and restoring serum calcium. During *in vivo* studies in thyroparathyroidectomized (TPTX) rats, LY627-2K was capable of increasing serum calcium over time, whilst at the same time avoiding the risk of hypercalciuria comparing favourably with PTH 1–84.

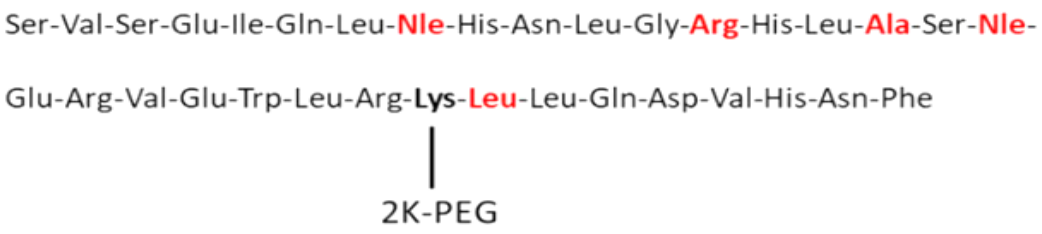

Figure 1.13: Sequence of LY627-2K.

The amino acid sequence of LY627-2K is consist of PTH (1–34) backbone with specific amino acid substitutions (red) is coupled to a 2 kDa polyethylene glycol (PEG) moiety linked to Lys26 (bold).

A recent novel approach used to improve the efficacy of PTH in circulation whilst minimising any potential side effects was tested by encasing PTH 1-34 in a TransCon carrier (Holten-Andersen et al., 2019). TransCon PTH is a PEG-PTH in which PTH 1-34 is transiently bound to an inert methoxy polyethylene glycol (mPEG) moiety through a proprietary TransCon linker. The release of the encapsulated PTH (TransCon PTH linker) is controlled by the body's physiological pH and temperature and provides a sustained release of PTH for an extended period. Using a single and repeat dosing regimen, the pharmacokinetics and pharmacodynamics of TransCon PTH were evaluated in intact rats, hypocalcemic TPTX rats, and monkeys. The results of TransCon PTH in animal models demonstrated a markedly prolonged half-life of free PTH of approximately 60 hours. A sustained serum calcium level and decrease in serum phosphate was also observed. This was significant as no increases in fractional calcium excretion was recorded for the rats treated with TransCon PTH. This suggested that TransCon PTH was well tolerated and the observed pharmacokinetics and pharmacodynamics were within physiological range of PTH which makes it suitable for use as a PTH replacement therapy (Holten-Andersen et al., 2019).

In a Phase 1 clinical trial with 170 healthy volunteers, TranCon showed potent calcemic, renal calcium reabsorption, and potent phosphaturic effects with no evidence of any anabolic effect. This result could be an important advancement in replacement therapy for hypoparathyroidism, providing physiological levels of PTH for 24 hours per day. Moreover, phase I trial result with TransCon PTH demonstrated a prolonged half-life of approximately 60 hours of free PTH (Karpf et al., 2020). These promising results supported further development of TransCon PTH into Phase 2 clinical trials which are currently under evaluation with preliminary results recently presented in an abstract form (Khan et al., 2020).

With most of the treatment options in various phases of clinical programs, the global hypoparathyroidism treatment market landscape is still in its infancy. Although the growth rate is expected to showcase similar trends, there is significant competition for the development of PTH analogues with prolonged actions that can be more effective as a treatment for hypoparathyroidism. In the European Union in the first half of 2018, sales of Natpara reached $109.8 Million. As per a recent analysis by Future Market Insights (FMI), by 2026 in terms of revenue, the valuation of global hypoparathyroidism treatment market holds the potential to exceed the $1.1 Billion (PharmiWeb.Com, 2021, Feb 23). The hypoparathyroidism competitive treatment landscape markets are summarised in Table 1.1 below.

Table 1.1: Hypoparathyroidism competitive landscape.

Company	**Product**	**Status**
Takeda	Natpara/ Natpara/Q-Cliq™ /1-84 PTH • US approval Jan-15 • EU approval Apr-17	• Black-box Warning • US recall Sep_19 • 2018 sales $230M
Ascendis Pharma	TransCon PTH/LA-prodrug of PTH + pen injector • Phase-II reported Apr-20	• Phase-III in Planning • FDA ODD in 2018
Chugi/Roche	PCO371/oral NCE of PTH1 receptor agonist • In Phase-I	• No recent updates
Entra Bio Inc.	Oral 1-34 PTH • Phase-IIa reported Jun-15	• No recent updates
Amolyt Pharma [fka Alize Pharma 3]	AZP-3601/PTH analogue • Built-to-sell	• Preclinical • Mass. Gen. Hospital
Eli Lilly & Co	LY627-2K/LA 1-34 PTH	• Preclinical since Jan-18 • Failed in osteoporosis

1.5 In House Development Long-Acting Parathyroid Hormone Preparations

One of the key features of the treatment of hypoparathyroidism is to a have a smooth profile after injection. Recently, replacement of PTH in hypoparathyroidism with Natpara (PTH 1-84) has been licensed but requires daily injections and is complicated by fluctuating calcium levels. Continuous pump therapy is effective but impractical for most patients. The biggest problem is the spike in PTH concentration which drives bone formation, which is ideal for osteoporosis but not for hypoparathyroidism (Zavatta and Clarke, 2020). Through subcutaneous injection, this hopefully will contribute to a slow release into the circulation therefore avoiding those spikes. Moreover, longer acting PTH biologicals with an increased control over serum calcium levels and reduced side effects are urgently needed to minimise the need for daily subcutaneous injections. There is therefore an unmet need for a long acting PTH molecule that provides constant physiological levels of PTH activity.

A viable long-acting PTH will exhibit the efficacy that is similar to that observed in PTH replacement therapy, but with an extended circulating half-life. This will both reduce the frequency of dose administration to patients of hypoparathyroidism and save cost expenditure. In this current study, we proposed to test a long-acting PTH which is a fusion of PTH 1-34 to a molecule with a longer circulating half-life. The idea was generated by the success of previous studies from our group: An independent in vivo study was completed, which tested both the pharmacokinetic (PK) and pharmacodynamic (PD) properties of long-acting growth hormone (GH) through a fusion of human GH to the growth hormone binding protein (GHBP, amino acids 1-238). GHBP is the ECD of the growth hormone receptor. The resulting ligand-receptor fusion exhibited a significantly reduced clearance rate of up to ~300 times compared to the native GH in rats (Wilkinson et al., 2007, Cawley et al., 2013) and 1.6–

2.8-fold reduced clearance in monkeys compared with rats. The terminal half-life was approximately 100 times that of GH when both are given intravenously (Ferrandis et al., 2010). With the success of the GH fusion, new long acting PTH fusions were developed utilising GHBP as the fusion partner in an attempt to reduce the clearance of PTH by increasing the molecular weight. To prevent GH binding in circulation, a single amino acid change of tryptophan-104 to alanine in the GHBP moiety (W104A) was introduced. All PTH fusion were expressed as secreted products using the naturally occurring PTH prepropeptide sequence.

This project concerns the testing of three long acting PTH molecules. The PTH fusions were predicted to have a prolonged circulating half-life through increased protein size, whilst retaining biological activity. Figure 1.14 shows the schematic designs of these PTH fusion molecules used in the study: 14A7 consist of PTH (residues 1-34) linked to GHBP (residues 1-238) containing the mutation W104A. GHBP is an inert moiety designed to increase molecular weight and delay clearance. 14A7 has a non-glycosylated molecular weight of 32 kDa.

Further PTH fusions were constructed after analysing the crystal structure of PTH with the N-domain PTH receptor in which PTH is shown to sit in a groove formed by the N-terminal receptor portion ((Pioszak et al., 2009), See Section 1.2.1.1). Consequently, PTH fusions were constructed that contained not only GHBP but also the extracellular PTH receptor domain (residues 29-187). In these fusions, it is expected that the binding of PTH to the PTH receptor domain (PTHrExt) will protect PTH from degradation and produce a pool of "inactive" PTH that is in equilibrium with active PTH, generating a more physiological PTH exposure. In the fusion 14A2c, PTH (1-34) is linked via flexible linkers to the N-terminal PTHrExt (residues 29-187) and GHBP (residues 1-238) (See Figure 1.14). The fusion 14A8 is the control molecule for 14A2c and consists of the same domain structure but also contains an Isoleucine-135 to lysine

(I135K) change in PTHrExt. The mutation is proposed to knock-out intramolecular PTH binding (Pioszak et al., 2010). Both fusion molecules have a non-glycosylated molecular weight of 52 kDa. Molecules are expressed under the control of the PTH secretion signal in a Chinese hamster ovary cell line (CHO). Full amino acid and nucleotide sequences can be found in Appendix A.

Glycosylation has a vital role in maintaining or forming glycoprotein integrity. Moreover, key features of glycosylation are an increase in molecular weight, protection against proteolytic degradation, decreases in immunogenicity and involvement in protein activity (Li and d'Anjou, 2009). The GHBP domain contains five potential N-linked glycosylation sites (Harding et al., 1994) and the PTH extracellular domain in 14A2c and 14A8 has four potential N-linked glycosylation sites (Bisello et al., 1996). An increase in molecular weight together with variable glycosylation outcomes across different domains is thus postulated.

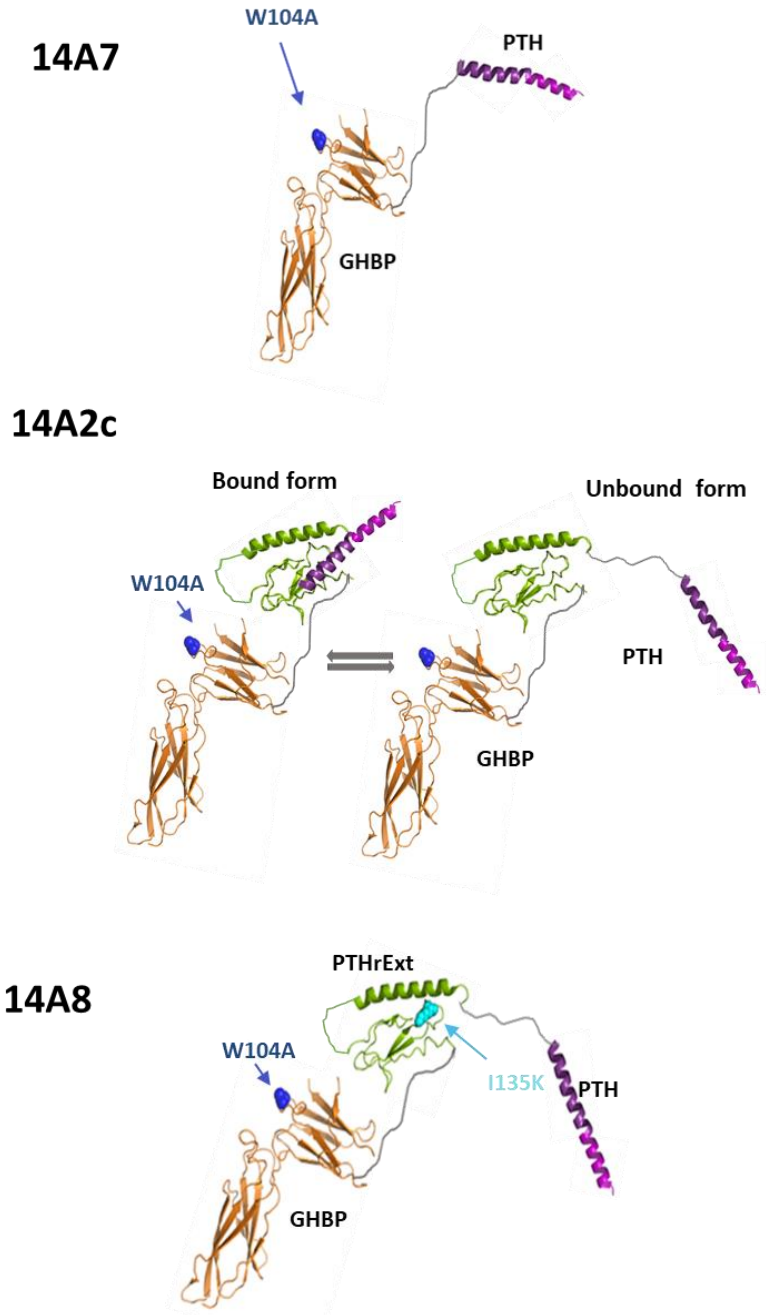

Figure 1.14: Schematics illustrate the difference in design of the PTH fusion molecules.

A number of PTH fusion molecules were constructed with a view to enhancing the potency of PTH and longevity of action; **14A7** consists of PTH linked directly to GHBP (14A7). All molecules contained the PTH signal/propeptide sequence and a W104A mutation **(Blue)** in GHBP to prevent interaction with growth hormone in circulation. **14A2c** consists of PTH **(Purple)** (residues 1-34) linked to PTH extracellular receptor **(Green)** (residues 29-187) and to GHBP **(Yellow)** (residues 1-238) using glycine-serine linkers (**Grey**) (Gly_4Ser). **(Bound form)** PTH binds to PTHrExt and this protects PTH from degradation. **(Unbound form)** PTH is free to bind receptor. There is hypothesised to be an equilibrium between A and B in the circulation. **14A8**, a control molecule for 14A2c, contains an I135K mutation **(Cyan)** in PTH extracellular receptor (residues 29-187) which abrogates PTH binding. Constructed by Pymol.

1.6 Hypothesis and Aims

It is hypothesised that PTH fusion molecules with GHBP will retain biological activity and their increased molecular weight will delay clearance and thereby extend the circulating plasma half-life. The use of flexible linkers in the fusion will facilitate intramolecular interactions of PTH with its cognate receptor. The introduction of the PTHrExt domain into the fusion is predicted to protect the ligand-moiety from proteolysis and will reduce *in vitro* bioactivity but prolong *in vivo* activity. To test this hypothesis a control has been generated with the introduction of a mutation in the PTHrExt with the expectation it will increase *in vitro* biological activity by reducing intra- and inter-molecular binding.

The aims of this research were:

1. To produce stable expression clones in a mammalian (CHO) cell line;

2. To express recombinant PTH fusion in mammalian cells;

3. To purify and test the biological activity of these PTH fusions in a suitable *in vitro* cell-based bioassay.

Chapter Two - Materials, Equipment & Methods

2.1 Materials

Acetic Acid	Thermo Fisher Scientific, UK (CAS: 64-19-7)
Acrylamide (30%)	Geneflow Ltd
Agarose	Sigma Aldrich, USA (Cas: 9012-36-6)
Ammonium Persulphate	Sigma Aldrich (Cat#7727-54-0)
Antihuman GHBP (10B8) antibody	Zida (GR1088)
Antihuman PTH muose antibody Ab144	GE healthcare, UK (Lot #GR293489-1)
Benzamidine Hydrochloride hydrate	Sigma Aldrich, USA (Lot# SLBJ2586V)
Bovine Serum Albumin	Sigma Aldrich, USA (Lot#SLBJ2586V)
Bradford	BioRad, Germany (Lot#5000006)
Bromophenol Blue	Sigma-Aldrich
cAMP Parameter Assay Kit	R&D systems Biotechne brand(Cat#KGE002B)
Chinese Hamster Ovary Cells	Thermo Fisher
Clarity Western Blot ECL substrate	BioRad, USA (Lot#1705060 S)
CNBr (cyanogen bromide)	Sigma (C9142)
Coomassie Blue R-250	BioRad, USA (Cat#20278)
Coomassie Blue Reagent	Sigma-Aldrich
Coomassie Colloidal Staining	EMBL Heidelberg
Cryogenic vials	Nalgen Nunc intl.
Deionised water	
Dithiothreitol (DTT)	Sigma-Aldrich
DNA Ladder 1Kb	Promega USA
Dual Luciferase Assay Kit	Promega, UK (Lot#E1910)
Dulbecco's Modified Eagle Medium F12	Life Technologies, UK (Cat#11320033)
EDTA	Thermo Fisher Scientific, UK (Cat#17892)
Ethanol	Fisher Scientific, UK (Cas: 64-17-5)
Expand Polymerase	Roche, UK
Flp-In CHO cell line	Invitrogen, USA (Cat #R75807)
Foetal Calf Serum (FCS)	Labtech
Forskolin	Sigma Aldrich, USA (Lot#F6886-10MG)
Fugene-6 transfection reagent	Roche Diagnostics
Gel loading dye (x6) Blue	New England BioLabs (Cat#B77021S)

GenElute™Gel Extraction Kit	Sigma Aldrich, UK
Glycerol	Fisher Scientific, UK (Cas : 56-81-5)
Glycine	Fisher Scientific, USA (Cas : 56-40-6)
Human PTH (1-34) Purified protein	Sigma Aldrich, USA (Lot#P3796-1MG)
Human PTH 1-34	AnaSpec AS-20708
Hyclone SFM4CHO Utility Media	Fisher Scientific, UK (Cat#SH3051602)
Hyclone media	Sigma-Aldrich
Hydrochloric Acid	Thermo Fisher Scientific, UK
Hygromycin B	Invitrogen, USA (Lot#HY068-L4)
IBMX	Sigma Aldrich, UK (Lot#I5879-100MG)
Isopropanol	Fisher Scientific, USA
Laemmli loading buffer	BioRad (x2)
Luciferase Assay System	Promega, UK (Cat#E1500)
Marvel Milk Protein Powder	Aldrich
Methanol	Fisher scientific, UK
$MgCl_2$	Sigma Aldrich
Midori Green Nucleic Acid Stain	Bulldog-Bio, USA
Mirus TransIT LT1	Geneflow (Cat#E7-0002)
NNN'N-tetremethylenediamine(TEMED)	Electran, Belgium
Phosphate Buffered Saline	Dubecco A, Oxoid, UK
Penicillin/Streptomycin	Sigma Aldrich, USA
pGLA 4.29[luc2P/CRE/Hygro]	Promega, UK (Lot#E8471)
Phosphate Buffer Saline	Oxoid, UK
Polyvinylidene fluoride membrane	GE Healthcare, UK
Precision Plus Protein All Blue Standards	BioRad, Germany (Lot#1610373)
ProSieve Quad Colour Protein Markers	Lonza, Switzerland
Protein Assay Dye Reagent Concentrate	Biorad, Germany (Lot #500-0006)
Protogel 30% solution	National diagnostics, USA
Renilla control plasmid (phRL-CMV)	Promega, UK (Lot#E2231)
Renilla control plasmid (phRL-TK)	Promega, UK
Resolving buffer (4x)	National diagnostics
Retroscript Kit	Ambion (AM1710)
RNeasy Mini Kit	QIAGEN (Cat#74104)
Running Buffer (x10)	National Diagnostics, USA

Sheep Anti-mouse IgG Horseradish Peroxidase	GE healthcare, UK Limited (Lot#9609128)
Snakeskin pleated dialysis tubing	Fisher Scientific, UK
Sodium Chloride	Sigma Aldrich, USA
Sodium Citrate	Sigma Aldrich, USA (Cas: 6132-04-3)
Sodium dodecyl sulfate (SDS)	Sigma-Aldrich, USA
Sodium Hydroxide	Sigma Aldrich, USA
Sodium Phosphate	Sigma Aldrich, USA
Stacking buffer (4x)	National diagnostics
Transferrin	Sigma-Aldrich
Tris-Glycine-SDS buffer (10x)	National diagnostics
Tris-Sodium Citrate	Sigma Aldrich, USA
Trizma Base >99.9% Titration	Sigma life Science
Trypan blue	Sigma-Aldrich, USA
Trypsin-EDTA	Gibco (Invitrogen Corp)
Tween20	Sigma Aldrich, USA
UMR-106 cells	ATCC, UK (Lot#CRL-1661)
X-ray developer and fixer	KODAK, USA
X-ray film Fujifilm	KODAK, USA
Zeocin antibiotic	Invitrogen

2.2 Equipment

Equipment	Product Name	Manufacturer
Balance	Mettler®PC440 Dleta Range	Mettler Toledo, USA
Centrifugal filter units	Centriprep	Merck Millipore Ltd, Ireland
Centrifuge	Avanti J-26XP	Beckman Coulter, USA
Centrifuge Rotors	JA 25.50 & JLA 16.250	Beckman
Centrifuge Tubes	50 & 250 mL	Beckman
Centrifuge (Benchtop)	Eppendorf Mini Spinner	Sigma Aldrich, USA
Chromatography Columns	XK 16/30	GE Healthcare Life Sciences
Crossflow Cassette	Viva Flow 200	Sartorius
Cell Culture flasks	T25 and T75 filtered	Nalgen Nunc intl
Cell Culture Shake Flasks	Baffled Shake Flask (2L)	Greiner Bio-one
Cell Culture plates	6/12/24/48 well plates	Costar
Cell Culture Incubator	Sanyo CO_2 Incubator	Sanyo North America Corp.
Cryogenic vials	Cryogenic vials	Nalgen Nunc intl
Gel viewer and imager	G: Box Viewer	Syngene, UK
Haemocytometer	Neubauer	Hawksley, USA
Heating block	Techne Dri Block	Sigma Aldrich, USA
Hypercassettte	Amersham 18 x 24	GE Healthcare
Large Balance	Metter PC440 Delta Range	Instrumente Zurich
Luminometer	AutoLumat LB 953	Berthold Technologies
Luminometer tubes	LP3	Sarstedt
Microscope	Olympus CK2 microscope	Olympus Optical C0. Ltd.
Microwave	Microwave	Sanyo
Multi-channel pipette	Alpha + Manual	Alpha Laboratories, UK
Nano Spectrophotometer	Nanodrop ND-1000	Thermo Scientific, UK
pH meter	3510 pH meter	Jenway, UK
Pippettes	StarPet	Star Lab, UK
Power Pack	250V PowerPac™	BioRad, Germany
Peristaltic Pump	Cole-Parmer Masterflex Precision Pump Tubing BioPharm Plus L/S	Fisher Scientific
Peristaltic pump	P1	GEHealthcare
Roller bottle	Roller bottle (2L)	Greiner Bio-one

Roller Bottle Mixer	Stuart SRT9	Stuart Scientific, UK
SDS-PAGE/Western blotting	Mini-Protean Gel Apparatus	BioRad, Germany
Cell Culture Shaker	ELMI Shaker S-3.01	Greiner Bio-one
Spectrophotometer	Jenway 7305	Progen Scientific LTD
		Geneflow Serial No: 36422
Tally counter	Tally counter	ENM
Tips (Pipettes)	TipOne®	StarLab, UK
Vortex	SA8 Vortex Mixer	Stuart Scientific, UK
Water bath	NB9 Water Bath	Nuve, Turkey
Blue Light Transilluminator	Safe Imager™ 2.0 Blue Light Transilluminator	ThermoFisher Scientific

2.3 General Methods

2.3.1 Protein analysis

2.3.1.1 Sodium Dodecyl Sulphate-Polyacrylamide Gel Electrophoresis (SDS-PAGE)

SDS-PAGE separates proteins based on their molecular size and was used for testing protein expression, purity and integrity. Variable charges on proteins are eliminated by heat and SDS which linearizes and coats the proteins with a uniform negative charge, thus standardising their charge: mass ratio. Acrylamide polymers with varying pore sizes form the molecular sieve used for proteins separation, and comprise of a stacking gel and a resolving gel. When an electric current is passed through the gel, the negatively charged proteins migrate toward the anode and the proteins are resolved based on their molecular weights - with lower molecular weight proteins moving faster through the gel.

2.3.1.1.1 Gel Preparation

BioRad Protean II gel equipment was set up and assembled in accordance with the manufacturer's instructions, thus ensuring that both the resolving gel and the stacking gel met the composition and quantity requirements outlined in Tables 2.1 and 2.2. The equation below was used as a benchmark for the calculation of the volumes in relation to the acrylamide percentage.

$$Vp = \frac{(XVt)}{30}$$

$\mathbf{V_p}$ = the volume of 30% Protogel.

$\mathbf{V_t}$ = total volume of the gel. X = monomer

Table 2.1: Components of 12% SDS-PAGE resolving gel (sufficient for 2 gels)

Component	**Volume**
Protogel 30% (w/v) Acrylamide: 0.8% Bis-Acrylamide Stock Solution (37.5:11)	4 mL
4x resolving buffer (1.5M Tris-HCl,), 0.4% SDS, pH 8.8)	2.5 mL
Deionised water	3.3 mL
10% (w/v) Ammonium persulphate (APS)	100 µL
TEMED	10 µL

Table 2.2: Components of SDS-PAGE 4% stacking (sufficient for 2 gels)

Component	**Volume**
Protogel 30% (w/v) Acrylamide: 0.8% Bis-Acrylamide Stock Solution (37.5:11)	0.65 mL
ProtoGel stacking buffer (0.5M Tris-HCl, 0.4% SDS, pH 6.8)	1.25 mL
Deionised water	3.05 mL
10% (w/v) Ammonium persulphate	25 µL
TEMED	5 µL

2.3.1.1.2 Preparation of Protein Samples for SDS-PAGE

Either cell culture media or purified protein samples were used for analysis. All protein samples were diluted in 2× laemmli buffer and heated for 15 minutes at 65°C. Protein standards were used to monitor protein separation and for molecular weight estimation.

Protein samples were separated at 100 V for ~90 minutes in 1× running buffer, which was diluted from a 10× stock as shown in Table 2.3. Separated proteins were visualised either by

coomassie Blue staining or transferred to polyvinylidene fluoride (PVDF) membrane for western blotting.

Table 2.3: Running buffer

Composition Elements	Volume
10x (0.25 M Tris HCl, 1.92 M Glycine and 1% SDS (w/v), pH 8.3) diluted in 1 Litre of H_2O	50 mL
Deionised water	450 mL

2.3.1.1.2.1 Visualisation of Proteins Using Coomassie Colloidal Blue

Instead of the standard Coomassie Brilliant Blue staining, Coomassie Colloidal blue staining was adopted in this work, and methanol was replaced by the less toxic ethanol. The Coomassie Colloidal blue staining protocol allows for fast and sensitive analysis, whereby proteins are visualised after separation by SDS-PAGE. In the Coomassie stain, ionic interactions occur between positive protein amine and sulfonic acid groups of the dye and positive amine groups of the separated proteins, staining them blue. The separated proteins were visualised by Coomassie staining (0.4% Coomassie Brilliant blue R-250 (w/v), 10% acetic acid (v/v), 8% ammonium sulphate (w/v), 20% ethanol (v/v), and make up with Deionised water). Any background stain is then removed using a simple water wash.

Gels were stained for ~30-60 minutes at room temperature, followed by rounds of rinsing with water, and shaking on an orbital shaker at room temperature until the desired background on the gel was achieved. Excess stain was absorbed by a paper towel. This process was repeated until all background staining had been eliminated. To visualise protein bands, the gels were photographed using a Syngene's G: Box Gel viewer.

2.3.1.1.2.2 Detection of Proteins by Western Blotting (WB)

Western blotting is used to identify proteins based on using protein specific antibodies primary and secondary antibodies. The primary antibody binds to the protein of interest, and the secondary antibody that is conjugated to horseradish peroxidase (HRP) binds to the primary antibody. A substrate reaction occurs due to the involvement of HRP and the addition of luminol into the mix, which produces light as a by-product that can be captured by X-ray film (See Figure 2.1).

In this work, a BioRad Trans-Blot Electrophoretic Transfer Cell was assembled as per manufacturer's instructions via the wet transfer technique and was used to transfer SDS-PAGE-separated proteins onto the PVDF membrane. Prior to gel transfer assembly the PVDF membrane was activated with methanol for 30 seconds, then both membrane and gel were equilibrated for at least 15 minutes in the transfer buffer (See Table 2.4 and Figure 2.2). The protein transfer was routinely carried out at 100 V for one hour, after which the PVDF membrane was blocked using a blocking solution comprising of 5% milk protein prepared in phosphate buffered saline + 0.5% Tween 20 (PBS-T) and left overnight at 4°C.

Table 2.4: Components of the transfer buffer

Components	**Amount**
Tris base	5.8 g
Glycine	2.0 g
Deionised water	1000 mL

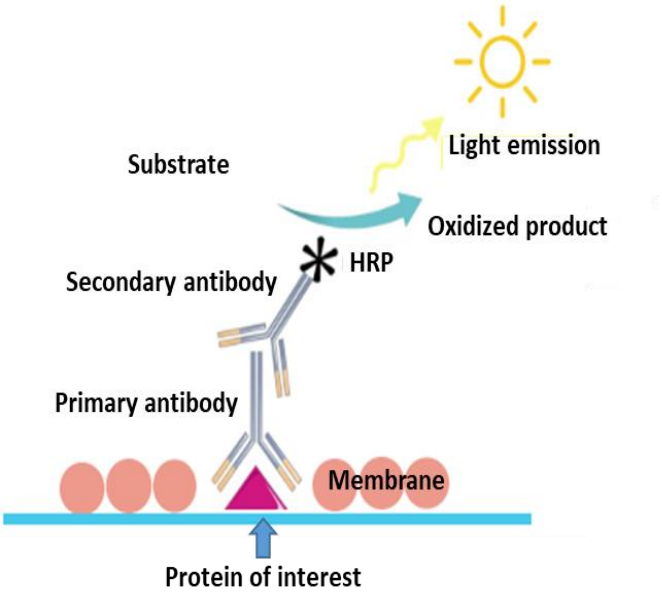

Figure 2.2: Schematic illustration of the chemiluminescent western blotting. Constructed using Venngage website (HRP: Horseradish peroxidase).

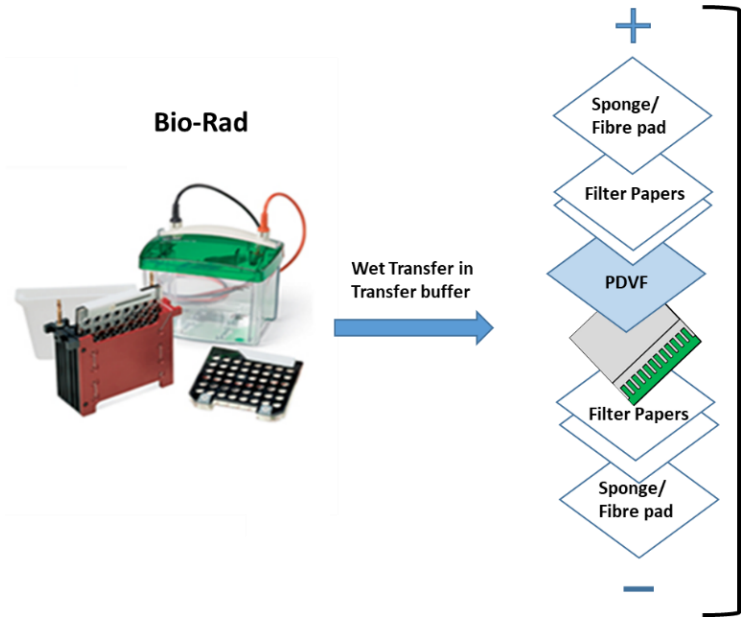

Figure 2.1: Western blot wet-transfer, gel and PVDF membrane assembly. Constructed using PowerPoint.

The membrane was subsequently probed with either a mouse anti-human PTH (Clone A1/70 used at 0.2 µg/mL) or mouse anti-human GHBP (Used at 1 µg/mL, clone 10B8, gift from Zida

Wu, Charite Mitte, Berlin) primary antibodies that were prepared in 1% milk protein/PBS-Tween (0.2 g of Marvel milk protein in 20 mL PBS-Tween) and incubated with the membrane for 2 hours with mixing. PBS-Tween was subsequently used to wash the PVDF membrane. The secondary antibody (goat anti-mouse IgG-HRP, GEHealthcare) was prepared at a 1:10,000 dilution in 1% milk protein/PBS-Tween blocking solution and incubated for 30 minutes with mixing. The membrane was washed four times - 15 minutes per wash - with PBS-Tween to remove non-specific binding. Next, the membrane was incubated in BioRad Clarity Western Blot ECL substrate with gentle shaking for 5 minutes before being placed in a Hypercassette with X-ray film in a darkroom for various exposure times. The X-ray films were placed in a developer solution (Kodak) until the appropriate development was observed after which they were washed in water followed by at least 1 minute incubation in a fixer solution (Kodak). Syngene's G: Box Gel viewer was utilised to photograph the developed X-ray films.

2.3.1.1.2.3 Agarose Gel Electrophoresis

Agarose gel electrophoresis is an effective way of separating a mixture of DNA fragments of varying sizes into discrete bands. In the current study, it was used for the estimation of DNA concentration and purity, as well as for enabling the separation and purification of both PCR products, and to assess the quality of RNA and cDNA (Section 2.3.4.2). The agarose percentage used was chosen based on the DNA size. The gel was prepared in a conical flask by adding a set amount of agarose to 50 mL 1 x TAE buffer (0.04 M Tris-acetate, 1 mM EDTA, pH 8.3) to inhibit metal-dependent endonucleases, followed by boiling for 60 seconds in the microwave. All equipment was set up and assembled in accordance with the manufacturer's instructions. Subsequently, 4 µL of midori green advance DNA stain was added to the cooled gel before being poured slowly into a casting chamber containing a thin comb and allowed to

solidify. Midori green is considered a safer stain than ethidium bromide and it emits green fluorescence when bound to DNA or RNA, producing two secondary excitation peaks at ~ λ = 270 and 290 nm, and one strong excitation peak at ~490 nm.

Once the gel was set, the well comb was removed, and samples were loaded into each well before being placed in electrophoresis buffer at 100 V (See Table 2.5). The DNA samples (including 1 kb DNA Ladder, New England Biolabs, NEB) were diluted with 6× DNA loading dye before loading them onto the gel.

In the event of DNA extraction and purification from the gel, 10% of each sample was loaded into an inner well for visualisation with ultraviolet (UV) light. The remaining 90% of the sample was loaded into another lane, which would be separated from the gel before exposure to UV. For the estimation of DNA product size after migration, DNA markers of 1 kb ladders were used. Finally, the DNA was visualised using Syngene's Genesnap Gel Viewer software.

Table 2.5: Electrophoresis buffer

Components	**Amount**
50X TAE electrophoresis running buffer	10 mL
Deionised water	500 mL

2.3.2 Protein Assays

2.3.2.1 Bradford Protein Assay

For the determination of total protein concentrations in samples, and to monitor the purification processes, the Bradford protein assay was used. For this purpose, protein samples were mixed with Bradford reagent, which consists of an acidic solution of Brilliant blue G-250 dye. Binding of the dye to the protein under these conditions yields a reddish-brownish to a

blue colour due to the change in absorbance from 465 nm to 595 nm as the protein-dye complex is formed. The colour intensity is proportional to the change in protein concentration. A spectrophotometer was used to measure the absorbance at 595 nm, and protein concentration was calculated using a BSA standard curve through linear regression.

2.3.2.1.1 Preparation of a BSA Standard Curve

The standard BSA curve (See Figure 2.3) was obtained by preparing 10 mg/mL of BSA solution in double distilled water (dd H_2O) and diluting this to 1 mg/mL and further to 100 µg/mL. The standards shown in Table 2.6 were prepared from the 100 µg/mL stock by serial dilution.

Table 2.6: Preparation of the BSA standard curve

Standard Stock BSA (µg/mL)	Final concentration in assay (µg/mL)	Dilution factor	Amount
25	20	x4	2 mL 100 µg/mL + 6 mL ddH_2O
12.5	10	x2	2.5 mL 25 µg/mL + 2.5 mL ddH_2O
6.25	5	x2	2.5 mL 12.5 µg/mL + 2.5 mL ddH_2O
2.5	2	x2.5	2 mL 6.25 µg/mL + 3 mL ddH_2O
1.25	1	x2	2 mL 2.5 µg/mL + 2 mL ddH_2O

A standard curve was prepared by pipetting 200 µL of BioRad Bradford reagent into a 1.5 mL Eppendorf tube which was mixed with 800 µL of each BSA standard (or distilled water for blanks). The solution was left for 5 minutes at room temperature before measuring absorbance at 595 nm. The absorbance readings as a function of concentration were plotted on a GraphPad Prism, as shown in Figure 2.3.

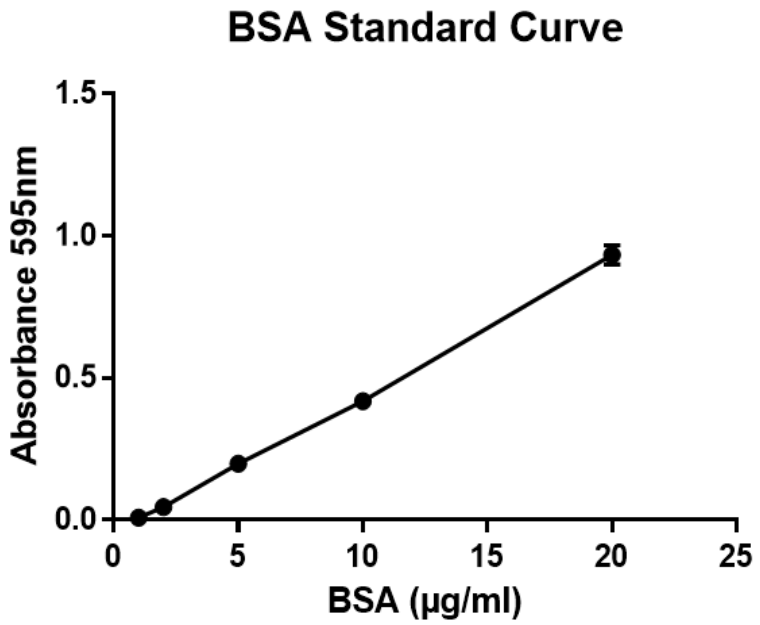

Y= 0.0478 X – 0.0385

R^2= 0.9978

Figure 2.3: Representative BSA standard curve used in the analysis.

2.3.2.1.2 Sample Analysis

The standard curve allows for an unknown sample concentration to be calculated. In this study, a solution containing 0.8 mL of a sample of unknown protein concentration and 0.2 mL of Bradford reagent was prepared in duplicate, as shown in previous Table 2.6. Protein concentration in the sample was determined based on the absorbance at 595 nm relative to the BSA standard curve using the GraphPad Prism.

2.3.2.2 Quantification of Protein by A_{280}

A Nanodrop spectrophotometer (ND-1000) was used to quantify the final purified product at an absorbance of A_{280} nm to determine the protein concentration. The calculations rely on the absorbance of ultraviolet light by aromatic amino acids - tryptophan, tyrosine and

cysteine - within the sample using the Nanodrop spectrophotometer. The purified protein concentration is thus obtained based on the A_{280} absorbance value. The extinction coefficient was obtained from the online tool ExPASy (http://ca.expasy.org/tools/protparam.html). The calculated extinction coefficient of a 1 mg/mL solution of our 14A7 fusion is 1.985 and that of 14A2c and 14A8 is 1.944 respectively. The equation given below was used to determine the purified protein concentration.

$$\mathbf{A = (C * E) * D}$$

$$\mathbf{Therefore: C\ (mg/mL) = A/E}$$

A: A_{280} absorbance value.

C: Analyte concentration (A/E).

E: Extinction coefficient.

D: Path length cm (This is zero when using the nanodrop).

2.3.2.3 Quantification of DNA/RNA by A_{260}

A Nano-drop spectrophotometer (ND-1000) was used to determine both DNA and RNA concentration from the absorbance at A_{260} nm. For this purpose, 1 µL of the sample was pipetted on the lower optical surface of the NanoDrop™, whereby the concentration of double stranded DNA (ng/µl) was calculated using: the optical density at 260 nm (OD_{260}) equals OD_{260} x dilution factor x 50 ng/µl (given that 1 OD of double stranded DNA at 260 nm is equivalent to 50 ng/µl). Whilst an OD of 1 at 260 nm is equivalent to 33 ng/µl RNA.

The absorbance ratio of OD_{260}/OD_{280} is used to determine the sample purity, whereby pure DNA and RNA samples have a ratio of ~1.8 to 2.0, respectively, whilst samples contaminated with protein or phenol have a ratio below 1.8.

2.3.3 Mammalian Cell Culture

2.3.3.1 General Culturing of Adherent CHO Flp-In Cells

Chinese Hamster Ovary (CHO) Flp-In cells are used routinely for stable cell line generation or transient transfection. Mammalian expression system, in general, is commonly adopted in research, as it allows the function of a particular protein to be studied in the most physiologically appropriate environment, given that it enables the best posttranslational protein processing and functional activity evaluations.

Adherent cells were routinely grown in complete media with zeocin antibiotic (100 μg/ml) and grown at 37°C, 5% CO_2. Passaging was conducted every 2−3 days or when cells were 80−90% confluent by washing with 5 mL of phosphate-buffered saline (PBS, pH 7.4) and treating cells with 2.5 mL of trypsin/ethylenediaminetetraacetic acid (TE), followed by incubation for 2−3 minutes. The trypsin enzyme acts to dissociate adherent cells from a vessel via proteolysis of proteins they use for adherence. After adding 10 mL of growing media to neutralise the enzymatic activity of trypsin, cells were transferred to a sterile 30 mL universal. Cells were centrifuged for 5 minutes at 1,000 rpm to remove the supernatant after which the cell pellet was resuspended in 10 mL of culture medium. The cells were subsequently counted before diluting in a 1:10 to 1:20 ratio using fresh T75 or T25 flasks. Additionally, cells used in the experiment were treated with TE, before being counted and diluted to specific concentrations prior to plating. Only cells that had been subjected to at least two passages post-thawing were used in experiments.

2.3.3.2 Stable Transfection

Flp-In Invitrogen cell line was used to generate stable clones of pSecTag plasmids containing genes of interest (See Appendix C1). The pSecTag plasmids contain not only the gene of interest but also a Flp recombinase recognition sequence, allowing for directional cloning into the CHO Flp-In cell line at a specific locus using the Flp-In recombinase enzyme. This enables rapid sites -specific generation of stable clones for high expression, as the Flp-In host cell lines (CHO Flp-In) have a single Flp recombinase target (FRT) site located at a transcriptionally active genomic locus. Stable cell lines are generated by co-transfection of the pSecTag plasmid (which also contains an FRT site) with the pOG44 (which constitutively transiently expresses Flp recombinase under the influence of the CMV promoter) into the Flp-In cell line. The Flp recombinase expressed from the pOG44 induces recombination between the FRT sites that are integrated into the CHO genome and are present on the pSecTag vector plasmid, thereby inserting the pSecTag construct into the genome at the integrated FRT site. This in turn brings the SV40 promoter into frame with the hygromycin resistance gene and inactivates lacZ-zeocin fusion gene, whereby stable cell lines are selected for hygromycin resistance.

In this study, CHO Flp-In cells were cultured in complete medium (DMEM/F12 containing 100 µg/mL streptomycin, 10% FCS, 2 mM L-glutamine, 100 U/mL penicillin, and 100 µg/mL zeocin) and were subjected to two passages before carrying out the transfection experiment. Cells were plated at 0.125×10^6 cells/mL in 2 mL complete media on a 6-well plate and were left overnight at 37°C/5% CO_2 to grow until approximately 60−70% confluency had been achieved. The next day, culture medium was replaced with complete media (without antibiotics).

For each transfection, a transfection mix was prepared by adding 92.5 µL of serum-free media to a 1.5 mL Eppendorf tube and 7.5 µL of the TransIT-LT1 (Mirus) reagent prior to mixing. In a

separate Eppendorf tube, 5 µg of pOG44 and 0.25 µg of plasmid of interest was pre-mixed and then added to the TransIT-LT1 solution followed by mixing and incubation for 15 minutes at room temperature. The transfection mixture was pipetted into individual wells as appropriate.

The cells were incubated at 37°C/5% CO_2 for 24 hours prior to replacing the initial media with complete media containing 600 µg/mL hygromycin B. The culture media were routinely changed every two days and when cells grew into clumps they were transferred to a T25 flask where they were kept until 60−70% confluency had been attained and were finally placed into a T75 flask. Cells were considered to be stable if all cells in the negative control plate had stopped growing and were dead. Approximately two weeks from transfection, the stable cells were frozen at -80°C (See Section 2.3.3.6), and were subsequently subjected to either protein expression testing by western blot or were adapted to the suspension culture (See Section 2.3.3.3)

2.3.3.3 Adaptation of Stable CHO Flp-In Cells to Serum-Free Suspension Culture

Stable cell lines expressing proteins of interest are routinely adapted to serum-free suspension culture. This process is used to reduce contamination with media components, in particular animal cell components such as FCS, and to achieve high cell densities for future protein expression experiments that may not be achieved using adherent cultures.

Adherent stable cell lines were adapted to Hyclone media by direct adaptation. Briefly, cells were grown in a T75 flasks to 80−90% confluency, after which the cells were washed with PBS and transferred to T75 flasks containing 15 mL of Hyclone media at a density of 1 x 10^6 cells /mL and incubated at 37°C/5% CO_2. Cells were checked every 2-3 days and media changed.

Any cells in suspension were taken and transferred to separate T75/T25 flasks. This process was continued until all cells were in suspension. Cells adapted quickly to Hyclone media without appreciable losses in viability and were deemed suspension adapted by visual confirmation and viability checking, adopting the criteria of >90% viability with a 24-48 hours doubling time. After the adaptation process hygromycin B was added to the media at ~250 µg/mL. Cells were expanded and token freeze (TF) stocks prepared (See Figure 2.4). One vial was then expanded out and cells frozen as master cell bank (MCB) stocks. Again, 1 vial was defrosted, and expanded as before and cells frozen as a working cell bank (WCB) stocks comprising at least five vials. Cells from this WCB were used for expression in large-scale roller bottles as described in Section 2.3.5.

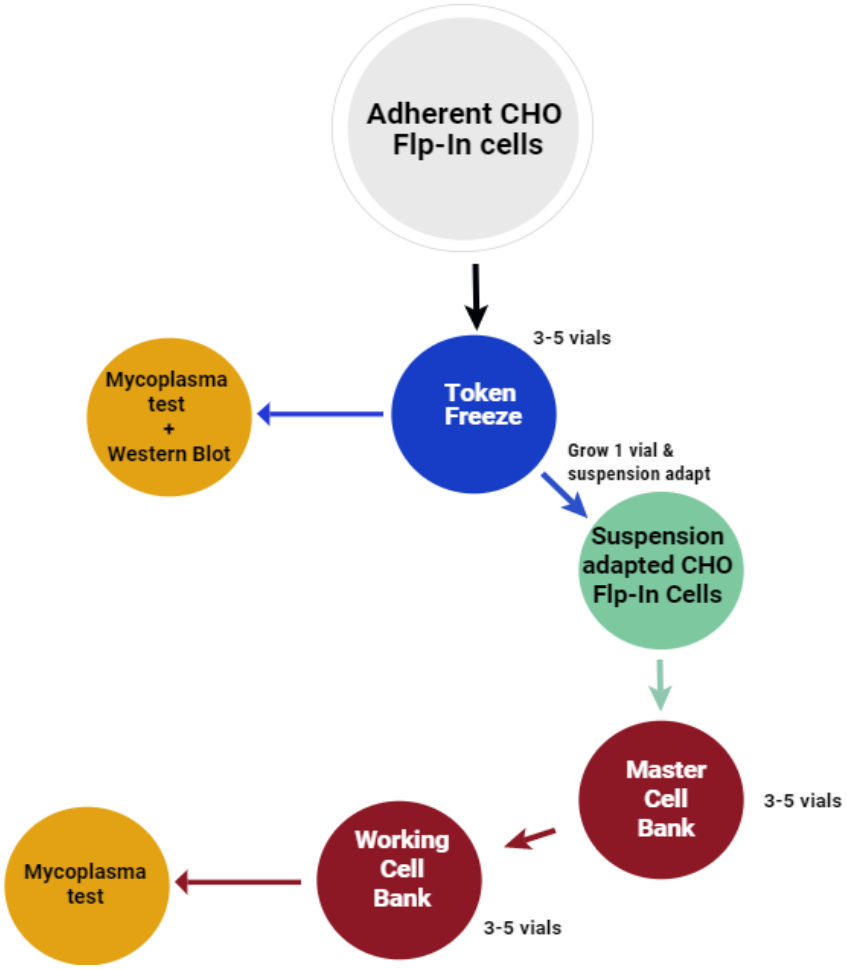

Figure 2.4: Schematic development of master and working cell banks from a stable cell line. Suspension adapted Cells line were immediately frozen at -80^{o}C by token freeze, as described in Section 2.3.3.6, this formed MCBs. One of the frozen vials was defrosted and grown until sufficient cells remained for token freezing of WCBs and checked for mycoplasma contamination. Constructed using Venngage website.

2.3.3.4 General Culturing of Adherent Rat Osteosarcoma (UMR-106) Cell Lines

For bioactivity studies, namely cAMP generation assays, the UMR-106 cells (rat osteosarcoma cells) were used, as these cells express endogenous parathyroid hormone (PTH) receptors and are thus responsive to stimulation with PTH/PTH fusions. Briefly, the UMR-106 cells were grown in T75 flasks containing DMEM: F12 (High-glucose), L-glutamine, 10% FCS and penicillin/streptomycin and incubated at 37°C/5% CO_2. Cells were passaged every 2–3 days or at ~ 80% confluency, as described in Section 2.3.3.1.

2.3.3.5 Monitoring Cell Number and Viability

Counting cells is imperative in order to establish a new culture with known cell numbers and to monitor growth rates. Thus, as a part of this investigation, suspension-adapted and adherent cell lines were counted, and viabilities were checked via the Trypan blue dye exclusion method and a haemocytometer by mixing cell suspension with dye in a 1:1 ratio. Dead cells were distinguished from living cells by appearance of blue colour resulting from dye absorbance by damaged cell membranes. The equation below was used for the calculation of cell density and viability (Figure 2.5). Two of the four "large" corner squares (1 mm × 1 mm) were typically used when counting (See Figure 2.6).

$$\text{Number of cells / ml} = \frac{\text{Number of cells}}{\text{Number of large square counted}} \times \text{Dilution of cells (2)} \times 10^4$$

Figure 2.5: The calculation of the number of cells.

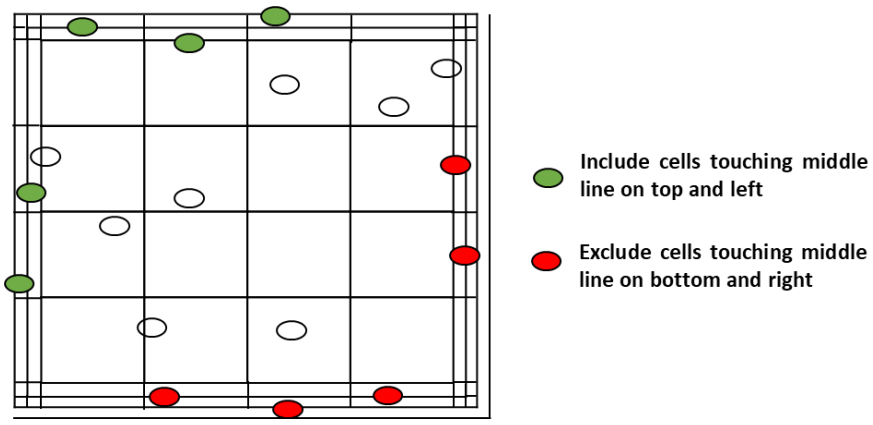

Figure 2.6: Schematic counting cell by haemocytometer.

Constructed using PowerPoint.

2.3.3.6 Freezing and Resuscitation of Mammalian Cell Lines

Freezing mammalian cells helps prevent any genetic changes in the continuously growing mammalian cell lines which may be caused by high passage numbers, and thus preserving cell stocks. In this work, cells were frozen and stored at -196°C at a low passage number in the presence of dimethyl sulfoxide (DMSO), acting as a cryoprotective agent.

Both suspension-adapted and adherent cells were frozen using the same process, as both cell types could be non-transfected or stably expressing a gene of interest. Once sufficient number of viable cells was established, they were centrifuged at 1,000 rpm for 5 minutes. Next, the cell pellet was resuspended in a volume of freezing mixture (See Table 2.7) required to yield a final cell density of 2−6 × 10^6 viable cells/mL. Subsequently, 1 mL of cell suspension was aliquoted into pre-chilled cryogenic vials, and placed in a CoolCell® Cell Freezing container and were stored at -80°C. After 72 hours, cells were transferred into liquid nitrogen for long-term storage. One vial of cells was then resuscitated, and viability was checked. Cells extracted from this vial were expanded and the freezing process described above was repeated to produce a MCB and thereafter a WCB, as described in Section 2.3.3.3. Throughout this process, cell media was routinely checked for mycoplasma contamination, which slowly alters the behaviour and the metabolism of cell culture, while reducing saturation density, thereby decreasing the cell proliferation rate without cell death or visible signs of infection.

Table 2.7: Freezing mixture formulation

Cells type	**Freezing medium**		
	FCS	**Serum-free medium (Hyclone)**	**DMSO**
Suspension cells	-	90%	10%
Adherent cells	90%	-	10%

To resuscitate cells from frozen - one vial was thawed in a water bath at 37°C until a few ice crystals remained. At this point, cells were diluted in an appropriate culture medium (usually 10−15 mL) and centrifuged at 1,000 rpm for 5 minutes to remove DMSO. The resulting cell pellet was resuspeded in an appropriate volume before being plated. Cells were subsequently subjected to at least two passages and viability checked using Trypan blue dye exclusion method before being used in further experiments.

2.3.4 Confirmation of Stable Cell Line Authenticity

To confirm that stable cell lines were expressing the correct protein, media samples from stable cell lines were subjected to western blotting (See Section 2.3.1.1.2.2), and inserted target gene DNA was confirmed by reverse transcription polymerase chain reaction (RT-PCR) and sequencing (See Section 2.3.4.2).

2.3.4.1 Confirmation of Expression by Western Blotting

Adherent stable cells were plated in T25 flasks in 4 mL at 0.25×10^6 cells/mL and left to grow until confluency had been attained. Cells were then washed with 4 mL PBS and media replaced with 4 mL serum-free media (without antibiotics) and incubated for 4−6 days. Cells that were adapted to suspension culture in Hyclone media were also tested for expression by seeding at 2.5×10^6 cells/mL and left for 2 days (See Section 2.3.3.3). Harvested media (day 6 and suspension) were centrifuged and concentrated before being western blotted with anti-PTH and anti-GHBP antibodies.

2.3.4.2 RT-PCR & cDNA Sequencing

2.3.4.2.1 RNA Extraction

RT-PCR was used to verify the stable cell line authenticity as described in Section 2.3.3.2. This required extraction of RNA to generate cDNA which in turn would be used for sequencing. For this purpose, total RNA was extracted from up to 5×10^6 cells using the RNeasy Mini Kit (Qiagen) as per the manufacturer's instructions. The RNA was quantified by absorbance at A_{260} nm using a Nanodrop spectrophotometer (See Section 2.3.2.3) before being frozen in aliquots at -80°C until required for cDNA synthesis.

2.3.4.2.2 Reverse Transcription Polymerase Chain Reaction (RT-PCR)

Total RNA was amplified using RT-PCR in order to generate cDNA for subsequent use as a template in PCR amplification. Oligodeoxynucleotide (oligo $d(T)_{20}$) primer was utilised to increase the specificity for mRNA only, as it binds to the poly(A) tail. The reverse transcription (RT) was conducted using Retroscript Kit Ambion (AM1710) according to the manufacturer's instructions.

To obtain three sterile Eppendorf tubes, 15 µL of RNA-primer volume, 2 µL of RNA per 15 µL reaction, and 1 µL of each negative control and positive control were combined. The reactions shown in Table 2.8 were generated using HeLa cell RNA controls (HeLa cDNA should produce a band at 353bp). The Eppendorf tubes were mixed briefly, and the components were centrifuged. Finally, the tubes were heated at 65°C for 5 minutes before incubating in ice for 1–2 minutes.

Table 2.8: Components of the anneal primer to template RNA

Component	RNA sample	+RT reaction	-RT reaction
50 µM oligo $d(T)_{20}$ Primer	1 µL	1 µL	1 µL
10 mM dNTP mix (10 mM each)	1 µL	1 µL	1 µL
10 µg/µl total HeLa RNA (10 ng total)	-	1 µL	1 µL
RNA sample	2 µL	-	-
Nuclease-free H_2O	Up to 15 µL	Up to 15 µL	Up to 15 µL

In the second step, three sterile Eppendorf tubes were set up to a 7 µL reaction volume, as described in Table 2.9.

Table 2.9: Components of the RT reaction mix

Component	RNA sample	+RT reaction	-RT reaction
5x SSIV Buffer	4 µL	4 µL	4 µL
100 mM DTT	1 µL	1 µL	1 µL
Ribonuclease Inhibitor	1 µL	1 µL	1 µL
SuperScript™ IV reverse transcription	1 µL	1 µL	-
Nuclease-free H_2O	-	-	1 µL

RT-PCR on total RNA derived from 14A8 and 14A7 cell lysates was subsequently performed as described in Section 2.3.4.2.2. The Control reactions outlined in the section pertaining to RT-PCR were used to verify that the RT reaction is working as expected by using both sense and antisense primers. The RT reaction components were added to the Eppendorf tubes and the reaction mixture was incubated in a PCR Thermocycler for 10 minutes at 50°C followed by 10 minutes at 80°C to inactivate the reaction. Next, *E. coli* RNase H (2 U/µL) was added to the cDNA sample and incubated at 37°C for 20 minutes. Finally, the sample was stored at -25°C until required for PCR.

2.3.4.2.3 Polymerase Chain Reaction (PCR)

PCR was used to amplify the required regions of a DNA fragment, using forward and reverse oligonucleotide primers. These primers were designed in our laboratory but synthesised by Eurofins Genetic Services Ltd (London, UK). Prior to their use, the primers were stored at -20°C at a concentration of 100 pmol/µL (100 µM). For the PCR reaction two Master Mixes (MMs) were prepared, as stated in Tables 2.10 and 2.11 (primer sequences are provided in Appendix C2). 14A2c was used as a positive control to verify that the PTHss primer set works whilst 14A4, which is a GH fusion with GHBP and contains the GH signal sequence, was used as a second positive control to verify that the GHss primer set works. cDNA was amplified by PCR using the PTHss primer and GHR reverse primer set. Negative controls without a template were set up for both primer sets.

Table 2.10: Master Mix I (25 µl per reaction)

Material	**cDNA sample**	**+ve 14A2c (cDNA)**	**Primer control 1**	**+ve 14A4 Plasmid**	**Primer control 2**
Forward primer: F1_Nhe1_PTHss (10 pmol/µl)	1 µl	1 µl	1 µl	_	_
Reverse primer: GHR_Q238 (10 pmol/µl)	1 µl	1 µl	1 µl	1 µl	1 µl
Primer GHss_Nhe1_F Plasmid (10 pmol/µl)	-	-	-	1 µl	1 µl
dNTPs (10 mM)	1.25 µl	1.25 µl	1.25 µl	1.25 µl	1.25 µl
Sterile water	16.75 µl	16.75 µl	21.75 µl	20.75 µl	21.75 µl
DNA template	5 µl	5 µl	-	1 µl	-
Total Volume (µl)	25	25	25	25	25

Table 2.11: Master Mix II: (25 µl per reaction)

Constituent	**6X Reactions**
x10 Polymerase buffer +$MgCl_2$ 1.5 mM final concentration)	30 µL
Sterile water	114.9 µL
Expand Polymerase (10 IU/µl)	5.1 µL

Next, 25 µL of MM II was added to each MM I, thus achieving a 50 µL reaction volume. The PCR reaction described in Table 2.12 was subsequently performed.

Table 2.12: PCR reaction

Stage	Time	Temperature
Denaturation	2 minutes	94°C
25 cycles (Annealing)	1 minute	56°C
	1 minute	56°C
	1 minute	56°C
Extension	10 minutes	72°C

When PCR did not work, a different method was used for a basic PCR reaction that utilised Go2 Taq polymerase (Taq polymerase isolated from Thermus Aquaticus). Master Mix II (MM II) was prepared, as shown in Table 2.13. PCR reactions were prepared separately for these controls, as outlined in Table 2.14. The number of cycles was increased to 35.

Table 2.13: Master Mix II (180 µl per reaction)

Constituent	1x Reaction	8x Reaction
5x Go2 Taq polymerase Flexi buffer (with Magnesium, 1.5mM final)	10 µL	80 µL
Sterile water	14.8 µL	118.4 µL
Go2 Taq polymerase	0.2 µL	1.6 µL

Table 2.14: RT-PCR controls (35 µl per reaction)

Component	Positive (with RT)	Negative (No RT)
	Volume (µL)	
Sterile water	19.8 µL	19.8 µL
Go2 Tag buffer (+ Mg)	10 µL	10 µL
dNTP's	1 µL	1 µL
Primer Sense	1 µL	1 µL
Primer antisense	1 µL	1 µL
cDNA from positive control (+RT) or No RT control	2 µL	2 µL
GoTaq polymerase	0.2 µL	0.2 µL

The resulting PCR products were analysed and separated on 0.8% agarose gel by electrophoresis and the DNA fragments visualised with Midori Green dye (See Section 2.3.1.1.3). For the estimation of DNA product size after migration, DNA markers of 1 kb ladders were used.

2.3.4.2.3.1 DNA Clean Up, Purification and Sequencing

GenElute™ Extraction Kit was used to extract and purify DNA after PCR, in accordance with the manufacturer's instructions. Subsequently, the extracted DNA was quantified using NanoDrop™ at A_{260} (See Section 2.3.2.3), and then sequenced in the Division of Genomic Medicine at the University of Sheffield. The PCR reaction was prepared at 10 µL/reaction using primer pairs of 1 pmol/µL concentration. The SeqMan software (Lasergene version 8; DNAStar Inc, Madison, WI) was used for analysing the sequence data.

2.3.5 Expression of PTH-Fusions in Roller Bottle (RB) and Shake Flask Cultures

Expansion of suspension-adapted CHO Flp-In cells stably expressing the protein of interest was conducted in RB and flask culture for protein expression. The cells were first incubated in a Cell Roll Cell Spine Control Unit with a stirrer operating at 6 rpm at 37°C/5% CO_2 to achieve an approximate density of 1×10^6 cells/mL, after which temperature was reduced to 31°C. Media samples were taken every 2−3 days, and cell counts and viabilities recorded. Media was harvested by centrifugation (25,000 × g for 20 minutes at 4°C using a JA 25.50 rotor) when cell viability began to decline below ~90% or after 12 days.

Proteolysis reduction was conducted by adding protease inhibitors, EDTA (5 mM final concentration) and benzamidine HCL (10 mM final concentration). A Vivaflow 200 concentrator with 10 kDa molecular weight cut-off (MWCO) and Masterflex pump were used

to concentrate clarified media by ~5- to 10-fold before being frozen at -25°C. Samples were analysed by western blotting prior to purification. Target protein was purified from concentrated media using anion exchange and affinity chromatography as described in Section 2.3.6.

2.3.6 PTH-fusion Purification Using Ion Exchange and Affinity Chromatography

PTH fusions were expressed as a secreted product from a CHO Flp-In cell line into the media due to the presence of PTH secretion and propeptide sequences. Prior to purification, the media was concentrated, as described in Section 2.3.5.

Purification of target protein from media was conducted using a combination of Q-Sepharose ion exchange (IEX) and affinity chromatography. This process consists of initial purification using a Q-Sepharose IEX column 20 mL (GE Healthcare Life Sciences) in flow-through mode combined with an anti-GHBP antibody column (monoclonal antibody used for purification was 10B8, gift from Zida Wu, Berlin). All purification steps were performed using XK16/30 column purification system (GE Healthcare Life Sciences) or other suitable columns. The aim was to obtain protein of >90% purity, as determined by SDS-PAGE, at >1.5 mg/mL, which was required for testing biological activity using the UMR-106 assay (See Section 2.3.3.4) as well as for further *in vivo* studies. Column buffers were prepared as per protocol instructions (See Appendix D1) and either filtered or autoclaved as appropriate and all column bindings were carried out at 4°C.

2.3.6.1 Preparation of Affinity Resin

To produce more affinity resin, 10B8 (anti GHBP monoclonal Ab) was coupled to Cyanogen Bromide-Activated Sepharose (CNBr activated). The 10B8 antibody - was a gift from Zida Wu, Berlin.

Prior to binding, 10B8 was dialysed against coupling buffer (See Appendix D2) at 4°C with the buffer replaced every 2 hours up to 3 times. The absorbance of the final antibody solution was measured at A_{280} nm. Column buffers were prepared as per protocol instructions (See Appendix D2) and either filtered or autoclaved as appropriate and all bindings were carried out at 4°C. For binding a minimum concentration of 2 mg/mL antibody solution is required. This was prepared by weighing out 2.5 g of CNBr activated resin in a 50 mL tube and the resin washed twice with 2 x 50 mL ice cold 1 mM HCl. The resin was harvested by centrifugation in between the washes. The resin was then incubated on ice with approximately 50 mL of ice cold 1mM HCl for at least 30 minutes to allow for swelling of resin (1 g resin swells to approximately 3-4 mL). Thereafter, the resin was transferred to a Millipore Filter unit and further rinsed with 350 mL of 1 mM HCl using the vacuum pump. The resin was washed with 500 mL MilliQ water followed by 500 mL coupling buffer. The swelled resin was transferred into coupling solution containing the antibody (Ab) ligand and incubated at room temperature for 2 hours on a rolling mixer. The ratio of ligand to resin was ~ 40 mg of Ab for a 10 mL column. Unreacted ligand was removed during a Millipore Stericup filtration followed by rinsing with at least 5 column volumes of coupling buffer. Next, the resin was rinsed with 100 mL blocking buffer. Unreacted sites were blocked by incubation in 200 mL 0.2M glycine, pH 8.0 for 2 hours at room temperature with intermittent mixing or overnight for 16 hours at 4°C. The resin was then washed with 10 CVs of coupling buffer, followed by 10 CV's of 0.1 M acetate, 0.5 M NaCl,

pH 4.0. The wash step was repeated 4 times. The resin was then stored in 20% ethanol at 4°C. Successful coupling was monitored by Bradford assay.

2.3.6.2 Q-Sepharose Anion Exchange Chromatography

Samples were purified by applying a flow-through technique. This allowed the majority of target protein to be collected in the unbound fraction (UB) whilst a considerable amount of the contaminating protein would bind to the column. As a result, the media samples were sufficiently cleaned to enable efficient binding of target proteins to the affinity column. Media were defrosted at 37°C (or overnight at 4°C) and clarified by centrifuging at 20,000 × g for 30 minutes at 4°C in a JA 25-50 rotor. The pellet was discarded, the supernatant was kept for loading and its conductivity measured. A conductivity of ~30 mS was considered acceptable as this was above that of the binding buffer which had a conductivity of ~ 17 mS.

All purifications were carried out at 4°C and buffers filtered and equilibrated to 4°C before use. A 20 mL Q-Sepharose (or Source-Q) stored in 20% ethanol at 4°C was washed with MilliQ water and equilibrated with 100-200 mL binding buffer (40 mM phosphate buffer, pH 8.0), at least 5 column volumes (CV's).

The cleared supernatant was loaded onto the Q-Sepharose column at a flow rate of 1.5 mL/minute and the UB fraction collected. The column was rinsed with 40 mL binding buffer and to remove any residual target protein; this was added to the unbound fraction. The unbound fraction pool contained the majority of target protein and was utilised for further purification via affinity chromatography. The Q-Sepharose column was washed with 5−10 CVs of binding buffer, followed by elution of bound protein with 30 mL of elution buffer composed

of binding buffer and 1 M sodium chloride. When not in use, the column was cleaned in place with 0.5 M NaOH followed by MilliQ then stored in 20% ethanol.

2.3.6.3 Purification Using Affinity Chromatography

Before use, the 20 ml affinity column (10B8 antibody bound to NHS-Sepharose, GEHealthcare, already available in laboratory or re-made as CNBr coupled resin (See Section 2.3.6.1) was washed with 0.2 M glycine, pH 2.7 followed by equilibration with 5−10 CVs of binding buffer (40 mM phosphate buffer, pH 8.0). The unbound fraction from the Q-Sepharose column was loaded at a rate of 1.5 mL/minute and UB fraction collected; this would be re-applied to the column). The column was washed with 5-10 CVs of binding buffer.

For the elution, the column was washed with 18 mL of 0.2 M glycine, pH 2.7, followed by the collection of a further 1 × 20 mL and 2 × 10 mL volumes and collected fractions neutralised with 1/10 volume of 1.5 M Tris, pH 8.8. The column was re-equilibrated with 5 CVs of binding buffer and the UB fraction re-applied and the process repeated. All samples were analysed by SDS-PAGE (See Section 2.3.1.1.2) and Bradford protein assay (See Section 2.3.2.1). Eluted samples were initially concentrated followed by dialysis (See Section 2.3.6.4). The column was subsequently washed with 5 CVs of distilled water, followed by 5 CVs of 20% ethanol before being stored at 4°C.

2.3.6.4 Concentration and Dialysis of Purified PTH-Fusions

Elution samples were polled and concentrated using a Centriprep-30 Centrifuge filter to reduce volume and increase protein concentration prior to dialysis. Samples were dialysed against 1−2 L of buffer with at least three changes for a total of 5 L at 4°C. If required the sample was further concentrated using the Centriprep-30 Centrifuge filter the next day to a

final protein concentration of 1−2 mg/mL, with the protein quantified at A_{280} nm using a Nanodrop. The final sample was centrifuged at 13,400 rpm for 1 minute on a benchtop centrifuge followed by a final quantification at A_{280} and analysis by SDS-PAGE. Samples were stored in aliquots at -80°C until required for the analysis.

2.3.7 Dual Luciferase Reporter Assay (DLRA)

In this study, the DLRA assay was used to test cells response to parathyroid hormone (PTH) and to compare the biological activity of purified PTH fusions, using the rat osteosarcoma cell line, UMR-106. The cell line expresses the endogenous PTH receptor and thus responds to PTH by producing the second messenger, cAMP. In turn, the cAMP levels in these cells can thus be quantified using a reporter gene assay, which is an indirect way of testing activity of the target protein.

For the assay, cells are transfected with a reporter plasmid that contains multiple copies of the cAMP Response Element (CRE) linked to the Firefly Luciferase gene and a minimal thymidine kinase promoter (pGL4.29/Luc2/Cre/Hygro plasmid, Promega), as well as a transfection control plasmid that expresses Renilla Luciferase under the control of either the cytomegalovirus promoter (pRL-CMV, Promega) or thymidine kinase promoter (pRL-TK, Promega).

Both Firefly and Renilla Luciferases' activities are quantified using the Promega Dual Luciferase Assay Reagent Kit and an AutoLumat LB 953 Multi-Tube Luminometer (Berthold Technologies).

In addition, Promega dual luciferase assay reagents contain two substrates: Luciferase Assay Substrate which contains luciferin, the substrate for Firefly Luciferase and Stop & Glo® Buffer

which contains ceolenterazine the substrate for Renilla. Both Firefly and Renilla Luciferase activity is measured sequentially from a single sample based on different substrate specificities of the two luciferases, thus minimising errors due to variability in pipetting volumes and providing a convenient means to measure both the experimental and control reporter activities. Firefly Luciferase activity is directly related to cAMP levels which in turn is related to activity of PTH or PTH fusions. Figure 2.7 shows the basic reaction of luciferase that catalyses the oxidation of luciferin (substrate) in the presence of ATP, Mg^{2+} in an O_2-dependent reaction. The luminometer then detects light emitted by the sample.

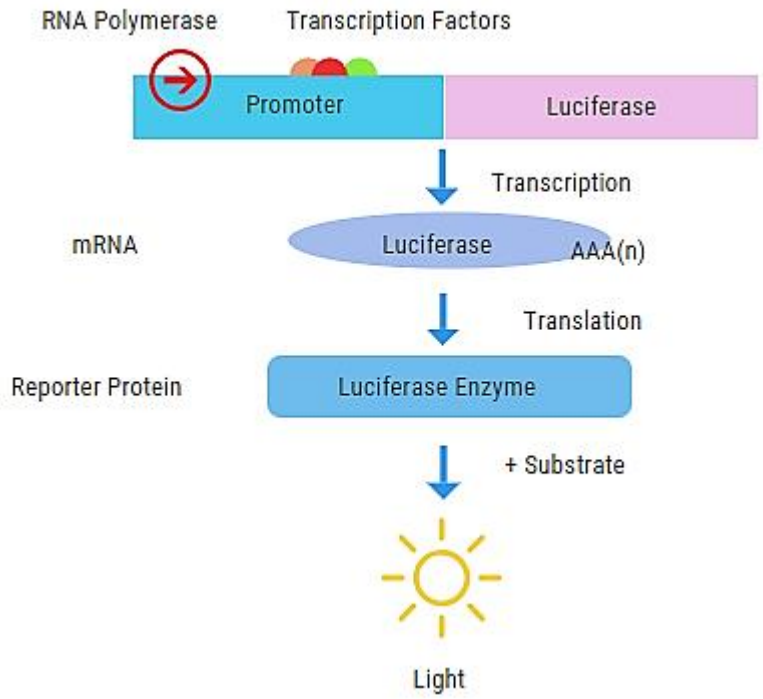

Figure 2.7: Schematic description of the principle of DLRA for detection of Luciferase activity. Constructed using Venngage website.

2.3.7.1 Trouble-shooting the DLRA

In vitro reporter assays utilise a reporter plasmid that in the presence of ligand generates a signal that is measurable and thus "reports" on ligand activity. To control for experimental

variations control plasmids that constitutively express a second reporter are included. However, control plasmids can interfere with or be influenced by the assay set up which could significantly affect the integrity of the assay. Consequently, two control plasmids were initially compared for interference, pRL-CMV and pRL-TK, expressing Renilla luciferase from the strong CMV (Cytomegalovirus) or the weaker TK (thymidine kinase) promoters.

The basic assay is as follows: on day one, 180 µL of UMR-106 cells at a density of 0.22×10^6 cells/mL were plated in 48-well plates (See Section 2.3.3.4) and incubated at 37°C/5% CO_2 for 24 hours. The following day, at approximately 50-60% confluence, cells were transfected using an in-house standard protocol. Briefly, 0.2 µg reporter plasmid per transfection were mixed with variable concentrations of control plasmid under test, ranging from 0.5 to 20 ng/transfection. Volumes of reagents were kept equal to avoid variations due to volume changes. Table 2.15 shows a typical transfection set up for testing pRL-TK and pRL-CMV from 0.5 to 10 ng/transfection. Each transfection mix includes sufficient reagents for 10 separate transfections as a minimum, in order to avoid variations due to using low µL volumes. Firstly, in one Eppendorf TransIT-LT1 was mixed with 200 µL of DMEM and in a second Eppendorf 2 µg pGL4.29/Luc2/Cre/Hygro was mixed with X ng Renilla plasmid (volume depends on experiment). Both tubes were incubated at room temperature for 15 minutes then mixed, followed by a further 15 minute incubation at room temperature after which 20 µL of this mix was added to each well of a 48 well plate containing 180 µL of cells and gently swirled to mix (See Table 2.15 for a typical transfection experiment).

Plates were incubated for 4 hours at 37°C/5% CO_2 after which media was replaced with 200 µL DB buffer (DMEM/0.1% BSA) and incubated for 24 hours at 37°C/5% CO_2.

Table 2.15: Basic transfection Master Mix (Number of transfection n=10)

Transfection Mix	Renilla plasmid per TFX mix (ng)	Firefly plasmid per TFX mix (µg)	DMEM	TransIT-LT1
pRL-TK Plasmid				
TFX 1	5 µL **1 ng/mL** plasmid = 5 ng (0.5 ng per Tfx)	2.55 µL plasmid = 2 µg (0.2 µg per Tfx)	200 µL	6 µL
TFX 2	5 µL **10 ng/mL** plasmid = 50 ng (5 ng per Tfx)	2.55 µL plasmid = 2 µg (0.2 µg per Tfx)	200 µL	6 µL
pRL-CMV plasmid				
TFX 3	5 µL **1 ng/mL** plasmid = 5 ng (0.5 ng per Tfx)	2.55 µL plasmid = 2 µg (0.2 µg per Tfx)	200 µL	6 µL
TFX 4	5 µL **10 ng/mL** plasmid = 50 ng (5 ng per Tfx)	2.55 µL plasmid = 2 µg (0.2 µg per Tfx)	200 µL	6 µL

Stocks of Renilla and reporters plasmids were adjusted to give an overall volume of 5 µL and 2.55 µL per transfection mix.

The following day, cells were challenged with PTH 1-34 from 0, 0.1, 1 and 10 nM. Table 2.16 describes the preparation of the standard concentrations used for samples/cells analysis, prepared as 10x stock concentrations. Firstly, DB buffer was replaced with 180 µL of fresh DB buffer along with 20 µL of either 10x PTH 1-34 standard or DB only, resulting in a final volume of 200 µL. The plates were incubated at 37°C/5% CO_2 for 5 hours, after which the media was removed, and 100-150 µL passive lysis buffer (5× concentrated solution diluted in distilled water) was added. Cells were allowed to lyse at room temperature for 15 minutes with mixing. Both Firefly and Renilla Luciferase were quantified using the Promega Dual Luciferase Assay Reagent Kit and an AutoLumat LB 953 Multi-Tube Luminometer (Berthold Technologies).

All samples were tested in duplicate and the ratio of Luciferase to Renilla was calculated using Excel software and data plotted using GraphPad Prism. Assay interference of both Renilla expressing plasmids was tested by calculating the fold difference (FD), which is mean difference in Renilla values from untreated controls. An increase in Renilla expression with increasing PTH 1-34 concentrations was taken as showing assay interference. Also, the % coefficient of variation (%CV) was calculated between duplicate values, whereby a %CV of

≤25% was acceptable. Validation of the assay with a particular control plasmid was obtained using the full PTH 1-34 standard curve

Table 2.16: Preparation of PTH 1-34 standards

PTH 1-34 (Mwt = 4117.72Da, AnaSpec). PTH 1-34 was resuspended at 2 mg/mL in DMEM/0.1 % BSA (DB buffer) and frozen in aliquots at -25°C; this provides a stock solution of 485000 nM.

Sample	Stock concentration (nM)	Volume of Sample (µL)	DMEM/0.1%BSA (µL)	Dilution	Final Concentration in assay (nM)
PTH	5000	5 µL 485000 nM Stock	485 µL	97	500
	1000	180 µL 5000 nM	720 µL	5	100
	500	180 µL 1000 nM Stock	180 µL	2	50
	250	180 µL 500 nM Stock	540 µL	2	25
	100	**180 µL 250 nM Stock**	**270 µL**	**2.5**	**10***
	50	180 µL 100 nM Stock	540 µL	4	2.5
	25	**180 µL 25 nM Stock**	**270 µL**	**2.5**	**1***
	10	180 µL 10 nM Stock	180 µL	2	0.5
	5	180 µL 5 nM Stock	180 µL	2	0.25
	1	**180 µL 2.5 nM Stock**	**270 µL**	**2.5**	**0.1***
DB					Neat

***For assay trouble-shooting cells were challenged with PTH 1-34 from 10, 1, and 0.1 nM.

The protocol described above was used to validate the suitability of pRL-TK and pRL-CMV plasmid in the DLRA. Any further variations in protocols are described in the relevant results sections.

2.3.7.2 *In Vitro* Potency Studies of PTH 1-34 and PTH Fusions by DLRA

For these investigations, PTH fusions were purified as described in Section 2.3.6, and DLRA was developed as described in Section 2.3.7.1. Using the established DLRA assay, full standard

curves for PTH fusions were compared to PTH 1-34 and EC_{50} values obtained (a full description of each PTH fusion is provided in Appendix E).

Experiments were set up following the method described in Section 2.3.7.1, while modifying the number and amount of transfections accordingly. Any variations in protocols are highlighted in the relevant result sections. Table 2.17 shows a typical transfection for a single 48 well plate. Standard curves for PTH 1-34 is shown in Table 2.18. See Appendix E for other standard curves of PTH fusions and PTH 1-34.

Table 2.17: Transfection Master Mix (MM)

This was multiplied by the number of wells + 10% extra to allow for pipetting differences, n = 50 transfections

Component	**Amount**
DMEM: F12	1000 µL
TransIT-LT1	30 µL
pGL4.29 (Firefly plasmid), 0.2 µg/TFX	12 µL (10 µg)
Renilla plasmid (pRL-TK) 20 ng/TFX	16.3 µL (1 µg)

Analysis was performed by uploading duplicate values for both Firefly and Renilla values to a prepared Excel sheet. From this the mean activity, a ratio of Firefly to Renilla Luciferase (FL/RL) was calculated together with standard deviation (StDev) and % coefficient of variation (%CV). Fold induction was obtained by calculating the fold difference in mean activity between samples and controls. Finally, % maximum fold induction was obtained by calculating the % change in fold induction of samples relative to the highest standard value.

To obtain EC_{50} values, data was fitted using GraphPad Prism software to a 3- or 4-parameter dose-response curve. Any duplicate FL/RL data with a %CV > 25% were removed from the analysis. Any data that showed a trend of increasing Renilla with increasing PTH 1-34 (or PTH fusion) concentrations were also dismissed from the study.

Table 2.18: Preparation of PTH 1-34 standards

PTH 1-34 (Mwt = 4117.72Da). PTH 1-34 was resuspended at 2 mg/mL in DMEM/0.1 % BSA (DB buffer) and frozen in aliquots at -25°C; this provides a stock solution of 485000 nM.

Sample	Stock concentration (nM)	Volume of Sample (µL)	DMEM/0.1%BSA (µL)	Dilution	Final Concentration in assay (nM)
PTH 1-34	3645	5 µL Stock	660 µL	133	364.5
	1215	30 µL 1000 nM	60 µL	3	121.5
	405	30 µL 1215 nM	60 µL	3	40.5
	135	30 µL 405 nM	60 µL	3	13.5
	45	30 µL 135 nM	60 µL	3	4.5
	15	30 µL 45 nM	60 µL	3	1.5
	5	30 µL 15 nM	60 µL	3	0.5
	1.66	30 µL 5 nM	60 µL	3	0.166
	0.55	30 µL 1.66 nM	60 µL	3	0.055
	0.185	30 µL 0.55 nM	60 µL	3	0.0185
	0.037	30 µL 0.185 nM	120 µL	5	0.0037
DB					Neat

Chapter Three - Confirmation of Stable Cell Line Authenticity and Expression of Target Protein

Abstract:

Aims:

1. To confirm stable clones contain the correct integrated gene of interest.
2. To confirm stable clones expresses target protein.

Methods: Both PTH fusion genes for 14A7 and 14A8 were cloned using the Invitrogen Flp-In system to create stable cell lines. Target gene integration from total RNA extraction was confirmed by reverse transcription polymerase chain reaction (RT-PCR) followed by sequencing using gene specific primers. Western blotting confirmed target protein expression from growth media of both adherent and suspension adapted cell lines. Confirmation of 14A2c target gene integration had already been carried out with success previously in the group.

Results: Extraction of total RNA generated 10 µg/µL and 1.5 µg/µL cDNA for 14A7 and 14A8 respectively. Sequence analysis confirmed gene authenticity. The expression of target protein from stable CHO Flp-In cell lines was confirmed by western blotting using anti PTH antibody giving an expected size of 37-100 and 50-250 kDa for 14A7 and 14A8, respectively.

Conclusion: Both 14A8 and 14A7 were successfully expressed from a stable CHO Flp-In cell line. It is therefore possible to create stable cell lines that express target PTH fusion proteins.

3.1 Verification of Stable Clone Integration by RT-PCR and Sequencing

Total ribonucleic acid (RNA) was extracted from approximately five million CHO-Flp-In cells, expressing either 14A7 or 14A8 (See Section 2.3.4.2.1). A total RNA of 85 µg (1767 ng/µL), for 14A7, and 65 µg (1363 ng/µL), for 14A8, was extracted and used for RT-PCR using gene specific primers (See Section 2.3.4.2.2). The expected sizes of the PCR fragments were 969 Base pair (bp) and 1506 bp for 14A7 and 14A8 respectively, as calculated using Lasergene software.

However, initial PCR using the primer pairs PTHss forward and GHR_Q238 reverse (See Appendix A for details and sequences) was unsuccessful, as both PTH-Fusions were not detected (See Figure 3.1 below, Lane 1).

Both PCR's generated a positive control band separating at the expected size of ~1.5 kb with a less distinct band running at ~1kb (Lane 3). In addition, a band of ~2kb was visible in Lane 3 for 14A7 which was also present in the negative control (Lane 2) thus suggesting it was an artefact. No such bands were present in 14A8 negative control. The integrity of the RNA was further confirmed by gel analysis (See Figure 3.2).

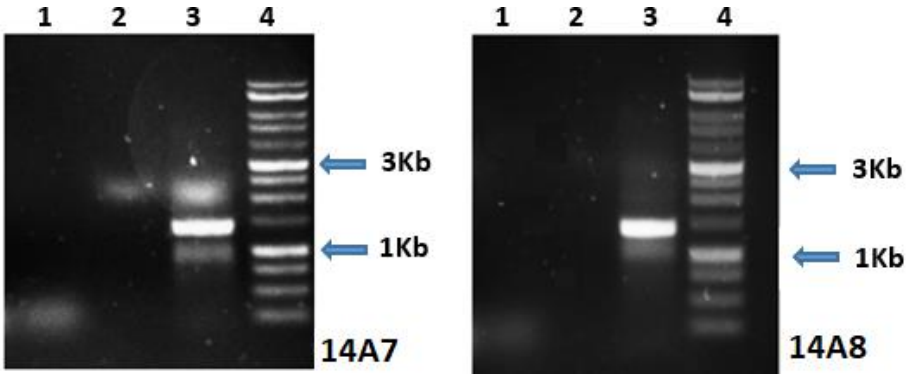

Figure 3.1: PCR of cDNA from 14A7 and 14A8 separated by 0.8% agarose/TAE gel and visualised using Midori green under ultraviolet light (UV).
Lane 1: 1/5 of PCR sample; **Lane 2:** Negative control (primers only); **Lane 3:** Positive control, PTH fusion 14A2c (See Appendix C2); **Lane 4**: Promega 1kb DNA ladder. A total 12 µL of a 50 µL PCR reaction was loaded per lane.

Ribosomal RNA is characterised by two subunits - 18S and 28S. Consistent with these subunits, 2 bands were observed on for both 14A7 and 14A8 RNA when analysed on agarose gels. This confirmed the integrity of the extracted RNA.

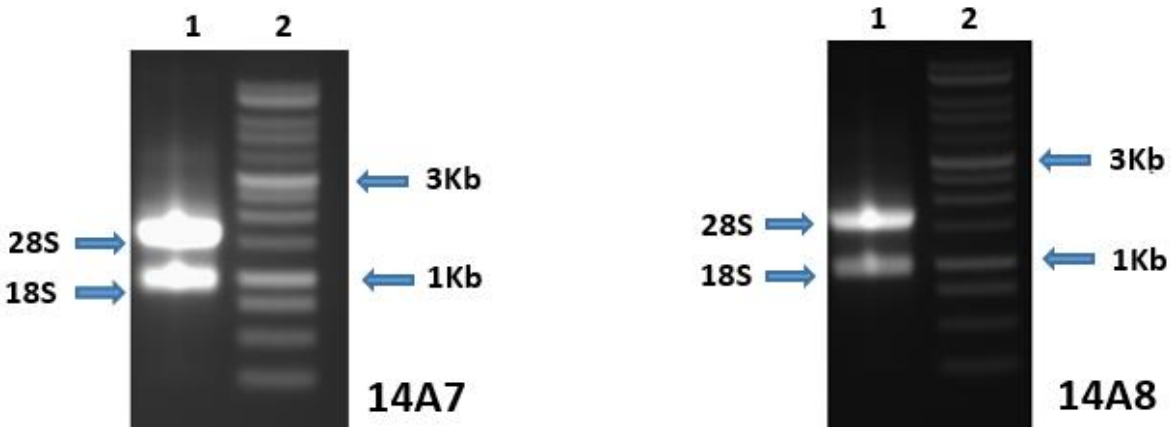

Figure 3.2: Total RNA extracted from 14A7 and 14A8 separated by 0.8% agarose/TAE gel and visualised using ethidium bromide under ultraviolet light (UV).
Lane 1: Total RNA sample was loaded 2.5 µL; **Lane 2:** Promega 1kb DNA ladder.

Following the confirmation of the integrity of RNA, RT-PCR was repeated with slight modifications. The addition of an RT positive and negative controls from the kit, increasing

the cycle number from 25 to 35, and using a selection of different primer pairs designed to provide both positive and negative outcomes (See Section 2.3.4.2.3 for details and Table 3.1 for primer pairs). The amplified PCR products were analysed by agarose gel electrophoresis against 1kb Promega DNA molecular weight ladder and the results are presented in Figures 3.3 and 3.4 for 14A7 and 14A8 respectively. In Gel A panel for both 14A7 and 14A8 constructs, PCR products generated using the PTH signal sequence (PTHss)_forward and GHBP reverse primers yielded single bands at approximately 1kb and 1.5kb (Figure 3.3 and 3.4, Gel A Lane 1). This is consistent with the expected sizes of 969 bp and 1506 bp for 14A7 and 14A8, respectively (See Appendix A). Additionally, the lack of amplified products in the negative control (Figures 3.3 and 3.4, Gel A Lane 2) suggests no contamination. A positive control consisting of purified 14A7 plasmid DNA (Figures 3.3 and 3.4, Gel A Lane 3) produced a band of approximately 1kb close to the expected size of 969 bp and showed that the PCR reaction was successful.

In contrast, in Gel B panel, analysis of PCR products amplified using the GH signal sequence specific primer, GHss_forward and GHBP reverse primer showed no bands in Lane 1 (Figures 3.3 and 3.4). This was an anticipated result as 14A7 and 14A8 both lack the GH signal sequence. The positive control was a purified 14A4 plasmid DNA, which contains the growth hormone signal sequence (See Appendix B1), and produced a band of ~1 kb for both 14A7 (Figure 3.3, Lane 3) and 14A8 (Figure 3.4, Lane 2) which was close to the expected size of 957 bp. This was an indication that the primers worked. The lack of bands in the negative controls (Figure 3.3, Lane 2 for 14A7 and Figure 3.4, Lane 3 or 14A8), confirmed there was no contamination of the PCR reaction.

Finally, in Gel C panel, PCR products generated from amplification with GHBP forward and GHBP reverse primers showed a prominent band at approximately 0.7kb for both 14A7 (Figure 3.3, Lane 5) and 14A8 (Figure 3.4, Lane 1), which corresponds to the predicted size of the GHBP fragment of 714 bp. As expected, no bands were detected in both negative controls (Figures 3.3 and 3.4, Lane 2). The RT positive control using HeLa cDNA produced a band between 0.25 and 0.5kb (Figures 3.3 and 3.4, Lane 3) close to the expected size of 353 bp. Negative controls (See Figures 3.3, and 3.4 Lane 4,) produced no bands.

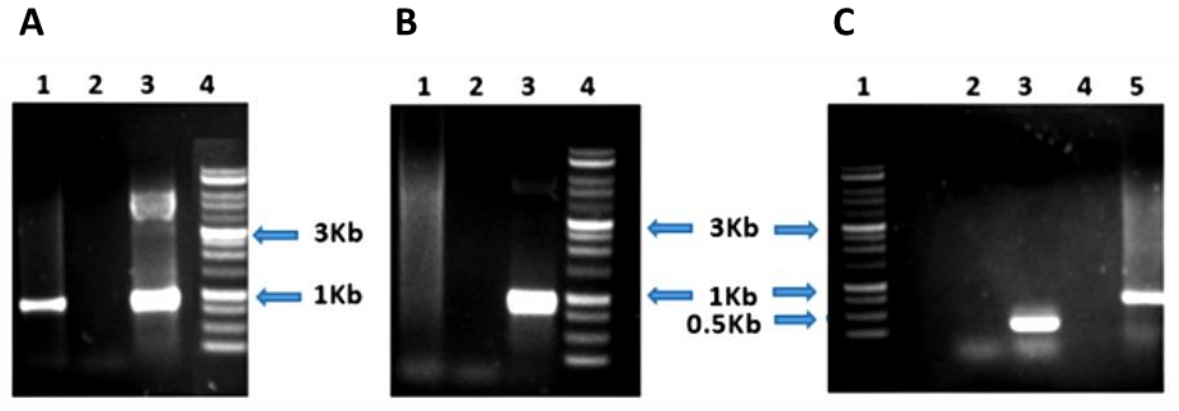

Figure 3.3: PCR of cDNA from 14A7 separated on a 0.8% agarose/TAE gel and visualised using Midori green under ultraviolet light (UV).

12 µL of PCR sample was loaded per well. **(Panel A)** PCR of 14A7 cDNA using primer pairs PTH signal sequence (PTHss) forward and GHBP reverse. **Lane 1:** (1/5) of PCR reaction; **Lane 2**: Negative control (primers only); **Lane 3:** Positive control, 14A7 plasmid; **Lane 4**: Promega 1kb DNA ladder. **(Panel B)** PCR of both 14A7 cDNA using primer pairs GH signal sequence (GHss) forward and GHBP reverse. **Lane 1:** (1/5) of 14A7 PCR sample; **Lane 2:** negative control (primers only); **Lane 3:** positive control consisting of a 14A4 (GH signal sequence); **Lane 4:** Promega 1kb DNA ladder. **(Panel C)** The PCR product was analysed by primer pairs GHBP forward and GHBP reverse. **Lane 1:** Promega 1kb DNA ladder; **Lane 2:** Negative control (primers only); **Lane 3**: Positive RT consisting of total Hela RNA from positive control kit (+RT) with sense and antisense primer; **Lane 4**: Negative RT consisting of a sense and antisense primer only; **Lane 5**: (1/5) of 14A7 PCR sample.

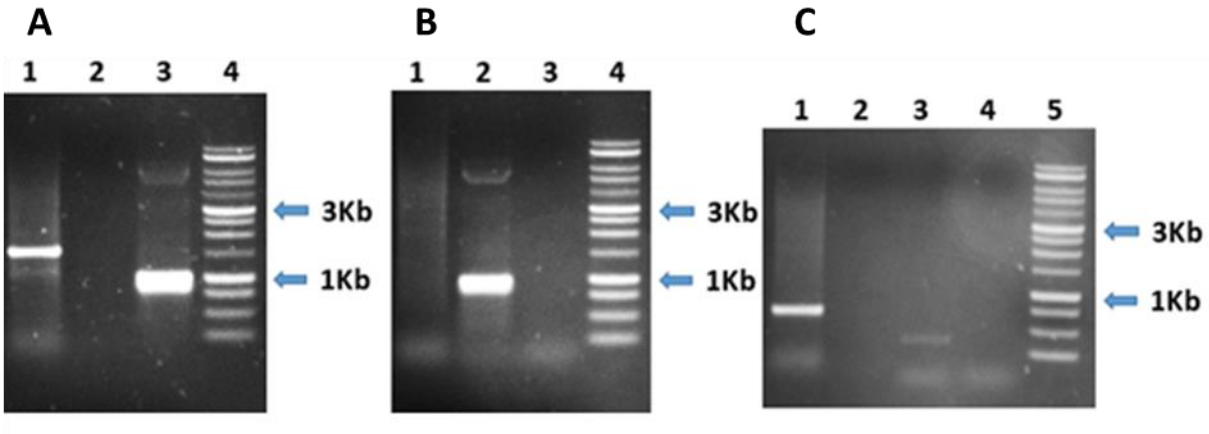

Figure 3.4: PCR of cDNA from 14A8 separated on a 0.8% agarose/TAE gel and visualised using Midori green under ultraviolet light (UV).

12 µL of PCR sample was loaded per well. **(Panel A)** PCR of 14A8 cDNA using primer pairs PTH signal sequence (PTHss) forward and GHBP reverse. **Lane 1:** (1/5) of PCR reaction; **Lane 2**: Negative control (primers only); **Lane 3:** Positive control, 14A7 plasmid; **Lane 4**: Promega 1kb DNA ladder. **(Panel B)** PCR of 14A8 cDNA using primer pairs GH signal sequence (GHss) forward and GHBP reverse. **Lane 1:** (1/5) of 14A8 PCR sample; **Lane 2:** positive control consisting of a 14A4 (GH signal sequence); **Lane 3:** negative control (primers only); **Lane 4:** Promega 1kb DNA ladder. **(Panel C)** The PCR product was analysed by primer pairs GHBP forward and GHBP reverse. **Lane 1:** (1/5) of 14A8 PCR sample; **Lane 2:** Negative control (primers only); **Lane 3**: Positive RT consisting of total Hela RNA from positive control kit (+RT) with sense and antisense primer; **Lane 4**: Negative RT consisting of a sense and antisense primer only; **Lane 5**: Promega 1kb DNA ladder.

Table 3.1: Primer Pairs

Gels	**Primers**	
	Forward	***Reverse***
A	PTH signal sequence PTHss_Forward	GHBP reverse
B	GH signal sequence GHss_For	GHBP reverse
C	GHBP_Forward	GHBP reverse

The 14A7 and 14A8 PCR fragments from Lane 1 of Gel A above were extracted, purified and quantified on a Nanodrop to give DNA concentrations of 10 µg/µL and 1.5 µg/µL, respectively (See Section 2.4.2.4). These were forwarded to the Gene Analysis Suite, Medical School Core

Facilities (University of Sheffield, Sheffield UK) for sequencing. The sequencing data generated demonstrated that the purified PCR products did contain the predicted 14A7 and 14A8 fusions' sequences (See Appendix A1 and A3). In conclusion, RT-PCR confirmed that the generation of a stable cell line was successful for 14A7 and 14A8.

3.2 Confirmation of 14A7 and 14A8 Protein Expression from Stable Cell Lines

For initial confirmation of protein expression, stable cells were grown as adherent cultures in T25 flasks and media taken on day 4 and 6 for analysis by western blotting. Cells were also adapted to suspension culture in Hyclone media (See Section 2.3.3.3) and culture media also tested for expression. Both non-concentrated and concentrated media were used for detection.

Figure 3.5 shows a western blotting analysis of media samples from both adherent and suspension adapted cultures using anti PTH antibody. The western blot shows that no target protein was detectable at day 4 and day 6 for non-concentrated adherent culture media for 14A7 and 14A8 (Lanes 1 and 2). However, protein expression was detected in concentrated media (Lane 3) and the proteins separated mainly as double bands between 37-50 kDa for 14A7 and as diffuse bands between ~50-250 kDa for 14A8. Expressed proteins were also detected in concentrated suspension adapted media showing distinct bands between ~37-100 and ~50-250 kDa for 14A7 and 14A8, respectively (Lane 4). The positive control of 14A2c produced an expected band running at ~50-75 kDa. A negative control sample, consisting of erythropoietin expression media, showed no background detection.

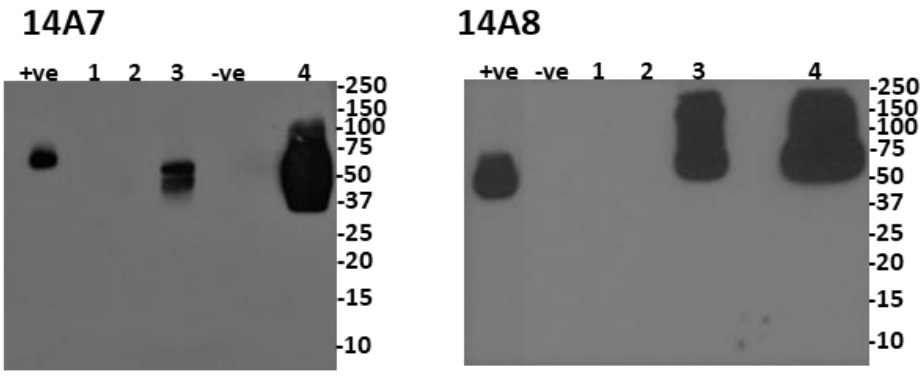

Figure 3.5: Western blot of expression media from adherent and suspension cultures of 14A7 and 14A8.

Samples were separated by 12% SDS-PAGE under non-reducing conditions and blots probed with a mouse anti-human PTH antibody. 20 µL of media sample was added to 10 µL of laemmli buffer and heated for 15 minutes at 65°C. 6 µL of Bio-Rad All Blue protein standards and 30 µL of samples were loaded per lane. **Lane +ve –** Positive control, 150 ng of 14A2c); **Lane -ve –** Negative control (10x concentrated EPO media only); **Lane 1 –** Day 4 sample; **Lane 2 –** Day 6 sample; **Lane 3 –** Concentrated adherent media; **Lane 4 –** Concentrated suspension media.

3.3 Discussion

Initial PCR's of cDNA derived from 14A7 and 14A8 were unsuccessful, even though the positive controls worked. This could be due to a number of experimental errors, such as the use of insufficient amounts or poor quality cDNA, contamination of the reaction with DNAse or omission of primers during sample preparation for the PCR reaction. The RNA was shown to be intact and of good quality for both preparations showing both the 18S and 28S ribosomal subunits by gel analysis. Both RT-PCR and PCR reactions were repeated using different primer pairs, and were ultimately successful. PCR's using primer pairs PTHss forward and GHBP reverse produced the expected band sizes of 969 bp and 1506 bp for both 14A7 and 14A8, respectively. This confirmed the presence of both PTH signal sequence and GHBP. As expected, PCR reactions using the GH signal sequence specific primer with GHBP reverse

primer showed no positive amplification of 14A7 and 14A8, due to a lack of GH signal sequence in both PTH fusions. In addition, PCR using GHBP forward and GHBP reverse primers showed an expected band size of 714 bp for GHBP, indicating the presence of GHBP in these fusions. The RT positive control using HeLa cell RNA detected bands close to the expected size of 353 bp and confirmed that the RT reaction worked.

Stable cell lines expressing PTH fusion proteins of interest were routinely adapted to serum-free suspension culture to achieve a high cell density for future protein expression experiments in roller bottle (RB) cultures. Secreted expression was directed by the PTH signal sequence and propeptide. Using western blotting protein analytical method, no protein was detected in both non-concentrated adherent media for both 14A7 and 14A8. This suggests that the PTH-fusions were expressed at low concentrations below the detection limit of the antibody. However, 14A7 and 14A8 proteins were detected in the western blots of concentrated adherent cell culture media showing diffuse bands at ~37–50 kDa and ~50-250 kDa respectively. Also, in concentrated cell suspension culture media target protein was detected as diffuse bands at ~37–100 kDa and ~50-250 kDa for 14A7 and 14A8, respectively. For both constructs western blotting analysis, there was no background detection in the negative control and the positive control produced a band running at 50-75 kDa confirming that the western blot was successful.

The molecular sizes observed during SDS-PAGE analysis were different from the expected non-glycosylated molecular sizes for 14A7 and 14A8 of 37 kDa and 52 kDa respectively. The observed diffuse bands and molecular weight differences could be attributed to glycosylation of either the PTHR, which has 4 sites in its extracellular domain (Bisello et al., 1996) or GHBP, which has ~5 putative sites (Harding et al., 1994). The influence of glycosylations on protein

expression is further discussed in more detail in chapter 5. In addition, the diffuse bands could be a result of the presence of higher order structures, such as dimers.

In conclusion, integration of target DNA into both stable cell lines was confirmed and expression of target protein from both adherent and suspension adapted cells was achieved by western blotting analysis of expression media. Therefore, the generation of a stable CHO Flp-In cell line of 14A7 and 14A8 was successful allowing for large-scale expression and downstream purification.

Chapter Four - Expression of PTH-Fusions

Abstract:

Aims:

1- To confirm expression using three different culture vessels

2- Large-scale expression and production of PTH fusions

Methods: All PTH fusions were expressed from a suspension adapted CHO stable cell line in roller bottle and shake flask culture as a secreted product. The media was harvested by centrifugation when cell viability was still around 90% or higher. Western blotting confirmed target protein expression from growth media.

Results: Vented RB's were taken forward for further protein expression. A comparative analysis of PTH fusions expression over 12 days revealed that the RB cultures produced a higher level of target protein. Analysis of media samples by western blotting showed that 14A7 appeared as diffuse bands between 37-75 kDa whilst both 14A2c and 14A8 were separating as diffuse bands between 50–75 kDa.

Conclusion: A sufficient amount of protein was obtained in the expression media for all PTH fusions.

4.1 Expression of PTH-Fusions

Stable CHO Flp-In cells expressing the gene of interest were adapted to suspension culture using Hyclone SMF4CHO Utility media or Hyclone media (Sigma-Aldrich) in T75 flasks. Cells were passaged every two or three days. For protein expression studies, cells were grown in roller bottles (RB's) and shake flasks at a starting density of 1 x 10^6 cells/mL at 31°C. Media samples were taken every 2 - 4 days to evaluate and record the cell counts and viabilities. The media was harvested by centrifugation when cell viability was still around 90% or higher. This took approximately 10-12 days. The culture medium was subsequently ~10-fold concentrated using a Vivaflow 200 Tangential Flow concentrator and frozen at -25°C prior to purification (See Section 2.3.5).

4.1.1 Expression of 14A7

14A7 expression was tested using three different culture vessels; non-vented RB, vented RB, and shake flasks. The vessel giving the best expression levels was selected for further investigation.

4.1.1.1 Testing Expression from Non-Vented Roller Bottle Cultures

Table 4.1 shows data for cell density and viability over a 4 day period from non-vented RB. The initial starting cell density was ~1 x 10^6 cells/mL in a volume of 500 mL at a temperature of 31°C. A peak viable cell density of 1.25 x 10^6 cells /mL was achieved on day 4 with a viability of 64%. The culture media on Day 4 was harvested and concentrated ~5-fold using a Vivaflow 200 Tangential Flow concentrator.

Table 4.1: Cell number and viability from non-vented RB culture

Day	Number of viable cells (x10^6/mL)	Number of dead cells (x10^6/mL)	Total number of cells (x10^6/mL)	Viability %
0	0.95	0	0.95	100
4	1.25	0.70	1.95	64

Figure 4.1 shows a western blot analysis of non-vented RB media samples using anti-PTH antibody. No target protein was detected at day 0 (Lane 1) but was detected at day 4, appearing mainly as a double band running between 37-50 kDa (Lane 2). The positive control produced an expected band running at ~50-75 kDa. A negative control sample, consisting of erythropoietin expression media, showed no background detection. Because of the poor performance of the non-vented RB, this was excluded from the study. Next, protein expression was compared between vented RB and shake flask cultures.

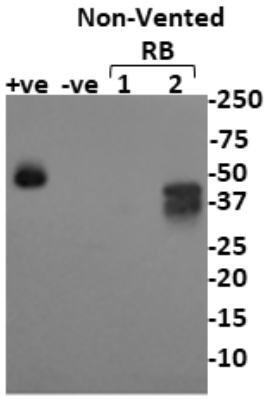

Figure 4.1: Western blot analysis of non-vented RB media samples.

20 µL of media sample was added to 10 µL of loading laemmli buffer before being heated for 15 minutes at 65°C. 6 µL of Bio-Rad All Blue protein standards and 30 µL media sample were loaded per lane. The samples were resolved on a 12% SDS-PAGE under non-reduced conditions followed by western blotting, probing with a mouse anti-human PTH primary antibody. Loading order: **Lane +ve –** Positive control,150 ng of 14A2c); **Lane -ve –** Negative control (10x concentrated EPO media only); **Lane 1 –** Day 0 sample; **Lane 2 –** Day 4 sample.

4.1.1.2 Testing Expression from Vented Roller Bottle and Shake Flask Cultures

This comparison study was repeated twice to validate the results. Both vented RB and shake flasks (both 2 litre volume vessels) were set up at 31°C containing 500 mL of Hyclone Utility media at a starting cell density of ~1 x 10^6 cells/mL. RB was mixed at 6 rpm/minute, whereas shake flasks were mixed at 100 rpm/minute. Samples were taken over the course of 12 days for analysis of cell density, viability and western blotting for target protein expression. Below is a representative example of one of these experiments (full details can be found in Appendix F1 for all experiments).

Experiment 1

Table 4.2 shows the data for cell density and viability over a 12 day period from vented RB and shake flask cultures. Viabilities were maintained at >90% from day 0 to day 12 with peak viable cell densities of 1.93 x10^6 and 2.39 x10^6 cells/mL for RB and shake flasks, respectively. The culture medium was harvested on day 12 and concentrated ~10-fold using a Vivaflow 200 Tangential Flow concentrator and frozen at -25°C.

Table 4.2: Cell number and viability from vented RB and shake flasks

Day	Number of viable cells (x10^6/mL)	Number of dead cells (x10^6/mL)	Total number of cells (x10^6/mL)	Viability %
Batch#1 vented RB's				
0	1.13	0	1.13	100
4	1.21	0	1.21	100
8	1.89	0.01	1.90	99
12	1.93	0.19	2.12	91
Batch #2 Shake flask				
0	1.00	0.02	1.02	98
4	1.86	0.03	1.89	98
8	2.05	0.07	2.12	96
12	2.39	0.15	2.54	94

Batch#1, Total Volume = 2 litres vented RB's (containing 500 mL per RB).
Batch #2 Total Volume = 2 litres shake flask (containing 500 mL per flask).

To confirm the integrity of the expressed 14A7, media samples collected over 12 days were analysed by western blotting using anti-PTH antibody (See Figure 4.2). For vented RBs, target protein was undetectable at day 0 (Lane 1). A progressive increase in target protein expression was noted from Day 4 to Day 12 and appeared as a diffuse band running between 37 and 50 kDa (Lane 2) and 37-75 kDa (Lanes 3 and 4).

In shake flasks, target protein was not detectable on day 0 (Lane 1). However, there was an increase in protein expression from day 4 to day 12, separating as a diffuse band between ~37-50 kDa (Lanes 2 and 3) and ~37-75 kDa (Lane 4). The positive control produced an expected band running at ~50-75 kDa.

Because the vented RB outperformed the shake flask culture in terms of target protein expression, shake flasks were excluded from further study. Therefore, vented RBs was taken forward for use in all subsequent protein expression. All media from these experiments was passed over for purification.

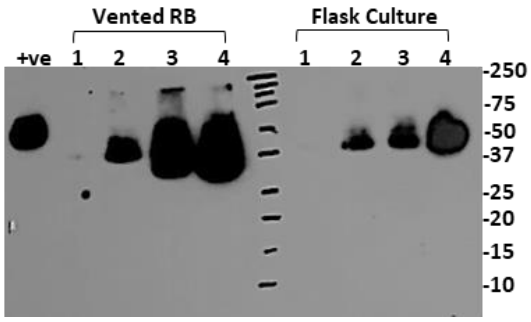

Figure 4.2: Comprising analysis vented RB vs shake flask media samples.

20 µL of media sample was added to 10 µL of loading laemmli buffer before being heated for 15 minutes at 65°C. 6 µL of Bio-Rad All Blue protein standards and 30 µL media sample were loaded per lane. The samples were resolved on a 12% SDS-PAGE under non-reduced conditions followed by western blotting, probing with a mouse anti-human PTH primary antibody. Loading order: **Lane +ve –** Positive control,150 ng of 14A2c); **Lane 1 –** Day 0 sample; **Lane 2 –** Day 4 sample; **Lane 3 –** Day 8 sample; **Lane 4 –** Day 12 sample.

4.1.1.3 Large Scale Expression of 14A7 from Vented Roller Bottle Cultures

Following confirmation of protein expression, stable cells were cultured in vented RB's. Three independent expression experiments were carried out, generating a total of 7 litres expression media (this include the media generated from Section 4.1.1.2) in order to obtain sufficient protein for purification (See Section 2.3.6). The results of these experiments were consistent, as similar results were achieved for cell viability and the day of protein target detection. Below is a representative example of one of these experiments (See Appendix F1 for full details of all experiments).

Experiment 1

Table 4.3 shows the data for cell density and viability over a 12-day period from vented RB. The initial starting cell density was 1.12 x 10^6 cells/mL per 500 mL Hyclone Utility medium in RB and cells were grown at a temperature of 31°C. The cumulative final culture volume was 2 litres (4 x 500 mL RB's). Throughout the experiment viability was maintained at >90% from day 0 to day 12 at which point the media was harvested and processed. Peak cell densities of 1.32 x10^6 cells/mL were achieved on day 12. The culture medium was harvested on Day 12 and concentrated ~10-fold using a Vivaflow 200 Tangential Flow concentrator and frozen at -25°C prior to purification.

Table 4.3: Cell number and viability from vented RB culture

Day	Number of viable cells (x10^6/mL)	Number of dead cells (x10^6/mL)	Total number of cells (x10^6/mL)	Viability %
0	1.12	0	1.12	100
4	1.23	0.02	1.25	99
8	1.25	0.05	1.30	96
12	1.32	0.13	1.45	91

Figure 4.3 shows a representative western blot analysis of 14A7 media samples collected at intervals over 12 days, probing with anti-PTH antibody. The target protein was undetectable at day 0 (Lane 1) but became increasingly detectable from day 4 to 12 (Lanes 2, 3 and 4). 14A7 protein separates as a diffuse band between 37-75 kDa. The positive control produced an expected band running at ~50-75 kDa.

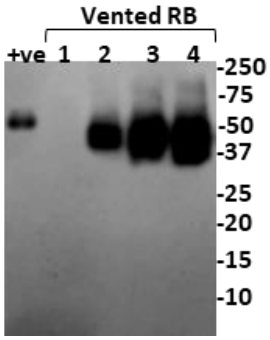

Figure 4.3: Western blot analysis of 14A7 media samples from vented RB.
20 µL of media sample was added to 10 µL of loading laemmli buffer before being heated for 15 minutes at 65°C. 6 µL of Bio-Rad All Blue protein standards and 30 µL media sample were separated on a 12% SDS-PAGE followed by western blotting using mouse anti-human PTH primary antibody. Loading order: **Lane +ve –** Positive control,150 ng of 14A2c); **Lane 1 –** Day 0 sample; **Lane 2 –** Day 4 sample; **Lane 3 –** Day 8 sample; **Lane 4 –** Day 12 sample.

4.1.2 Expression of 14A2c

14A2c protein expression was tested using two different culture vessels, vented RB and shake flasks. The vessel giving the best expression levels was selected for further investigation.

4.1.2.1 Comparison of Vented Roller Bottle and Shake Flask Expression

An initial comparison study was carried out to assess the optimum protein expression vessel between vented RBs and shake flasks. Both vented RB and shake flasks (2 litres volume vessels) were set up at 31°C with each containing 500 mL of Hyclone Utility media at a starting cell

density of ~1 x 10^6 cells/mL. RB's were mixed at 6 rpm/minute, whereas shake flasks were mixed at 100 rpm/minute.

Table 4.4 shows the resulting data for cell density and viability over a 12-day period from vented RB and shake flask cultures. Throughout the experiment, viability was maintained at >90% from day 0 to day 12 with peak cell densities on day 12: 1.93 x10^6 cells/mL for RB and 1.85 x10^6 cells/mL for Shake flasks. The culture medium was harvested on day 12 and concentrated ~10-fold using a Vivaflow 200 Tangential Flow concentrator and frozen at -25°C.

Table 4.4: Cell number and viability from vented RB culture and shake flask

Day	Number of viable cells (x10^6/mL)	Number of dead cells (x10^6/mL)	Total number of cells (x10^6/mL)	Viability %
Batch#1 vented RB's				
0	0.98	0	0.98	100
4	1.28	0.01	1.29	99
8	1.44	0.4	1.48	97
12	1.93	0.15	2.08	92
Batch #2 Shake flask				
0	1.05	0	1.05	100
4	1.16	0.1	1.17	99
8	1.32	0.7	1.39	95
12	1.85	0.11	1.96	94

Batch#1, Total Volume = 2 litre vented RB's (containing 500 mL per RB),
Batch #2 Total Volume = 2 litre Shake flask (containing 500 mL per flask).

To confirm the integrity of the expressed 14A2c protein, media samples were analysed by western blotting using anti-PTH antibody (See Figure 4.4). For the vented RB samples, target protein was detected at day 0 as a faint band at ~75 kDa (Lane 1), followed by an increase in detectable protein expression from day 4 to 12 (Lanes 2, 3 and 4), separating as a diffuse band between 50-75 kDa. The positive control produced an expected band running at ~50-75 kDa.

In shake flasks, target protein was not detectable on day 0 and day 4 (Lanes 1 and 2), but was detected at day 8 as a faint band at ~75 kDa (Lane 3). Expression increased dramatically from

day 8 to 12 and appeared as a diffuse band on day 12, running between 50-75 kDa (Lane 4). Although both vented RB's and shake flask cultures produced reasonable levels of expression, however, RB's were taken forward for use in further protein expression, consistent with earlier established methodology for 14A7. Consequently, use of shake flask was excluded from further expression study.

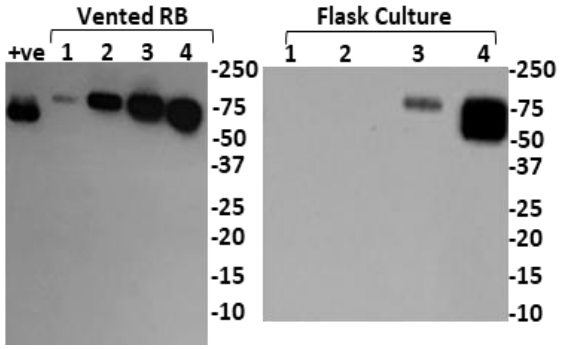

Figure 4.4: Western blot analysis of media samples from vented RB vs shake flask media samples.

20 µL of media sample was added to 10 µL of loading laemmli buffer before being heated for 15 minutes at 65°C. 6 µL of Bio-Rad All Blue protein standards and 30 µL media sample were loaded per lane. The samples were resolved on a 12% SDS-PAGE under non-reduced conditions followed by western blotting, probing with a mouse anti-human PTH primary antibody. Loading order: **Lane +ve –** Positive control,150 ng of 14A2c) **Lane 1 –** Day 0 sample; **Lane 2 –** Day 4 sample; **Lane 3 –** Day 8 sample; **Lane 4 –** Day 12 sample.

4.1.2.2 Large Scale Expression of 14A2c from Vented Roller Bottle Cultures

Following confirmation of protein expression in vented RB's, the stable cells were cultured and expanded for large-scale protein expression (See Section 2.3.5). The initial starting cell density was 1.16 x 10^6 cells/mL in a 500 mL culture volume per RB, and cells were grown at a temperature of 31°C. The sum-total culture volume for expression was 2 litres (4 x 500 mL RB's). Table 4.5 shows data for cell density and viability over a 12 day period from vented RB. Throughout the experiment viability was maintained at >90% from day 0 to day 12 with a

viable peak cell density of 1.91 x10^6 cells/mL on day 12. The culture medium was harvested on day 12 and concentrated ~10-fold using a Vivaflow 200 Tangential Flow concentrator and frozen at -25°C prior to purification.

Table 4.5: Cell number and viability from vented RB culture

Day	Number of viable cells (x10^6/mL)	Number of dead cells (x10^6/mL)	Total number of cells (x10^6/mL)	Viability %
0	1.16	0.0	1.16	100
4	1.66	0.00	1.66	100
8	1.75	0.04	1.79	96
12	1.91	0.15	2.06	92

Figure 4.5 shows a western blot using anti-PTH antibody of samples collected over 12 days. Target protein expression was undetectable at day 0 (Lane 1) but became increasingly detectable from day 4 to 12 (Lanes 2, 3 and 4). 14A2c separates as a diffuse band between 50-75 kDa. The positive control produced an expected band running at ~50-75 kDa.

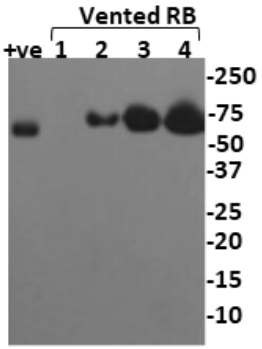

Figure 4.5: Western blot analysis of 14A2c from vented RB media samples.
20 µL of media sample was added to 10 µL of loading laemmli buffer before being heated for 15 minutes at 65°C. Then 6 µL of Bio-Rad All Blue protein standards and 30 µL media sample were loaded per lane and resolved on a 12% SDS-PAGE followed by western blotting probing with a mouse anti-human PTH primary antibody. Loading order: **Lane +ve –** Positive control,150 ng of 14A2c); **Lane 1 –** Day 0 sample; **Lane 2 –** Day 4 sample; **Lane 3 –** Day 8 sample; **Lane 4 –** Day 12 sample.

4.1.3 Expression of 14A8

14A8 expression was tested using two different culture vessels, vented RB and shake flasks. The vessel giving the best expression level was selected for further investigation.

4.1.3.1 Comparison of Vented Roller Bottle and Shake flask Expression

This comparison study was used to assess 14A8 protein expression levels in vented RB's and shake flask. Vented RB and shake flasks (both 2 litre volume vessels) were set up at 31°C each containing 500 mL of Hyclone Utility media at a starting cell density of ~1 x 10^6 cells/mL. RB's were mixed at 6 rpm/minute, whereas shake flasks were mixed at 100 rpm/minute.

Table 4.6 shows the resulting data of cell density and viability from vented RB and shake flask cultures, taken at intervals over a 12-day period. Throughout the experiment, viability was maintained at >90% from day 0 to day 12 with peak viable cell densities of 1.55 x 10^6 and 1.22 x 10^6 cells/mL achieved for RB and shake flasks on day 12, respectively. Culture medium was harvested on day 12 and concentrated ~10-fold using a Vivaflow 200 Tangential Flow concentrator and frozen at -25°C.

Table 4.6: Cell number and viability from vented RB culture and shake flask

Day	Number of viable cells (x10^6/mL)	Number of dead cells (x10^6/mL)	Total number of cells (x10^6/mL)	Viability %
Batch#1 vented RB's				
0	1.02	0.04	1.06	96
4	1.19	0.01	1.20	99
8	1.26	0.07	1.33	95
12	1.55	0.11	1.66	93
Batch #2 Shake flask				
0	0.96	0	0.96	100
4	0.98	0	0.98	100
8	1.02	0.07	1.09	93
10	1.22	0.16	1.38	89

Batch#1, Total Volume = 2 litre vented RB's (containing 500 mL per RB).
Batch #2 Total Volume = 2 litre Shake flask (containing 500 mL per flask).

To confirm the integrity of the expressed 14A8, media samples were analysed by western blotting using anti-PTH antibody (See Figure 4.6). From vented RBs, the target protein expression was undetectable at day 0 (Lane 1) but became increasingly detectable from day 4 to 12 (Lanes 2, 3 and 4), separating as a diffuse band between 50-250 kDa.

In shake flasks, target protein was not detectable on day 0 and day 4 (Lanes 1 and 2). Target protein gradually increased in expression from day 8 to 12. At day 8 it appeared as a band at ~50-75 kDa (Lane 3) and at day 12 appeared as a more diffuse band running between 50-250 kDa (Lane 4). The positive control produced an expected band running at ~50-75 kDa.

Whilst both vented RB's and shake flask cultures produce reasonable levels of expression, RB's were taken forward for use in protein expression.

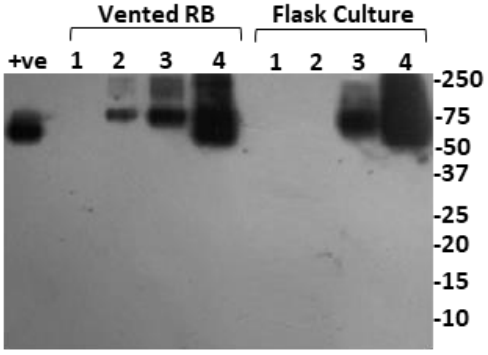

Figure 4.6: Western Blot Analysis of 14A8 from Vented RB Media Samples
20 µL of media sample was added to 10 µL of loading laemmli buffer before being heated for 15 minutes at 65°C. Then 6 µL of Bio-Rad All Blue protein standards and 30 µL media sample were loaded per lane and resolved on a 12% SDS-PAGE followed by western blotting probing with a mouse anti-human PTH primary antibody**.** Loading order: **Lane +ve –** Positive control,150 ng of 14A2c); **Lane 1 –** Day 0 sample; **Lane 2 –** Day 4 sample; **Lane 3 –** Day 8 sample; **Lane 4 –** Day 12 sample.

4.1.3.2 Large Scale Expression of 14A8 from Vented Roller Bottle Cultures

Following confirmation of protein expression, the stable cells were cultured and expanded into 2 Litres vented RB's for large-scale protein expression (See Section 2.3.5). The initial starting cell density was ~1 x 10^6 cells/mL. Cultures were grown at a temperature of 31°C in a final volume of 2 Litres (4 x 500 mL RB's) in Hyclone Utility medium.

Table 4.7 shows the expression profile (cell density and viability) of the culture at intervals over a 12-day period. Throughout the experiment, viability was maintained at >90% from day 0 to day 12 with a peak viable cell density of 1.45 x10^6/mL on day 12. The culture medium was harvested on Day 12 and concentrated ~10-fold using a Vivaflow 200 Tangential Flow concentrator and frozen at -25°C prior to purification.

Table 4.7: Cell number and viability from vented RB culture

Day	Number of viable cells (x10^6/mL)	Number of dead cells (x10^6/mL)	Total number of cells (x10^6/mL)	Viability %
0	1.02	0.02	1.04	98
4	1.25	0.03	1.28	98
8	1.34	0.05	1.39	96
12	1.45	0.15	1.60	91

Figure 4.7 shows a western blot of media samples collected over 12 days, when probed with an anti-PTH antibody. Target protein expression was undetectable at day 0 (Lane 1) but became increasingly detectable from day 4 to 12 (Lanes 2, 3 and 4), separating as a diffuse band between 50-250 kDa. The positive control produced an expected band running at ~50-75 kDa. The negative control sample, consisting of erythropoietin expression media, showed no background detection.

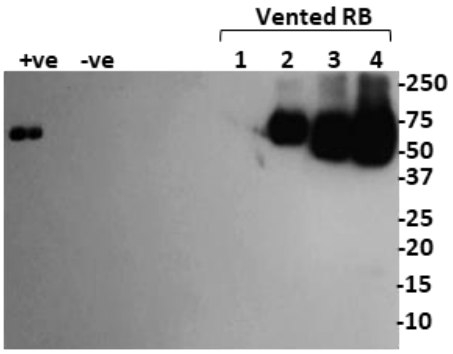

Figure 4.7: Western blot analysis of 14A8 from vented RB media samples.
20 µL of media sample was added to 10 µL of loading laemmli buffer before being heated for 15 minutes at 65°C. Then 6 µL of Bio-Rad All Blue protein standards and 30 µL media sample were loaded per lane and resolved on a 12% SDS-PAGE followed by western blotting probing with a mouse anti-human PTH primary antibody. Loading order: **Lane +ve –** Positive control,150 ng of 14A2c); **Lane -ve –** Negative control (10x concentrated EPO media only); **Lane 1 –** Day 0 sample; **Lane 2 –** Day 4 sample. **Lane 3 –** Day 8 sample; **Lane 4 –** Day 12 sample.

4.2 Discussion

All PTH fusions were expressed as secreted proteins directed by the PTH signal sequence and propeptide. In the previous chapter, it was successfully shown that all PTH fusions contained the correct integrated gene of interest and could be stably expressed from a CHO cell line. Protein expression experiments under mild hypothermic conditions confirmed expression of the PTH-fusions by western blotting of media samples.

Both vented RB and shake flask cultures 14A7 maintained a high viability of ~90% up to day 12, when media was harvested. Analysis of media samples by western blotting showed that 14A7 appeared as diffuse bands between 37-75 kDa and that the RB cultures produced a higher level of target protein. The reasons for this are unknown but could be due to a lack of adaptation time to shake flask culture, as cells were cultured directly from RB cultures. Another reason may be aeration factor as RB's were mixed at 6 rpm/minute, and the larger

surface area may have facilitated better aeration. It may also be that these particular proteins express better in RB cultures. Shake flask cultures were consequently discarded as a possible expression system.

On the other hand, non-vented RB's did not retain the same viability or productivity as vented RB's and shake flask cultures and expression was halted after 4 days due to a dramatic loss in viability (< 65%). The observed low viability could be attributed to inefficient aeration, as cells were cultured in 500 mL of media in a 2 litres RB (according to the personal communication from Dr Ian Wilkinson: expression was more consistent using 100-200 mL of media per RB which helped improve aeration and cell viabilities). Therefore, the non-vented RB was demonstrated to be an inefficient system for expressing 14A7 as the cell viability was low and the protein expression poor. If lower volumes were used then this would lower the overall amount of expression media generated from a single run and would not be viable to produce sufficient protein required for downstream studies. In view of these outcomes, vented RB's were chosen to carry out large-scale expression in order to increase the culture volume and density, and thereby maximise culture productivity for 14A7 protein expression.

In 14A2c and 14A8 vented RB and shake flask cultures, a high viability of >90% was maintained over the 12-day culture. Analysis of media samples by western blotting showed both fusions separating as diffuse bands between 50–75 kDa. Although there were indications of similar levels of expression for these fusions in both RB and Shake flask cultures, RB's were taken forward for further protein expression. One main reason was that with the laboratory facilities available, a higher volume of culture media could be used for RB's cultures, up to 4 litres (8 x RB's), as compared to a shake flask volume of only 1 litre (2 x shake flasks).

In this study, we utilised the Chinese hamster ovary (CHO) cell line as it is well characterised, easy to grow and is ideal for high expression levels of target protein. Stable cell lines were constructed using the Flp-In system (Invitrogen) which allowed for the quick establishment of a stable isogenic clone. Also, all PTH fusions were expressed under the control of the CMV promoter as a secreted product directed by the native secretion signal sequence and cells were easily adapted to serum free media conditions using Hyclone SFM4CHO media. There are other cell lines that could also have been utilised, such as Human Embryonic Kidney (HEK) cells which can mimic the glycosylation pattern that occurs in humans (Dumont et al., 2016, Swiech et al., 2012). However, comparatively CHO cells have the ability to efficiently perform posttranslational processes and recombinant proteins produced by CHO cells possess similar glycosylation profiles to native proteins (Damiani et al., 2009). Furthermore, the CHO cell line is an industry standard for recombinant therapeutic proteins production and many protein drugs are manufactured in this system (mostly antibodies) without problems (Wurm, 2004, Jayapal et al., 2007). They are able to produce ~ 3-10 g/L of recombinant protein (Wurm and Hacker, 2011).

We utilised mild hypothermic conditions to try and improve protein expression and prolong the viability of the culture. Many studies have shown that low culture temperature improves recombinant protein production in mammalian cells and may protect our protein from proteolysis. The advantages of using low temperatures is that it maintains high cell viability, suppresses medium consumption, and extends the production phase through maintaining a higher proportion of cells in G1 phase of the cell cycle (Kaufmann et al., 2001, Yoon et al., 2003, Ritacco et al., 2018, Damiani et al., 2009). This observation was consistent with a published expression study in which Yoon et al. (2003) showed that the erythropoietin

expression in CHO cells was increased 2.5-fold when the temperature was decreased to 33°C compared to growing cells at the higher temperature of 37°C.

In addition to low temperature, other simple media additions have proved useful in increasing protein expression, which are cheap and easy to do and could perhaps be included in future expression studies. A good example is lithium chloride, which arrests the cell cycle in the G2/M phase and regulates apoptosis (Pastor et al., 2009). Furthermore, Ha et al. (2014) showed that adding 10 mM of lithium chloride to the media increased expression of an Fc-fusion protein by 2.1-5 fold in a CHO cell line. Additionally, small peptides such as insulin-like growth factor-I (IGF-I) has been demonstrated to improve growth and productivity by inhibition of apoptosis (Adamson and Walum, 2007). Other media additions that are known to inhibit histone deacetylases and arrest cells in the G1 phase, such as valproic acid and sodium butyrate, have been evaluated for their effect on recombinant protein expression in CHO and other mammalian cell lines (Backliwal et al., 2008, Chen et al., 2011). For example, Backliwal et al. (2008) showed that adding valproic acid to the media increased the expression yield at least 1.5-fold in yield for an antibody produced in CHO cells.

Future experiments optimising culture conditions in combination with low temperature may be beneficial in increasing the expression yield of PTH-fusions. This view is consistent with a published expression study by Kantardjieff et al. (2010) showing that the production of recombinant IgG in CHO cells increased 6-fold when the temperature was decreased to 33°C in combination with 2 mM sodium butyrate compared to untreated cells at 37°C. Moreover, in a recent study by Johari et al. (2021) the combination of reduced temperature and valproic acid increased viable cell density at least 1.4-fold but also increased production of trimeric SARS-CoV-2 spike protein by CHO cells up to ~53 mg/L.

There are various methods of making stable cell lines such as creating a stable cell line followed by clonal selection in antibiotic selection media. However, this can be very time consuming. There are many advantages to using the Flp-In stable cell line generation method which is quick and easy and cells adapt well to Hyclone media. It is also a proven system of protein expression used in previous work on GH fusions (Wilkinson et al., 2016). Future experiments optimising culture conditions may be beneficial in increasing the expression yield of PTH-fusions.

In conclusion, for all constructs, a sufficient amount of expressed protein was obtained and progressed to downstream purification studies.

Chapter Five - PTH Fusion Purification

Abstract:

Aims:

1- Purify three protein fusions through a combination of ion exchange and affinity chromatography and analyse by Coomassie staining and Western blotting.

2- Resultant final purified protein preparations to be taken forward for bioactivity assessment *in vitro*.

Methods: Fusions were expressed in suspension culture in roller bottles as a secreted product and purified by ion exchange and affinity chromatography. Samples were analysed by SDS-PAGE followed by Coomassie staining and Western blotting using both anti-GHBP and anti-PTH antibodies.

Results: Protein expression for all PTH fusions was confirmed by western blotting. 14A7 separated as diffuse bands between 37 and 50 kDa and purified to 0.93 mg/mL. 14A2c and 14A8 separated as diffuse bands between 75 and 100 kDa and purified to 2.57 mg/mL and 2.29 mg/mL, respectively.

Conclusion: Preliminary purification of PTH fusion molecules was achieved and samples taken forward for *in vitro* bioactivity measurements.

5.1 Purification of PTH-Fusions

Characterisation of protein function, structure, and interactions is vital for understanding all fundamental biological phenomena. This requires protein purification, which involves a series of processes designed to isolate a single protein type from a mixture of biomolecules that were produced in a heterologous expression system. The choice of these processes and the success with which they are performed will impact the outcome of the subsequent functional and structural investigations of the protein of interest (Walls et al., 2010). In the present study, PTH fusions were stably expressed in a CHO cell line adapted to suspension culture. The CHO cells utilised for this purpose were grown in roller bottle (RB) cultures and expression media taken and centrifuged to pellet cell debris. The supernatant was subsequently collected and 10 mM of benzamidine HCl and 5 mM of EDTA added. Finally, media samples were concentrated ~10-fold using a Vivaflow 200 concentrator, and frozen at -25°C until required for purification.

In preparation for the purification process, concentrated media samples were defrosted overnight at 4°C and centrifuged to clear. Purification commenced by loading the media on to a Q-Sepharose column (GE Healthcare Life Sciences) run in a flow-through mode (as described in Section 2.3.6.1). This step allowed for a clean-up of target protein prior to binding in the affinity column. The unbound fraction containing the majority of the target protein, was loaded on to a 10B8 (anti-GHBP) affinity column as described in Section 2.3.6.2. The unbound fraction was collected whilst bound protein eluted using 0.2 M glycine, pH 2.7. To maximise the amount of purified product obtained the unbound fraction was passed over the affinity column once again and protein eluted as described above. After a series of concentration and

dialysis steps, purified protein was quantified spectrophotometrically at A_{280} and samples aliquoted and frozen at -80°C.

Samples were collected at each stage of the purification process and protein concentrations calculated using Bradford assay (Section 2.3.2.1) and/or A_{280} (Section 2.3.2.2). Finally, analyses were performed by SDS-PAGE (Section 2.3.1.1) followed by coomassie staining (Section 2.3.1.1.2.1) and western blotting (Section 2.3.1.1.2.2).

5.1.1 Purification of 14A7

Frozen media samples were defrosted overnight at 4°C, centrifuged to clear, and purified using two purification resins, as discussed in the preceding section. The conductivities of media samples and binding buffer used for purification were confirmed to be ≥30 mS and 15−20 mS, respectively. For the purification of 14A7, a total of 7 litres media sample from RB culture was used. Throughout this process, all protein samples were analysed by SDS-PAGE followed by coomassie staining and western blotting. Final purified protein was pooled, concentrated and taken forward for *in vitro* bioactivity assessment. A representative example of the methodology adopted is described below. Purification analysis is described in Appendix G1.

Experiment 1

14A7 expression media from a 2 litres RB culture (Section 4.1.1.3) was concentrated to 215 mL containing 895 mg of protein (See Table 5.1). The concentrated sample was loaded onto a Q-Sepharose column followed by rinsing with 40 mL of binding buffer. Spectrophotometric analyses confirmed that the unbound fraction (Q-Unbound) contained 602 mg of protein - equivalent to ~70% of the total protein loaded. The wash and elution steps contained a total

of 270 mg, about 30% of the total protein loaded. Next, the Q-Unbound fraction was passed over the affinity column and 481 mg of protein recovered – equivalent to ~80% of total protein in the unbound fraction. A further 4.7 mg, ~1 % of total protein, was obtained in the wash step. Bound protein was eluted with 0.2 M glycine, pH 2.7 in 3 elution volumes. The first 20 mL elution fraction (E1) yielded 2.9 mg of protein followed by two further 10 mL elution fractions (E2 and E3) with 0.22 mg and 0.18 mg of protein recovered, respectively. All elution fractions with a detectable amount of protein were pooled together, resulting in a total volume of 40 mL containing 5.8 mg of protein, ~ 1.2% recovery. This was further concentrated to 2 mL (PC1) with an 85% loss and final 0.88 mg of protein recovery. The sample was dialysed in citrate buffer, pH 6.0 resulting in a further loss of ~41% and 0.52 mg of protein recovered (PD1) in a final volume of 1.2 mL.

To increase total protein recovery, the unbound fraction from the initial purification run was passed over the affinity column once again and the process described above repeated with 466.4 mg of protein obtained, ~80% of the total protein loaded. The first elution fraction (E1) yielded 1.06 mg of protein. However, no protein was recovered from other elution fractions. Therefore, the first eluted fraction was concentrated to 1.4 mL volume (PC2) and contained 0.59 mg of protein; 44% protein was lost during the concentration step. Finally, the sample was dialysed in citrate buffer pH 6.0, resulting in a further ~32% protein loss with 0.72 mg of protein (PD2) recovered in a final volume of 1 mL.

The purified protein obtained in both runs was quantified spectrophotometrically by measuring the absorbance at 280nm wavelength (A_{280}), giving 0.53 mg and 0.4 mg, respectively. Thus, 2.2 mL containing 0.93 mg of protein was obtained.

Subsequent 14A7 purification experiments yielded variable protein recovery rates, with protein losses ranging from 33% to 85% during the concentration steps and 20% to 40% in the dialysis steps. Details are available in Appendix G4.

Table 5.1: Protein assays of 14A7 samples taken during the purification

Protein levels were calculated using Bradford Assay and A_{280}

Samples	Volume (mL)	µg/mL	Total protein (mg)	% Recovery
Source-Q Purification				
Load	215	4164.4	895.3	100
Q-UB	240	2511.7	602.8	70
Q-Wash_Elute	100	2708.3	270.8	30
Affinity Purification				
Run #1				
UB-1	260	1850	481	80
Wash-1	100	47.4	4.7	1
Elution 1	20	138.2	2.9	0.46
Elution 2	10	22.3	0.22	0.04
Elution 3	10	19	0.18	0.03
Pooled elutions (PE1)	40	147.1	5.8	1.2
Post-concentration (PC1)	2	441	0.88	15*
Post-dialysis (PD1)	1.2	433.7	0.52	59**
Run #2				
UB-2	280	1665.9	466.5	97
Wash-2	100	26.5	2.6	1
Elution 1	20	52.8	1.06	0.22
Elution 2	10	0	0	0
Elution 3	10	0	0	0
Pooled elutions (PE1)	20	52.8	1.06	0.22
Post-concentration (PC2)	1.4	423.2.2	0.59	56*
Post-dialysis (PD2)	1	717.1	0.72	68**
Final Analysis of Purified Protein by A_{280}				
Samples	**Volume (mL)**	**Mean A_{280}**	**mg/mL**	**Total protein (mg)**
Post-dialysis (PD1)	1.2	0.87	0.44	0.53
Post-dialysis (PD2)	1	0.79	0.40	0.40

Source-Q Purification; Q-Sepharose column was run in flow-through mode.

Affinity Purification (Run #1): The unbound fraction from the Source-Q column was used as the load for the first run (Run #1) on the 10B8 affinity column

Affinity Purification (Run #2): The unbound fraction from the first run was passed again over the 10B8 affinity column (Run #2).

***** PC1&2 percentage recoveries were derived from comparison with PE1&2

****** PD1&2 percentage recoveries were derived from comparison with PC1&2

Coomassie and western blotting analyses of the purification samples from both Q-Sepharose and affinity columns are shown in Figures 5.1A and 5.1B respectively. In Figure 5.1B the western blot of samples from the first purification step using Q-Sepharose revealed that the majority of 14A7 separated between 37 and 75 kDa and was captured in the unbound fraction. However, a small fraction of higher molecular-weight species, containing ~30% of the total protein and running between 50−250 kDa, were present in the wash/elution fractions. In Figure 5.1A, Coomassie stain analysis showed a large amount of protein present in the unbound fractions from the affinity column (Lanes 4 and 7). Western blotting confirmed the presence of 14A7 (Figure 5.1B, Lanes 4 and 7). It is noteworthy that the band intensity of 14A7 remained unchanged even after two passes over the affinity column indicating that 14A7 did not bind efficiently to the affinity column and detectable amount of this protein was still present in all unbound fractions (Lanes 4 and 7). Even though the purification process was inefficient, sufficient amount of target protein was successfully purified as seen in Figure 5.1 Lanes 6 and 9, as bands separating between ~37 and 50 kDa. The final product was >95% pure as no degradation and contamination was observed during the post-purification processes, as evidenced by coomassie stain and western blotting analysis. The post-concentrated (PC) and post-dialysis (PD), samples for both purification are seen as diffuse bands running between 37 and 50 kDa (Figures 5.2A and 5.2B).

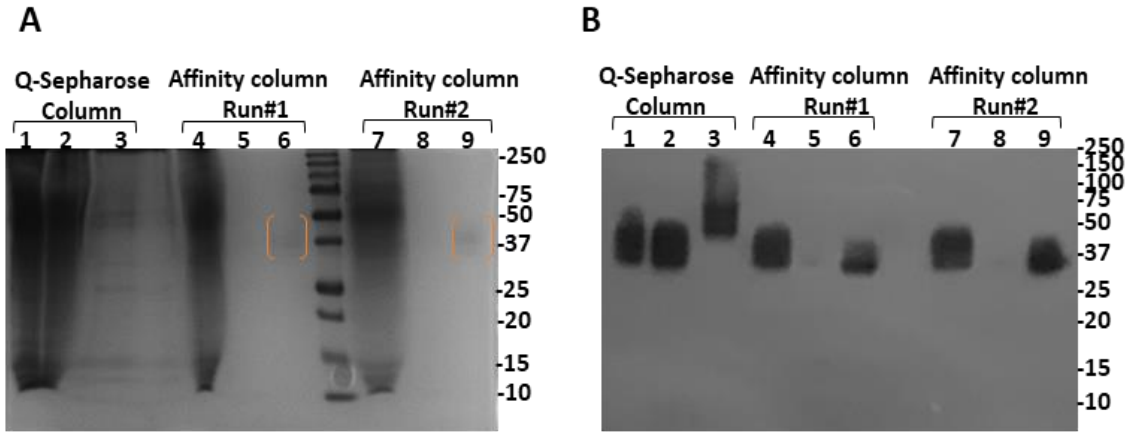

Figure 5.1: 12% SDS-PAGE under non-reduced conditions of 14A7 samples collected from Q-Sepharose and Affinity columns for Run #1 and Run #2.

(A) Coomassie staining and **(B)** Western blot using mouse anti-human PTH primary antibody. 40 µL of a sample was added to 20 µL of loading laemmli buffer before being heated for 15 minutes at 65°C. 30 µL were loaded for Coomassie staining and 6 µL for Western blotting; **Lane 1 –** Load sample; **Lane 2 –** Q-Unbound fraction; **Lane 3 –** Wash/Elution sample; **Lane 4 –** 10B8-Unbound fraction; **Lane 5 –** Wash sample; **Lane 6 –** Pooled elution sample; **Lane 7 –** 10B8-Unbound fraction; **Lane 8 –** Wash sample; **Lane 9 –** Pooled elution sample. Bio-Rad All Blue protein standards 6 µL were loaded.

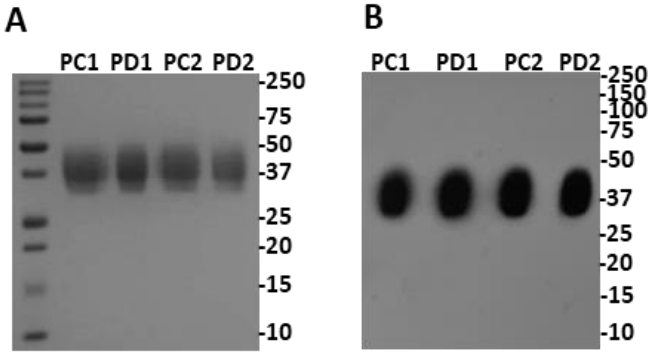

Figure 5.2: 12% SDS-PAGE under non-reducing conditions of 14A7 samples from Run #1 and Run #2.

(A) Coomassie staining (5µg/lane) and **(B)** Western blot using mouse anti-human PTH primary antibody (~150 ng/lane). 40 µL of a sample was added to 20 µL of loading laemmli buffer before being heated for 15 minutes at 65°C. Bio-Rad All Blue protein standards (6 µL per lane); **Lane 1 –** Post-concentration (PC1); **Lane 2 –** Post-Dialysis (PD2); **Lane 3 –** Post-concentration (PC2); **Lane 4 –** Post-Dialysis (PD2).

5.1.1.1 Final 14A7 Sample Preparation

Three separate purification experiments were carried out to generate sufficient pure protein for bioactivity assessment and *in vivo* studies. For preparation final sample, all PC samples were then pooled from each experiment (PPD). Samples were then concentrated (PDC) followed by a final spin (Final).

Table 5.2 shows the amount of 14A7 recovered from each experiment with the amount of purified protein obtained varying considerably, from 0.23 to 0.465 mg/L. Further details can be found in Appendix G1.

As indicated in Table 5.3, all dialysed and concentrated samples were pooled (PPD) to obtain 2.25 mg of protein in a total volume of 4.5 mL. Samples were then concentrated to 1.5 mL (PDC) followed by a final spin (Final) to give 1.3 mg of protein at 0.93 mg/mL obtained from 7 litres of culture media. This was equivalent to an overall loss of 42%, mainly stemming from inefficiency of the concentration step. Coomassie staining and western blot analysis of these samples are presented in Figures 5.3A and 5.3B, and show diffuse banding at 37−50 kDa with no signs of degradation or contamination. Samples were considered suitable for further testing of bioactivity.

Table 5.2: The amount of recovered 14A7 from the 3 separate purifications.

Experiment	Culture volume	Total protein recovered (mg/L)	Total protein (mg)
1	2L	0.84	0.93
2	2L	1.03	0.92
3	3L	1.73	0.7

Table 5.3: Final analysis of purified 14A7 samples were calculated using A_{280}

Sample	Volume (mL)	Mean A_{280}	mg/mL	Total protein (mg)
All Dialysed elutions (PPD)	4.5	1	0.50	2.25
post-con (PDC)	1.5	1.80	0.91	1.36
Final	1.4	1.85	0.93	1.30

PPD; all dialysed sample from all three experiment 14A7 were defrosted and pooled together.

PDC; pooled dialysed sample were concentrated using Centriprep-30 concentrator at 2500 rpm ((Millipore Inc.) for 20 minutes.

Final: 1 minute spin at 13k rpm on bench top centrifuge.

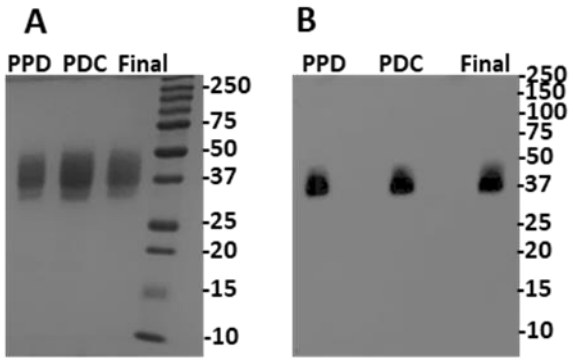

Figure 5.3: Analysis of final purified samples by 12% SDS-PAGE under non-reducing conditions. **(A)** Coomassie staining (5 µg per lane) and **(B)** Western blot of 14A7 samples (150 ng per lane) using mouse anti-human PTH primary antibody. Samples were heated for 15 minutes at 65°C. Bio-Rad All Blue protein standards (6 µL per lane); **Lane 1 –** Pooled, Post Dialysis (PPD); **Lane 2 –** Post-concentration (PDC); **Lane 3 –** Final.

5.1.2 Purification of 14A2c

Frozen media samples were defrosted overnight at 4°C, centrifuged to clear, and purified using two purification resins, as discussed in the preceding section. The conductivities of the media samples and binding buffer were confirmed to be ≥30 mS and 15−20 mS, respectively. Next, a 2 litres 14A2c RB culture was purified, consistent with 14A7 purification methodology. Throughout this process, all samples were assessed by SDS-PAGE followed by coomassie staining and western blotting. Final purified protein factions were pooled, concentrated, and

taken forward for *in vitro* bioactivity assessment. A representative example of the methodology adopted is described below. Purification analysis is described in Appendix G2.

Experiment 1

14A2c expression media from a 1-litre RB culture (Section 4.1.2.2) was concentrated to 105 mL containing 233 mg of protein (Table 5.4). The concentrated sample was subsequently loaded onto a Q-Sepharose column followed by rinsing with 40 mL of binding buffer. The unbound fraction (Q-Unbound) contained 185.8 mg of protein, equivalent to ~80% of the total protein loaded. Next, 50.8 mg of protein - approximately 22% of the total protein loaded - was recovered from the wash and elution steps. To increase total protein recovery, the Q-Unbound fraction from above was passed over the affinity column and 170 mg of protein - equivalent to ~92% of the total protein in the unbound fraction - was obtained in the unbound fraction. A further 3.8 mg – equivalent to ~2 % of total protein - was obtained after the wash step. The first elution (E1) was carried out using 20 mL of 0.2 M glycine, pH 2.7 yielded 2.4 mg of protein and a subsequent 10 mL elution yielded a further 0.22 mg. Further protein elution attempts failed to yield any protein. Therefore, the two elution fractions with a detectable amount of protein were pooled together, resulting in a total volume of 30 mL containing 3.9 mg of protein. This amounted to ~2% recovery of the load sample. Next, the pooled elution fractions were further concentrated to 3.2 mL (PC1) with 3.3 mg of protein recovered and a 15 % loss of protein. Subsequent dialyses of concentrated samples in citrate buffer pH 6.0 resulted in a further loss of ~28% to give a final protein yield (PD1) of 2.4 mg in 1.9 mL volume.

In the next purification run, the unbound fraction was passed over the affinity column once again as described above, and 152.4 mg of protein was retained in the unbound fraction which was equivalent to ~90% of the total protein loaded. The first elution fraction (E1) was

obtained using 20 mL of 0.2 M glycine pH 2.7 with 3.1 mg of protein recovered. Additional 1.2 mg of protein was recovered upon further elution with 10 mL glycine elution buffer to give a total elution yield of 2.7mg in 30mL (equivalent to ~1.6% recovery). Subsequent elution attempts yielded no protein. Next, the two elution fractions were pooled and concentrated to 3 mL and 2.2 mg of protein recovered post-concentration (PC2). Approximately 19% of protein was lost during this concentration step and additional 37% loss was observed when concentrated sample was dialyses in citrate buffer, pH 6.0 to give a final protein yield of 1.4 mg in 1.7 mL post-dialysis (PD2).

The final protein yields obtained from both purification runs were 1.28 mg and 1.11 mg, estimated using A_{280} quantification and an extinction coefficient of 1.944 for a 1 mg/mL solution. The extinction coefficient was obtained using online Expasy Protoparam software (See Section 2.3.2.2). In summary, 3.6 mL of media containing 2.39 mg of protein was obtained in these experiments.

Table 5.4: Protein assays of 14A2c samples taken during the purification

Protein levels were calculated using the Bradford Assay and A_{280}

Samples	Volume (ml)	µg/ml	Total protein (mg)	% Recovery
Source-Q Purification				
Load	105	2218.8	233.0	100
Q-UB	145	1281.6	185.8	80
Q-Wash_Elute	100	507.5	50.8	22
Affinity Purification				
Run #1				
UB_1	175	971.9	170.1	92
Wash-1	100	38.2	3.8	2
Elution 1	20	121.8	2.4	1.31
Elution 2	10	21.8	0.22	0.12
Elution 3	10	0	0	0
Pre-Dialysis (PE1)	30	129.2	3.9	2
Post-concentration (PC1)	3.2	1032.2	3.3	85*
Post-Dialysis (PD1)	1.9	1243.3	2.4	72**
Run #2				
UB2	195	781.5	152.4	90
Wash-2	100	28.5	2.9	2
Elution 1	20	153.2	3.1	1.8
Elution 2	10	120.6	1.2	0.71
Elution 3	10	0	0	0
Pre-Dialysis (PE2)	30	90.1	2.7	1.59
Post-concentration (PC2)	3	728.7	2.2	81*
Post-Dialysis (PD2)	1.7	812.3	1.4	63**
Final Analysis of Purified Protein by A_{280}				
Samples	**Volume (mL)**	**Mean A_{280}**	**mg/ml**	**Total protein (mg)**
Post-Dialysis (PD1)	1.9	1.31	0.67	1.28
Post-Dialysis (PD2)	1.7	1.27	0.66	1.11

Source-Q Purification; Q-Sepharose column was run in flow-through mode.

Affinity Purification (Run #1); The unbound fraction from the Source-Q column was used as the load for the first run (Run #1) on the 10B8 affinity column.

Affinity Purification (Run #2); The unbound fraction from the first run was passed again over the 10B8 affinity column (Run #2).

***** PC1&2 percentage recoveries were derived from comparison with PE1&2

****** PD1&2 percentage recoveries were derived from comparison with PC1&2

Coomassie and western blotting analyses of purification samples from both Q-Sepharose and affinity columns are shown in Figures 5.4A and 5.4B. In the first purification step using Q-Sepharose, the majority of 14A2c was retained in the unbound fraction which is seen running between 50 and 100 kDa. Also, a large amount of protein was in the unbound fractions from the affinity chromatography (Figure 5.4, Lanes 4 and 7). The western blotting analyses confirmed that these fractions contained 14A2c (Figure 5.4B, Lanes 4 and 7). However, 14A2c did not bind efficiently to the affinity column as it was still detectable in the unbound fractions after two passes over the affinity column, as evidenced by no observable changes to the band intensity of the unbound fractions (Lanes 4 and 7). Despite the inefficiency of the purification process, some target protein could be purified, as separated bands were detected in the pooled elution samples from both runs when analysed by western blotting (between ~ 75 and 100 kDa, Lanes 6 and 9). The purified products from the two experimental runs were pooled, concentrated, and dialysed in citrate buffer. Coomassie staining and western blot analysis of the samples are presented in Figures 5.5A and 5.5B, respectively, and showed 14A2c separated as a diffuse band at 75-100 kDa. Additional faint bands at ~37 kDa (possible cleaved fusion protein) were also observed in the coomassie stained gel analysis. In summary, even though the overall protein loss was high across all purification stages, the amount of protein recovered was sufficient for further characterisation studies.

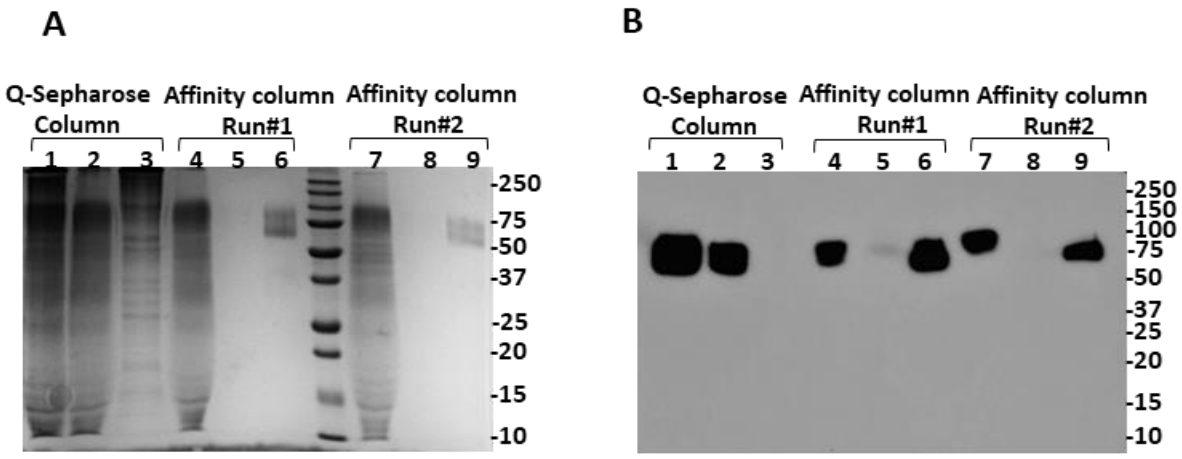

Figure 5.4: 12% SDS-PAGE under non-reduced conditions of 14A2c samples collected from Q-Sepharose and Affinity columns for Run #1 and Run #2.

(A) Coomassie staining and **(B)** Western blot using mouse anti-human PTH primary antibody. 40 µL of a sample was added to 20 µL of loading laemmli buffer before being heated for 15 minutes at 65°C. 30 µL were loaded for Coomassie staining and 6 µL for western blotting; **Lane 1 –** Load sample; **Lane 2 –** Q-Unbound fraction; **Lane 3 –** Wash/Elution sample; **Lane 4 –** 10B8-Unbound fraction; **Lane 5 –** Wash sample; **Lane 6 –** Pooled elution sample; **Lane 7 –** 10B8-Unbound fraction**; Lane 8 –** Wash sample**; Lane 9 –** Pooled elution sample. Bio-Rad All Blue protein standards 6 µL were loaded.

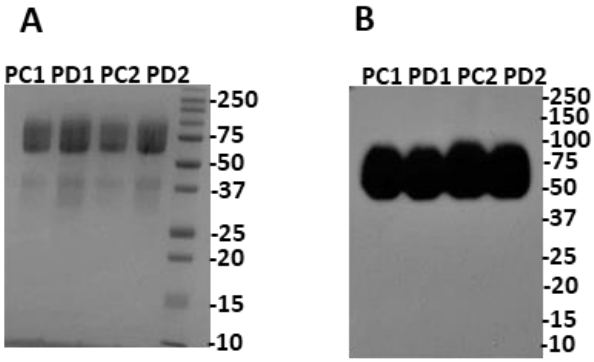

Figure 5.5: 12% SDS-PAGE under non-reducing conditions of 14A2c samples from Run #1 and Run #2. (**A)** Coomassie staining (5µg/lane) and **(B)** Western blot using mouse anti-human PTH primary antibody (~150 ng/lane). 40 µL of a sample was added to 20 µL of loading laemmli buffer before being heated for 15 minutes at 65°C. Bio-Rad All Blue protein standards (6 µL per lane); **Lane 1 –** Post-concentration (PC1); **Lane 2 –** Post-Dialysis (PD2); **Lane 3 –** Post-concentration (PC2); **Lane 4 –** Post-Dialysis (PD2).

5.1.2.1 Final 14A2c Sample Preparation

Table 5.5 shows the amount of recovered 14A2c protein from two separate purification experiments, and the results showed that consistent recovery rates were achieved as 2.39 mg/L and 2.22 mg/L of protein were purified in the first and second experiments, respectively (more details are provided in Appendix G2).

Table 5.6, all dialysed and concentrated samples were pooled (PPD) to give a 4.9 mg of protein in 4.8 mL total volume. The samples were further concentrated to 1.5 mL (PDC) to give a final protein (Final) product of 3.6 mg at 2.57 mg/mL obtained from 2 litres of culture media. About 26% of protein was lost during the concentration step. The final samples were subsequently analysed by coomassie staining and western blotting and the results presented in Figure 5.6A and 5.6B, reveal diffuse banding between 75−100 kDa.

Further probing of the lower band in a western blotting using mouse anti-human PTH 1-34 and anti-GHBP monoclonal antibodies confirmed that the band between 50-100 kDa was the intact 14A2c fusion protein (Figures 5.7A and 5.7B respectively). The less intense band of lower molecular weight at 37−50 kDa was confirmed to contain GHBP when probed with anti-GHBP monoclonal antibodies (Figure 5.7A). All samples were deemed suitable for further bioactivity testing.

Table 5.5: The amount of recovered 14A2c from the 2 separate purifications

Experiment	Culture volume	Total protein recovered (mg/L)	Total protein (mg)
1	1L	1.33	2.39
2	1L	1.7	2.22

Table 5.6: Final analysis of purified 14A2c samples were calculated using A_{280}

Sample	Volume (mL)	Mean A_{280}	mg/mL	Total protein (mg)
All Dialysed elutions (PPD)	4.8	1.70	0.86	4.9
post-con (PDC)	1.5	4.94	2.50	3.8
Final spin	1.4	5.07	2.57	3.6

PPD; all dialysed sample from all three experiment 14A2c were defrosted and pooled together.
PDC; pooled dialysed sample were concentrated using Centriprep-30 concentrator at 2500 rpm ((Millipore Inc.) for 20 minutes.
Final: 1 minute spin at 13k rpm on bench top centrifuge.

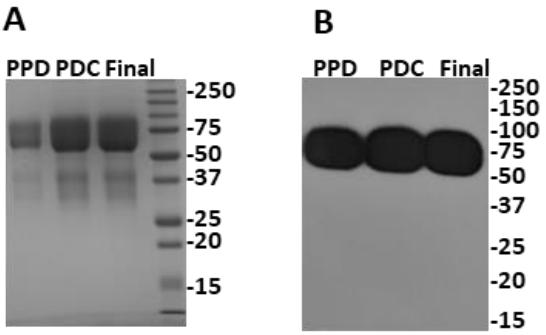

Figure 5.6: Analysis of final purified samples by 12% SDS-PAGE under non-reducing conditions.
(A) Coomassie staining (5 µg per lane) and **(B)** Western blot of 14A2c samples (150 ng per lane) using mouse anti-human PTH primary antibody. Samples were heated for 15 minutes at 65°C. Bio-Rad All Blue protein standards (6 µL per lane); **Lane 1 –** Pooled, Post Dialysis (PPD); **Lane 2 –** Post-concentration (PDC); **Lane 3 –** Final.

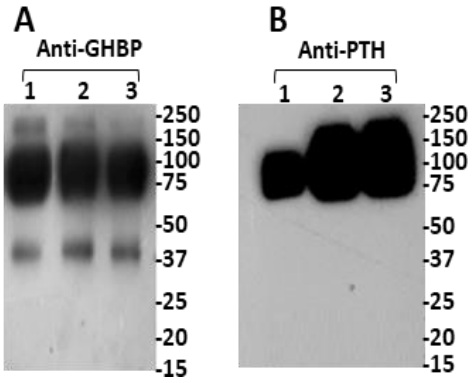

Figure 5.7: Analysis of final purified 14A2c samples by 12% SDS-PAGE under non-reducing conditions followed by western blotting using an anti-GHBP and anti-PTH antibody.
Samples were blotted using two different monoclonal antibodies **(A)** anti-GHBP antibody, and **(B)** anti-PTH antibody, with a loading of **Lane 1 –** 100 ng; **Lane 2 –**150 ng; **Lane 3 –** 250 ng. Bio-Rad All Blue protein standards (6 µL per lane).

5.1.3 Purification of 14A8

Frozen 14A8 expression media samples were defrosted overnight at 4°C, centrifuged to clear, and purified using two purification resins, as discussed in the preceding section. The conductivities of the media samples and binding buffer were ≥30 mS and 15−20 mS, respectively. 14A8 protein was purified from a 2 litres RB culture volume recovered from 2 successive experiments. All in- process and final purified samples were assessed by SDS-PAGE followed by coomassie staining and western blotting. Purified protein was pooled, concentrated, and taken forward for *in vitro* bioactivity assessment. A representative example of the methodology adopted is described below whilst purification analysis is described in Appendix G3.

Experiment 1

14A8 expression media from a 1-litre RB culture (Section 4.1.3.2.) was concentrated to 115 mL containing 319 mg of protein (See Table 5.7). The concentrated sample was subsequently loaded onto a Q-Sepharose column followed by rinsing with 40 mL of binding buffer. The unbound fraction (Q-Unbound) contained 226 mg of protein, equivalent to ~70% total protein loaded. Additional 95.5 mg protein, approximately 30% total protein loaded, was recovered from the wash/elution step.

The Q-Unbound fraction was passed over the affinity column and obtained 193.5 mg of protein in the unbound fraction, which was ~85% of the total protein loaded. A total of 5.7 mg of protein was obtained after the wash step (~3% of the total protein loaded).

The first elution (E1) with 20 mL of 0.2 M glycine, pH 2.7 yielded 1.76 mg of protein and a subsequent (10 mL) elution yielded further 0.32 mg. Subsequent elution attempts yielded no

protein. Consequently, the two elution fractions with detectable amounts of protein were pooled to give 2.8 mg of protein in 30 mL total volume. This amounted to ~1.22% recovery from the load samples. The pooled sample was further concentrated to 3.2 mL (PC1) and 2.17 mg of protein. Approximately 22% of the protein was lost during the concentration step and with a further loss of ~35% when sample was dialysed into citrate buffer, pH 6.0 to give a final yield of 1.40 mg of protein in 1.8 mL post-dialysis (PD1).

In the subsequent 14A8 protein purification from the expression media of the second experiment, the unbound fraction from the preceding run was passed over the affinity column once again and the process described above was repeated. 185.5 mg of protein was obtained in the unbound fraction, which was equivalent to ~96% of total protein loaded. 1.91 mg of protein was recovered during the initial elution (E1) with 20 mL of elution buffer (0.2 M glycine, pH 2.7) and a further 10 mL elution volume yielded 0.2 mg protein. The two elution fractions were pooled together to give a total volume of 30 mL containing 2.42 mg of protein, indicating ~1.0% protein recovery. Next, the pooled sample was concentrated to 2.8 mL (PC2) containing 1.94 mg of protein. Approximately ~20% loss of the purified protein was lost during the concentration step and a further ~38% loss observed when the sample was dialysed in citrate buffer, pH 6.0 to give 1.21 mg of protein in 1.5 mL post-dialysis (PD2).

The final amount of purified protein was quantified at A_{280} using an extinction coefficient of 1.944 obtained from online Expasy Protoparam software (See Section 2.3.2.2) and gave 1.61 mg and 1.3 mg from both purifications. In summary, 3.3 mL of media containing 2.91 mgs of protein was obtained in these experiments.

Table 5.7: Protein assays of 14A8 samples taken during the purification

Protein levels were calculated using Bradford assay and A_{280}.

Samples	Volume (mL)	µg/mL	Total protein (mg)	% Recovery
Source-Q Purification				
Load	115	2779.4	319.6	100
Q-UB	155	1461.5	226.5	70
Q-Wash_Elute	100	955.230	95.5	30
Affinity Purification				
Run #1				
UB_1	175	1105.8	193.5	85
Wash-1	100	57.0	5.7	3
Elution 1	20	89.6	1.79	0.79
Elution 2	10	32.3	0.32	0.14
Elution 3	10	0	0	0
Pre-Dialysis (PE1)	30	93.6	2.8	1.24
Post-concentration (PC1)	3	724.5	2.17	78*
Post-Dialysis (PD1)	1.8	778.9	1.40	65**
Run #2				
UB2	195	951.046	185.5	96
Wash-2	100	19.372	1.93	1
Elution 1	20	95.523	1.91	1
Elution 2	10	20.628	0.20	0.11
Elution 3	10	0	0	0
Pre-Dialysis (PE2)	30	80.9	2.42	1.07
Post-concentration (PC2)	2.8	695.2	1.94	80*
Post-Dialysis (PD2)	1.5	808.2	1.21	62**
Final Analysis of Purified Protein by A_{280}				
Samples	**Volume (mL)**	**Mean A_{280}**	**mg/mL**	**Total protein (mg)**
Post-Dialysis (PD1)	1.8	1.77	0.90	1.61
Post-Dialysis (PD2)	1.5	1.72	0.87	1.30

Source-Q Purification; Q-Sepharose column was run in flow-through mode.
Affinity Purification (Run #1); the unbound fraction from the Source-Q column was used as the load for the first run (Run #1) on the 10B8 affinity column
Affinity Purification (Run #2); the unbound fraction from the first run was passed again over the 10B8 affinity column (Run #2). ***** PC1 & 2 percentage recoveries were derived from comparison with PE1 & 2.
****** PD1 & 2 percentage recoveries were derived from comparison with PC1 & 2.

Samples from both Q-Sepharose and affinity columns were assessed by coomassie staining and western blotting (Figures 5.8A and 5.8B respectively). Figure 5.8B shows that using Q-Sepharose, the majority of 14A8 was recovered in the unbound fraction running between 75 and 150 kDa, with a small fraction of higher-molecular-weight species present in the wash/elution fraction, separating at about 100−150 kDa. In the affinity column purification, a large amount of protein was observed in the unbound fractions upon coomassie staining (Figure 5.8A, Lanes 4 and 7) and a corresponding western blotting analysis confirmed that these fractions contained 14A8 protein (Figure 5.8B, Lanes 4 and 7). This suggests that 14A8 does not bind efficiently to the affinity column. Despite the inefficiency of the purification process, sufficient target protein of high purity was purified as 14A8 is seen as a diffuse band between 50 and 100 kDa in the final processed sampled (Figures 5.9A and 5.9B). Coomassie staining showed an additional lower band between 37−50 kDa which was later confirmed to be the GHBP fragment of the 14A8 fusion (further details provided in Section 5.1.3.1 below). In summary, even though the overall protein loss was high across all purification stages, the amount of protein recovered was sufficient for conducting relevant tests.

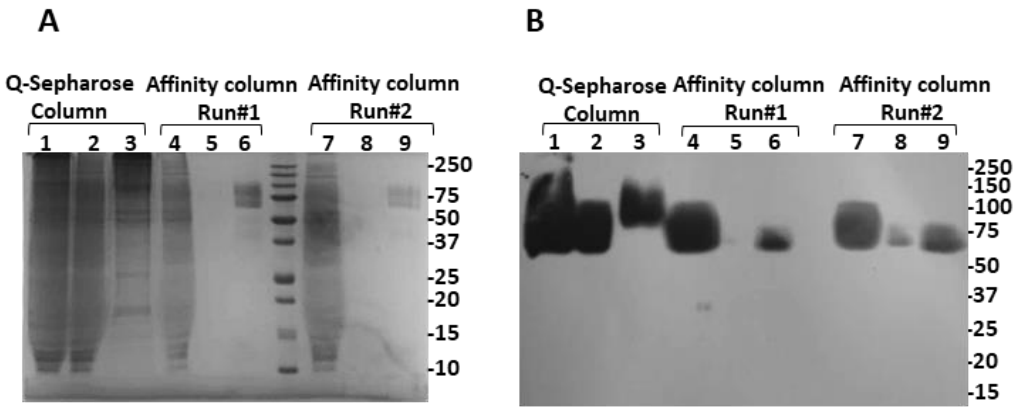

Figure 5.8: 12% SDS-PAGE under non-reduced conditions of 14A8 samples collected from Q-Sepharose column and Affinity column for Run #1 and Run #2.

(A) Coomassie staining and **(B)** Western blot using mouse anti-human PTH primary antibody. 40 µL of a sample was added to 20 µL of loading laemmli buffer before being heated for 15 minutes at 65°C. 30 µL for Coomassie staining and 6 µL for western blot were loaded; **Lane 1 –** Load sample; **Lane 2 –** Q-Unbound fraction; **Lane 3 –** Wash/Elution sample; **Lane 4 –** 10B8-Unbound fraction; **Lane 5 –** Wash sample; **Lane 6 –** Pooled elution sample; **Lane 7 –** 10B8-Unbound fraction; **Lane 8 –** Wash sample; **Lane 9 –** Pooled elution sample. Bio-Rad All Blue protein standards 6 µL were loaded.

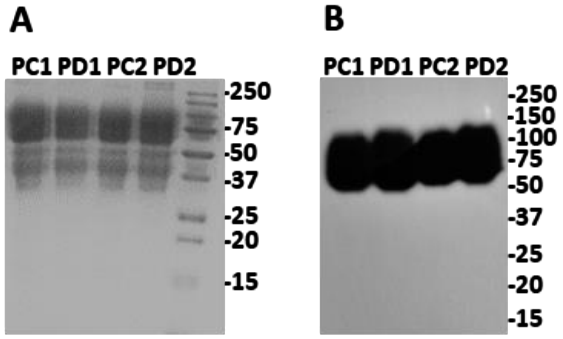

Figure 5.9: 12% SDS-PAGE under Non-reducing Conditions of 14A8 Samples from Run #1 and Run #2.

(A) Coomassie staining (5µg/lane) and **(B)** western blot using mouse anti-human PTH primary antibody (~150 ng/lane). 40 µL of a sample was added to 20 µL of loading laemmli buffer before being heated for 15 minutes at 65°C. Bio-Rad All Blue protein standards 6 µL were loaded. **Lane 1 –** Post-concentration (PC1); **Lane 2 –** Post-Dialysis (PD2); **Lane 3 –** Post-concentration (PC2); **Lane 4 –** Post-Dialysis (PD2).

5.1.3.1 Final 14A8 Sample Preparation

Table 5.8 is a summary of 14A8 protein recovered from the two separate purification experiments. The data showed that consistent recovery rates were achieved as 2.91 mg/L and 3.03 mg/L of proteins were purified (more details are provided in Appendix G4). As indicated in Table 5.9, when all dialysed and concentrated samples were pooled (PPD), the resulting 6 mL volume contained 3.95 mg of protein. These samples were further concentrated to 1.5 mL (PDC) and the final product (Final) contained 3.21 mg at 2.29 mg/mL. Figures 5.10A and 5.10B show the results of coomassie staining and western blotting analyses of the prepared samples, PPD and PDC and Final. A diffuse band was detected between 50−100 kDa and a further secondary lower band was observed in the coomassie stained gel at 37−50 kDa. Further probing of the lower band in a western blotting using mouse anti-human PTH 1-34 and anti-GHBP monoclonal antibodies confirmed that the band between 50-100 kDa was the 14A8 fusion protein (Figures 5.11A and 5.11B respectively). However, the lower band at ~37 kDa was only observed when probed with anti-GHBP antibody suggesting this to be a cleaved fragment of 14A8 that co-purified with the fusion protein (See Figure 5.11A). All samples were deemed suitable for use in further bioactivity testing.

Table 5.8: The amount of recovered 14A8 from the 2 separate purifications

Experiment	Culture volume	Total protein recovered (mg/L)	Total protein (mg)
1	1L	1.77	2.91
2	1L	2.03	3.03

Table 5.9: Final analysis of purified 14A8 samples were calculated using A_{280}.

Samples	Volume (mL)	Mean A_{280}	mg/mL	Total protein (mg)
All Dialysed elutions (PPD)	6	1.30	0.66	3.95
post-con (PDC)	1.5	4.61	2.33	3.5
final spin	1.4	4.53	2.29	3.21

PPD; all dialysed sample from all three experiment 14A8 were defrosted and pooled together.
PDC; pooled dialysed sample were concentrated using Centriprep-30 concentrator at 2500 rpm ((Millipore Inc.) for 20 minutes to pellet debris.

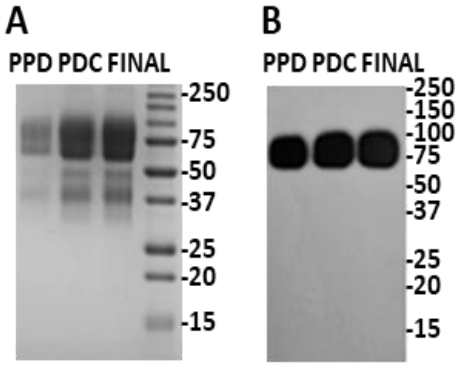

Figure 5.10: Analysis of final purified samples by 12% SDS-PAGE under non-reducing conditions.
(A) Coomassie staining (5 µg per lane) and **(B)** Western blot of 14A8 samples (150 ng per lane) using mouse anti-human PTH primary antibody. Samples were heated for 15 minutes at 65°C. Bio-Rad All Blue protein standards (6 µL per lane); **Lane 1 –** Pooled, Post Dialysis (PPD); **Lane 2 –** Post-concentration (PDC); **Lane 3 –** Final.

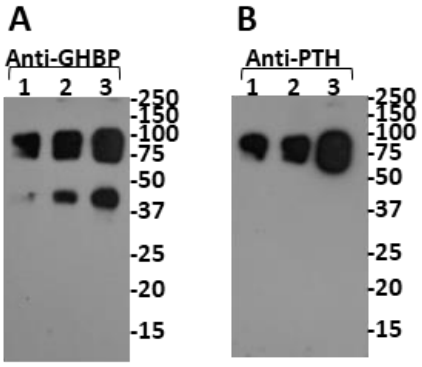

Figure 5.11: Analysis of final purified 14A8 samples by 12% SDS-PAGE under non-reducing conditions followed by western blotting using an Anti-GHBP vs Anti-PTH antibody.
Samples were blotted using two different monoclonal antibodies **(A)** anti-GHBP antibody, and **(B)** anti-PTH antibody, with a loading of **Lane 1 –** 100 ng; **Lane 2 –** 150 ng; **Lane 3 –** 250 ng. Bio-Rad All Blue protein standards 6 µL were loaded.

5.2 Analysis of Concentrated Media and Final Purified Samples for 14A2c and 14A8

As discussed in Chapter 4, during western blotting analyses of concentrated media from roller bottle cultures and final purified samples of 14A2c and 14A8 probing with anti-GHBP antibody, lower-molecular-weight bands were detected separating between ~37 and 50 kDa (See Figures 5.12A and 5.12B). The results indicate that these low-molecular-weight products were carried through from the concentrated media to the purification process; the same bands were detected in the final purified preparations of 14A2c and 14A8.

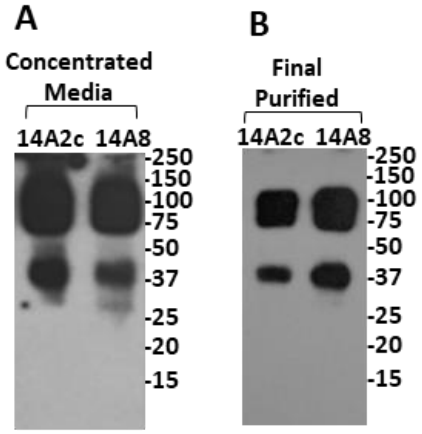

Figure 5.12: Analysis of concentrated media and final purified samples by 12% SDS-PAGE under non-reducing conditions followed by western blotting using an anti-GHBP for 14A2c and 14A8.
(A) Concentrated media sample **(B)** Final purified sample (250 ng per lane): Samples were blotted using anti-GHBP antibody. Bio-Rad All Blue protein standards 6 µL were loaded.

5.3 Discussion

In this study, a two-stage chromatography method was used for protein purification. In the initial step, a Q-Sepharose Ion Exchange Chromatography (IEX) column was used in a flow-through mode to reduce the amount of initial total protein contamination and thus allow for more effective binding to the anti-GHBP antibody column. Q-Sepharose was shown to be

efficient, resulting in a ~30% loss of total protein whilst retaining most of the target protein in the flow through.

In the next step, the affinity chromatography column was used to capture the target protein from other protein contaminants. However, the binding efficiency of the column was very low, as appreciable amounts of target protein was still present in the unbound fractions for all purified fusion proteins, as revealed by the western blotting data. Several approaches could be considered to potentially improve the binding of target protein to the affinity column. Firstly, increasing the contact time of the target protein with the resin will increase the protein binding and yield. This strategy could be tested by mixing the affinity resin with the load sample, for example, 2 hours or more and then analysing the supernatant. Alternatively, reducing the flow rate to 0.2 mL/minute will also increase the contact time and target protein binding to the column, as the flow rate of 1 mL/minute which was used in these studies may be too high for effective binding of the target protein. However, if large volumes are involved, lowering the flow rate may not be feasible. Another option is to use a different affinity chromatography column could be tested using an anti-PTH 1-34 polyclonal antibody recently developed in our laboratory. Similarly, other purification methods could be explored, such as further experimentation with both cation (SP-Sepharose) and anion exchange resins, or the use of hydrophobic interaction chromatography (HIC) for separating the proteins based on their hydrophobicity (Walls et al., 2010).

In this study a Bradford assay was used for measuring total protein concentration, and final product concentration was obtained using A_{280} quantification. However, when these methods were adopted, it was challenging to estimate how much of the target protein was recovered from the starting material. Thus, a more targeted protein-specific assay, such as Enzyme-

linked immunosorbent assay (ELISA) could be used to assess protein yield, as well as loss and recovery percentages in each purification stage. Recently, the lab has validated an ELISA using anti-PTH 1-34 and anti-GHBP antibodies, making this approach a viable alternative for future studies.

Protein loss was observed during both concentration and dialysis steps. Protein losses were particularly noticeable in the experiments involving 14A7 with up to 85% loss during both the dialysis and concentration steps. It is speculated that most 14A7 losses occurred during dialysis could potentially be due to non-specific binding, whereas those arising during concentration could be in part attributed to the similarity between the molecular weight cut-off (MWCO) and the molecular weight of 14A7. This view was supported by evaluating the molecular properties of 14A7 in relation to the protein losses. Whilst all the fusions are glycosylated, 14A7 has a non-glycosylated molecular weight of 32 kDa which increased to 37−50 kDa following glycosylation as observed by SDS-PAGE analysis. Despite utilising a dialysis membrane with a 10 kDa MWCO, which was well below the molecular weight of 14A7, losses of 20−40% were still observed during dialysis. However, when a 30 kDa MWCO was used in the concentration step, losses increased to 57−85%. Nonetheless, as significant variations in losses obtained in different experiments were noticed, it is evident that these could be due to other factors including poor performance of the concentrators (according to the personal communication from Dr Ian Wilkinson, certain batches of these concentrators were shown to be faulty and increased protein losses were noted).

On the other hand, the size of non-glycosylated 14A2c and 14A8 is ~52 kDa, which increases to 75−100 kDa when glycosylated. In both cases, up to 27−29% protein losses were noted during the concentration step, whereby dialysis resulted in up to 48−55% losses. These losses

during dialysis were surprisingly greater compared to 14A7 especially since 14A2c and 14A8 are larger molecules than 14A7. Thus, these losses cannot be attributed solely to loss due to the MWCO of concentrators. To circumvent potential loss due to small protein size, a lower MWCO concentrator, such as 10 kDa, could be employed. This could be particularly useful for 14A7 as most protein losses occurred during the concentration step, but less so for 14A2c and 14A8 and needs further study.

Another potential cause of loss of protein during the purification step could be due to protein instability caused by pH change during dialysis. During dialysis, the elution buffer, 0.2 M glycine at pH 2.7, was replaced with 20 mM citrate buffer at pH 6.0 (containing 0.15M NaCl and 10% Glycerol). Whilst the stability of fusion proteins containing two or even three different protein domains is difficult to predict, the theoretical pI of 14A7 is 6.19 and 6.34 for other fusions. A pH too close to the pI point of 14A7 may cause problems with stability because the protein is approaching a point in which it has no net charge. As a reference, PTH is known to be stored in acidic pH (Shimizu et al., 2016) and other fusions utilising GHBP produced in the laboratory, such as the growth hormone-GHBP fusions are all stored in citrate buffer, pH 6.5 without loss in stability (Wilkinson, personal communication). The stability of the PTH fusions in the current studies could be further investigated by testing different pH ranges of buffers.

During analysis by SDS-PAGE, proteins separated as diffuse bands. The GHBP domain contains five potential N-linked glycosylation sites (Harding et al., 1994) and the PTH extracellular domain in 14A2c and 14A8 has four potential N-linked glycosylation sites (Bisello et al., 1996). The increase in molecular weight together with variable glycosylation outcomes across different domains is hypothesised to have resulted in the diffuse nature of the target protein

band. In addition to the diffuse high molecular weight bands of 14A2c and 14A8, other bands at ~37−50 kDa were also noted. These lower bands may be present in 14A7, but owing to its lower molecular weight, may be obscured. It was hypothesised that at least some of these lower bands contain a cleaved GHBP component. The detection of lower bands at ~37 kDa for both 14A2c and 14A8 in a western blotting using anti-GHBP antibodies but absent when probed with anti-PTH antibody supported the hypothesis. Also, as these lower bands were detected in the expression media prior to purification when analysed by western blotting with anti-GHBP antibody, it was apparent that these bands were carried through the purification process onto the final purified preparations. As these lower bands contained GHBP fragments they potentially bound to the affinity column.

However, it possible that the lower band(s) also contains PTH, PTHR or linker, albeit in quantities that are below detection. Therefore, to investigate these peptide fragments further, mass spectrometry could be utilised to determine the components of the purified sample.

In conclusion, the purification aims were met as sufficient quantities of each target protein were obtained in order to carry out bioactivity analyses. All fusions were successfully purified, obtaining 1.31 mg (0.93 mg/mL) of 14A7, 3.6 mg (2.57 mg/mL) of 14A2c and 3.44 mg (2.29 mg/mL) of 14A8.

Chapter Six: Bioactivity Studies – Dual-Luciferase Reporter Assay (DLRA)

Abstract:

Aims

1. To develop and validate a Dual Luciferase Reporter Assay (DLRA) in which assay interference and variability are reduced to a minimum.
2. To use this assay to determine an EC_{50} for human PTH 1-34.
3. To confirm biological activity for PTH fusion and to compare potency (EC_{50}) to PTH 1-34.

Methods: Initial experiments were designed to evaluate the use of the pRL-TK and pRL-CMV plasmids as transfection controls for use in the DLRA. These plasmids constitutively express Renilla luciferase. UMR-106 cells that endogenously express full length PTHR1 were transfected with a range of concentrations of either pRL-TK or pRL-CMV plasmids, along with the cAMP reporter plasmid pGL4.29 that expresses Firefly Luciferase in response to cAMP. Transfected cells were challenged for 5 hours with PTH 1-34 at 0, 0.1, 1 & 10 nM after which cells were lysed and samples analysed for both Firefly and Renilla luciferase activities using the Promega Dual-Luciferase Reporter Assay. For generation of EC_{50} values, full standard curves were generated for PTH 1-34 and PTH fusions. Data was plotted using GraphPad prism software.

Results: During the validation process, pRL-TK was shown to be superior to pRL-CMV as an internal control. pRL-TK at 10 or 20 ng per transfection yielded more consistent results with no variation in Renilla expression noted with increasing concentrations of PTH 1-34 or PTH fusions. Using the validated DLRA, EC_{50}'s (EC_{50} ± StDev nM) for PTH 1-34 of 2.39 ± 0.58 (n = 8),

14A7, 68.02 ± 4.01 (n = 4), 14A2c, 699.4 ± 55.6 (n = 3), and 14A8, 253.8 ± 26.3 (n = 3) were obtained.

Conclusions: DLRA development was completed using the optimised DLRA assay methodology. Using the established DLRA assay, EC_{50}'s were generated for PTH fusions and compared to PTH. 14A7 (PTH linked to GHBP) is the smallest molecule and is hypothesised to be the most active due to less steric hindrance from the GHBP moiety. Conversely, 14A2c (PTH linked to PTHrExt and GHBP) is hypothesised to be the least active due to its increased size as well as steric hindrance, but also because PTH may potentially undergo intramolecular interactions with the PTHrExt, thus reducing PTH availability. 14A8 is a control for 14A2c and contains the I135K mutation, which prevents PTH from binding to PTHrExt. The retention of biological activity was confirmed for all PTH fusions. It is essential that the PTH fusions retain their biological activity for them to be a potential treatment for hypoparathyroidism.

6.1 Dual-Luciferase Reporter Assay (DLRA)

The DLRA was used to test the response of rat osteosarcoma cell line (UMR-106) to parathyroid hormone (PTH) and to compare the biological activity of purified PTH fusions. Briefly, UMR-106 cells were transfected with a reporter plasmid containing the Firefly Luciferase gene that contains multiple copies of the cAMP response element linked to the minimal thymidine kinase promoter (pGL4.29 [luc2P/CRE/Hygro] plasmid, Promega), as well as a transfection control plasmid expressing Renilla Luciferase under the control of the either the cytomegalovirus immediate-early enhancer/promoter region (pRL-CMV, Promega) or Herpes Simplex Virus thymidine kinase promoter (pRL-TK, Promega). The pLG4.29 [luc2P/CRE/Hygro] vector contains a destabilised luc2P Firefly Luciferase gene and has been codon-optimised for more efficient expression, resulting in low backgrounds and high levels of induction. The vector also contains a hygromycin resistance selectable marker, allowing use in both transient transfections and for stable cell line selection. The control plasmid contains hRluc which has also been optimised for expression in mammalian cells.

Using the Promega Dual Luciferase Assay Kit and a luminometer, Firefly Luciferase and Renilla Luciferase activity can be assayed with high sensitivity and linearity over several orders of magnitude. Both Firefly and Renilla Luciferase activity is measured sequentially from a single sample based on different substrate specificities of the two luciferases. The luminometer injects 2 different buffers sequentially. Firefly Luciferase is detected using the Luciferase assay substrate buffer which contains Luciferin. A “Stop & Glow” solution is then injected which stops the reaction with Firefly Luciferase and allows the detection of Renilla Luciferase using the substrate coelenterazine. The activities are given as relative light units (RLU). This minimises errors due to variability in pipetting volumes and providing a more convenient

means to measure both the experimental and control reporter activities. Firefly Luciferase activity is directly related to cAMP levels which in turn is related to activity of PTH or PTH fusions. (See Section 2.3.7 for full assay details).

6.2 Bioassay Development

In this chapter, a number of issues with the DLRA have been addressed (See Section 2.3.7.1). Initial studies used the transfection control plasmid pRL-CMV (See Section 6.1.3.1). This was found to be unreliable as a control due to variations in Renilla expression. A comparison was then made between 2 control plasmids, pRL-CMV and pRL-TK (both obtained from Promega). The basic assay consisted of transfection of UMR-106 cells with varying concentrations of each plasmid, along with a set concentration of reporter plasmid and analysing primarily the effect on Renilla expression (See Sections 6.2.2.1 to 6.2.2.4). Any assays that showed assay interference in the form of an increase in Renilla values with increasing PTH were disregarded. The final sections are concerned with the validation of the assay using a full PTH 1-34 standard curve (See Section 6.2.3) and analysis of PTH fusion bioactivities (See Sections 6.3.2 to 6.3.4). Throughout these sections emphasis is placed on the fold difference in Renilla values from the untreated controls and the %CV between duplicate FL/RL ratios (Ratio of Firefly to Renilla Luciferase) which should to be ≤25% for acceptance. From these data an acceptance criteria for the assay was established (See Section 6.2.4). Data was plotted using GraphPad Prism software. EC_{50} values were obtained from 4-Parameter plots of FL/RL vs Log concentration. Data is also displayed as % Maximum Fold induction.

6.2.1 Use of pRL-CMV as Transfection Control

Initial bioactivity experiments were conducted using pRL-CMV as the transfection control plasmid at 0.5 ng per transfection (See Section 2.3.7.1) using a full standard curve for PTH 1-34. Representative data from one experiment is presented in Figure 6.1. The data shows that with increasing concentrations of PTH 1-34 there is an increase in Renilla expression across the experiment, with a maximum fold difference of 3.7-fold attained at 100 nM PTH 1-34. Firefly Luciferase activity as expected increases with increasing PTH 1-34 as does the FL/RL ratio, as shown in Figures 6.2A and 6.2B. However, large errors (%CV >25%) were noted for several duplicate samples, as reflected in high percent coefficient of variation (%CV) values.

These initial findings raised doubts about the applicability of the pRL-CMV as a control for the PTH assay. Therefore, the assay was further developed in the subsequent sections in order to reduce interference or variability to a minimum and maintain stable Renilla values across all PTH concentrations.

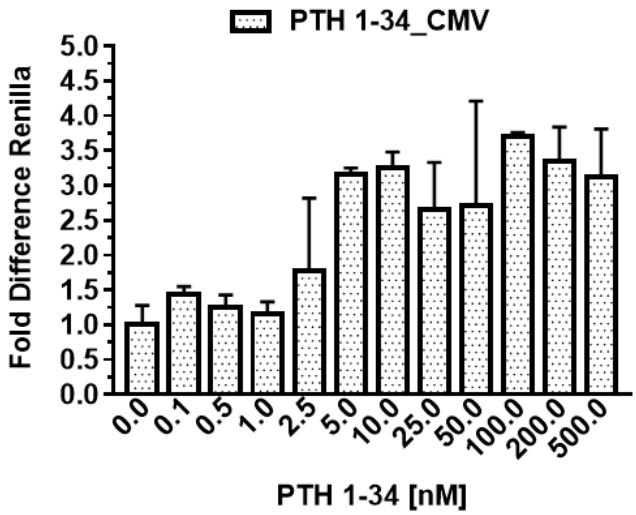

Figure 6.1: Representative of PTH assays for measuring PTH 1-34 bioactivity using a pRL-CMV plasmid. Fold Difference bars plotted against PTH 1-34 treatment (0-500 nM) for transfections using pRL-CMV plasmid at 0.5 ng per transfection. Data are presented as mean ± StDev for fold difference Renilla value and data analysed using GraphPad Prism.

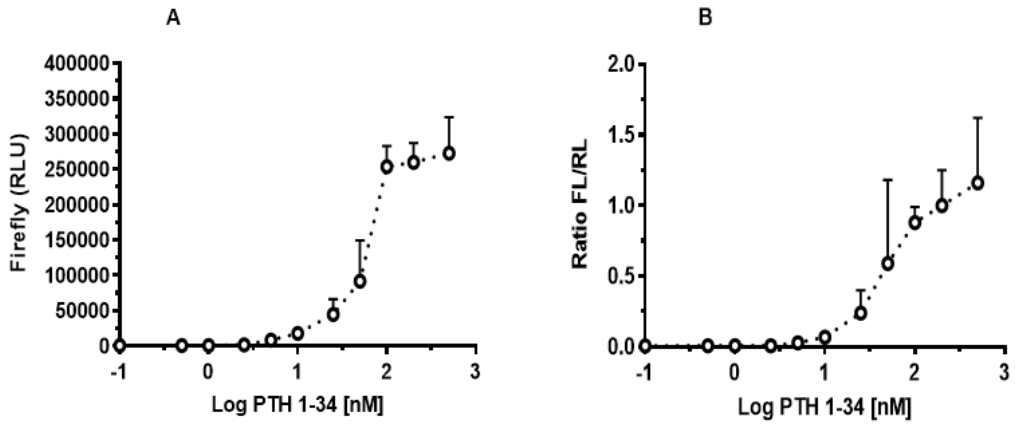

Figure 6.2: Representative of PTH assays for measuring PTH 1-34 bioactivity using a pRL-CMV plasmid. The transfection was at 0.5 ng per transfection plotted against log PTH 1-34 treatment (0-500 nM). **(A)** Firefly Luciferase (RLU). **(B)** Ratio for Firefly Luciferase (RLU) to Renilla Luciferase (RL). Data are presented as mean ± StDev for RLU and FL/RL ratio. Data analysed using GraphPad Prism.

6.2.2 Evaluation of pRL-TK as an Alternative Transfection Control

Since Renilla expression was shown to be variable when pRL-CMV plasmid was used at 0.5 ng/transfection, the suitability of another plasmid, pRL-TK as a transfection control was assessed in comparison to pRL-CMV.

The evaluation of the assay was an iterative process consisting of the transfection of UMR-106 cells with varying concentrations of either pRL-TK or pRL-CMV, along with a set concentration of the cAMP reporter plasmid pGL4.29 that expresses Firefly Luciferase. Transfected cells were challenged with PTH 1-34 at 0, 0.1, 1, and 10 nM and samples analysed using the Promega DLRA kit, as described in Section 2.3.7.1.

6.2.2.1 Effect of Control Plasmids at 0.5 and 5 ng per transfection

Briefly, cells were transfected with 0.5 and 5 ng/transfection of each control plasmid (pRL-CMV and pRL-TK) along with reporter plasmid. Cells were challenged with PTH 1-34 and lysed in 150 µL lysis buffer prior to analysis using 25 µL of lysate. The effect of pRL-CMV and pRL-TK on Renilla Luciferase expression is presented in Table 6.1 and Figure 6.3. All data were compared with the zero-background control for the transfection (untreated control). Figure 6.3 shows that when pRL-TK is at 0.5 ng/transfection, Renilla values increase with increasing PTH up to a maximum fold difference of 4.8-fold at 10 nM PTH. However, this trend is not observed at 5 ng/transfection at 0−1 nM PTH, with no notable fold-increase in Renilla values. The only change observed occurs at 10 nM PTH, whereby Renilla values increased by 1.28-fold, albeit at a very high %CV of 30%.

In contrast to pRL-TK, pRL-CMV at 0.5 ng /transfection gives Renilla values higher than untreated controls at all PTH concentrations. However, at 5 ng/transfection, Renilla values

cannot be differentiated from untreated controls at 0.1 nM PTH but vary considerably in the 1−10 nM range, with a maximum fold difference of 1.4-fold (See Figure 6.3).

As expected Firefly Luciferase activity increases with increasing PTH 1-34 irrespective of transfection mode (See Figure 6.4A). The fact that these values are comparable for all transfections irrespective of whether it is pRL-CMV or pRL-TK, confirms that Firefly values are not affected by the assay. However, due to the increased expression of Renilla from the pRL-CMV plasmid the FL/RL ratio are reduced in comparison to pRL-TK. This change is due to the stronger promoter qualities of CMV resulting in overexpression of Renilla (See Figure 6.4B).

Table 6.1: Testing the effect of pRL-TK and pRL-CMV on Renilla Luciferase values in the DLRA. UMR-106 cells were transfected with plasmids at 0.5 and 5 ng/transfection and treated with PTH 1-34 at 0.1, 1 & 10 nM. Readouts were Firefly and Renilla Luciferase given in relative light units (RLU). Data is presented either as a ratio of Firefly to Renilla (RL) Luciferase or as Fold difference (FD) in Renilla Luciferase from untreated controls. StDev; Standard deviation, %CV; Coefficient of variation.

PTH (nM)	Firefly Luciferase RLU	Renilla Luciferase (RL) RLU	Ratio FL/RL	Mean: Ratio FL/RL	StDev: Ratio FL/RL	% CV: FL/RL	Fold Difference (FD) (Renilla)	Mean FD	StDev FD	%CV FD
pRL-TK at 0.5 ng/transfection										
0	3631	162	22.414	20.296	2.995	15	0.837	1.00	0.230	23
0	4090	225	18.178				1.163			
0.1	40120	543	73.886	79.476	7.905	10	2.806	2.948	0.201	7
0.1	50869	598	85.065				3.090			
1	136136	1116	121.986	229.87	152.57	66	5.767	3.987	2.518	63
1	144222	427	337.756				2.207			
10	360344	835	431.550	401.90	41.918	10	4.315	4.809	0.698	15
10	381947	1026	372.268				5.302			
pRL-TK at 5 ng/transfection										
0	3753	2722	1.379	1.571	0.271	17	1.073	1.00	0.103	10
0	4145	2352	1.762				0.927			
0.1	32888	2273	14.469	15.597	1.596	10	0.896	0.947	0.072	8
0.1	42350	2532	16.726				0.998			
1	142120	3031	46.889	48.574	2.383	5	1.195	0.948	0.349	37
1	89361	1778	50.259				0.701			
10	345995	3934	87.950	106.05	25.608	24	1.551	1.279	0.384	30
10	317491	2557	124.165				1.008			
pRL-CMV at 0.5 ng/transfection										
0	3854	108361	0.036	0.037	0.001	4	0.973	1.00	0.037	4
0	4285	114263	0.038				1.027			
0.1	44748	178268	0.251	0.271	0.028	10	1.602	1.564	0.053	3
0.1	49442	169951	0.291				1.527			
1	219713	183110	1.200	1.219	0.027	2	1.645	1.492	0.216	15
1	184460	149045	1.238				1.339			
10	467332	163319	2.861	2.986	0.177	6	1.467	1.311	0.221	17
10	400031	128565	3.112				1.155			
pRL-CMV at 5 ng/transfection										
0	2770	1148010	0.002	0.002	0.0001	3	1.022	1.00	0.032	3
0	2533	1097599	0.002				0.978			
0.1	17456	1325463	0.013	0.015	0.002	16	1.180	1.035	0.205	20
0.1	16470	999732	0.016				0.890			
1	146005	1662396	0.088	0.083	0.006	7	1.481	1.405	0.106	8
1	118077	1493491	0.079				1.330			
10	425639	1676933	0.254	0.253	0.001	1	1.494	1.427	0.095	7
10	384520	1526588	0.252				1.360			

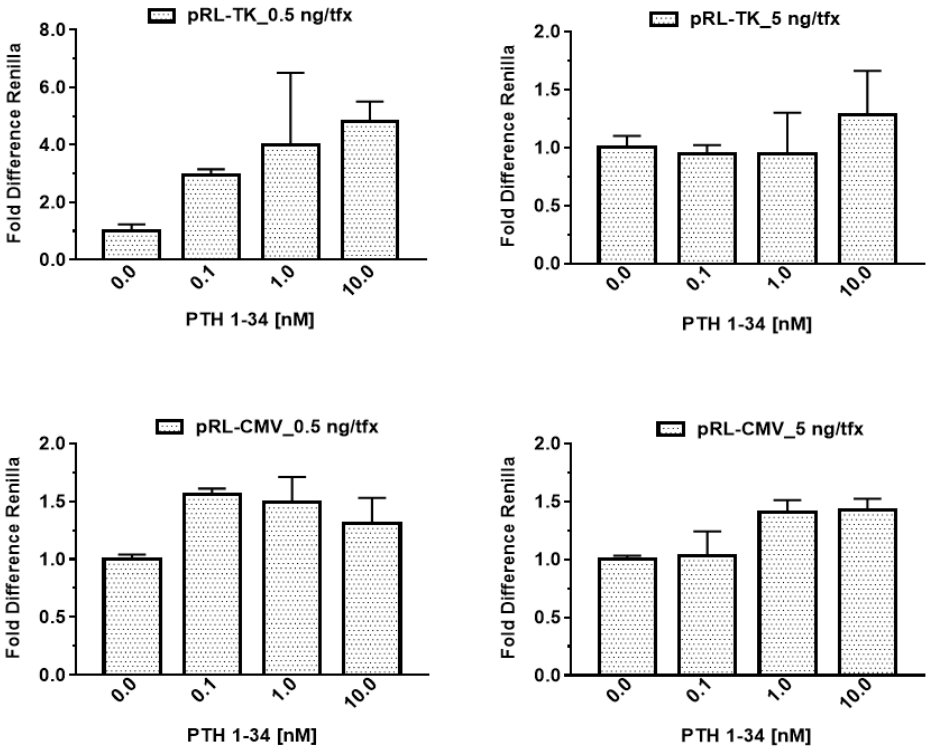

Figure 6.3: Fold difference in Renilla values from untreated controls for pRL-TK and pRL-CMV transfections.

Fold Difference bars plotted against PTH 1-34 treatment (0, 0.1, 1 & 10 nM) for transfections using pRL-TK and pRL-CMV plasmid at 0.5 and 5 ng per transfection. Data are presented as mean ± StDev for fold difference Renilla value and data analysed using GraphPad Prism.

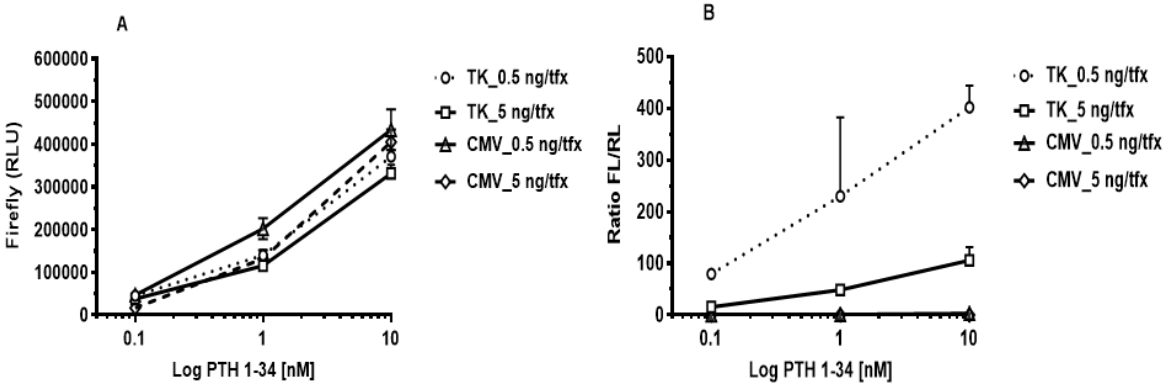

Figure 6.4: Represented the firefly luciferase density and FL/RL ratio by using pRL-TK and pRL-CMV plasmids.

The transfection was at 0.5 and 5 ng per transfection plotted against log PTH 1-34 treatment (0, 0.1, 1 & 10 nM). **(A)** Firefly Luciferase (RLU) values. **(B)** FL/RL ratio value. Data are presented as mean ± StDev for RLU and FL/RL ratio. Data analysed using GraphPad Prism.

A repeat assay was completed that confirmed the above result (See Appendix H1). As more consistent results were obtained when higher pRL-TK plasmid concentrations were used, the effect of further increases in pRL-TK plasmid concentrations on fold difference of Renilla was tested. The pRL-CMV plasmid was excluded from further investigation as fold differences in Renilla values were consistently higher than those in untreated controls. These increases in Renilla have been attributed the potential increase in gene expression from the binding of cAMP response element binding (CREB) to the CMV promoter. These issues will be discussed later.

6.2.2.2 Testing pRL-TK at 2-20 ng per transfection

To further validate the suitability of pRL-TK plasmid for use in the DLRA assay, a broader range of plasmid concentrations from 2, 5, 10, 20 ng/transfection were tested. Cells were lysed in 150 µL of lysis buffer and 50 µL were used for analysis. Data were compared with the zero-background control for the transfection (untreated control). The results are presented in Table 6.2 and Figure 6.5. pRL-TK at 2 ng/transfection, shows an increase in Renilla values with increasing PTH up to a maximum fold difference of 4-fold at 10 nM PTH, albeit at a relatively high %CV for FL/RL of 20%. A similar trend is observed with 5 ng/transfection where Renilla values increased up to 2.65-fold at 10 nM PTH, an effect that had previously been observed.

However, when using 10 ng/transfection this induced a minimal change in Renilla values relative to controls across all PTH concentrations, with a maximum fold difference of 1.09-fold and low %CV for FL/RL of 13%. This trend was also seen for 20 ng/transfection at PTH concentrations from 0.1-1 nM, but showed an increase of 1.37 fold at 10 nM (See Figure 6.5).

As expected, Firefly Luciferase increases with increasing PTH concentrations, giving similar values across all transfections (Figure 6.6A). These findings imply that Firefly values are not affected by the assay. Moreover, as shown in Figure 6.6B, both Firefly Luciferase activity and FL/RL increase with increasing PTH for all transfections.

Table 6.2: Testing the effect of pRL-TK on Renilla Luciferase values in the DLRA

UMR-106 cells were transfected with plasmids at 2, 5, 10 and 20 ng/transfection and treated with PTH 1-34 at 0.1, 1 & 10 nM. Readouts were Firefly and Renilla Luciferase given in relative light units (RLU). Data is presented either as a ratio of Firefly to Renilla (RL) Luciferase or as Fold difference (FD) in Renilla Luciferase from untreated controls. StDev; Standard deviation, %CV; Coefficient of variation.

PTH (nM)	Firefly Luciferase RLU	Renilla Luciferase (RL) RLU	Ratio FL/RL	Mean: Ratio FL/RL	StDev: Ratio FL/RL	% CV: FL/RL	Fold Difference (FD) (Renilla)	Mean FD	StDev FD	%CV FD
pRL-TK at 2 ng/transfection										
0	6426	2580	2.49	2.48	0.02	1	1.06	1.00	0.08	8
0	5645	2288	2.47				0.94			
0.1	24680	2292	10.77	11.18	0.58	5	0.94	0.97	0.04	4
0.1	28239	2436	11.59				1.00			
1	175197	3722	47.07	53.14	8.58	16	1.53	1.32	0.30	23
1	159676	2697	59.21				1.11			
10	577789	11124	51.94	60.29	11.81	20	4.57	3.95	0.88	22
10	555857	8098	68.64				3.33			
pRL-TK at 5 ng/transfection										
0	3622	5633	0.64	0.61	0.04	7	0.92	1.00	0.12	12
0	3865	6660	0.58				1.08			
0.1	13599	6573	2.07	2.00	0.10	5	1.07	1.12	0.07	6
0.1	13805	7185	1.92				1.17			
1	114377	6432	17.78	19.89	2.98	15	1.05	1.20	0.22	18
1	182769	8307	22.00				1.35			
10	578420	19228	30.08	33.96	5.48	16	3.13	2.65	0.68	26
10	502845	13292	37.83				2.16			
pRL-TK at 10 ng/transfection										
0	4538	16728	0.27	0.27	0.01	2	0.98	1.00	0.03	3
0	4591	17529	0.26				1.02			
0.1	16637	16586	1.00	1.15	0.21	18	0.97	0.92	0.07	8
0.1	19265	14834	1.30				0.87			
1	164994	16559	9.96	9.03	1.32	15	0.97	0.94	0.04	4
1	126403	15605	8.10				0.91			
10	505857	20521	24.65	23.67	1.39	6	1.20	1.09	0.15	13
10	385335	16988	22.68				0.99			
pRL-TK at 20 ng/transfection										
0	8063	39942	0.20	0.19	0.01	8	0.96	1.00	0.06	6
0	7886	43596	0.18				1.04			
0.1	20782	37249	0.56	0.50	0.08	15	0.89	1.00	0.15	15
0.1	20654	45948	0.45				1.10			
1	187108	50828	3.68	3.98	0.42	11	1.22	1.03	0.26	26
1	150602	35240	4.27				0.84			
10	721718	55148	13.09	14.53	2.04	14	1.32	1.35	0.04	3
10	916311	57381	15.97				1.37			

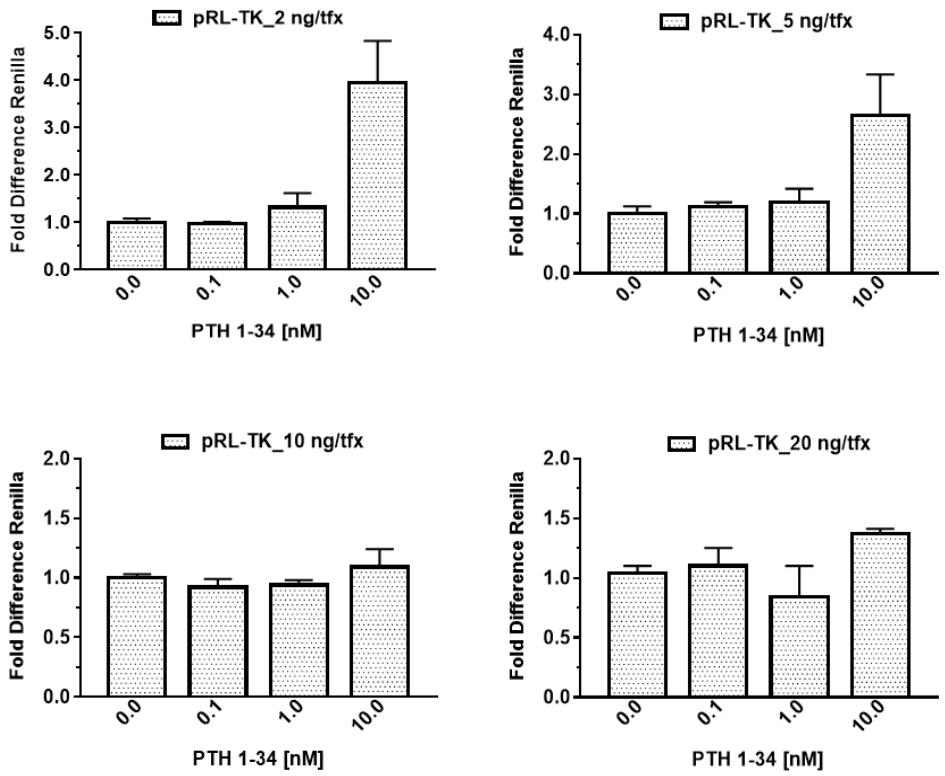

Figure 6.5: Fold difference in Renilla values from untreated controls for pRL-TK transfections. Fold Difference bars plotted against PTH 1-34 treatment (0, 0.1, 1 & 10 nM) for transfections using pRL-TK plasmid at 2, 5, 10, and 20 ng per transfection. Data are presented as mean ± StDev for fold difference Renilla value and data analysed using GraphPad Prism.

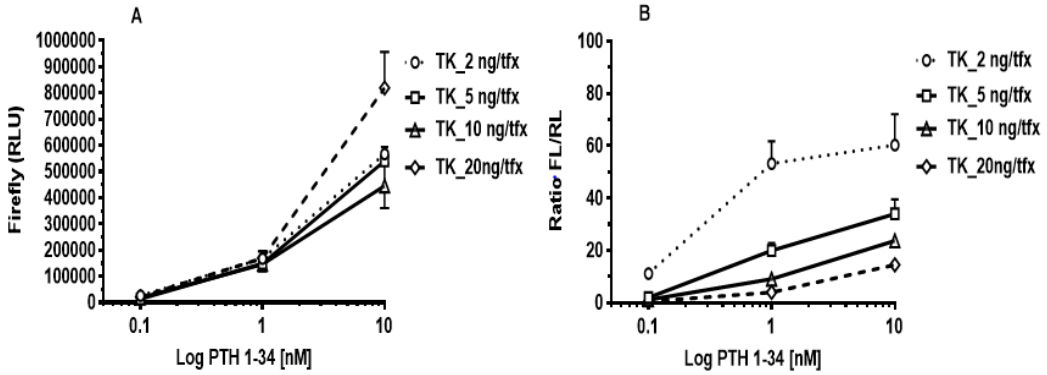

Figure 6.6: Presented the firefly luciferase density and FL/RL ratio values by using pRL-TK plasmid. Data is presented at 2, 5, 10 and 20 ng per transfection plotted against log PTH 1-34 treatment (0, 0.1, 1 & 10 nM) for transfections. **(A)** Firefly Luciferase (RLU) values. **(B)** FL/RL ratio value. Data are presented as mean ± StDev for RLU and FL/RL ratio. Data analysed using GraphPad Prism.

In summary, in line with the findings reported in Figure 6.3 and Figure 6.5, Renilla values were more variable when using lower pRL-TK plasmid concentrations per transfection. This is particularly apparent when data from 2 and 5 ng/transfection were compared to values obtained for 10 and 20 ng/transfection, which were more consistent. For this reason and to confirm these results the assay was repeated using only pRL-TK at 10 and 20 ng per transfection.

6.2.2.3 Validating pRL-TK at 10 and 20 ng per transfection

For this experiment, the previously described setup used for testing pRL-TK plasmid at 10 & 20 ng/transfection was employed and the FL/RL and FD data are presented in Table 6.3 and Figure 6.7. The results show consistent Renilla values across all PTH concentrations studied, with a maximum FD of 1.19 and 1.12 for 10 and 20 ng/transfection, respectively. The %CV for FD are also consistent and remain below 25%. As expected, Firefly Luciferase levels increase with increasing PTH and are similar across all treatments (Figure 6.8A). Moreover, the FL/RL activity ratio increases with increasing PTH for all transfections. Renilla values for 20 ng/transfection are close to double those values for 10 ng/transfection and are directly related to an increase in plasmid per transfection. This increase in Renilla in turn leads to a decreased FL/RL ratio for 20 ng/transfection compared to 10 ng/transfection, as shown in Figure 6.8B.

Table 6.3: Testing the effect of pRL-TK on Renilla Luciferase values in the DLRA.

UMR-106 cells were transfected with plasmids at 10 and 20 ng/transfection and treated with PTH 1-34 at 0.1, 1 & 10 nM. Readouts were Firefly and Renilla Luciferase given in relative light units (RLU). Data is presented either as a ratio of Firefly to Renilla (RL) Luciferase or as Fold difference (FD) in Renilla Luciferase from untreated controls. StDev; Standard deviation, %CV; Coefficient of variation.

PTH (nM)	Firefly Luciferase RLU	Renilla Luciferase (RL) RLU	Ratio FL/RL	Mean: Ratio FL/RL	StDev: Ratio FL/RL	% CV: FL/RL	Fold Difference (FD) (Renilla)	Mean FD	StDev FD	%CV FD
pRL-TK at 10 ng/transfection										
0	3331	11812	0.28	0.28	0.001	0.3	1.01	1.00	0.02	2
0	3246	11562	0.28				0.99			
0.1	47144	15185	3.10	2.66	0.62	23	1.30	1.16	0.19	17
0.1	26652	11996	2.22				1.03			
1	158641	13696	11.58	10.35	1.74	17	1.17	1.19	0.03	2
1	128950	14134	9.12				1.21			
10	467170	13774	33.92	32.24	2.36	7	1.18	1.19	0.01	1
10	427627	13987	30.57				1.20			
pRL-TK at 20 ng/transfection										
0	2667	19486	0.14	0.118	0.027	23	0.89	1.0	0.162	16
0	2432	24537	0.10				1.11			
0.1	24943	20954	1.19	0.812	0.535	66	0.95	0.924	0.040	4
0.1	8549	19707	0.43				0.90			
1	88280	21775	4.05	4.27	0.30	7	0.99	1.04	0.07	7
1	107987	24094	4.48				1.09			
10	368191	25122	14.66	14.92	0.375	3	1.14	1.12	0.02	2
10	370114	24371	15.19				1.11			

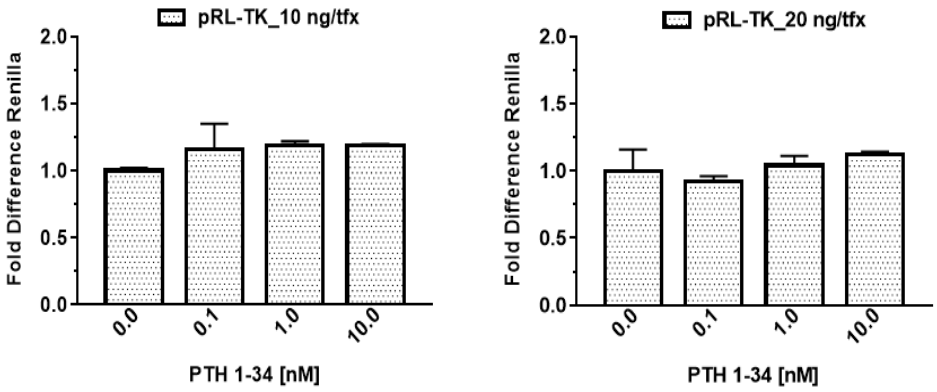

Figure 6.7: Fold difference in Renilla values from untreated controls for pRL-TK transfections.

Fold Difference bars plotted against PTH 1-34 treatment (0, 0.1, 1 & 10 nM) for transfections using pRL-TK plasmid at 10, and 20 ng per transfection. Data are presented as mean ± StDev for fold difference Renilla value and data analysed using GraphPad Prism.

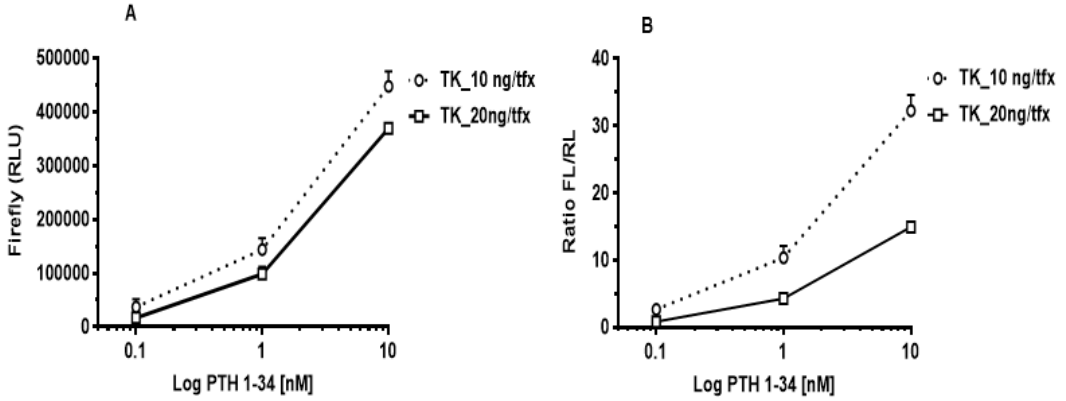

Figure 6.8: Represented the firefly luciferase density and FL/RL ratio values by using pRL-TK plasmid. Data is presented at 10 and 20 ng per transfection plotted against log PTH 1-34 treatment (0, 0.1, 1 & 10 nM) for transfections. (**A)** Firefly Luciferase (RLU) values. **(B)** FL/RL ratio value. Data are presented as mean ± StDev for RLU and FL/RL ratio. Data analysed using GraphPad Prism.

6.2.2.4 Final Analysis of Mean FD for Renilla Using pRL-TK

Using pRL-TK at 10 and 20 ng/transfection produced more consistent results in Renilla values. The mean fold differences from two independent experiments, measured at different PTH concentrations 0, 0.1, 1, and 10 nM, were evaluated and are presented in Table 6.4 and Figure 6.9. Renilla values increased very slightly as PTH concentrations increased, with a maximum FD of 1.13 and 1.27 at 10 and 20 ng/transfection, respectively. Moreover, the %CV FD values remained below 25%. Based on these results, pRL-TK at 20 ng/transfection was adopted for all future assays and validated in the next section using a full standard curve for PTH 1-34.

Table 6.4: The mean of FD for Renilla from two separate experiments using pRL-TK at 10 and 20 ng/transfection and treated with PTH 1-34 at 0.1, 1 & 10 nM**.**

Mean fold difference (FD) in Renilla Luciferase from untreated controls. StDev; Standard deviation, %CV; Coefficient of variation.

PTH (nM)	Mean FD	StDev FD	%CV FD
Mean pRL-TK at 10 ng/transfection			
0	1.0	0.014	1
0.1	1.01	0.121	12
1	1.04	0.013	1
10	1.13	0.081	7
Mean pRL-TK at 20 ng/transfection			
0	1.0	0.097	10
0.1	0.97	0.083	9
1	1.03	0.147	14
10	1.27	0.016	1

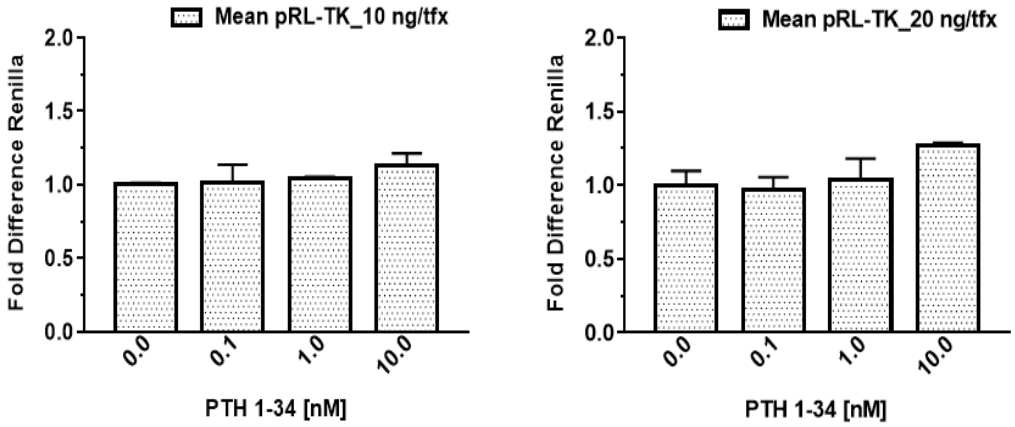

Figure 6.9: Mean fold difference in Renilla values from untreated controls for pRL-TK transfections. Mean fold Difference bars plotted against PTH 1-34 treatment (0, 0.1, 1 & 10 nm) for transfections using pRL-TK plasmid (n=2) at 10 and 20 ng per transfection. Data are presented as mean FD ± StDev (FD) and data analysed using GraphPad Prism.

6.2.3 Testing a Full Standard Curve for PTH 1-34

The assay was tested using PTH 1-34 adopting the previously determined parameters, along with pRL-TK plasmid at 20 ng/transfection (as described in Section 6.2.2.4). Briefly,

transfected cells were challenged with increasing PTH concentrations and samples analysed using the Promega Dual-Luciferase Reporter Assay kit (as described in Section 2.3.7). Cells were lysed in 150 µL of lysis buffer and 50 µL of the cell lysate was taken for analysis.

All samples were tested in duplicate and the ratio of Firefly to Renilla Luciferase (FL/RL ratio) for each sample was calculated using Excel software and an average ratio for each sample as well as StDev and %CV for these measurements were obtained. The mean activity was calculated from the average FL/RL ratio, and fold induction was obtained by calculating the fold difference in mean activity between samples and controls. Next, the % maximum fold induction was obtained by calculating the % change in fold induction of all samples relative to the highest value. Finally, EC_{50}s were calculated using GraphPad Prism software with a 3- or 4-parameter fit.

As shown in Table 6.5 and Figure 6.10, Renilla expression does not increase with increasing PTH concentrations and FD remains stable, with a maximum fold difference of 1.22 (StDev = 0.10) at 364.5 nM and the %CV of FD remains below 20%. As expected, both Firefly Luciferase and FL/RL value increase with increasing PTH, as previously observed (Figure 6.11).

A plot of the % maximum fold induction vs PTH produces a sigmoidal curve in which the maximum fold induction of 73.9 (StDev = 3.9) corresponds to ~40.5 nM (Figure 6.12). The EC_{50} values obtained from plots of mean activity (FL/RL ratio) against log PTH 1-34 concentration for two independent experiments are presented in Table 6.6 and show a mean EC_{50} of 2.23 (StDev = 0.16) with a %CV of 7%. The assay activity peaks at 40.5 nM and shows a sensitivity down to ~ 0.055 nM, giving an assay range of 0.055−40.5 nM.

Table 6.5: The mean FD for Renilla from two separate PTH 1-34 experiments testing the effect of pRL-TK at 20 ng/transfection on Renilla Luciferase values in the DLRA.

UMR-106 cells were transfected with pRL-TK plasmids at 20 ng/transfection and treated with PTH 1-34 (n=2) at (0 - 364.5 nm). Mean Fold difference (FD) in Renilla Luciferase from untreated controls. StDev; Standard deviation, %CV; Coefficient of variation

PTH (nM)	Mean FD	StDev FD	%CV FD
DB*	1.00	0.10	10
0.0037	1.04	0.09	9
0.0185	1.08	0.05	4
0.055	0.96	0.07	7
0.166	0.88	0.03	4
0.5	0.92	0.10	11
1.5	0.97	0.04	4
4.5	0.92	0.09	10
13.5	0.98	0.18	18
40.5	0.93	0.02	2
121.5	0.97	0.14	14
364.5	1.22	0.10	8

*DB: DMEM Buffer/0.1% BSA

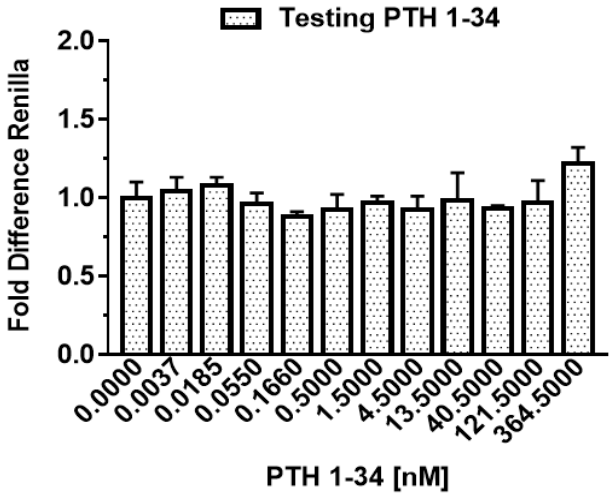

Figure 6.10: The mean fold difference in Renilla from testing pRL-TK plasmid at 20 ng per transfection plotted against PTH 1-34 (n=2) treatment (0-364.5 nM).

Data are presented as mean ± StDev for fold difference Renilla and analysed using GraphPad Prism.

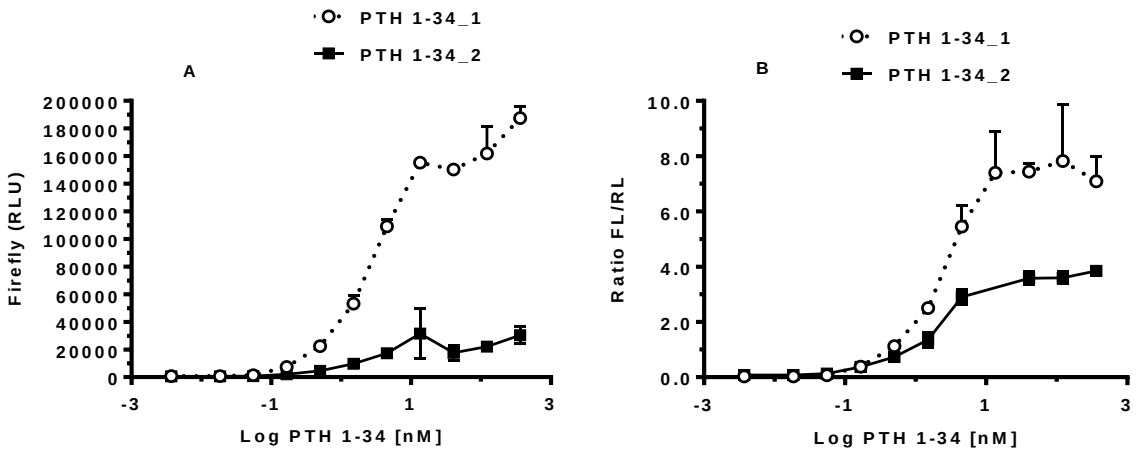

Figure 6.11: DLRA of PTH 1-34 testing pRL-TK at 20 ng per transfection (n=2).

Standard curves were produced from a range of concentrations, 364.5-0.0037 nM for PTH 1-34. **(A)** Firefly Luciferase (RLU) plotted against log10 PTH 1-34. **(B)** FL/RL ratio plotted against log10 PTH 1-34. Data are presented as mean ± StDev for RLU and FL/RL ratio. Data analysed using GraphPad Prism.

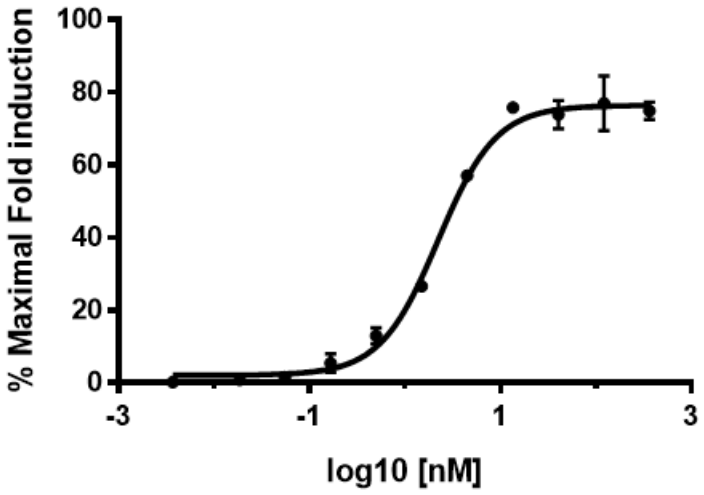

Figure 6.12: Mean % Maximum fold induction plotted against Log10 PTH 1-34 [nM].

The standard curve was produced from a range of concentrations, 364.5-0.0037 nM for PTH 1-34. Data are presented as the mean of 2 independent experiments ±StDev.

Table 6.6: The EC50 values calculated for PTH 1-34 (n= 2)

Each EC_{50} value is given as mean (nM), standard deviation (StDev), and Coefficient of variation (%CV).

Assay (EC_{50})			Mean	StDev	%CV
Test Sample	**1**	**2**			
PTH	2.342	2.199	**2.23**	**±0.16**	**7%**

6.2.4 Establishing the Acceptance Criteria

Based on the studies described in the preceding sections, assay acceptance criteria were established. Specifically, Renilla values should not exhibit an upward trend with increasing PTH concentrations. Assays showing this trend will be discarded. In addition, %CV's of duplicate FL/RL ratios should not exceed 25%. Values greater than this will be discarded from the analysis. In summary, the data is accepted as valid if the FL/RL ratio is ≤25% and Renilla values do not increase with increasing PTH.

6.3 Bioactivity Studies

PTH fusions were purified as described in Chapter 5, and DLRA development was completed using the optimised DLRA assay methodology described in Section 6.2. Using the established DLRA assay, EC_{50}'s were generated for PTH fusions and compared to PTH (See Appendix B1 for a full description of all fusion constructs). 14A7 (PTH linked to GHBP) is the smallest molecule and is hypothesised to be the most active due to less steric hindrance from the GHBP moiety. Conversely, 14A2c (PTH linked to PTHrExt and GHBP) is hypothesised to be the least active due to its increased size as well as steric hindrance, but also because PTH may potentially undergo intramolecular interactions with the PTHrExt, thus reducing PTH

availability. 14A8 is a control for 14A2c and contains the I135K mutation, which prevents PTH from binding to PTHrExt.

Each assay was conducted using duplicate samples and assays were repeated for a total of 3 independent experiments. Mean activity (FL/RL), fold induction, and % maximum fold induction were calculated using Excel software, and data plotted in GraphPad Prism using a 4-parameter fit to obtain EC_{50}'s (See Section 6.2.3).

6.3.1 Bioactivity of PTH 1-34

Based on the criteria described in Section 6.2.4, PTH 1-34 bioactivity analysis was performed for a total of ten times and data analysed as outlined in Section 6.3.

A plot of mean % maximum fold induction vs log PTH (based on eight independent experiments) produced a sigmoidal curve with peak activity at 40.5 nM (StDev = 5.6) and a sensitivity of 0.055 nM (StDev = 0.6; 0.055−40.5 nM), resulting in a >700 fold spread in concentrations (See Figure 6.13). The EC_{50}'s were obtained from the mean activity (FL/RL ratio) vs log PTH concentration plots and a mean EC_{50} of 2.39 (StDev = 0.58) obtained with a %CV of 24% (See Table 6.7). It is worth noting that, although ten assays were performed, two were omitted due to the increase in Renilla values across PTH concentrations. The EC_{50} values for these two assays were 0.38 and 17 nM, respectively.

Analysis of the mean fold difference showed that Renilla expression did not exhibit any obvious trends across the tested PTH concentrations, while FD remained stable with a maximum fold difference of 1.32 (StDev = 0.06) at 40.5 nM (Table 6.8 and Figure 6.14). The %CV of FD was below 25% across all PTH concentrations. As expected, both Firefly

Luciferase and FL/RL value increased with increasing PTH. Thus, these assays were accepted for analysis as they met the criteria outlined in Section 6.2.4.

As noted earlier, two assays were omitted from the analysis due to errors and not meeting the acceptance criteria (See Section 6.2.4). Figures 6.15A and 6.15B depict the results of these omitted assays, revealing an upward trend of 16.7 and 2.78-fold, respectively in Renilla values with increasing PTH. Moreover, several duplicate FL/RL samples were discarded as %CV exceeded 25%.

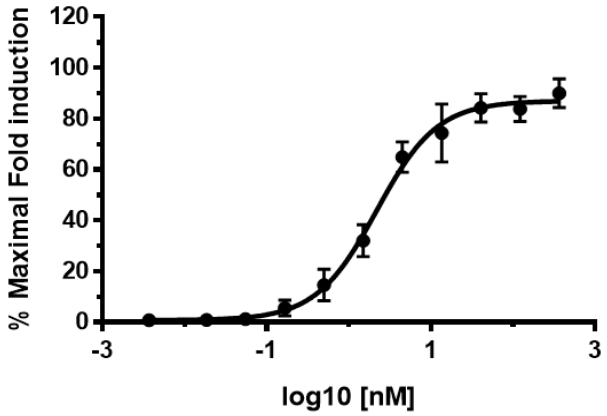

Figure 6.13: Mean % Maximal Fold Induction of PTH 1-34 (n=8) against log10 concentration (nM). The standard curve was produced from a range of concentrations, (364.5-0.0037 nM) for PTH 1-34. Data analysed by GraphPad Prism and presented as mean maximal fold induction ± StDev calculated from an average of 8 separate experiments.

Table 6.7: EC_{50} values calculated for PTH 1-34 (n= 8)

Each EC_{50} value is given as mean (nM), standard deviation (StDev), and Coefficient of variation (%CV).

Assay (EC_{50})											Mean	StDev	%CV
Test Sample	**1***	**2***	**3****	**4****	**5#**	**6#**	**7##**	**8##**	**9x**	**10x**			
PTH	2.24	2.19	1.97	1.66	3.09	2.49	3.37	1.98	0.38	17	**2.39**	**±0.58**	**24%**

***** **Assay tested in section 6.2.3**
****** **Assay tested with 14A7**
**Assay tested with 14A2c**
**Assay tested with 14A8**
x **Assays Discarded**

Table 6.8: The mean fold differences in Renilla for n = 8 separate experiments
UMR-106 cells were transfected with pRL-TK plasmids at 20 ng/transfection and treated with PTH 1-34 (n=8) at (0 - 364.5 nm). Mean Fold difference (FD) in Renilla Luciferase from untreated controls. StDev; Standard deviation, %CV; Coefficient of variation.

PTH (nM)	Mean FD	StDev FD	%CV FD
DB*	1.00	0.20	20
0.0037	0.91	0.09	10
0.0185	0.99	0.05	5
0.055	0.85	0.18	21
0.166	1.00	0.13	13
0.5	1.03	0.05	5
1.5	1.00	0.01	1
4.5	1.10	0.12	11
13.5	1.14	0.17	15
40.5	1.32	0.06	5
121.5	1.22	0.04	3
364.5	1.30	0.07	6

*DB: DMEM Buffer/0.1% BSA

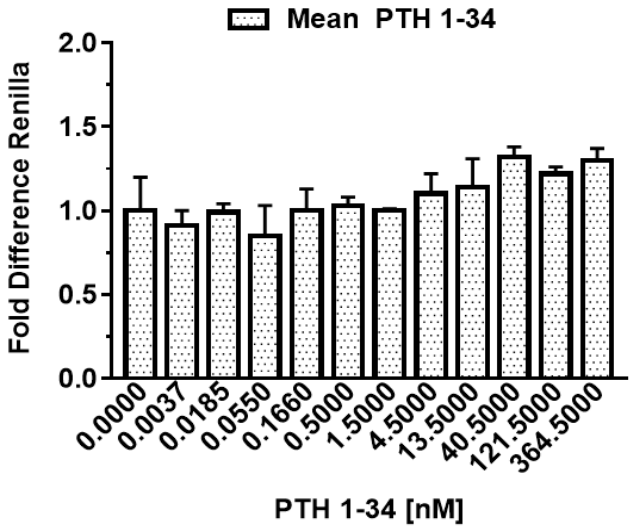

Figure 6.14: Mean Fold difference in Renilla values for PTH 1-34 (n=8) assays.

Fold Difference bars plotted against PTH 1-34 treatment (0-364.5 nM) for transfections using pRL-TK at 20 ng per transfection. Data are presented as mean FD ± StDev (FD) and data analysed using GraphPad Prism.

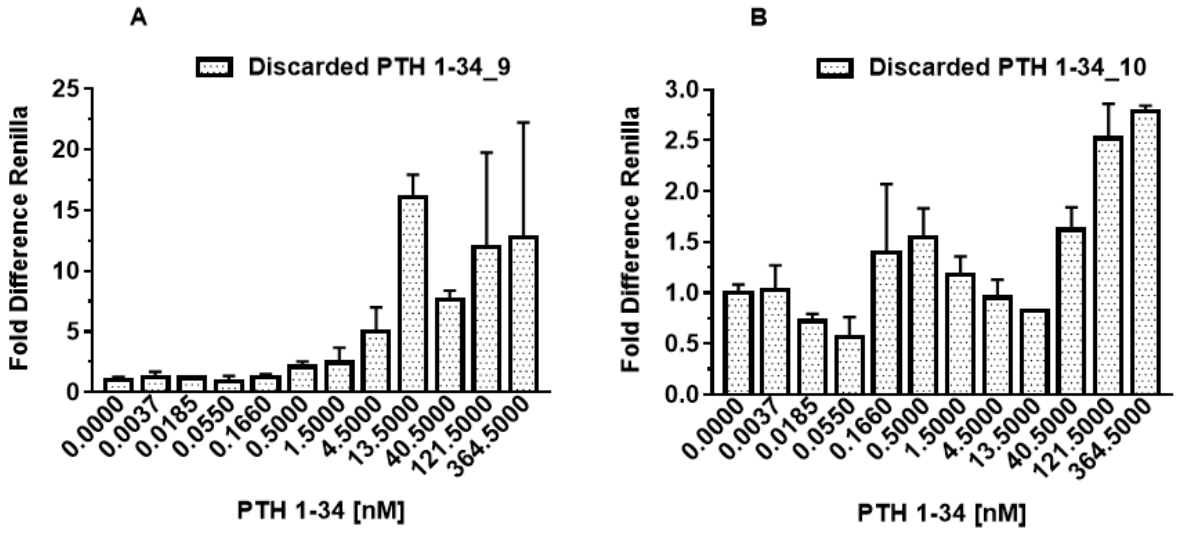

Figure 6.15: Presented fold difference in Renilla values for discarded two PTH 1-34 assays.

Fold Difference bars plotted against PTH 1-34 treatment (0-364.5 nM) for transfections using pRL-TK 20 ng per transfection. This data was dismissed. **A)** PTH 1-34_9, **B)** PTH 134_10. Data are presented as mean FD ± StDev (FD) and data analysed using GraphPad Prism.

In summary, EC_{50}'s obtained for eight assays met the acceptance criteria, and mean EC_{50} values compare to PTH fusion molecules (See Appendix H2 for graphical displays of FD and FL/RL vs log plots for all remaining assays).

6.3.2 Bioactivity of PTH-Fusion 14A7

Figure 6.16 shows a plot of mean % maximum fold induction for 14A7 (based on n = 4 experiments) and PTH 1-34 (n = 8). It is evident that the sigmoidal curve for 14A7 has shifted to the right with a maximum stimulation obtained at 5000 nM (StDev = 1.71) compared to PTH 1-34 that produced a sigmoidal curve with a maximum stimulation at 40.5 nM (StDev = 5.6).

EC_{50} values were obtained from the mean activity (FL/RL) vs log plot (See Table 6.9). These gave a mean EC_{50} of 69.24 nM (StDev = 2.819) compared to 2.39 nM (StDev = 0.58) for PTH 1-34. These results demonstrate that 14A7 is approximately ~35 fold less potent compared to PTH 1-34.

Analysis of the mean fold difference in Renilla Luciferase reveals an absence of any trend of increasing Renilla values relative to controls across all concentrations (See Table 6.10 and Figure 6.17). In addition, %CV's remain at ≤25% between duplicate FL/RL ratios. As expected, the FL/RL ratio increases with increasing 14A7 for all transfections. However, one assay failed to meet the aforementioned criteria, as shown in Figure 6.18A, and was omitted from the analysis due to an increase in Renilla values of up to 18-fold at 150 nM. Also several duplicate FL/RL samples had to be discarded as the %CV of the exceeded 25%. Due to these variations, maximum stimulation was not achieved and a sigmoidal curve was not produced, as shown

in Figure 6.18B. All other assays were accepted for analysis, as they met the criteria outlined in Section 6.2.4.

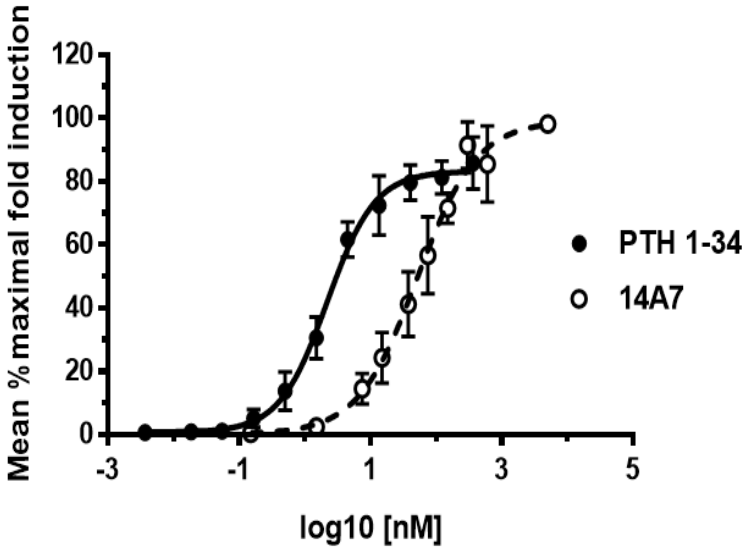

Figure 6.16: Mean % Maximal Fold Induction of 14A7 and PTH 1-34 against log10 concentration (nM). PTH 1-34 (n=8) (•) and 14A7 (n=4) (○). The standard curve was produced from a range of concentrations, (0.0037-364.5 nM) for PTH and (0.15-5000 nM) for 14A7 on the challenge of UMR-106 cells. Data presented by GraphPad Prism and presented as maximal fold induction ± StDev calculated from an average of duplicate values.

Table 6.9: EC_{50} values calculated for 14A7 (n= 5)

Each EC_{50} value is given as mean (nM), standard deviation (StDev), and Coefficient of variation (%CV).

Assay (EC_{50})						**Mean**	**StDev**	**%CV**
Test Sample	**1**	**2**	**3**	**4**	**5[x]**			
14A7	66.44	72.24	70.22	63.21	202	**68.02**	**4.01**	**6**

X Assay Discarded

Table 6.10: The mean fold difference of four separate 14A7 experiments

UMR-106 cells were transfected with pRL-TK plasmids at 20 ng/transfection and treated with 14A7 at (0 – 5000 nM). Mean Fold difference (FD) in Renilla Luciferase from untreated controls. StDev; Standard deviation, %CV; Coefficient of variation.

14A7 (nM)	Mean FD	StDev FD	%CV FD
DB*	1.00	0.022	2
0.15	1.06	0.13	12
1.5	0.84	0.027	3
15	0.99	0.102	10
37.5	1.10	0.07	7
75	1.17	0.08	7
150	1.21	0.03	3
300	0.94	0.19	20
600	1.24	0.16	13
5000	1.30	0.08	6

*DB: DMEM Buffer/0.1% BSA

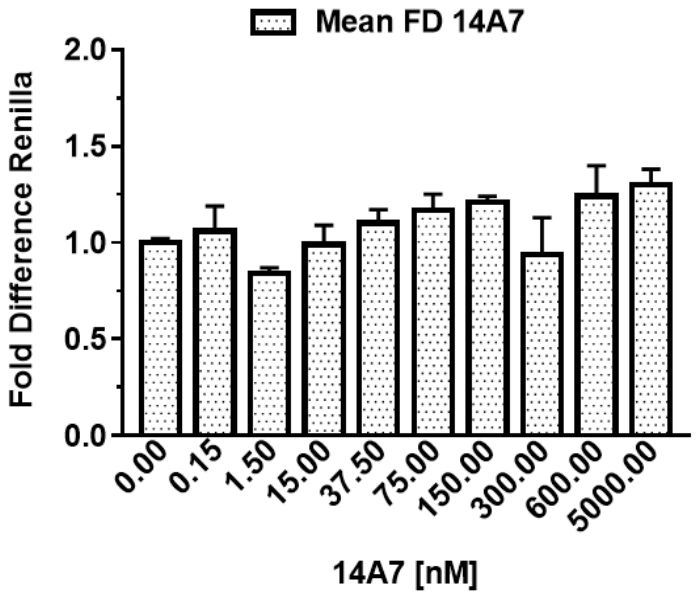

Figure 6.17: Mean fold difference in Renilla values for 14A7 (n=4) assay.

Fold Difference bars plotted against 14A7 treatment (0–5000 nM) for transfections using pRL-TK 20 ng per transfection. Data are presented as mean FD ± StDev (FD) and data analysed using GraphPad Prism.

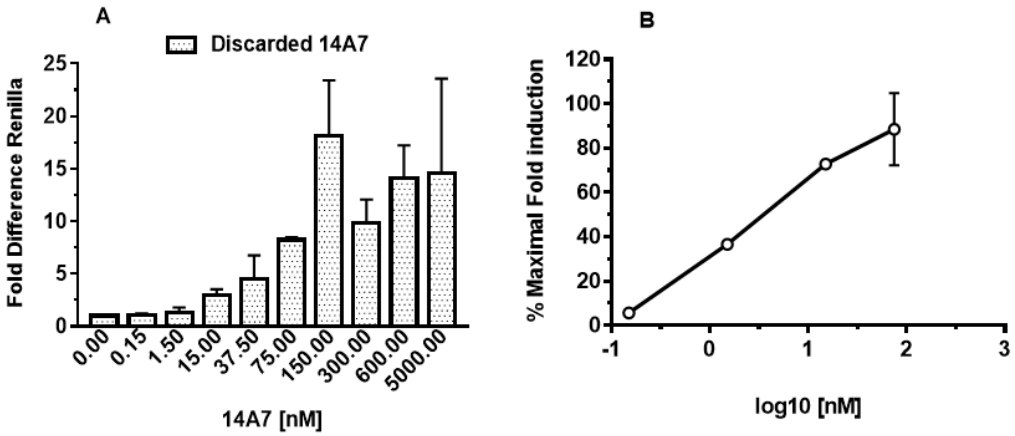

Figure 6.18: Represents the discarded 14A7 assay data.

(A) Mean Fold difference in Renilla values for 14A7_5 assay. Fold Difference bars plotted against 14A7 treatment (0–5000 nM) for transfections using pRL-TK 20 ng per transfection. Data are presented as mean FD ± StDev (FD). **(B)** % Maximal Fold Induction of 14A7_5 vs log10 concentration (0.15-5000 nM) for 14A7 on challenge of UMR-106 cells. Data presented by GraphPad Prism and presented as mean maximal fold induction ± StDev calculated from an average of duplicate values.

6.3.3 Bioactivity of PTH-Fusion 14A2c

Mean % maximum fold induction for 14A2c (n = 3) and PTH 1-34 (n = 8) is presented in Figure 6.19. 14A2c produced a sigmoidal curve that is shifted to the right relative to PTH 1-34, with a maximum stimulation at 49162 nM (StDev = 2.82) whereas PTH 1-34 exhibited a maximum stimulation at 40.5 nM (StDev = 5.6).

Also, for 14A2c, an EC_{50} of 699.24 nM (StDev = 55.6) with a %CV of 8% was obtained compared to an EC_{50} of 2.39 nM (StDev = 0.58) PTH 1-34 (See Table 6.11). Data show that 14A2c is ~292 fold less potent compared to PTH 1-34. No trends in increasing Renilla values relative to controls across all 14A2c concentrations were observed (See Table 6.12 and Figure 6.20). As expected, the FL/RL ratio increases with increasing 14A2c. It should, however, be noted that some individual points were removed from the analysis as the FL/RL ratios CV exceeded 25%.

Nonetheless, all assays met the criteria outlined in Section 6.2.4 and were accepted for analysis.

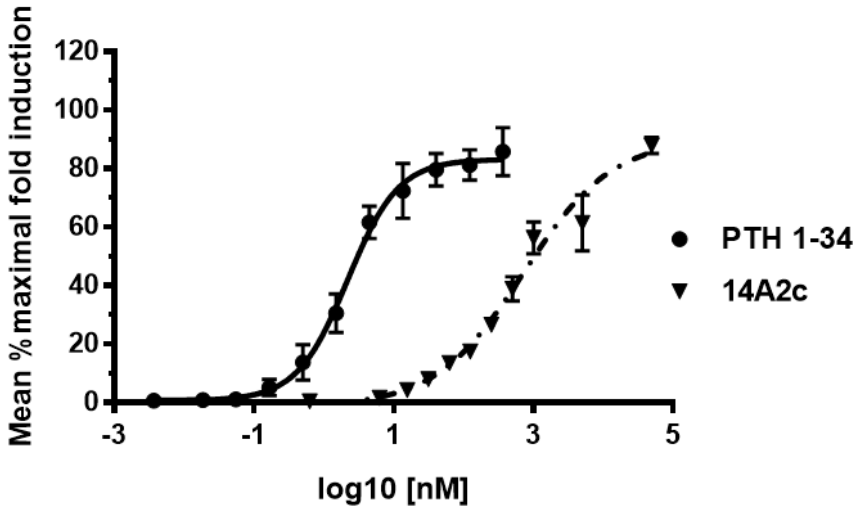

Figure 6.19: Mean % maximal fold induction of 14A2c and PTH 1-34 against log10 concentration (nM). PTH 1-34 (n=8) (•) and 14A2c (n=3) (▼). The standard curve was produced from a range of concentrations, (364.5-0.0037 nM) for PTH and (49162-0.625 nM) for 14A2c fusion on the challenge of UMR-106 cells. Data presented by GraphPad Prism and presented as maximal fold induction ± StDev calculated from an average of duplicate values.

Table 6.11: EC_{50} values calculated for 14A2c (n= 3)

Each EC_{50} value is given as mean (nM), standard deviation (StDev), and Coefficient of variation (%CV).

Assay (EC_{50})				**Mean**	**StDev**	**%CV**
Test Sample	**1**	**2**	**3**			
14A2c	721	636.2	741	**699.4**	**55.6**	**8**

Table 6.12: The mean fold difference of three separate 14A2c experiments

UMR-106 cells were transfected with pRL-TK plasmids at 20 ng/transfection and treated with 14A2c at (0 - 49162 nM). Mean Fold difference (FD) in Renilla Luciferase from untreated controls. StDev; Standard deviation, %CV; Coefficient of variation.

14A2c (nM)	Mean FD	StDev FD	%CV FD
DB*	1.00	0.07	7
0.625	1.09	0.01	1
6.25	1.02	0.02	2
15.6	0.98	0.11	11
31.25	0.82	0.08	9
62.5	1.17	0.12	11
125	1.31	0.24	18
250	1.20	0.03	3
500	1.19	0.02	1
1000	1.27	0.32	25
5000	1.40	0.03	2
49162	1.19	0.28	23

*DB: DMEM Buffer/0.1% BSA

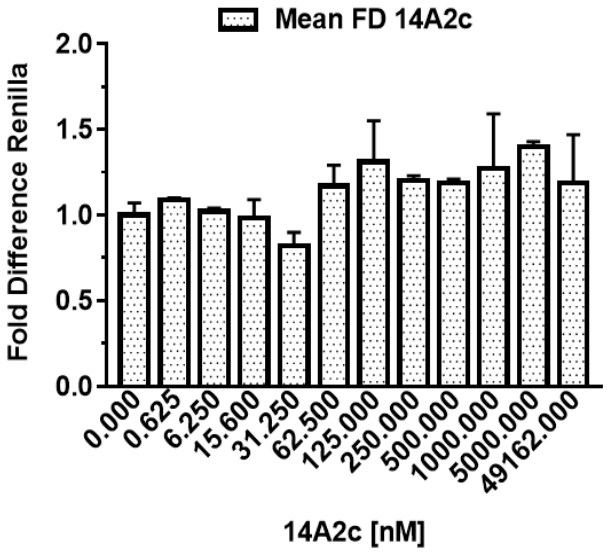

Figure 6.20: Mean fold difference in Renilla values for 14A2c (n=3) assay.

Fold Difference bars plotted against 14A2c treatment (0–49162 nM) for transfections using pRL-TK 20 ng per transfection. Data are presented as mean FD ± StDev (FD) and data analysed using GraphPad Prism.

6.3.4 Bioactivity of PTH-Fusion 14A8

Mean % maximum fold induction plots for 14A8 (n = 3) and PTH 1-34 (n = 8) are presented in Figure 6.21. Similar to previously PTH-fusions, 14A8 produced a sigmoidal curve that is shifted to the right compared to PTH 1-34, with a maximum stimulation at 5000 nM (StDev = 7.83). The EC_{50}s obtained from the mean activity (FL/RL) vs log plots are presented in Table 6.13. An EC_{50} of 253.8 nM (StDev = 26.31) was obtained with a %CV of 10%. This equates to ~106-fold reduction in potency compared to PTH 1-34.

No trend was observed in the mean fold difference values in Renilla Luciferase and with the %CV below 25% between duplicate FL/RL ratios in all assays (See Table 6.14 and Figure 6.22). As all assays met the acceptance criteria, all were accepted for analysis.

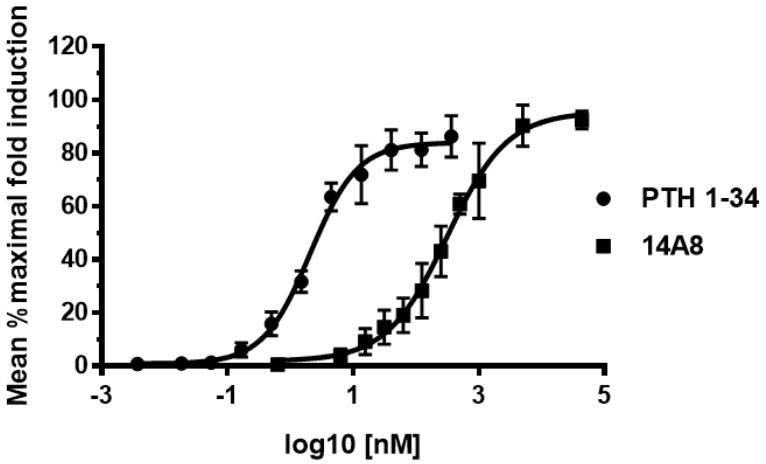

Figure 6.21: Mean % Maximal Fold Induction of 14A8 and PTH 1-34 against log10 concentration (nM). PTH 1-34 (n=8) (•) and 14A8 (n=3) (■). The standard curve was produced from a range of concentrations, (0.0037-364.5 nM) for PTH (1-34) and (0.625-43812 nM) for 14A8 fusion on the challenge of UMR-106 cells. Data presented by GraphPad Prism and presented as maximal fold induction ± StDev calculated from an average of duplicate values.

Table 6.13: The EC_{50} values calculated for 14A8 (n= 3)

Each EC_{50} value is given as mean (nM), standard deviation (StDev), and Coefficient of variation (%CV).

Assay (EC_{50})				Mean	StDev	%CV
Test Sample	**1**	**2**	**3**			
14A8	224.5	275.4	261.5	**253.8**	**26.3**	**10**

Table 6.14: The mean fold difference of three separate 14A8 experiments

UMR-106 cells were transfected with pRL-TK plasmids at 20 ng/transfection and treated with 14A8 at (0–43812 nM). Mean Fold difference (FD) in Renilla Luciferase from untreated controls. StDev; Standard deviation, %CV; Coefficient of variation.

14A8 (nM)	Mean FD	StDev FD	%CV FD
DB*	1.00	0.20	20
0.625	0.97	0.01	1
6.25	0.95	0.01	1
15.6	1.02	0.00	0
31.25	0.70	0.02	4
62.5	0.85	0.10	12
125	0.80	0.02	2
250	0.81	0.11	13
500	0.75	0.04	5
1000	0.88	0.04	5
5000	0.91	0.02	2
43812	1.12	0.17	15

*DB: DMEM Buffer/0.1% BSA

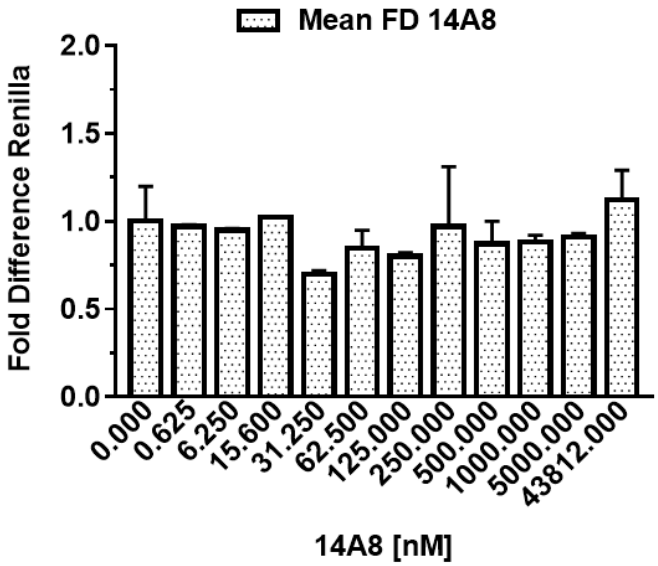

Figure 6.22: Mean fold difference in Renilla values for 14A8 (n=3) assay.
Fold Difference bars plotted against 14A8 treatment (0–43812 nM) for transfections using pRL-TK 20 ng per transfection. Data are presented as mean FD ± StDev (FD) and data analysed using GraphPad Prism.

6.3.5 Comparison of EC_{50}s and Statistical Significance

Percentage maximum fold induction vs log nM curves for all PTH fusions were compared and all produced sigmoidal curves shifted to the right in comparison to PTH 1-34, indicating reduced potency in the following sequence, PTH 1-34 > 14A7 > 14A8 > 14A2c (See Figure 6.23). To assess the significance of these findings, the null hypothesis (stipulating that there are no statistically significant differences between the EC_{50} values of PTH 1-34 and PTH fusion molecules) was tested by carrying out a one-way ANOVA. As differences between samples were noted at $p \leq 0.0001$ significance level, Tukey's multiple comparisons test was conducted. The results, reported in Table 6.15, revealed a significant difference in each comparison across these groups. Thus, null hypothesis was rejected.

Therefore, the alternative hypothesis was accepted, that the EC_{50} values of PTH 1-34 and PTH fusions were significantly different from each other. PTH has an EC_{50} 2.39 ± 0.58 nM (based on eight experiments) and is ~29-fold more potent than 14A7 (EC_{50} = 68.02 ± 4.01 nM, n = 4), 106-fold more potent than 14A8 (EC_{50} = 253.8 ± 26.3 nM, n =3) and 296-fold more potent than 14A2c (EC_{50} = 699.4 ± 55.6 nM, n = 3). Data was analysed using GraphPad Prism version 9 (GraphPad Software, San Diego California USA).

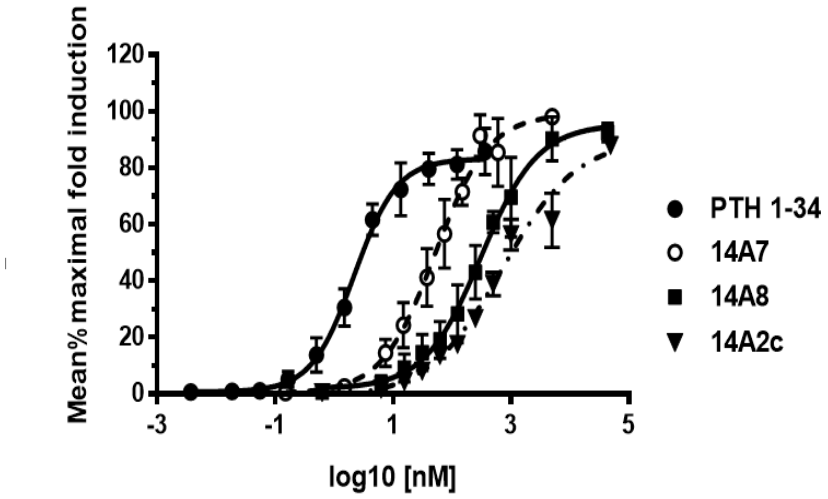

Figure 6.23: Mean % maximum fold induction against log10 concentration (nM) for all ligands. Data presented as Mean % maximal fold induction ± StDev for PTH 1-34 (n=8, •), 14A7 (n=4, ○), 14A2c (n=3, ▼), 14A8 (n=3, ■) and produced by GraphPad Prism.

Table 6.15: Comparative statistics of EC_{50} values of PTH 1-34 and PTH fusion proteins
GraphPad Prism was used for this Tukey's multiple comparisons test. **(A)** Each EC_{50} value is given as mean, standard deviation **(B)** A significance level is generated for the comparison of all Fusions.

(A)

	Fusion	N	Mean	StDev	FD related to PTH 1-34
EC_{50}	PTH (1-34)	8	2.39	0.58	-
	14A7	4	68.02	4.01	29-fold
	14A8	3	253.8	26.3	106-fold
	14A2c	3	699.4	55.6	269-fold

(B)

Tukey's multiple comparisons test	Adjusted *P* Value	Mean Diff.
PTH 1-34 vs. 14A7	0.0021	-65.65
PTH 1-34 vs. 14A8	<0.0001	-251.4
PTH 1-34 vs. 14A2c	<0.0001	-697.0
14A7 vs. 14A8	<0.0001	-185.8
14A7 vs. 14A2c	<0.0001	-631.4
14A2c vs. 14A8	<0.0001	445.6

6.4 Discussion

A Dual-Luciferase Reporter Assay (DLRA) was used in this investigation as it is a suitable method for comparing PTH 1-34 and PTH fusions activity. The DLRA was developed based on Firefly and Renilla Luciferase activity using UMR-106 cells (rat osteosarcoma cell line) that endogenously express PTHR1. The DLRA assay offers several advantages for measuring gene expression, including reduction in inherent variability that can undermine experimental accuracy. Moreover, as a control reporter gene is coupled to a constitutive promoter, experimental variations, such as differences in cell number, pipetting errors, and cell transfection and lysis efficiency, can be mitigated (Sherf et al., 1996).

To correct for variations in transfection efficiency, control plasmids constitutively expressing Renilla luciferase under two different promoters (CMV and TK) were transfected in to UMR-106 at different concentrations, along with the cAMP reporter plasmid pGL4.29 that expresses Firefly Luciferase. Cells were challenged with ligand, and cell lysis was followed by measuring the activity of both luciferases in a luminometer (Sherf et al., 1996) applying the method described in Section 2.3.7. Initial data using the plasmid pRL-CMV showed that the CMV promoter might not be compatible with the chosen assay protocol because Renilla values were inconsistent and increased with increasing PTH concentrations implying assay interference. As a result, the assay was validated using both control plasmids pRL-CMV and pRL-TK. In the latter control plasmid, Renilla is under the control of the thymidine kinase promoter from HSV. During the validation process, pRL-TK was found to be superior to pRL-CMV, as pRL-TK at 10 or 20 ng per transfection yielded more consistent results with no variation in Renilla expression noted with increasing PTH 1-34 concentrations. Similar results were also obtained for Renilla when PTH fusions were tested.

The conflicting results obtained with these two promoters can potentially be attributed to the presence of numerous transcription factor binding sites in the CMV promoter, including one for CREB, which in turn induces Renilla Luciferase expression and may well be the main source of variation (Badding et al., 2012, Shan and Storm, 2010). It is also worth noting that, although the TK promoter also contains transcription factor binding sites, including those of Sp1, Nurr1, skNAC (Matuszyk et al., 2002, Sims et al., 2003), and several GATA transcription factors (Ho and Strauss, 2004), TK is suggested to be a weak promoter (Jiwaji et al., 2010). The TK promoter also contains no CREB transcription binding sites (Ho and Strauss, 2004).

The potential pitfalls of using certain control plasmids in the DLRA, such as pRL-TK, are well documented. According to Ibrahim et al. (2000) the hormone dependence of any control promoter must be first established. They showed that when CV-1 (African Green Monkey Kidney) cells were co-transfected with androgen receptor, pRL-TK Renilla expression increased in response to dihydroxytestosterone and when co-transfected with the glucocorticoid receptor, Renilla expression decreased in response to dexamethasone. The authors argued that these effects are cell type specific and likely reflect different sets of transcription factors and cofactors in the different cell lines used (Ibrahim et al., 2000).

In another study, Ho and Strauss (2004) showed that several GATA transcription factors when expressed from a plasmid stimulated Renilla expression from pRL-TK in the monkey kidney cell line, COS-7. To control this, they created two mutant control plasmids from which putative GATA response elements were deleted which reduced the response of pRL-TK. However, there is no evidence to suggest that PTH stimulates GATA transcription factor expression in UMR-106 cells. In a more recent study, Meir et al. (2014) found that in UMR-106 cells, PTH can activate Nurr1 to induce fibroblast growth factor-23 (FGF-23) transcription. Therefore, taking these findings into account, activation of Renilla expression from pRL-TK by the transcription factor Nurr1 in the presence of PTH may potentially induce problems with background expression in UMR-106 cells.

Interestingly, our results show that by increasing pRL-TK plasmid concentrations per transfection we were able to overcome problems in Renilla expression. However, using lower pRL-TK plasmid concentrations there was variability in Renilla expression. The reason may be due in part to expression of the transcription factor, Nurr1, induced by PTH (Ibrahim et al., 2000, Meir et al., 2014). Despite these apparent pitfalls, we have successfully developed the

DLRA and found no variation in Renilla values across all PTH and PTH fusion concentrations used. In addition, Firefly Luciferase values were not affected by Renilla plasmid concentrations during assay development (See Section 6.2.3). Based on these consistent observations, acceptance criteria were formulated, comprising of: (i) Renilla values must not increase as ligand values increase, and (ii) FL/RL ratio must not exceed 25% between duplicates.

The PTH fusion molecules were shown to retain *in vitro* bioactivity in the DLRA. 14A7 (PTH linked to GHBP) is the smallest molecule and is hypothesised to be the most active due to less steric hindrance from the GHBP moiety. Conversely, 14A2c (PTH linked to PTHrExt and GHBP) is hypothesised to be the least active due to its increased size as well as steric hindrance, but also because PTH may potentially undergo intra and inter molecular interactions with the PTHrExt, thus reducing PTH availability. 14A8 is a control for 14A2c and contains the I135K mutation, which prevents PTH from binding to PTHrExt.

Preliminary potency assays demonstrated that PTH 1-34 is significantly more potent than any of the tested PTH fusion molecules. 14A7, for example, exhibited a 29-fold reduction in potency compared to PTH 1-34 with an EC_{50} of 68.02 ± 4.01 nM vs 2.39 ± 0.58 nM. This finding is attributed to increased steric hindrance from the GHBP part of the fusion. 14A2c, which contains PTH 1-34 linked to GHBP and PTHrExt, exhibited an EC_{50} of 699.4 ± 55.6 nM and was 296-fold less active than PTH 1-34, likely due to intra- and inter-molecular interactions between PTH within the fusion and the PTH receptor portion, which would reduce PTH availability for binding. Alternatively, these results could have arisen due to steric hindrance. According to X-ray crystallography measurements of PTH bound to its ECD (extracellular domain), PTHR1, performed by Pioszak et al. (2010), PTH binds to a groove in the ECD. The

same process is hypothesised to occur in 14A2c, in which PTH is protected at the C-terminus by attachment to PTHrExt. Therefore, the molecule may exhibit low biological activity *in vitro*, but *in vivo* PTH will be partially protected by the interactions with PTHrExt and may thus exhibit prolonged activity.

While these assertions are only tentative and require experimental validation. It is worth noting that, 14A8, is a control fusion molecule for 14A2c and contains the mutation I135K in PTHrExt which was shown by Pioszak et al. (2010) to reduce binding of PTH with PTH receptor. Thus, due to the abrogation of interactions of PTH with PTHrExt in 14A8, it was hypothesised that the fusion would demonstrate an increased potency. This hypothesis was confirmed as an EC_{50} of 253.8 ± 26.3 nM was obtained for 14A8, indicating a small increase in activity of 2.7-fold compared to 14A2c. However, the fact that 14A8 was 106-fold less active than PTH 1-34 imply that other factors may also be responsible for its low activity. As hypothesised, compared to 14A7, both 14A2c and 14A8 are less active by approximately 10.3 and 4.3-fold, respectively, and is hypothesised to be due to both size (steric hindrance) and increased intra-inter-molecular interactions, in particular with respect to 14A2c.

Although a number of different *in vitro* methods have been utilised to determine the bioactivity of both PTH and its analogues, our DLRA bioactivity assay methodology produced comparable data. For instance, some studies used the GloSensor cAMP reporter which provides a platform of flexible luciferase-based biosensors for real-time detection of signalling events in live cells, including intracellular cAMP production by luminescence readout (Binkowski et al., 2011, Yu et al., 2018). Recently, Noda et al. (2020) used the GloSensor reporter cell lines UGS-56 cells (derived from the UMR-106) that endogenously express PTHR1 or GP-2.3 cells (derived from Hek293 cells) that stably express the hPTHR1. They reported

EC_{50}'s of 0.2 nM and 1.4 nM respectively, for PTH 1-34. In another study Daley et al. (2020) used the endogenously expressing PTHR1 glosensor cell lines, UGS-56 and SGS-72 (derived from SaOS-2, human osteoblastic cell line), obtaining EC_{50}'s of 0.13 nM and 0.82 nM respectively.

In contrast to the use of glosensor cell lines, other studies have directly analysed cAMP from cell lines that express endogenous receptors. Reidhaar-Olson et al. (2000) used both UMR-106 and Saos-2 stimulated with PTH 1-34 to obtain EC_{50}'s of 0.65 nM and 2.1 nM respectively. Other studies have utilised other reporter assays, for example, Murrills et al. (2004) used Saos-H3 cells that were stably transfected with a cAMP response element (CRE) reporter and obtained an EC_{50} of 1.89 nM for PTH 1-34. Although some variations in EC_{50} determinations were observed in some of these reported studies, our bioactivity assay showed that PTH 1-34 has an EC_{50} 2.39 ± 0.58 nM which is comparable to many of the published data.

The variations in EC_{50} determinations in some of the aforementioned studies can be attributed to the use of different cells lines and whether these cells lines express endogenous receptors or have been manipulated to stably express the PTHR1. Differences may also occur in cell lines from different species expressing their own endogenous receptors i.e. Human as opposed to rat receptors. The mode of analysis whether it be direct cAMP measurements or the measurement of luminescence from a reporter assay may also be a factor. Moreover, the sources of PTH could have also contributed to the observed inconsistencies, as Noda et al. (2020) reported different results based on proprietary sources compared to those obtained by Shimizu et al. (2016) who used PTH international standards. Overall, the main observation from all the above studies is that all assays give low nM EC_{50} values for PTH 1-34 and are comparable to those results achieved in this study.

In summary, future investigations using DLRA could be improved by removing transfection variability. The stable transfection of UMR-106 cells with the reporter plasmid pGL4.29, could be generated to avoid repeated transfections for each experimental DLRA assay. Also, to further investigate the reason for differences in activities between PTH and PTH fusions, other mutations can be investigated in the 14A8 molecule, as Pioszak et al. (2010) demonstrated that both I135K and D137A mutations diminish PTH binding.

Overall, the retention of biological activity of PTH fusions was confirmed by DLRA and may show therapeutic potential for the treatment of hypoparathyroidism.

Chapter Seven: General Discussion

In this thesis three PTH fusion molecules were designed, expressed purified and tested for biological activity. PTH fusion molecules were tested with a view to enhancing the potency and longevity of action of PTH. 14A7 (PTH linked to GHBP) is the smallest molecule and is hypothesised to be the most active due to less steric hindrance from the GHBP moiety. Conversely, 14A2c (PTH linked to PTHrExt and GHBP) is hypothesised to be the least active due to its increased size as well as steric hindrance, but also because PTH may potentially undergo intra and inter molecular interactions with the PTHrExt, thus reducing PTH availability. 14A8 is a control for 14A2c and contains the I135K mutation, which prevents PTH from binding to PTHrExt. All fusions contained the PTH signal/propeptide sequence. We demonstrated that it was possible to express and purify all fusions whilst retaining biological activity.

PTH fusion molecules were tested with a view to enhancing the potency and longevity of action of PTH. The molecule 14A7, a fusion of PTH 1-34 to GHBP, showed biological activity approximately 20 to 30 fold less than PTH 1-34 itself. This molecule has the potential to provide a therapeutic. Based on previous work 14A7 is predicted to have reduced clearance with a potential for a weekly injection with a smoother prolonged physiological activity *in vivo* without peaks and troughs in biological activity. The other two molecules 14A2c and 14A8 had greatly reduced *in vitro* activity making it unlikely that these fusions will provide therapeutics; however, 14A8, contained a mutation in the PTHrExt domain that prevented intramolecular binding of PTH to the extracellular PTH receptor, had greater activity than 14A2c, suggesting the hypothesis that there is intramolecular binding in 14A2c is correct.

Future studies will need to test in vivo activity of these PTH fusion molecules, in particular 14A7.

Current treatments for hypoparathyroidism, including treatment with calcium and vitamin D, and parathyroid hormone result in fluctuating calcium levels with intermittent hypercalcuria and the risk of renal complications. There is an unmet need for a longer-acting PTH biological that controls calcium at physiological levels over 24 hours without peaks and troughs in PTH and calcium levels.

One of the key features of the treatment of hypoparathyroidism is to have a smooth profile after injection. Recently, the replacement of PTH in hypoparathyroidism with Natpara (PTH 1-84) has been licensed but requires daily injections and is complicated by fluctuating calcium levels. Although continuous pump therapy is effective it is impractical for most patients. The most problem is the spike in PTH concentration which drives bone formation. Whilst this is a beneficial side effect for patients with osteoporosis, however, it causes significant health challenges in patients with Hypoparathyroidism. It is envisaged that, like the GH-GHBP fusion, the PTH-fusion molecules developed in this study will deliver a smooth pharmacokinetic profile (Wilkinson et al., 2007) without the peaks and troughs associated with PTH delivery. Similarly, it is envisaged that bioactivity will be maintained over a prolonged period of time whilst keeping calcium levels within the normal range without causing hypercalcemia.

There is a significant competition for the development of PTH analogues with prolonged actions that can be more effective as a treatment for hypoparathyroidism. In the European Union, in the first half of 2018, sales of Natpara reached $109.8 Million. As per a recent analysis by Future Market Insights (FMI), by 2026 in terms of revenue, the valuation of global

hypoparathyroidism treatment market holds the potential to exceed the $1.1 Billion (PharmiWeb.Com, 2021, Feb 23).

One of the drawbacks of testing both pharmacokinetic (PK) and pharmacodynamics (PD) properties of PTH compounds that are developed for hypoparathyroidism therapy is the lack of an easy to use animal model. Other groups have used a variety of different animal models including rat, mice and monkey in the generation of long acting PTH molecules. The thyroparathryoidectomised (TPTX) rat was used as a specific animal model to test the PK and PD properties of a long acting PTH (Shimizu et al., 2016). Because the parathyroid glands of rodents are very small, the removal of the parathyroid glands is often accompanied by thyroidectomy (Jung et al., 2016). Therefore, the drawbacks of using certain animal models is that they are complex, expensive, and time limited.

During the write up of this PhD, an independent *in vivo* study was completed by our group that tested both the PK and PD properties of 14A7. In the study, a suitable *in vivo* animal model was developed using the calcium mimetic, Cinacalcet-HCl (Ramezani-Pour et al., 2020). Rats gavaged with 30 mg/kg Cinacalcet-HCl showed a robust and reproducible lowering of calcium between 2-24 hours with a nadir at ~8 hours post dosing, returning to baseline at 48-72 hours. This effect was shown to be abrogated for up to 2 hours by a single dose of PTH at 20 nmol/kg. Using this animal model, the effectiveness of 14A7 was then tested (Wilkinson et al., 2020). Results showed that a single dose at 20 nmol/kg of 14A7 had a delayed and prolonged response that reduced the impact of cinacalcet-HCl induced low ionised calcium levels between 4 to 24 hours post dosing (Wilkinson et al., 2020). These findings provided proof of concept of biological activity over a prolonged period for 14A7. Moreover, this non-

surgical animal model has a valuable potential in testing the pharmacodynamics of PTH analogues for hypoparathyroidism in the future.

It is hoped that this maintenance of biological activity over a prolonged period will translate into good management of calcium within the normal range without causing hypercalcemia in adults. In addition to studying the effects on calcium and phosphate, any immunological effects that might occur should be investigated. The GH-GHBP fusions that inspired the PTH-fusions were non-toxic and non-immunogenic, and therefore it is hypothesised that the PTH-fusions will be the same (Wilkinson et al., 2007). The success of one of the PTH-fusions as a therapy for hypoparathyroidism would satisfy the current need for long-term treatment. It is expected that the PTH-fusion may have a gold standard treatment for hypoparathyroidism in the future. Therefore, further work in the described areas is needed to continue the development of the molecule that would further advance the concept of a long-acting treatment for hypoparathyroidism.

References

ABATE, E. G. & CLARKE, B. L. 2016. Review of Hypoparathyroidism. *Frontiers in Endocrinology,* 7**,** 172.

ADAMSON, L. & WALUM, E. 2007. Insulin and IGF-1 mediated inhibition of apoptosis in CHO cells grown in suspension in a protein-free medium. *Altern Lab Anim,* 35**,** 349-52.

ALBRIGHT, F. & ELLSWORTH, R. 1929. STUDIES ON THE PHYSIOLOGY OF THE PARATHYROID GLANDS: I. Calcium and Phosphorus Studies on a Case of Idiopathic Hypoparathyroidism. *J Clin Invest,* 7**,** 183-201.

ALLGROVE, J. & O'RIORDAN, J. L. H. 1985. Biological half-life of parathyroid hormone in the circulation. *Bone (New York, N.Y.),* 6**,** 59-59.

AMOLYTPHARMA.COM. 2020, September 20. *Amolyt Pharma Presents First Clinical Data for AZP-3601, its Parathyroid Hormone Analog for Hypoparathyroidism, at the Endocrine Society's Virtual Annual Meeting (ENDO 2021)* [Online]. Available: https://amolytpharma.com/#our-programs. [Accessed].

BACKLIWAL, G., HILDINGER, M., KUETTEL, I., DELEGRANGE, F., HACKER, D. L. & WURM, F. M. 2008. Valproic acid: a viable alternative to sodium butyrate for enhancing protein expression in mammalian cell cultures. *Biotechnol Bioeng,* 101**,** 182-9.

BADDING, M. A., VAUGHAN, E. E. & DEAN, D. A. 2012. Transcription factor plasmid binding modulates microtubule interactions and intracellular trafficking during gene transfer. *Gene Ther,* 19**,** 338-46.

BARDEN, J. A. & KEMP, B. E. 1993. NMR solution structure of human parathyroid hormone(1-34). *Biochemistry,* 32**,** 7126-7132.

BERGWITZ, C. & JUPPNER, H. 2010. Regulation of phosphate homeostasis by PTH, vitamin D, and FGF23. *Annu Rev Med,* 61**,** 91-104.

BHATTACHARYA, P., YAN, Y. L., POSTLETHWAIT, J. & RUBIN, D. A. 2011. Evolution of the vertebrate pth2 (tip39) gene family and the regulation of PTH type 2 receptor (pth2r) and its endogenous ligand pth2 by hedgehog signaling in zebrafish development. *J Endocrinol,* 211**,** 187-200.

BI, R., FAN, Y., LAUTER, K., HU, J., WATANABE, T., CRADOCK, J., YUAN, Q., GARDELLA, T. & MANNSTADT, M. 2016. Diphtheria Toxin- and GFP-Based Mouse Models of Acquired Hypoparathyroidism and Treatment With a Long-Acting Parathyroid Hormone Analog. *J Bone Miner Res,* 31**,** 975-84.

BINKOWSKI, B. F., BUTLER, B. L., STECHA, P. F., EGGERS, C. T., OTTO, P., ZIMMERMAN, K., VIDUGIRIS, G., WOOD, M. G., ENCELL, L. P., FAN, F. & WOOD, K. V. 2011. A luminescent biosensor with increased dynamic range for intracellular cAMP. *ACS Chem Biol,* 6**,** 1193-7.

BISELLO, A., GREENBERG, Z., BEHAR, V., ROSENBLATT, M., SUVA, L. J. & CHOREV, M. 1996. Role of Glycosylation in Expression and Function of the Human Parathyroid Hormone/Parathyroid Hormone-Related Protein Receptor. *Biochemistry,* 35**,** 15890-15895.

BISELLO, A., MANEN, D., PIERROZ, D. D., USDIN, T. B., RIZZOLI, R. & FERRARI, S. L. 2004. Agonist-specific regulation of parathyroid hormone (PTH) receptor type 2 activity: structural and functional analysis of PTH- and tuberoinfundibular peptide (TIP) 39-stimulated desensitization and internalization. *Mol Endocrinol,* 18**,** 1486-98.

BLAINE, J., CHONCHOL, M. & LEVI, M. 2015. Renal Control of Calcium, Phosphate, and Magnesium Homeostasis. *Clinical Journal of the American Society of Nephrology : CJASN,* 10**,** 1257-1272.

BOLLERSLEV, J., REJNMARK, L., MARCOCCI, C., SHOBACK, D. M., SITGES-SERRA, A., VAN BIESEN, W. & DEKKERS, O. M. 2015. European Society of Endocrinology Clinical Guideline: Treatment of chronic hypoparathyroidism in adults. *Eur J Endocrinol,* 173**,** G1-20.

BRANDI, M. L., BILEZIKIAN, J. P., SHOBACK, D., BOUILLON, R., CLARKE, B. L., THAKKER, R. V., KHAN, A. A. & POTTS, J. J. T. 2016. Management of Hypoparathyroidism: Summary Statement and Guidelines. *The Journal of Clinical Endocrinology & Metabolism,* 101**,** 2273-2283.

BROWN, E. M. 1983. Four-parameter model of the sigmoidal relationship between parathyroid hormone release and extracellular calcium concentration in normal and abnormal parathyroid tissue. *J Clin Endocrinol Metab,* 56**,** 572-81.

CAWLEY, P., WILKINSON, I. & ROSS, R. J. 2013. Developing long-acting growth hormone formulations. *Clin Endocrinol (Oxf),* 79**,** 305-9.

CHELOHA, R. W., GELLMAN, S. H., VILARDAGA, J.-P. & GARDELLA, T. J. 2015. PTH receptor-1 signalling—mechanistic insights and therapeutic prospects. *Nature Reviews Endocrinology,* 11**,** 712.

CHEN, F., KOU, T., FAN, L., ZHOU, Y., YE, Z., ZHAO, L. & TAN, W.-S. 2011. The combined effect of sodium butyrate and low culture temperature on the production, sialylation, and biological activity of an antibody produced in CHO cells. *Biotechnology and Bioprocess Engineering,* 16**,** 1157-1165.

CLARKE, B. L., BROWN, E. M., COLLINS, M. T., JÜPPNER, H., LAKATOS, P., LEVINE, M. A., MANNSTADT, M. M., BILEZIKIAN, J. P., ROMANISCHEN, A. F. & THAKKER, R. V. 2016. Epidemiology and Diagnosis of Hypoparathyroidism. *The Journal of Clinical Endocrinology & Metabolism,* 101**,** 2284-2299.

CLARKE, B. L., KAY BERG, J., FOX, J., CYRAN, J. A. & LAGAST, H. 2014. Pharmacokinetics and pharmacodynamics of subcutaneous recombinant parathyroid hormone (1-84) in patients with hypoparathyroidism: an open-label, single-dose, phase I study. *Clin Ther,* 36**,** 722-36.

CLEMENS, T. L., CORMIER, S., EICHINGER, A., ENDLICH, K., FIASCHI-TAESCH, N., FISCHER, E., FRIEDMAN, P. A., KARAPLIS, A. C., MASSFELDER, T., ROSSERT, J., SCHLUTER, K. D., SILVE, C., STEWART, A. F., TAKANE, K. & HELWIG, J. J. 2001. Parathyroid hormone-related protein and its receptors: nuclear functions and roles in the renal and cardiovascular systems, the placental trophoblasts and the pancreatic islets. *Br J Pharmacol,* 134**,** 1113-36.

COLLIP, J. B. 1925. THE EXTRACTION OF A PARATHYROID HORMONE WHICH WILL PREVENT OR CONTROL PARATHYROID TETANY AND WHICH REGULATES THE LEVEL OF BLOOD CALCIUM. *Journal of Biological Chemistry,* 63**,** 395-438.

CONIGRAVE, A. D. & WARD, D. T. 2013. Calcium-sensing receptor (CaSR): Pharmacological properties and signaling pathways. *Best Practice & Research Clinical Endocrinology & Metabolism,* 27**,** 315-331.

COOPER, M. S. & GITTOES, N. J. L. 2008. Diagnosis and management of hypocalcaemia. *BMJ,* 336**,** 1298-1302.

CUSANO, N. E., RUBIN, M. R. & BILEZIKIAN, J. P. 2015. Parathyroid hormone therapy for hypoparathyroidism. *Best Practice & Research Clinical Endocrinology & Metabolism,* 29**,** 47-55.

CUSANO, N. E., RUBIN, M. R., MCMAHON, D. J., IRANI, D., ANDERSON, L., LEVY, E. & BILEZIKIAN, J. P. 2014. PTH(1-84) is associated with improved quality of life in hypoparathyroidism through 5 years of therapy. *J Clin Endocrinol Metab,* 99**,** 3694-9.

CUSANO, N. E., RUBIN, M. R., MCMAHON, D. J., ZHANG, C., IVES, R., TULLEY, A., SLINEY, J. J., CREMERS, S. C. & BILEZIKIAN, J. P. 2013. Therapy of Hypoparathyroidism with PTH(1–84): A Prospective Four-Year Investigation of Efficacy and Safety. *The Journal of Clinical Endocrinology & Metabolism,* 98**,** 137-144.

CUSANO, N. E., RUBIN, M. R., WILLIAMS, J. M., AGARWAL, S., TABACCO, G., TAY, D., MAJEED, R., OMERAGIC, B. & BILEZIKIAN, J. P. 2020. Changes in Skeletal Microstructure Through Four Continuous Years of rhPTH(1-84) Therapy in Hypoparathyroidism. *J Bone Miner Res,* 35**,** 1274-1281.

D'AMOUR, P., RAKEL, A., BROSSARD, J. H., ROUSSEAU, L., ALBERT, C. & CANTOR, T. 2006. Acute regulation of circulating parathyroid hormone (PTH) molecular forms by calcium: utility of PTH fragments/PTH(1-84) ratios derived from three generations of PTH assays. *J Clin Endocrinol Metab,* 91**,** 283-9.

DALEY, E. J., KHATRI, A., DEAN, T., VILARDAGA, J. P., ZAIDI, S. A., KATRITCH, V. & GARDELLA, T. J. 2020. Ligand-Dependent Effects of Methionine-8 Oxidation in Parathyroid Hormone Peptide Analogs. *Endocrinology*.

DAMIANI, R., OLIVEIRA, J. E., VORAUER-UHL, K., PERONI, C. N., VIANNA, E. G., BARTOLINI, P. & RIBELA, M. T. 2009. Stable expression of a human-like sialylated recombinant thyrotropin in a Chinese hamster ovary cell line expressing alpha2,6-sialyltransferase. *Protein Expr Purif,* 67**,** 7-14.

DOBOLYI, A., DIMITROV, E., PALKOVITS, M. & USDIN, T. B. 2012. The Neuroendocrine Functions of the Parathyroid Hormone 2 Receptor. *Frontiers in Endocrinology,* 3**,** 121.

DOBOLYI, A., PALKOVITS, M. & USDIN, T. B. 2010. The TIP39–PTH2 receptor system: Unique peptidergic cell groups in the brainstem and their interactions with central regulatory mechanisms. *Progress in Neurobiology,* 90**,** 29-59.

DUMONT, J., EUWART, D., MEI, B., ESTES, S. & KSHIRSAGAR, R. 2016. Human cell lines for biopharmaceutical manufacturing: history, status, and future perspectives. *Critical reviews in biotechnology,* 36**,** 1110-1122.

EGBUNA, O. I. & BROWN, E. M. 2008. Hypercalcaemic and hypocalcaemic conditions due to calcium-sensing receptor mutations. *Best practice & research. Clinical rheumatology,* 22**,** 129-148.

FERRANDIS, E., PRADHANANGA, S. L., TOUVAY, C., KINOSHITA, C., WILKINSON, I. R., STAFFORD, K., WU, Z., STRASBURGER, C. J., SAYERS, J. R., ARTYMIUK, P. J. & ROSS, R. J. 2010. Immunogenicity, toxicology, pharmacokinetics and pharmacodynamics of growth hormone ligand-receptor fusions. *Clin Sci (Lond),* 119**,** 483-91.

FERRANDON, S., FEINSTEIN, T. N., CASTRO, M., WANG, B., BOULEY, R., POTTS, J. T., GARDELLA, T. J. & VILARDAGA, J. P. 2009. Sustained cyclic AMP production by parathyroid hormone receptor endocytosis. *Nat Chem Biol,* 5**,** 734-42.

GARDELLA, T. J. & JUPPNER, H. 2001. Molecular properties of the PTH/PTHrP receptor. *Trends Endocrinol Metab,* 12**,** 210-7.

GARDELLA, T. J. & VILARDAGA, J.-P. 2015. International Union of Basic and Clinical Pharmacology. XCIII. The Parathyroid Hormone Receptors—Family B G Protein–Coupled Receptors. *Pharmacological Reviews,* 67**,** 310.

GENSURE, R. C., GARDELLA, T. J. & JUPPNER, H. 2005. Parathyroid hormone and parathyroid hormone-related peptide, and their receptors. *Biochem Biophys Res Commun,* 328**,** 666-78.

GOSWAMI, R., GOEL, S., TOMAR, N., GUPTA, N., LUMB, V. & SHARMA, Y. D. 2010. Prevalence of clinical remission in patients with sporadic idiopathic hypoparathyroidism. *Clin Endocrinol (Oxf),* 72**,** 328-33.

GRANT, M. P., STEPANCHICK, A. & BREITWIESER, G. E. 2012. Calcium Signaling Regulates Trafficking of Familial Hypocalciuric Hypercalcemia (FHH) Mutants of the Calcium Sensing Receptor. *Molecular Endocrinology,* 26**,** 2081-2091.

GRAUSCHOPF, U., LILIE, H., HONOLD, K., WOZNY, M., REUSCH, D., ESSWEIN, A., SCHAFER, W., RUCKNAGEL, K. P. & RUDOLPH, R. 2000. The N-terminal fragment of human parathyroid hormone receptor 1 constitutes a hormone binding domain and reveals a distinct disulfide pattern. *Biochemistry,* 39**,** 8878-87.

GUO, J., KHATRI, A., MAEDA, A., POTTS, J. T., JR., JUPPNER, H. & GARDELLA, T. J. 2017. Prolonged Pharmacokinetic and Pharmacodynamic Actions of a Pegylated Parathyroid Hormone (1-34) Peptide Fragment. *J Bone Miner Res,* 32**,** 86-98.

GUO, J., LIU, M., YANG, D., BOUXSEIN, M. L., THOMAS, C. C., SCHIPANI, E., BRINGHURST, F. R. & KRONENBERG, H. M. 2010. Phospholipase C Signaling via the Parathyroid Hormone (PTH)/PTH-Related Peptide Receptor Is Essential for Normal Bone Responses to PTH. *Endocrinology,* 151**,** 3502-3513.

HA, T. K., KIM, Y. G. & LEE, G. M. 2014. Effect of lithium chloride on the production and sialylation of Fc-fusion protein in Chinese hamster ovary cell culture. *Appl Microbiol Biotechnol,* 98**,** 9239-48.

HABENER, J. F., ROSENBLATT, M., KEMPER, B., KRONENBERG, H. M., RICH, A. & POTTS, J. T. 1978. Pre-proparathyroid hormone; amino acid sequence, chemical synthesis, and some biological studies of the precursor region. *Proceedings of the National Academy of Sciences,* 75**,** 2616-2620.

HARDING, P. A., WANG, X. Z., KELDER, B., SOUZA, S., OKADA, S. & KOPCHICK, J. J. 1994. In vitro mutagenesis of growth hormone receptor Asn-linked glycosylation sites. *Molecular and Cellular Endocrinology,* 106**,** 171-180.

HERMANS, E. 2003. Biochemical and pharmacological control of the multiplicity of coupling at G-protein-coupled receptors. *Pharmacol Ther,* 99**,** 25-44.

HIREMATH, M. & WYSOLMERSKI, J. 2013. Parathyroid hormone-related protein specifies the mammary mesenchyme and regulates embryonic mammary development. *J Mammary Gland Biol Neoplasia,* 18**,** 171-7.

HO, C. K. & STRAUSS, J. F., 3RD 2004. Activation of the control reporter plasmids pRL-TK and pRL-SV40 by multiple GATA transcription factors can lead to aberrant normalization of transfection efficiency. *BMC Biotechnol,* 4**,** 10.

HOARE, S. R., CLARK, J. A. & USDIN, T. B. 2000. Molecular determinants of tuberoinfundibular peptide of 39 residues (TIP39) selectivity for the parathyroid hormone-2 (PTH2) receptor. N-terminal truncation of TIP39 reverses PTH2 receptor/PTH1 receptor binding selectivity. *J Biol Chem,* 275**,** 27274-83.

HODSMAN, A. B., BAUER, D. C., DEMPSTER, D. W., DIAN, L., HANLEY, D. A., HARRIS, S. T., KENDLER, D. L., MCCLUNG, M. R., MILLER, P. D., OLSZYNSKI, W. P., ORWOLL, E. & YUEN,

C. K. 2005. Parathyroid Hormone and Teriparatide for the Treatment of Osteoporosis: A Review of the Evidence and Suggested Guidelines for Its Use. *Endocrine Reviews,* 26**,** 688-703.

HOLTEN-ANDERSEN, L., PIHL, S., RASMUSSEN, C. E., ZETTLER, J., MAITRO, G., BARON, J., HEINIG, S., HOFFMANN, E., WEGGE, T., KRUSCH, M., FALTINGER, F., KILLIAN, S., SPROGOE, K., KARPF, D. B., BREINHOLT, V. M. & CLEEMANN, F. 2019. Design and Preclinical Development of TransCon PTH, an Investigational Sustained-Release PTH Replacement Therapy for Hypoparathyroidism. *J Bone Miner Res,* 34**,** 2075-2086.

IBRAHIM, N. M., MARINOVIC, A. C., PRICE, S. R., YOUNG, L. G. & FRÖHLICH, O. 2000. Pitfall of an internal control plasmid: response of Renilla luciferase (pRL-TK) plasmid to dihydrotestosterone and dexamethasone. *Biotechniques,* 29**,** 782-4.

ICHIKAWA, F., NODA, H., OKAZAKI, M. & NAKAGAWA, C. 2008. A New Long-Acting PTH/PTHrP Hybrid Analog that Binds to a Distinct PTHR Conformation has Superior Efficacy in a Rat Model of Hypoparathyroidism. *Journal of bone and mineral research* Vol.23**,**, p.S128-S128.

JAYAPAL, K. P., WLASCHIN, K. F., HU, W. & YAP, M. G. S. 2007. Recombinant protein therapeutics from CHO cells-20 years and counting. *Chemical engineering progress,* 103**,** 40.

JIN, L., BRIGGS, S. L., CHANDRASEKHAR, S., CHIRGADZE, N. Y., CLAWSON, D. K., SCHEVITZ, R. W., SMILEY, D. L., TASHJIAN, A. H. & ZHANG, F. 2000. Crystal structure of human parathyroid hormone 1-34 at 0.9-A resolution. *J Biol Chem,* 275**,** 27238-44.

JIWAJI, M., DALY, R., PANSARE, K., MCLEAN, P., YANG, J., KOLCH, W. & PITT, A. R. 2010. The Renilla luciferase gene as a reference gene for normalization of gene expression in transiently transfected cells. *BMC Mol Biol,* 11**,** 103.

JOHARI, Y. B., JAFFÉ, S. R. P., SCARROTT, J. M., JOHNSON, A. O., MOZZANINO, T., POHLE, T. H., MAISURIA, S., BHAYAT-CAMMACK, A., LAMBIASE, G., BROWN, A. J., TEE, K. L., JACKSON, P. J., WONG, T. S., DICKMAN, M. J., SARGUR, R. B. & JAMES, D. C. 2021. Production of trimeric SARS-CoV-2 spike protein by CHO cells for serological COVID-19 testing. *Biotechnology and Bioengineering,* 118**,** 1013-1021.

JOHN, M. R., ARAI, M., RUBIN, D. A., JONSSON, K. B. & JUPPNER, H. 2002. Identification and characterization of the murine and human gene encoding the tuberoinfundibular peptide of 39 residues. *Endocrinology,* 143**,** 1047-57.

JUNG, S. Y., KIM, H. Y., PARK, H. S., YIN, X. Y., CHUNG, S. M. & KIM, H. S. 2016. Standardization of A Physiologic Hypoparathyroidism Animal Model. *PLOS ONE,* 11**,** e0163911.

JUPPNER, H., ABOU-SAMRA, A. B., FREEMAN, M., KONG, X. F., SCHIPANI, E., RICHARDS, J., KOLAKOWSKI, L. F., JR., HOCK, J., POTTS, J. T., JR., KRONENBERG, H. M. & ET AL. 1991. A G protein-linked receptor for parathyroid hormone and parathyroid hormone-related peptide. *Science,* 254**,** 1024-6.

KANTARDJIEFF, A., JACOB, N. M., YEE, J. C., EPSTEIN, E., KOK, Y. J., PHILP, R., BETENBAUGH, M. & HU, W. S. 2010. Transcriptome and proteome analysis of Chinese hamster ovary cells under low temperature and butyrate treatment. *J Biotechnol,* 145**,** 143-59.

KARPF, D. B., PIHL, S., MOURYA, S., MORTENSEN, E., KOVOOR, E., MARKOVA, D. & LEFF, J. A. 2020. A Randomized Double-Blind Placebo-Controlled First-In-Human Phase 1 Trial of TransCon PTH in Healthy Adults. *Journal of Bone and Mineral Research,* 35**,** 1430-1440.

KATRITCH, V., CHEREZOV, V. & STEVENS, R. C. 2013. Structure-Function of the G-protein-Coupled Receptor Superfamily. *Annual review of pharmacology and toxicology,* 53**,** 531-556.

KAUFMANN, H., MAZUR, X., MARONE, R., BAILEY, J. E. & FUSSENEGGER, M. 2001. Comparative analysis of two controlled proliferation strategies regarding product quality, influence on tetracycline-regulated gene expression, and productivity. *Biotechnol Bioeng,* 72**,** 592-602.

KHAN, A. A., REJNMARK, L., SCHWARZ, P. E., VOKES, T. J., CLARKE, B. L., RUBIN, M. R., HOFBAUER, L. C., ERIKSON, E., PALERMO, A., PAGOTTO, U., MARCOCCI, C., AHMED, I., MOURYA, S., MARKOVA, D. & KARPF, D. B. 2020. SAT-LB72 Design of the PaTH Forward Phase 2 Trial of TransCon PTH, a Long-Acting PTH, in Patients With Hypoparathyroidism. *Journal of the Endocrine Society,* 4.

KOBILKA, B. K. 2007. G protein coupled receptor structure and activation. *Biochimica et Biophysica Acta (BBA) - Biomembranes,* 1768**,** 794-807.

KOBRYNSKI, L. J. & SULLIVAN, K. E. 2007. Velocardiofacial syndrome, DiGeorge syndrome: the chromosome 22q11.2 deletion syndromes. *Lancet,* 370**,** 1443-52.

KOSTENUIK, P. J., FERRARI, S., PIERROZ, D., BOUXSEIN, M., MORONY, S., WARMINGTON, K. S., ADAMU, S., GENG, Z., GRISANTI, M., SHALHOUB, V., MARTIN, S., BIDDLECOME, G., SHIMAMOTO, G., BOONE, T., SHEN, V. & LACEY, D. 2007. Infrequent delivery of a long-acting PTH-Fc fusion protein has potent anabolic effects on cortical and cancellous bone. *J Bone Miner Res,* 22**,** 1534-47.

KUMAR, R. & THOMPSON, J. R. 2011. The Regulation of Parathyroid Hormone Secretion and Synthesis. *Journal of the American Society of Nephrology : JASN,* 22**,** 216-224.

LEDERER, E. 2014. Regulation of serum phosphate. *The Journal of Physiology,* 592**,** 3985-3995.

LI, H. & D'ANJOU, M. 2009. Pharmacological significance of glycosylation in therapeutic proteins. *Curr Opin Biotechnol,* 20**,** 678-84.

LIEBMAN, S. E., TAYLOR, J. G. & BUSHINSKY, D. A. 2006. Idiopathic hypercalciuria. *Curr Rheumatol Rep,* 8**,** 70-5.

LOUPY, A., RAMAKRISHNAN, S. K., WOOTLA, B., CHAMBREY, R., DE LA FAILLE, R., BOURGEOIS, S., BRUNEVAL, P., MANDET, C., CHRISTENSEN, E. I., FAURE, H., CHEVAL, L., LAGHMANI, K., COLLET, C., ELADARI, D., DODD, R. H., RUAT, M. & HOUILLIER, P. 2012. PTH-independent regulation of blood calcium concentration by the calcium-sensing receptor. *The Journal of Clinical Investigation,* 122**,** 3355-3367.

MAEDA, A., OKAZAKI, M., BARON, D. M., DEAN, T., KHATRI, A., MAHON, M., SEGAWA, H., ABOU-SAMRA, A. B., JUPPNER, H., BLOCH, K. D., POTTS, J. T., JR. & GARDELLA, T. J. 2013. Critical role of parathyroid hormone (PTH) receptor-1 phosphorylation in regulating acute responses to PTH. *Proc Natl Acad Sci U S A,* 110**,** 5864-9.

MANNSTADT, M., CLARKE, B. L., BILEZIKIAN, J. P., BONE, H., DENHAM, D., LEVINE, M. A., PEACOCK, M., ROTHMAN, J., SHOBACK, D. M., WARREN, M. L., WATTS, N. B., LEE, H. M., SHERRY, N. & VOKES, T. J. 2019. Safety and Efficacy of 5 Years of Treatment With Recombinant Human Parathyroid Hormone in Adults With Hypoparathyroidism. *J Clin Endocrinol Metab,* 104**,** 5136-5147.

MARCUCCI, G., DELLA PEPA, G. & BRANDI, M. L. 2016. Natpara for the treatment of hypoparathyroidism. *Expert Opinion on Biological Therapy,* 16**,** 1417-1424.

MARINISSEN, M. J. & GUTKIND, J. S. 2001. G-protein-coupled receptors and signaling networks: emerging paradigms. *Trends Pharmacol Sci,* 22**,** 368-76.

MARX, U. C., AUSTERMANN, S., BAYER, P., ADERMANN, K., EJCHART, A., STICHT, H., WALTER, S., SCHMID, F. X., JAENICKE, R., FORSSMANN, W. G. & ET AL. 1995. Structure of human parathyroid hormone 1-37 in solution. *J Biol Chem,* 270**,** 15194-202.

MATUSZYK, J., ZIOLO, E., CEBRAT, M., KOCHEL, I. & STRZADALA, L. 2002. Nurr1 affects pRL-TK but not phRG-B internal control plasmid in genetic reporter system. *Biochem Biophys Res Commun,* 294**,** 1036-9.

MEIR, T., DURLACHER, K., PAN, Z., AMIR, G., RICHARDS, W. G., SILVER, J. & NAVEH-MANY, T. 2014. Parathyroid hormone activates the orphan nuclear receptor Nurr1 to induce FGF23 transcription. *Kidney Int,* 86**,** 1106-15.

MELICK, R. A., GILL, J. R., JR., BERSON, S. A., YALOW, R. S., BARTTER, F. C., POTTS, J. T., JR. & AURBACH, G. D. 1967. Antibodies and clinical resistance to parathyroid hormone. *N Engl J Med,* 276**,** 144-7.

MURRAY, T. M., RAO, L. G., DIVIETI, P. & BRINGHURST, F. R. 2005. Parathyroid Hormone Secretion and Action: Evidence for Discrete Receptors for the Carboxyl-Terminal Region and Related Biological Actions of Carboxyl-Terminal Ligands. *Endocrine Reviews,* 26**,** 78-113.

MURRILLS, R. J., MATTEO, J. J., SAMUEL, R. L., ANDREWS, J. L., BHAT, B. M., COLEBURN, V. E., KHARODE, Y. P. & BEX, F. J. 2004. In vitro and in vivo activities of C-terminally truncated PTH peptides reveal a disconnect between cAMP signaling and functional activity. *Bone,* 35**,** 1263-72.

NA, D. H. & LEE, K. C. 2004. Capillary electrophoretic characterization of PEGylated human parathyroid hormone with matrix-assisted laser desorption/ionization time-of-flight mass spectrometry. *Anal Biochem,* 331**,** 322-8.

NAYLOR, S. L., SAKAGUCHI, A. Y., SZOKA, P., HENDY, G. N., KRONENBERG, H. M., RICH, A. & SHOWS, T. B. 1983. Human parathyroid hormone gene (PTH) is on short arm of chromosome 11. *Somatic Cell Genetics,* 9**,** 609-616.

NECHAMA, M., BEN-DOV, I. Z., SILVER, J. & NAVEH-MANY, T. 2009. Regulation of PTH mRNA stability by the calcimimetic R568 and the phosphorus binder lanthanum carbonate in CKD. *Am J Physiol Renal Physiol,* 296**,** F795-800.

NODA, H., OKAZAKI, M., JOYASHIKI, E., TAMURA, T., KAWABE, Y., KHATRI, A., JUEPPNER, H., POTTS JR, J. T., GARDELLA, T. J. & SHIMIZU, M. 2020. Optimization of PTH/PTHrP Hybrid Peptides to Derive a Long-Acting PTH Analog (LA-PTH). *JBMR Plus,* 4**,** e10367.

PALCZEWSKI, K. & ORBAN, T. 2013. From Atomic Structures to Neuronal Functions of G Protein–Coupled Receptors. *Annual review of neuroscience,* 36**,** 139-164.

PALERMO, A., SANTONATI, A., TABACCO, G., BOSCO, D., SPADA, A., PEDONE, C., RAGGIUNTI, B., DORIS, T., MAGGI, D., GRIMALDI, F., MANFRINI, S. & VESCINI, F. 2018. PTH(1–34) for Surgical Hypoparathyroidism: A 2-Year Prospective, Open-Label Investigation of Efficacy and Quality of Life. *The Journal of Clinical Endocrinology & Metabolism,* 103**,** 271-280.

PASTOR, N., KAPLAN, C., DOMÍNGUEZ, I., MATEOS, S. & CORTÉS, F. 2009. Cytotoxicity and mitotic alterations induced by non-genotoxic lithium salts in CHO cells in vitro. *Toxicol In Vitro,* 23**,** 432-438.

PHARMIWEB.COM. 2021, Feb 23. *hypoparathyroidism treatment market* [Online]. Available: (https://www.pharmiweb.com/press-release/2021-02-23/hypoparathyroidism-treatment-market-will-reach-at-a-cagr-of-8-from-2018-to-2026. [Accessed].

PIOSZAK, A. A., HARIKUMAR, K. G., PARKER, N. R., MILLER, L. J. & XU, H. E. 2010. Dimeric arrangement of the parathyroid hormone receptor and a structural mechanism for ligand-induced dissociation. *J Biol Chem,* 285**,** 12435-44.

PIOSZAK, A. A., PARKER, N. R., GARDELLA, T. J. & XU, H. E. 2009. Structural basis for parathyroid hormone-related protein binding to the parathyroid hormone receptor and design of conformation-selective peptides. *J Biol Chem,* 284**,** 28382-91.

PIOSZAK, A. A. & XU, H. E. 2008. Molecular recognition of parathyroid hormone by its G protein-coupled receptor. *Proceedings of the National Academy of Sciences,* 105**,** 5034-5039.

PISERCHIO, A., BISELLO, A., ROSENBLATT, M., CHOREV, M. & MIERKE, D. F. 2000. Characterization of Parathyroid Hormone/Receptor Interactions: Structure of the First Extracellular Loop. *Biochemistry,* 39**,** 8153-8160.

POTTS, J. T. 2005. Parathyroid hormone: past and present. *Journal of Endocrinology,* 187**,** 311-325.

POTTS, J. T., KRONENBERG, H. M., HABENER, J. F. & RICH, A. 1980. BIOSYNTHESIS OF PARATHYROID HORMONE. *Annals of the New York Academy of Sciences,* 343**,** 38-55.

PRADHANANGA, S., WILKINSON, I. & ROSS, R. J. M. 2002. Pegvisomant: structure and function. *Journal of molecular endocrinology,* 29**,** 11-14.

PUZZIELLO, A., ROSATO, L., INNARO, N., ORLANDO, G., AVENIA, N., PERIGLI, G., CALÒ, P. G. & DE PALMA, M. 2014. Hypocalcemia following thyroid surgery: incidence and risk factors. A longitudinal multicenter study comprising 2,631 patients. *Endocrine,* 47**,** 537-542.

RAISZ, L. G. 1963. Stimulation of Bone Resorption by Parathyroid Hormone in Tissue Culture. *Nature,* 197**,** 1015.

RAMEZANI-POUR, N., ESFAHANI, S. H. Z., PRADHANANGA, S., NEWELL-PRICE, J. D. C., ROSS, R. J. M. & WILKINSON, I. R. 2020. SAT-396 A Non-Surgical Animal Model of Hypoparathyroidism for Testing PTH Analogues. *Journal of the Endocrine Society,* 4.

REIDHAAR-OLSON, J. F., DAVIS, R. M., DE SOUZA-HART, J. A. & SELICK, H. E. 2000. Active variants of human parathyroid hormone (1-34) with multiple amino acid substitutions. *Mol Cell Endocrinol,* 160**,** 135-47.

RITACCO, F. V., WU, Y. & KHETAN, A. 2018. Cell culture media for recombinant protein expression in Chinese hamster ovary (CHO) cells: History, key components, and optimization strategies. *Biotechnol Prog,* 34**,** 1407-1426.

SANTONATI, A., PALERMO, A., MADDALONI, E., BOSCO, D., SPADA, A., GRIMALDI, F., RAGGIUNTI, B., VOLPE, R., MANFRINI, S. & VESCINI, F. 2015. PTH(1-34) for Surgical Hypoparathyroidism: A Prospective, Open-Label Investigation of Efficacy and Quality of Life. *J Clin Endocrinol Metab,* 100**,** 3590-7.

SCHIPANI, E. & PROVOT, S. 2003. PTHrP, PTH, and the PTH/PTHrP receptor in endochondral bone development. *Birth Defects Res C Embryo Today,* 69**,** 352-62.

SHAN, Q. & STORM, D. R. 2010. Optimization of a cAMP response element signal pathway reporter system. *J Neurosci Methods,* 191**,** 21-5.

SHERF, B., NAVARRO, S. L., HANNAH, R. & WOOD, K. Dual-Luciferase TM Reporter Assay: An Advanced Co-Reporter Technology Integrating Firefly and Renilla Luciferase Assays. 1996.

SHIGENO, C., HIRAKI, Y., WESTERBERG, D. P., POTTS, J. T., JR. & SEGRE, G. V. 1988. Parathyroid hormone receptors are plasma membrane glycoproteins with asparagine-linked oligosaccharides. *J Biol Chem,* 263**,** 3872-8.

SHIMIZU, M., JOYASHIKI, E., NODA, H., WATANABE, T., OKAZAKI, M., NAGAYASU, M., ADACHI, K., TAMURA, T., POTTS, J. T., JR., GARDELLA, T. J. & KAWABE, Y. 2016. Pharmacodynamic Actions of a Long-Acting PTH Analog (LA-PTH) in

Thyroparathyroidectomized (TPTX) Rats and Normal Monkeys. *J Bone Miner Res,* 31**,** 1405-12.
SHOBACK, D. 2008. Hypoparathyroidism. *New England Journal of Medicine,* 359**,** 391-403.
SIKJAER, T., AMSTRUP, A. K., ROLIGHED, L., KJAER, S. G., MOSEKILDE, L. & REJNMARK, L. 2013. PTH(1-84) replacement therapy in hypoparathyroidism: a randomized controlled trial on pharmacokinetic and dynamic effects after 6 months of treatment. *J Bone Miner Res,* 28**,** 2232-43.
SIKJAER, T., REJNMARK, L. & MOSEKILDE, L. 2011a. PTH treatment in hypoparathyroidism. *Curr Drug Saf,* 6**,** 89-99.
SIKJAER, T., REJNMARK, L., ROLIGHED, L., HEICKENDORFF, L. & MOSEKILDE, L. 2011b. The effect of adding PTH(1-84) to conventional treatment of hypoparathyroidism: a randomized, placebo-controlled study. *J Bone Miner Res,* 26**,** 2358-70.
SIMS, R. J., 3RD, LISS, A. S. & GOTTLIEB, P. D. 2003. Normalization of luciferase reporter assays under conditions that alter internal controls. *Biotechniques,* 34**,** 938-40.
SMRCKA, A. V. 2008. G protein βγ subunits: Central mediators of G protein-coupled receptor signaling. *Cellular and molecular life sciences : CMLS,* 65**,** 2191-2214.
SPRANG, S. R. 2016. Activation of G proteins by GTP and the mechanism of Gα-catalyzed GTP hydrolysis. *Biopolymers,* 105**,** 449-462.
STRATFORD, R., JR., VU, C., SAKON, J., KATIKANENI, R., GENSURE, R. & PONNAPAKKAM, T. 2014. Pharmacokinetics in rats of a long-acting human parathyroid hormone-collagen binding domain peptide construct. *J Pharm Sci,* 103**,** 768-75.
SUBRAMANIAN, H., DÖRING, F., KOLLERT, S., RUKOYATKINA, N., STURM, J., GAMBARYAN, S., STELLZIG-EISENHAUER, A., MEYER-MARCOTTY, P., EIGENTHALER, M. & WISCHMEYER, E. 2016. PTH1R Mutants Found in Patients with Primary Failure of Tooth Eruption Disrupt G-Protein Signaling. *PLoS ONE,* 11**,** e0167033.
SWIECH, K., PICANÇO-CASTRO, V. & COVAS, D. T. 2012. Human cells: new platform for recombinant therapeutic protein production. *Protein Expr Purif,* 84**,** 147-53.
TAYLOR, C. W. 2017. Regulation of IP(3) receptors by cyclic AMP. *Cell Calcium,* 63**,** 48-52.
UREÑA, P., KONG, X. F., ABOU-SAMRA, A. B., JÜPPNER, H., KRONENBERG, H. M., POTTS, J. J. T. & SEGRE, G. V. 1993. Parathyroid hormone (PTH)/PTH-related peptide receptor messenger ribonucleic acids are widely distributed in rat tissues. *Endocrinology,* 133**,** 617-623.
USDIN, T. B., BONNER, T. I. & HOARE, S. R. 2002. The parathyroid hormone 2 (PTH2) receptor. *Receptors Channels,* 8**,** 211-8.
USDIN, T. B., GRUBER, C. & BONNER, T. I. 1995. Identification and functional expression of a receptor selectively recognizing parathyroid hormone, the PTH2 receptor. *J Biol Chem,* 270**,** 15455-8.
VILARDAGA, J.-P., GARDELLA, T. J., WEHBI, V. L. & FEINSTEIN, T. N. 2012. Non-canonical signaling of the PTH receptor. *Trends in pharmacological sciences,* 33**,** 423-431.
VILARDAGA, J.-P., JEAN-ALPHONSE, F. G. & GARDELLA, T. J. 2014. Endosomal generation of cAMP in GPCR signaling. *Nature Chemical Biology,* 10**,** 700.
VILARDAGA, J. P., ROMERO, G., FRIEDMAN, P. A. & GARDELLA, T. J. 2011. Molecular basis of parathyroid hormone receptor signaling and trafficking: a family B GPCR paradigm. *Cell Mol Life Sci,* 68**,** 1-13.
WALLS, D., MCGRATH, R. & LOUGHRAN, S. T. 2010. A Digest of Protein Purification. *Methods Mol Biol,* 681**,** 3-23.

WEHBI, V. L., STEVENSON, H. P., FEINSTEIN, T. N., CALERO, G., ROMERO, G. & VILARDAGA, J.-P. 2013. Noncanonical GPCR signaling arising from a PTH receptor–arrestin–Gβγ complex. *Proceedings of the National Academy of Sciences,* 110**,** 1530-1535.

WETTSCHURECK, N. & OFFERMANNS, S. 2005. Mammalian G proteins and their cell type specific functions. *Physiol Rev,* 85**,** 1159-204.

WILKINSON, I. R., FERRANDIS, E., ARTYMIUK, P. J., TEILLOT, M., SOULARD, C., TOUVAY, C., PRADHANANGA, S. L., JUSTICE, S., WU, Z., LEUNG, K. C., STRASBURGER, C. J., SAYERS, J. R. & ROSS, R. J. 2007. A ligand-receptor fusion of growth hormone forms a dimer and is a potent long-acting agonist. *Nature Medicine,* 13**,** 1108.

WILKINSON, I. R., PRADHANANGA, S. L., SPEAK, R., ARTYMIUK, P. J., SAYERS, J. R. & ROSS, R. J. 2016. A long-acting GH receptor antagonist through fusion to GH binding protein. *Scientific Reports,* 6**,** 35072.

WILKINSON, I. R., RAMEZANI-POUR, N., ESFAHANI, S. H. Z., EASTELL, R. & ROSS, R. J. M. 2020. SAT-408 Bioactivity of Long Acting PTH Fusion Molecules Tested in a Novel Non-Surgical Animal Model of Hypoparathyroidism. *Journal of the Endocrine Society,* 4.

WINER, K. K., KO, C. W., REYNOLDS, J. C., DOWDY, K., KEIL, M., PETERSON, D., GERBER, L. H., MCGARVEY, C. & CUTLER, G. B., JR. 2003. Long-term treatment of hypoparathyroidism: a randomized controlled study comparing parathyroid hormone-(1-34) versus calcitriol and calcium. *J Clin Endocrinol Metab,* 88**,** 4214-20.

WINER, K. K., YANOVSKI, J. A., CUTLER, G. B. & JR 1996. Synthetic human parathyroid hormone 1-34 vs calcitriol and calcium in the treatment of hypoparathyroidism: Results of a short-term randomized crossover trial. *JAMA,* 276**,** 631-636.

WINER, K. K., YANOVSKI, J. A., SARANI, B. & CUTLER, G. B., JR. 1998. A randomized, cross-over trial of once-daily versus twice-daily parathyroid hormone 1-34 in treatment of hypoparathyroidism. *J Clin Endocrinol Metab,* 83**,** 3480-6.

WINER, K. K., ZHANG, B., SHRADER, J. A., PETERSON, D., SMITH, M., ALBERT, P. S. & CUTLER, G. B., JR. 2012. Synthetic human parathyroid hormone 1-34 replacement therapy: a randomized crossover trial comparing pump versus injections in the treatment of chronic hypoparathyroidism. *J Clin Endocrinol Metab,* 97**,** 391-9.

WONG, S. K. 2003. G protein selectivity is regulated by multiple intracellular regions of GPCRs. *Neurosignals,* 12**,** 1-12.

WURM, F. M. 2004. Production of recombinant protein therapeutics in cultivated mammalian cells. *Nat Biotechnol,* 22**,** 1393-8.

WURM, F. M. & HACKER, D. 2011. First CHO genome. *Nat Biotechnol,* 29**,** 718-20.

YOON, S. K., SONG, J. Y. & LEE, G. M. 2003. Effect of low culture temperature on specific productivity, transcription level, and heterogeneity of erythropoietin in Chinese hamster ovary cells. *Biotechnol Bioeng,* 82**,** 289-98.

YU, L., SHI, X., HAN, C., RAO, C. & WANG, J. 2018. A rapid reporter assay for recombinant human brain natriuretic peptide (rhBNP) by GloSensor technology. *J Pharm Anal,* 8**,** 297-301.

ZAVATTA, G. & CLARKE, B. L. 2020. Challenges in the management of chronic hypoparathyroidism. *Endocrine connections,* 9**,** R229-R240.

ZHOU, A. T., ASSIL, I. & ABOU-SAMRA, A. B. 2000. Role of Asparagine-Linked Oligosaccharides in the Function of the Rat PTH/PTHrP Receptor. *Biochemistry,* 39**,** 6514-6520.

Appendices

Appendix A: Nucleotide and Protein Sequences of PTH fusions Key

PTH signal sequence: **Uppercase**

Propeptide: **Lowercase and underlined**

PTH (1-34); **Uppercase and bold**

Linker region (g4s)4: **Lowercase and italics**

PTHrExt (amino acids 29-187): **Uppercase and underlined (14A2c & 14A8 only)**

GHBP (1-238): **Uppercase and italics**

W104A_mutation in GHBP: **Bold and underlined**

I135K_mutation in PTHrExt: **Bold and italics (14A8 only)**

A1: 14A7 nucleic acid and protein sequence

Nucleotide Sequence: 969bp

ATGATACCTGCAAAAGACATGGCTAAAGTTATGATTGTCATGTTGGCAATTTGTTTTCTTACAAAATC

GGATGGGaaatctgttaagaagaga**TCTGTGAGTGAAATACAGCTTATGCATAACCTGGGAAAACATCT**

GAACTCGATGGAGAGAGTAGAATGGCTGCGTAAGAAGCTGCAGGATGTGCACAATTTT*ggtggcgg*

aggtagtggtggcggaggtagcggtggcggaggttctggtggcggaggttccTTTTCTGGAAGTGAGGCCACAGCA

GCTATCCTTAGCAGAGCACCCTGGAGTCTGCAAAGTGTTAATCCAGGCCTAAAGACAAATTCTTCTAA

GGAGCCTAAATTCACCAAGTGCCGTTCACCTGAGCGAGAGACTTTTTCATGCCACTGGACAGATGAG

GTTCATCATGGTACAAAGAACCTAGGACCCATACAGCTGTTCTATACCAGAAGGAACACTCAAGAAT

GGACTCAAGAATGGAAAGAATGCCCTGATTATGTTTCTGCTGGGGAAAACAGCTGTTACTTTAATTC

*ATCGTTTACCTCCATC***GCA***ATACCTTATTGTATCAAGCTAACTAGCAATGGTGGTACAGTGGATGAAA*

AGTGTTTCTCTGTTGATGAAATAGTGCAACCAGATCCACCCATTGCCCTCAACTGGACTTTACTGAAC

GTCAGTTTAACTGGGATTCATGCAGATATCCAAGTGAGATGGGAAGCACCACGCAATGCAGATATTC

AGAAAGGATGGATGGTTCTGGAGTATGAACTTCAATACAAAGAAGTAAATGAAACTAAATGGAAAA

TGATGGACCCTATATTGACAACATCAGTTCCAGTGTACTCATTGAAAGTGGATAAGGAATATGAAGT

GCGTGTGAGATCCAAACAACGAAACTCTGGAAATTATGGCGAGTTCAGTGAGGTGCTCTATGTAACA

CTTCCTCAGATGAGCCAA

Amino acid sequence (includes signal and propeptide sequence)

MIPAKDMAKVMIVMLAICFLTKSDGksvkkr**SVSEIQLMHNLGKHLNSMERVEWLRKKLQDVHNF***ggg gsggggsggggsggggsFSGSEATAAILSRAPWSLQSVNPGLKTNSSKEPKFTKCRSPERETFSCHWTDEVH HGTKNLGPIQLFYTRRNTQEWTQEWKECPDYVSAGENSCYFNSSFTS***I***AIPYCIKLTSNGGTVDEKCFSVD EIVQPDPPIALNWTLLNVSLTGIHADIQVRWEAPRNADIQKGWMVLEYELQYKEVNETKWKMMDPILT TSVPVYSLKVDKEYEVRVRSKQRNSGNYGEFSEVLYVTLPQMSQ*

A2: 14A2c nucleic acid and protein sequence

Nucleotide Sequence: 1506bp

ATGATACCTGCAAAAGACATGGCTAAAGTTATGATTGTCATGTTGGCAATTTGTTTTCTTACAAAATC GGATGGGaaatctgttaagaagaga**TCTGTGAGTGAAATACAGCTTATGCATAACCTGGGAAAACATCT GAACTCGATGGAGAGAGTAGAATGGCTGCGTAAGAAGCTGCAGGATGTGCACAATTTT***ggtggcgg aggtagtggtggcggaggtagcggtggcggaggttctggtggcggaggttcc*GATGACGTCATGACTAAAGAGGA ACAGATCTTCCTGCTGCACCGTGCTCAGGCCCAGTGCGAAAAACGGCTCAAGGAGGTCCTGCAGAG GCCAGCCAGCATAATGGAATCAGACAAGGGATGGACATCTGCGTCCACATCAGGGAAGCCCAGGA AAGATAAGGCATCTGGGAAGCTCTACCCTGAGTCTGAGGAGGACAAGGAGGCACCCACTGGCAGC AGGTACCGAGGGCGCCCCTGTCTGCCGGAATGGGACCACATCCTGTGCTGGCCGCTGGGGGCACCA GGTGAGGTGGTGGCTGTGCCCTGTCCGGACTACATTTATGACTTCAATCACAAAGGCCATGCCTACC GACGCTGTGACCGCAATGGCAGCTGGGAGCTGGTGCCTGGGCACAACAGGACGTGGGCCAACTAC AGCGAGTGTGTCAAATTTCTCACCAATGAGACTCGTGAACGGGAGGTGTTTGACCGCCTG*ggtggcgg aggtagtggtggcggaggtagcggtggcggaggttctggtggcggaggttccTTTTCTGGAAGTGAGGCCACAGCA GCTATCCTTAGCAGAGCACCCTGGAGTCTGCAAAGTGTTAATCCAGGCCTAAAGACAAATTCTTCTAA GGAGCCTAAATTCACCAAGTGCCGTTCACCTGAGCGAGAGACTTTTTCATGCCACTGGACAGATGAG GTTCATCATGGTACAAAGAACCTAGGACCCATACAGCTGTTCTATACCAGAAGGAACACTCAAGAAT GGACTCAAGAATGGAAAGAATGCCCTGATTATGTTTCTGCTGGGGAAAACAGCTGTTACTTTAATTC ATCGTTTACCTCCATC***GCA****ATACCTTATTGTATCAAGCTAACTAGCAATGGTGGTACAGTGGATGAAA AGTGTTTCTCTGTTGATGAAATAGTGCAACCAGATCCACCCATTGCCCTCAACTGGACTTTACTGAAC GTCAGTTTAACTGGGATTCATGCAGATATCCAAGTGAGATGGGAAGCACCACGCAATGCAGATATTC AGAAAGGATGGATGGTTCTGGAGTATGAACTTCAATACAAAGAAGTAAATGAAACTAAATGGAAAA TGATGGACCCTATATTGACAACATCAGTTCCAGTGTACTCATTGAAAGTGGATAAGGAATATGAAGT GCGTGTGAGATCCAAACAACGAAACTCTGGAAATTATGGCGAGTTCAGTGAGGTGCTCTATGTAACA CTTCCTCAGATGAGCCAA*

Amino acid sequence (includes signal and propeptide sequence)

MIPAKDMAKVMIVMLAICFLTKSDGksvkkr**SVSEIQLMHNLGKHLNSMERVEWLRKKLQDVHNF***ggg gsggggsggggsggggs*svdaddvmtkeeqifllhraqaqcekrlkevlqrpasimesdkgwtsastsgkprkdkasgklypes eedkeaptgsryrgrpclpewdhilcwplgapgevvavpcpdyiydfnhkghayrrcdrngswelvpghnrtwanysecvkfl tnetrerevfdrl*ggggsggggsggggsgggg FSGSEATAAILSRAPWSLQSVNPGLKTNSSKEPKFTKCRSPERE TFSCHWTDEVHHGTKNLGPIQLFYTRRNTQEWTQEWKECPDYVSAGENSCYFNSSFTS***I***AIPYCIKLTSN GGTVDEKCFSVDEIVQPDPPIALNWTLLNVSLTGIHADIQVRWEAPRNADIQKGWMVLEYELQYKEVNE TKWKMMDPILTTSVPVYSLKVDKEYEVRVRSKQRNSGNYGEFSEVLYVTLPQMSQ*

A3: 14A8 nucleic acid and protein sequence.

Nucleotide Sequence: 1506bp

ATGATACCTGCAAAAGACATGGCTAAAGTTATGATTGTCATGTTGGCAATTTGTTTTCTTACAAAATC

GGATGGGaaatctgttaagaagaga**TCTGTGAGTGAAATACAGCTTATGCATAACCTGGGAAAACATCT GAACTCGATGGAGAGAGTAGAATGGCTGCGTAAGAAGCTGCAGGATGTGCACAATTTT***ggtggcgg aggtagtggtggcggaggtagcggtggcggaggttctggtggcggaggttcc*gatgacgtcatgactaaagaggaacagatc ttcctgctgcaccgtgctcaggcccagtgcgaaaaacggctcaaggaggtcctgcagaggccagccagcataatggaatcagaca agggatggacatctgcgtccacatcagggaagcccaggaaagataaggcatctgggaagctctaccctgagtctgaggaggacaa ggaggcacccactggcagcaggtaccgagggcgcccctgtctgccggaatgggaccacatcctgtgctggccgctgggggcacca ggtgaggtggtggctgtgccctgtccggactac***aag***tatgacttcaatcacaaaggccatgcctaccgacgctgtgaccgcaatgg cagctgggagctggtgcctgggcacaacaggacgtgggccaactacagcgagtgtgtcaaatttctcaccaatgagactcgtgaac gggaggtgtttgaccgcctg*ggtggcggaggtagtggtggcggaggtagcggtggcggaggttctggtggcggaggttcc TTTTCTGGAAGTGAGGCCACAGCAGCTATCCTTAGCAGAGCACCCTGGAGTCTGCAAAGTGTTAATCCA GGCCTAAAGACAAATTCTTCTAAGGAGCCTAAATTCACCAAGTGCCGTTCACCTGAGCGAGAGACTT TTTCATGCCACTGGACAGATGAGGTTCATCATGGTACAAAGAACCTAGGACCCATACAGCTGTTCTAT ACCAGAAGGAACACTCAAGAATGGACTCAAGAATGGAAAGAATGCCCTGATTATGTTTCTGCTGGG GAAAACAGCTGTTACTTTAATTCATCGTTTACCTCCATC***GCA****ATACCTTATTGTATCAAGCTAACTAGC AATGGTGGTACAGTGGATGAAAAGTGTTTCTCTGTTGATGAAATAGTGCAACCAGATCCACCCATTG CCCTCAACTGGACTTTACTGAACGTCAGTTTAACTGGGATTCATGCAGATATCCAAGTGAGATGGGA AGCACCACGCAATGCAGATATTCAGAAAGGATGGATGGTTCTGGAGTATGAACTTCAATACAAAGA AGTAAATGAAACTAAATGGAAAATGATGGACCCTATATTGACAACATCAGTTCCAGTGTACTCATTG*

AAAGTGGATAAGGAATATGAAGTGCGTGTGAGATCCAAACAACGAAACTCTGGAAATTATGGCGAG
TTCAGTGAGGTGCTCTATGTAACACTTCCTCAGATGAGCCAA

Amino acid sequence (includes signal and propeptide sequence)

MIPAKDMAKVMIVMLAICFLTKSDGksvkkr**SVSEIQLMHNLGKHLNSMERVEWLRKKLQDVHNF***ggg*
*gsggggsggggsggggs*vdaddvmtkeeqifllhraqaqcekrlkevlqrpasimesdkgwtsastsgkprkdkasgklypes
eedkeaptgsryrgrpclpewdhilcwplgapgevvavpcpdy***k***ydfnhkghayrrcdrngswelvpghnrtwanysecvkf
ltnetrerevfdrl*ggggsggggsggggsgggg**FSGSEATAAILSRAPWSLQSVNPGLKTNSSKEPKFTKCRSPER*
*ETFSCHWTDEVHHGTKNLGPIQLFYTRRNTQEWTQEWKECPDYVSAGENSCYFNSSFTS**I**AIPYCIKLTSN*
GGTVDEKCFSVDEIVQPDPPIALNWTLLNVSLTGIHADIQVRWEAPRNADIQKGWMVLEYELQYKEVNE
TKWKMMDPILTTSVPVYSLKVDKEYEVRVRSKQRNSGNYGEFSEVLYVTLPQMSQ

Appendix B: PTH Fusions used in the Current Study

Molecule Code	Design	Comments
14A7	PTHss-pp-PTH (1-34)-4(G4S)- GHBP_W104A (1-238)	Contains PTH linked to GHBP. Includes PTHss & pp sequence
14A2c	PTHss-pp-PTH (1-34)-4(G4S)-PTHrExt (29-187)-4(G4S)-GHBP_W104A (1-238)	Contains PTH linked to both PTHrExt & GHBP. Includes PTHss & pp sequence
14A8	PTHss-pp-PTH (1-34)-4(G4S)-PTHrExt_I135K (29-187)-4(G4S)-GHBP_W104A (1-238)	Control molecule for 14A2c. Contains the I135K mutation
14A4	GHss-PTH (1-34)-4(G4S)-GHBP_W104A (1-238)	As for 14A7 but has GHss sequence.

PTH= human Parathyroid hormone (amino acids 1-34), GHBP = growth hormone binding protein (amino acids 1-238), PTHrExt = extracellular PTH receptor portion (amino acids 29-187), PTHss = PTH signal sequence and propeptide (pp), W104A = Tryptophan-104 change to alanine in GHBP, I135K = Isoleucine-135 to Lysine change in PTHr (Knocks out binding of PTH to receptor). GHss = Growth hormone signal sequence, 4(G4S) = 4 repeat sequences of Gly-Gly-Gly-Gly-Ser

Appendix C: Plasmid Map and Primer sequences

C1: Plasmid Map: pSecTag_Link

Invitrogen's Flp-In cell line was used to generate stable clones of pSecTag plasmids containing genes of interest plasmid consist of multiple cloning site (MCS), Cytomegalovirus promoter (CMV), Polyadenylation site, hygromycin B resistant gene, FRT site.

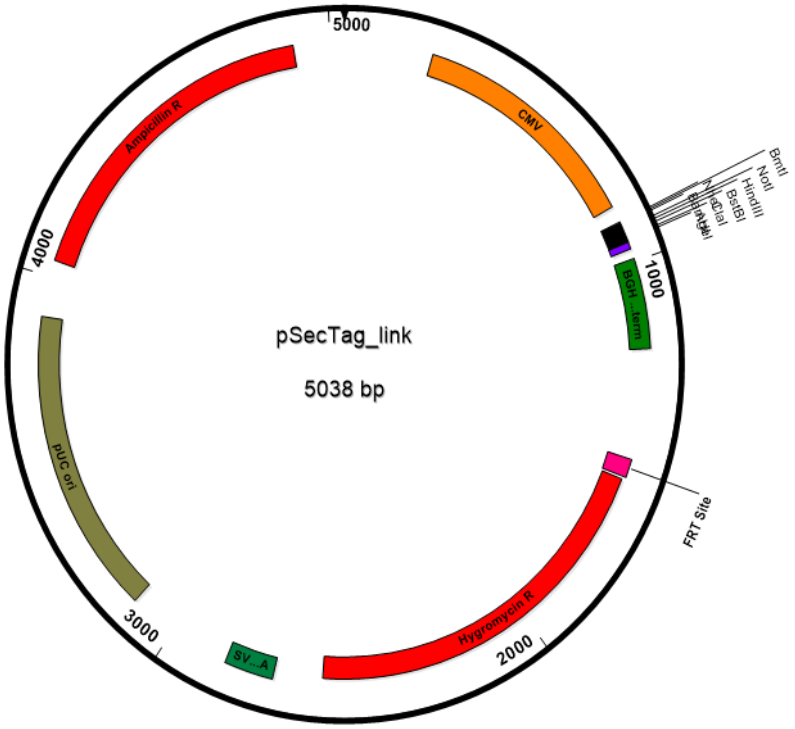

C2: Primer sequences used in study

Primer	**Sequence 5' > 3'**
PTHss_ Nhe1_ F1_ For	AAGAAAGCTAGCCACCATGATACCTGCAAAAG
GHss_Nhe1_F	AAATTTGCTAGCCACCATGGCTACAGGCTCCCGG
GHR_Q238_Rev (GRBP_REV)	TTTCCCAAGCTTTTATTGGCTCATCTGAGGAAGTGTTAC
GHBP_For	TTTTCTGGAAGTGAGGCC
Control sense primer (10 µM)	GCTCGTCGTCGACAACGGCTC
Control antisense primer (10 µM)	CAAACATGATCTGGGTCATCTTCTC

Appendix D: Buffer Preparation

D1: Buffer Preparation for Protein Purification

Buffers	Preparation
1. Binding buffer for Source-Q/10B8: 40 mM Sodium Phosphate, pH 8.0	Prepare the following stock solutions (a) 0.2 M sodium phosphate monobasic; 13.8 g/L (monohydrate, M.W. 138.0) (b) 0.2 M sodium phosphate dibasic; 26.8 g/L (heptahydrate, M.W. 268.0) Filter and autoclave
	pH 200 mL Sodium Phosphate Dibasic with Sodium Phosphate Monobasic to 8.0 using a sensitive pH meter. Take 200 mL and adjust the final volume to 1 Litres with distilled water to give a 40mM solution. Filter and autoclave.
Elution buffer (Source-Q): 40mM Phosphate/ 1M NaCl, pH 8.0 buffer	To prepare 40mM phosphate/ 1M NaCl, pH 8.0 buffer 10 mL 0.2 M phosphate buffer (from 1 above) 12.5 mL 4 M NaCl Make up to 50 mL with MilliQ/distilled.
Elution buffer (Affinity column: 0.2M Glycine, pH 2.7	To prepare 0.2M glycine, pH 2.7. 15g dissolved in 800 mL distilled water and pH with HCL (37% solution) to 2.7. Make volume up to 1 Litre with distilled water (3 g per 200 mL). Filter and autoclave.
Dialysis buffer: 20mM citrate, pH 6.0, 0.15M, 10% glycerol.	To prepare 20mM citrate, pH 6.0, 0.15M, 10% glycerol. Prepare stock solutions of 0.1M citric acid, Tri-sodium citrate & 4M NaCl. pH 1 Litre 0.1M Tri sodium citrate with 0.1M citric acid to 6.0. To 1 Litre of this add 500 mL glycerol, 187.5 mL 4M NaCl and make up to 5 Litres with MilliQ/Distilled.
0.5M NaOH	Dissolve 10g NaOH in 0.5 Litre distilled water. Filtered only (DO NOT AUTOCLAVE).
20% Ethanol	Add 200 mL ethanol and make volume up to 1 Litre with distilled water. Filtered only (DO NOT AUTOCLAVE).

D2: Buffers for Preparation of Affinity Resin

Coupling/Wash buffer

Component (Final Concentration)	**Weight/Volume ***
0.1M Sodium Bicarbonate	42.5g
0.5M Sodium Chloride	146g
distilled H_2O	Up to 5 Litres

*Mix Sodium Bicarbonate and Sodium Chloride in the proportions indicated, pH to 8.5. Adjust the final volume to 5 Litres with distilled water.

Acetate Wash buffer

Component (Final Concentration)	**Weight/Volume ***
0.1M Sodium acetate	14g
0.5M Sodium Chloride	58g
distilled H_2O	Up to 2 Litres

*Mix Sodium Acetate and Sodium Chloride in the proportions indicated and pH to 4. Adjust the final volume to 2 Litres with distilled water.

Other buffers

Component (Final Concentration)	**Weight/Volume (L)**
1mM HCL for swelling of resin (ice cold)*	Up to 3 L
0.2M Glycine, pH 8.0, for blocking (15g)	15 g make up to 1 L

*Diluted from 10M stock

Appendix E: Preparation of PTH Fusion Standards for Bioassay

E1: Preparation of 14A7 Standards

PTH-fusion (Mwt = 32626Da, 930 µg/mL/32626 = 28.5 µM stock solution = 28504 nM) Stock 28504 nM. Then 5-fold in the assay i.e. 40 µL per well (plus 160 µL DB). All the remaining samples will be diluted x10 (20 µL per well (plus 180 µL DB).

Sample	Stock Concentration (nM)	14A7 (µL)	DMEM/0.1%BSA (µL)	Dilution	Final concentration in assay (nM)
14A7	**50000**	40 µL neat	-	-	**5000**
	25000	60 µL 50000 nM	60 µL	2	**2500**
	10000	60 µL 25000 nM	90 µL	2.5	**1000**
	2500	60 µL 10000 nM	180 µL	4	**250**
	1250	60 µL 2500 nM	60 µL	2	**125**
	625	60 µL 1250 nM	60 µL	2	**62.5**
	312.5	60 µL 625 nM	60 µL	2	**31.25**
	156.25	60 µL 312 nM	60 µL	2	**15.6**
	62.5	50 µL 156 nM	75 µL	2.5	**6.25**
	6.25	10 µL 62.5 nM	90 µL	10	**0.625**
	1.25	20 µL 6.25 nM	80 µL	5	**0.125**
DB					**Neat**

E2: Preparation of 14A2c Standards

PTH-fusion (Mwt = 52.268kDa, 2570 µg/mL/52268 = 49.16 µM stock solution = 49162 nM).
Stock 25000 nM will be diluted 5-fold in the assay i.e. 40 µL per well plus 160 µL DB. All the remaining samples will be diluted x10 (20 µL per well plus 180 µL DB).

Sample	Stock Concentration (nM)	14A2c (µL)	DMEM/0.1 %BSA (µL)	Dilution	Final concentration in assay (nM)
14A2c	**49162**	40 µL neat	-	5	**9832.4**
	25000	100 µL neat nM	9 µL	1.96	**5000**
	10000	50 µL 25000 nM	75 µL	2.5	**1000**
	5000	60 µL 10000 nM	60 µL	2	**500**
	2500	60 µL 5000 nM	60 µL	2	**250**
	1250	60 µL 2500 nM	60 µL	2	**125**
	625	60 µL 1250 nM	60 µL	2	**62.5**
	312.5	60 µL 625 nM	60 µL	2	**31.25**
	156.25	60 µL 312.5 nM	60 µL	2	**15.6**
	62.5	50 µL 156 nM	75 µL	2.5	**6.25**
	6.25	10 µL 62.5 nM	90 µL	10	**0.625**
DB					**Neat**

E3: Preparation of 14A8 Standards

PTH-fusion (Mwt = 52.268kDa, 2290 µg/mL/52268 = 43.81 µM stock solution = 43812 nM).
Stock 25000 nM will be diluted 5-fold in the assay i.e. 40 µL per well plus 160 µL DB. All the remaining samples will be diluted x10 (20 µL per well plus 180 µL DB).

Sample	Stock Concentration (nM)	14A2c (µL)	DMEM/0.1 %BSA (µL)	Dilution	Final concentration in assay (nM)
14A8	**43812**	40 µL neat	-	**5**	**8762**
	25000	98 µL 43812 nM	73.5 µL	1.75	**5000**
	10000	50 µL 25000 nM	75 µL	2.5	**1000**
	5000	60 µL 10000 nM	60 µL	2	**500**
	2500	60 µL 5000 nM	60 µL	2	**250**
	1250	60 µL 2500 nM	60 µL	2	**125**
	625	60 µL 1250 nM	60 µL	2	**62.5**
	312.5	60 µL 625 nM	60 µL	2	**31.25**
	156.25	60 µL 312.5 nM	60 µL	2	**15.6**
	62.5	50 µL 156 nM	75 µL	2.5	**6.25**
	6.25	10 µL 62.5 nM	90 µL	10	**0.625**
DB					**Neat**

Appendix F: Cell Number and Viability from vessels culture for PTH Fusions

F1: 14A7

Cell Number and viabilities from vented roller bottles (RB) and shake flasks from three independent expression experiments

Experiment 1:

Day	Number of viable cells (x10^6/mL)	Number of dead cells (x10^6/mL)	Total number of cells (x10^6/mL)	Viability %
Batch#1 vented RB's				
0	1.23	0.02	1.34	96
4	1.21	0.00	1.21	99
8	1.89	0.01	1.90	96
12	2.12	0.08	2.20	90
Batch #2 Shake flask				
0	1.00	0.02	1.02	96
4	1.86	0.02	1.88	99
8	2.05	0.01	2.06	96
12	2.50	0.05	2.55	90

Experiment 2:

Day	Number of viable cells (x10^6/mL)	Number of dead cells (x10^6/mL)	Total number of cells (x10^6/mL)	Viability %
Batch#1 vented RB's				
0	1.09	0.0	1.09	100
4	2.48	0.0	2.48	100
8	2.26	0.07	2.33	97
11	1.97	0.11	2.11	94
Batch #2 Shake flask				
0	1	0.0	1	100
4	2.10	0.0	2.10	100
8	1.87	0.05	1.92	97
11	2.05	0.15	2.20	93

Experiment 3:

Day	Number of viable cells (x10^6/mL)	Number of dead cells (x10^6/mL)	Total number of cells (x10^6/mL)	Viability %
0	1.12	0.0	1.12	96
4	1.23	0.00	1.23	99
8	1.25	0.05	1.30	96
11	1.32	0.07	1.39	90

F2: 14A2c

Cell Number and viabilities from vented RB (3L)

Day	Number of viable cells (x10^6/mL)	Number of dead cells (x10^6/mL)	Total number of cells (x10^6/mL)	Viability %
0	1.16	0.0	1.16	100
4	1.66	0.0	1.66	100
8	1.85	0.04	1.89	96
12	2.35	0.15	2.50	90

F3: 14A8

Cell Number and viabilities from vented RB (3L)

Day	Number of viable cells (x10^6/mL)	Number of dead cells (x10^6/mL)	Total number of cells (x10^6/mL)	Viability %
0	1.02	0.04	1.06	96
4	1.19	0.01	1.20	99
8	1.26	0.07	1.33	96
12	1.02	0.11	1.13	90

Appendix G: Protein Assays for all Remaining PTH Fusion Purification experiments

Protein levels were calculated using Bradford assay and A280.

G1: Experiment 2: 14A7

Samples	Volume (ml)	µg/ml	Total protein (mg)	% Recovery
Load	215	2323.4	478.6	100
Q-UB	240	1348.5	331.7	69
Q-Wash_Elute	100	1896.7	189.7	40
		Run#1		
10B8-UB_1	260	1036.2	274.6	83
10B8-Wash	100	16.0	1.6	0.48
Elution 1	20	131.5	2.6	0.79
Elution 2	10	24.4	0.2	0.07
Elution 3	10	18.5	0.2	0.06
Pre Dialysis (PE1)	40	69.1	2.8	0.83
Post concentration (PC1)	1.3	587.1	0.8	28
Post Dialysis (PD1)	0.8	667.7	0.5	70
		Run#2		
10B8-UB_2	280	126.2	35.3	13
10B8-Wash	100	33.2	3.3	1.21
Elution 1	20	53.7	1.1	0.39
Elution 2	10	0.0	0.0	0.00
Elution 2	10	0.0	0.0	0.00
Pre Dialysis (PE2)	20	53.7	1.1	0.32
Post concentration (PC2)	1.2	480.4	0.6	54
Post Dialysis (PD2)	0.7	582.9	0.4	71
		A_{280}		
Samples	**Volume (mL)**	**Mean of A_{280}**	**mg/ml**	**Total pure protein mg**
Post Dialysis (PD1)	0.8	1.35	0.68	0.55
Post Dialysis (PD2)	0.7	1.06	0.53	0.37

Experiment 3: 14A7

Samples	Volume (ml)	µg/ml	Total protein (mg)	% Recovery
Load	320	3741.8	1197.3	100
Q-UB	360	2390.3	860.4	72
Q-Wash_Elute	100	2407.1	240.7	20
		Run#1		
10B8-UB_1	360	1619.9	583.15	68
10B8-Wash	100	46.2	4.62	0.54
Elution 1	20	103.1	2.06	0.24
Elution 2	10	25.2	0.25	0.03
Elution 3	10	0	0	0
Pre Dialysis (PE1)	30	103.1	2.06	0.24
Post concentration (PC1)	1.5	885.6	1.33	43
Post Dialysis (PD1)	0.8	1203.6	0.96	72
		Run#2		
10B8-UB_2	380	808.2	323.26	55
10B8-Wash	100	18.1	1.81	0.31
Elution 1	20	53.3	1.07	0.18
Elution 2	10	0	0	0
Elution 2	10	0	0	0
Pre Dialysis (PE2)	20	53.3	1.07	0.12
Post concentration (PC2)	1.4	511.1	0.72	67
Post Dialysis (PD2)	1	575.9	0.58	80

A_{280}

Samples	Volume (mL)	Mean of A_{280}	mg/ml	Total pure protein mg
Post Dialysis (PD1)	0.8	1.81	0.92	0.73
Post Dialysis (PD2)	1	1.61	0.81	0.81

G2: Experiment 2: 14A2c

Samples	Volume (ml)	µg/ml	Total protein (mg)	% Recovery
Source-Q Purification				
Load	105	3729.3	391.58	100
Q-UB	145	1766.9	256.21	65
Q-Wash_Elute	100	1202.1	120.21	31
Affinity Purification				
Run #1				
UB_1	175	1285.8	225.01	88
Wash-1	100	81.3	8.13	3.17
Elution 1	20	177.9	3.56	1.39
Elution 2	10	34.0	0.34	0.13
Elution 3	10	19.8	0.20	0.08
Pre-Dialysis (PE1)	40	186.3	7.45	3
Post-concentration (PC1)	3.2	1655.4	5.30	71
Post-Dialysis (PD1)	1.4	1718.2	2.41	45
Run #2				
UB2	195	1072.4	209.12	93
Wash-2	100	28.6	2.86	1.22
Elution 1	20	153.3	3.07	1.30
Elution 2	10	21.5	0.21	0.09
Elution 3	10	0	0	0
Pre-Dialysis (PE2)	20	153.3	3.07	1
Post-concentration (PC2)	2.8	1004.8	2.81	92
Post-Dialysis (PD2)	1.2	1327.0	1.59	57
Final Analysis of Purified Protein by A_{280}				
Samples	**Volume (mL)**	**Mean A_{280}**	**mg/ml**	**Total protein (mg)**
Post-Dialysis (PD1)	1.4	1.85	0.94	1.31
Post-Dialysis (PD2)	1.2	1.51	0.76	0.91

G3: Experiment 2: 14A8

Samples	Volume (ml)	µg/ml	Total protein (mg)	% Recovery
Source-Q Purification				
Load	115	2365.3	272	100
Q-UB	155	1231.4	190.8	70
Q-Wash_Elute	100	628.9	62.8	23
Affinity Purification				
Run #1				
UB_1	175	822.8	143.9	75
Wash-1	100	38.2	3.8	2.00
Elution 1	20	118.5	2.3	1.24
Elution 2	10	28.8	0.287	0.15
Elution 3	10	25.6	0.256	0.13
Pre-Dialysis (PE1)	40	128.2	5.1	2.69
Post-concentration (PC1)	3.8	994.4	3.7	74
Post-Dialysis (PD1)	1.5	1306.1	1.9	52
Run #2				
UB2	195	393.9	76.8	53
Wash-2	100	20.2	2	1.40
Elution 1	20	82.1	1.6	1.14
Elution 2	10	21.5	0.21	0.15
Elution 3	10	17.7	0.17	0.12
Pre-Dialysis (PE2)	30	86.3	2.6	1.36
Post-concentration (PC2)	2	945.3	1.8	73
Post-Dialysis (PD2)	1.5	1140.8	1.7	91
Final Analysis of Purified Protein by A_{280}				
Samples	**Volume (mL)**	**Mean A_{280}**	**mg/ml**	**Total protein (mg)**
Post-Dialysis (PD1)	1.5	2.07	1.05	1.57
Post-Dialysis (PD2)	1.5	1.93	0.98	1.46

G4: Protein losses during concentration and dialysis for all fusions.

The percentage loss of protein was calculated from recoveries such as (14A7) total of protein of PC1 divided the total protein of PE1 and multiply by 100 then the outcome minus a 100 to get the percentage of loss of protein ((PC1/EP1*100) – 100) and PC2 same equation. For PD1 as ((PD1/PC1*100)-100) and PD2 same equation.

Sample 14A7

Sample 14A7	Experiment 1		Experiment 2		Experiment 3	
Experiment	Run#1	Run#2	Run#1	Run#2	Run#1	Run#2
Concentration (PC)	85%	44%	72%	46%	57%	33%
Dialysis (PD)	40%	32%	30%	29%	28%	20%

Sample 14A2c

Sample 14A2c	Experiment 1		Experiment 2	
Experiment	Run#1	Run#2	Run#1	Run#2
Concentration (PC)	29%	8%	15%	19%
Dialysis (PD)	55%	43%	28%	46%

Sample 14A8

Sample 14A8	Experiment 1		Experiment 2	
Experiment	Run#1	Run#2	Run#1	Run#2
Concentration (PC)	26%	27%	22%	20%
Dialysis (PD)	48%	9%	35%	38%

Appendix H: PTH 1-34 & PTH Fusion Bioassay Data

H1: Repeat Experiment using pRL-TK at 0.5 and 5 ng/transfection
The assay was repeated using 100 µL of lysis buffer and 50 µL used for analysis.

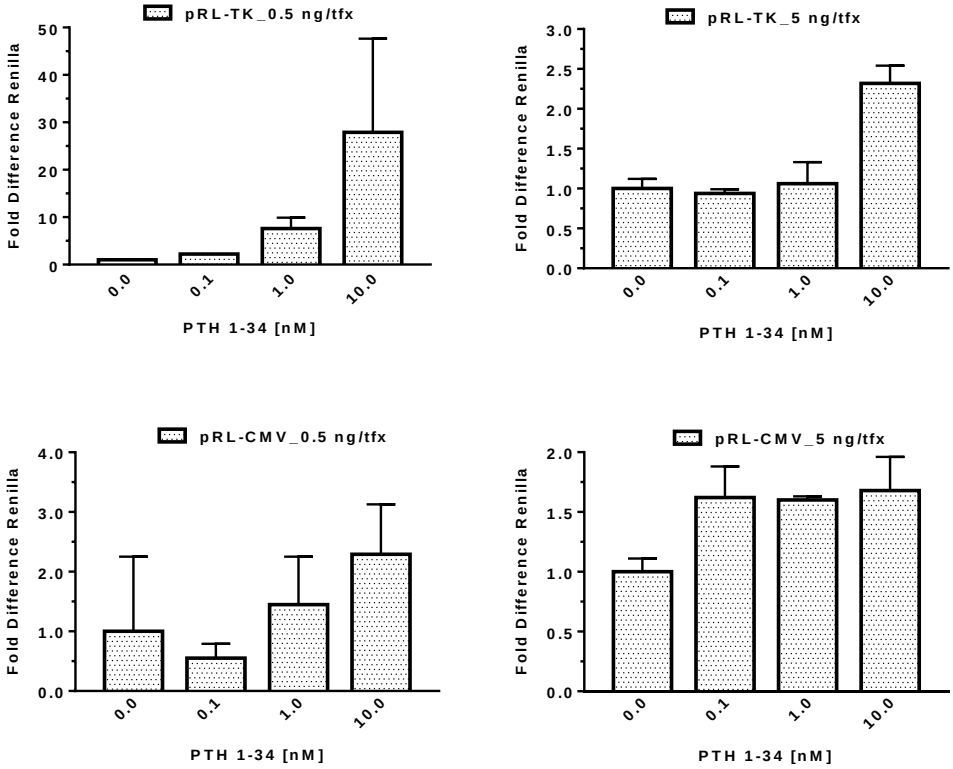

Figure H1: Fold difference in Renilla values from untreated controls for pRL-TK and pRL-CMV transfections. Fold Difference bars plotted against PTH 1-34 treatment (0, 0.1, 1 & 10 nM) for transfections using pRL-TK and pRL-CMV plasmid at 0.5 and 5 ng per transfection. Data are presented as mean ± StDev for fold difference Renilla value and data analysed using GraphPad Prism.

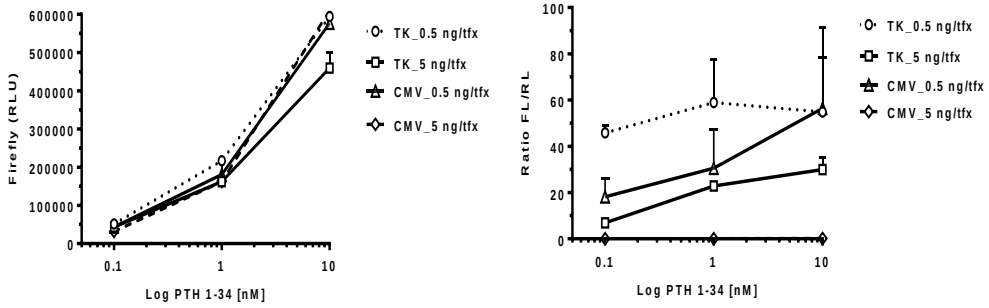

Figure H1: Represented the firefly luciferase density and ratio FL/RL by using pRL-TK and pRL-CMV plasmids.

The transfection was at 0.5 and 5 ng per transfection plotted against log PTH 1-34 treatment (0, 0.1, 1 & 10 nM). A) Firefly Luciferase (RLU) values. B) FL/RL ratio value. Data are presented as mean ± StDev for RLU value and FL/RL ratio. Data analysed using GraphPad Prism.

H2: Fold differences in Renilla values for bioactivity assays of PTH 1-34 (n = 8 experiments). Some individual points were removed from the analysis as the FL/RL ratios exceeded a %CV of 25%.

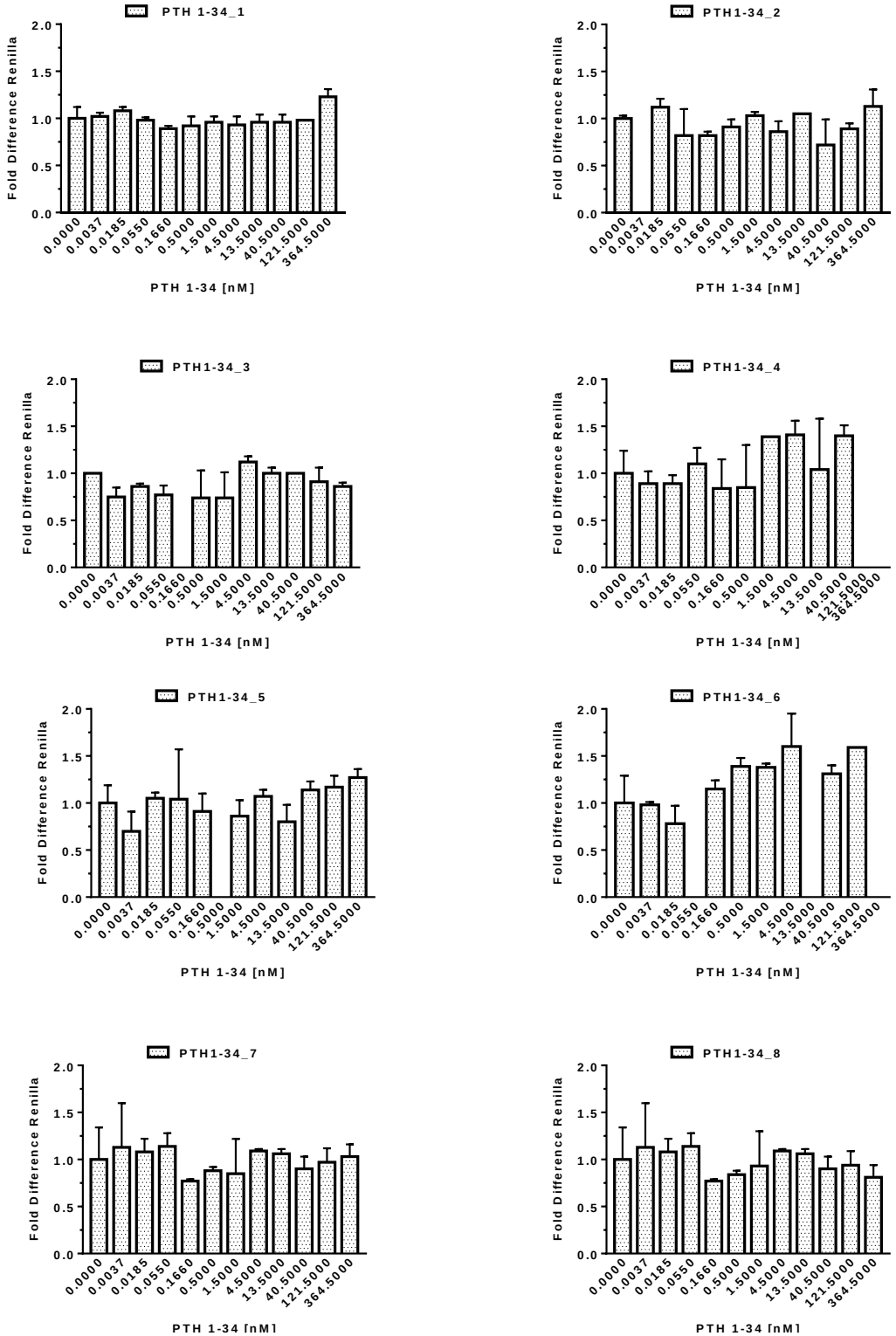

Figure H2: The fold difference in Renilla for eight independent PTH bioactivity assay experiments for testing pRL-TK plasmid at 20 ng per transfection plotted against PTH 1-34 treatment (0-364.5 nm). Data are presented as mean ± StDev for fold difference Renilla value and data analysed using GraphPad Prism.

H3: Fold differences in Renilla values for bioactivity assays of 14A7 (n =4 experiments). Some individual points were removed from the analysis as the FL/RL ratios exceeded a %CV of 25%.

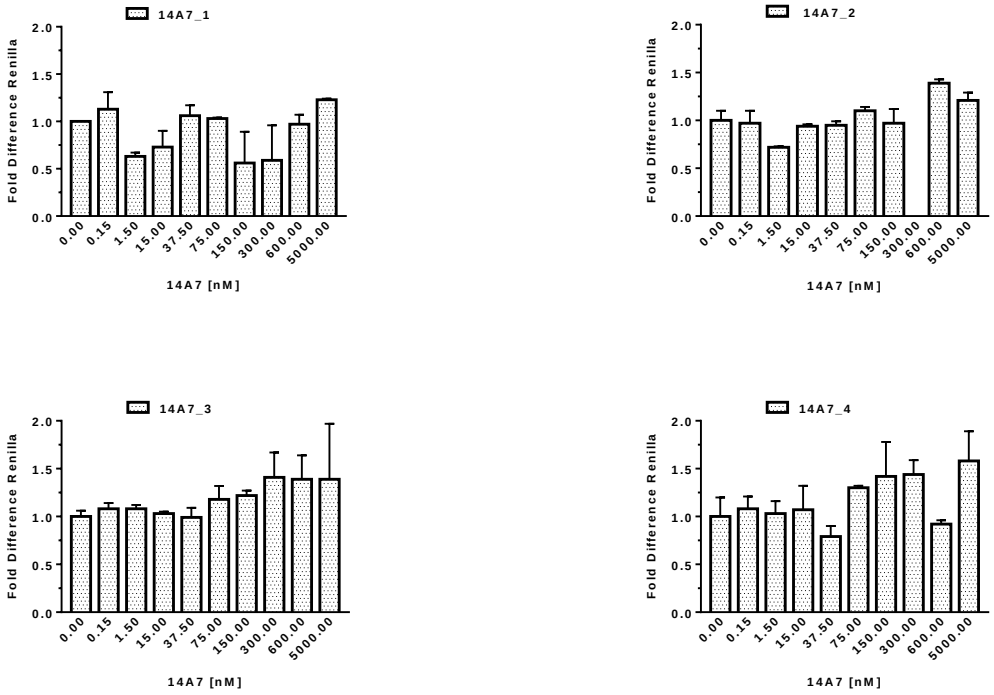

Figure H3: The fold difference in Renilla values for four independent 14A7 bioactivity assay experiments. Fold difference bars plotted against 14A7 treatment (0–5000 nM) for transfections using pRL-TK 20 ng per transfection. Data are presented as mean FD ± StDev (FD) and data analysed using GraphPad Prism.

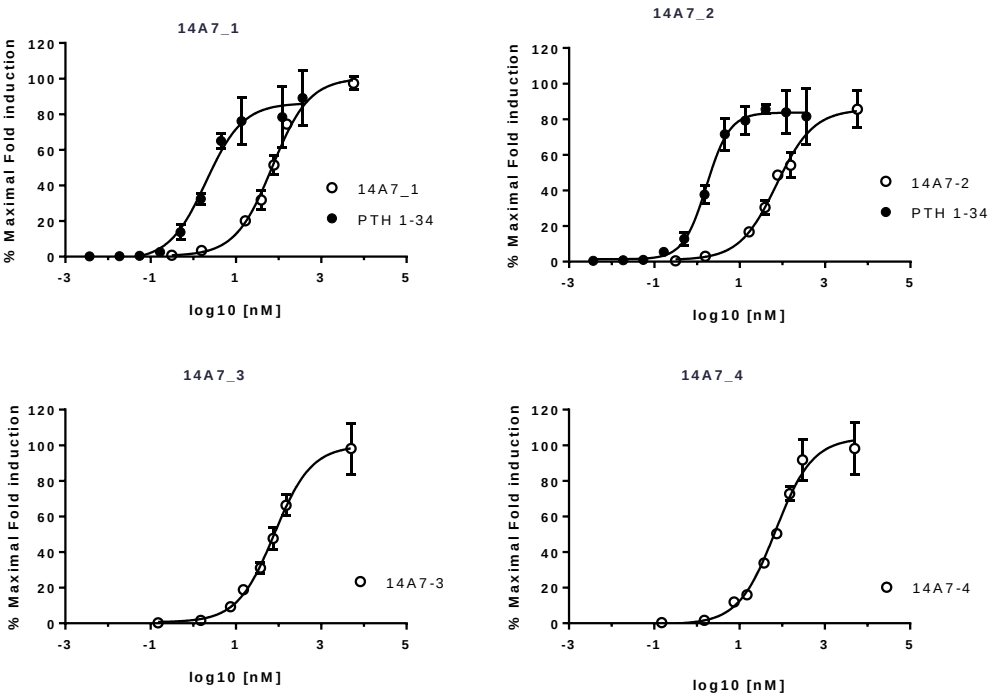

Figure H3: Mean % Maximal Fold Induction of four independent 14A7 bioactivity assay experiments and two PTH 1-34 against log10 concentration (nM). PTH 1-34 (•) and 14A7 (○). The standard curve was produced on the challenge of UMR-106 cells. Data presented by GraphPad Prism and presented as maximal fold induction ± StDev calculated from an average of duplicate values.

H4: Fold differences in Renilla values for bioactivity assays of 14A2c (n =3 experiments). Some individual points were removed from the analysis as the FL/RL ratios exceeded a %CV of 25%.

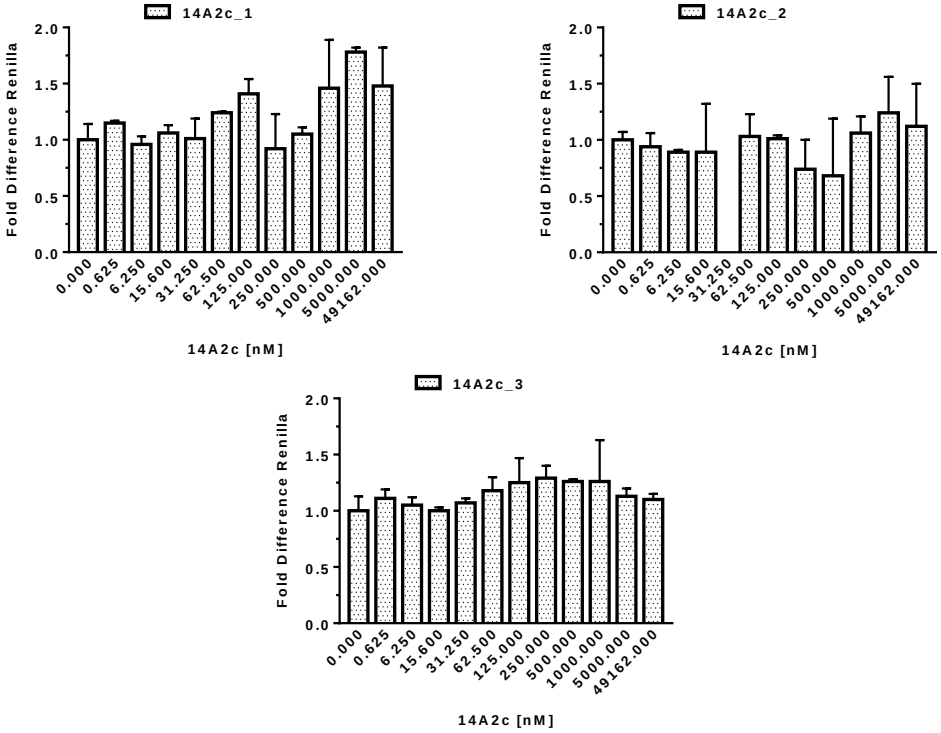

Figure H4: The fold difference in Renilla values for three independent 14A2c bioactivity assay experiments. Fold Difference bars plotted against 14A2c treatment (0–49162 nM) for transfections using pRL-TK 20 ng per transfection. Data are presented as mean FD ± StDev (FD) and data analysed using GraphPad Prism.

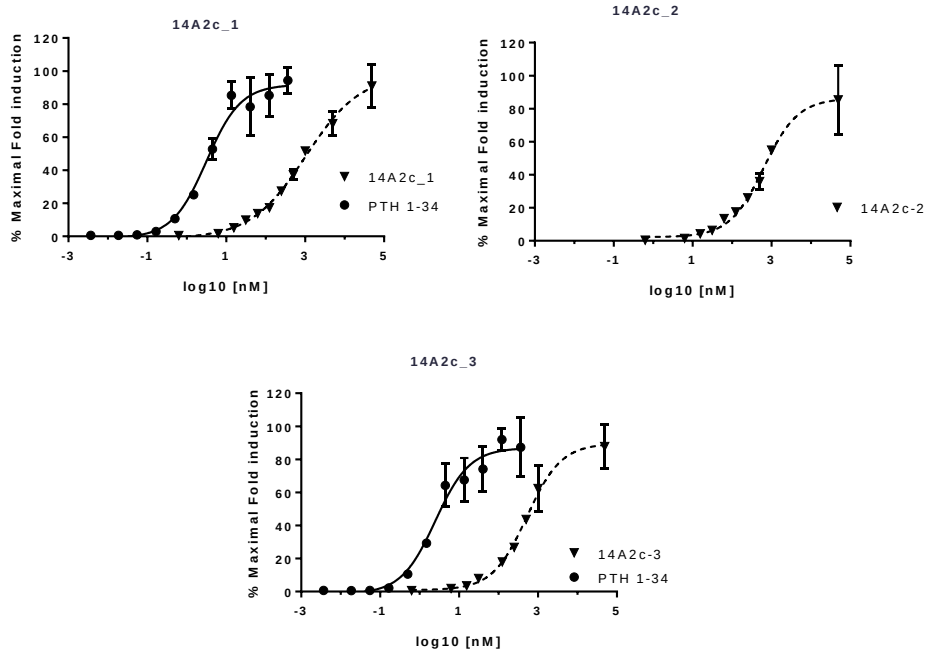

Figure H4: Mean % Maximal Fold Induction of three independent 14A2c bioactivity assay experiments and two PTH 1-34 against log10 concentration (nM). PTH 1-34 (•) and 14A2c (▼). The standard curve was produced on the challenge of UMR-106 cells. Data presented by GraphPad Prism and presented as maximal fold induction ± StDev calculated from an average of duplicate values.

H5: Fold differences in Renilla values for bioactivity assays of 14A8 (n = 3 experiments).

Some individual points were removed from the analysis as the FL/RL ratios exceeded a %CV of 25%.

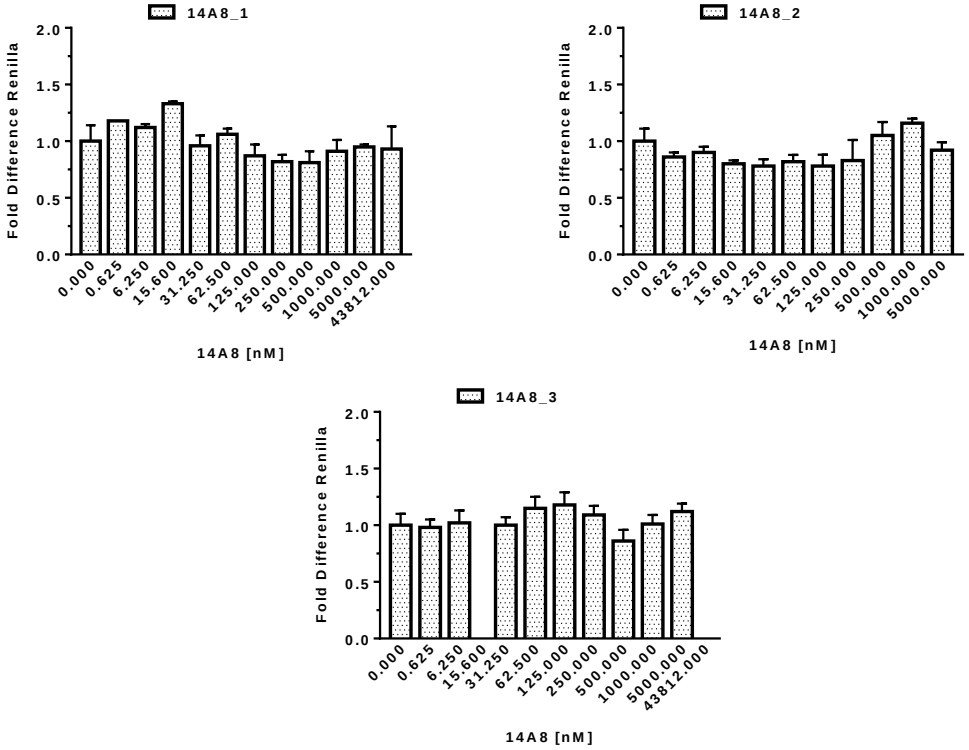

Figure H5: The fold difference for three independent 14A8 bioactivity assay experiments. Fold Difference bars plotted against 14A8 treatment (0–43812 nM) for transfections using pRL-TK 20 ng per transfection. Data are presented as mean FD ± StDev (FD) and data analysed using GraphPad Prism.

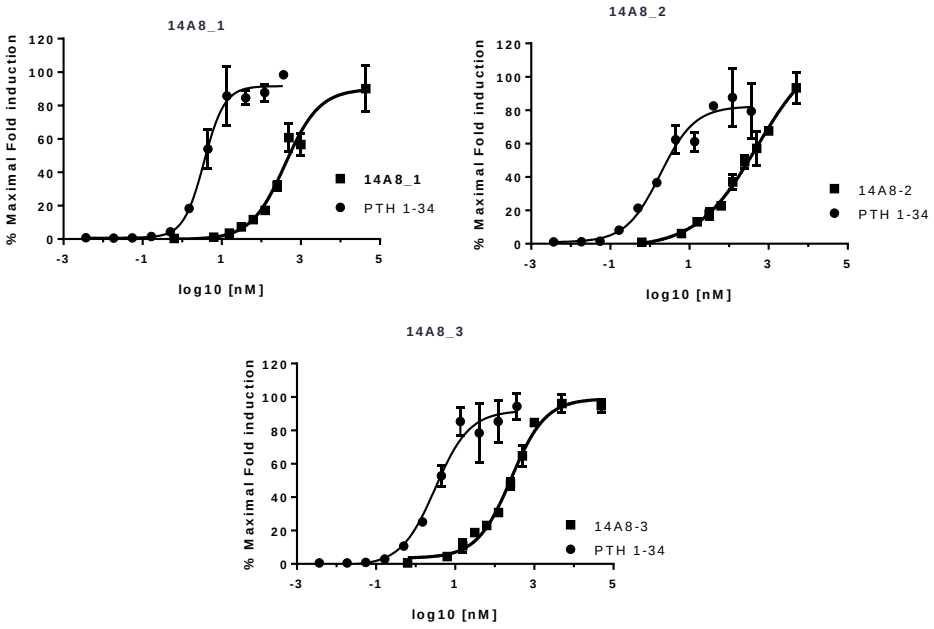

Figure H5: Mean % Maximal Fold Induction of three independent 14A8 bioactivity assay experiments and PTH 1-34 against log10 concentration (nM). PTH 1-34 (•) and 14A8 (■). The standard curve was produced on the challenge of UMR-106 cells. Data presented by GraphPad Prism and presented as maximal fold induction ± StDev calculated from an average of duplicate values.